Head Office:
UNIVERSITÀ DEGLI STUDI DI PADOVA

DEPARTMENT OF PHYSICS AND ASTRONOMY
"GALILEO GALILEI"

Ph.D. COURSE IN PHYSICS
XXXIV CYCLE

Statistical Physics approach to ecological and biological topics

Thesis written with the financial contribution of
Fondazione Cassa di Risparmio di Padova e Rovigo

Coordinator
Prof. Franco Simonetto

Supervisor
Prof. Amos Maritan

Co-supervisor
Prof. Sandro Azaele

***Ph.D.* candidate**
Stefano Garlaschi

"Research is what I'm doing when I don't know what I'm doing."

Wernher von Braun

"The most exciting phrase to hear in science, the one that heralds new discoveries, is not 'Eureka!' but 'That's funny...'"

Isaac Asimov

Abstract

Natural scientists have been always attracted by the study of the phenomenon of Life, since it displays a plethora of curious and yet puzzling behaviors. In the last decades it has been registered an increasing interest in the investigations of ecological and biological systems by the Physics community. This stems from the fact that the physical discipline of Statistical Mechanics offers many tools, frameworks and ideas that have turned out to be naturally adapted, as well as very efficient, to deal with systems affected by an huge degree of *complexity*, like living systems are.

In this Thesis we embrace such a perspective and so we tackle ecological and biological topics employing a Statistical Mechanics mindset.

We firstly model ecological communities in which several different species compete for the consumption of a shared pool of resources with the aim of understanding how the huge biodiversity empirically encountered can originate. To do so, we extended the celebrated MacArthur's consumer-resource model to account for spatial contributions, originating from a variety of ecological mechanisms, in an effective way. Thanks to this, we show analytically the model predicts several species coexisting while competing for a limited number of resources, in complete agreement with evidences coming from empirical observations. This is solely due to the modification we introduce, based on both physical and ecological arguments, since such a result can not be obtained within the classical formulation of the model.

Then, we move our attention to study the universal features of self-organized regular spatial structures, which can be found in both empirical and theoretical ecological investigations. Due to their wide diffusion also in other scientific fields, we search for any universal behavior in their spatio-temporal evolution, regardless the microscopic peculiarities characterizing a certain system. We provide a mathematical framework able to state whether such patterns emerge or not. More interestingly, in the pattern formation phase of the model, we are able to show that it exists a regime in which the evolution of the envelope of such spatial structures on long timescales and large spatial scales is model independent, i.e., it is governed by an equation, whose shape does not dependent on the dynamics details.

Finally, motivated by real-world biological scenarios, we build a theoretical framework, which acquires the form of a generalized Langevin dynamics, accounting for demographic stochastic contributions and temporal delays effects. Hence we model systems whose evolution, subjected to noisy effects, is determined also by the past states visited by the system. We demonstrate how such a framework predicts quite naturally the emergence of almost regular oscillating behaviors, in the form of noise-induced cycles, in the temporal evolution of the system. We then apply these theoretical findings to understand the experimental results studying gene expression regulatory networks, in which noise and delay contributions indeed are at stake.

Acknowledgements

Well, where, or rather with whom shall I start? It has been a $3 + 5$ years long adventure and I had the pleasure to cross my path with a lot of people, who indeed deserve to be acknowledged here.

I'd start by thanking Amos. Besides being an amazing scientist, he has always been a great person to work and spend time with. Thank you for your guidance, but more importantly for your constant support and encouragement.

Tons of credit have to be acknowledged also to Sandro. After his arrival, we undertook a fervid research activity, during which he patiently taught me a lot. Indeed, from him I learnt to never stop searching for the correct answers in front of initial failures and discouragements.

Although we didn't have the opportunity to work much together, I think Marco deserves to be explicitly thanked here. He always had comforting words, which helped me so much academically and personally. It was a real pleasure to have met you.

Along with Amos, Sandro and Marco, I spent my days at university with the Liph Lab guys. I feel lucky to have been part of such a fantastic group of people and to have shared my Ph.D. experience with you, past and present members. Shout-out to you all!

I have to admit that it hasn't been always easy and I've been through tough periods, but I am blessed to have an enormous number of friends to cheer my days up. They are too many to be mentioned one by one, but I want them to know I am grateful for their friendship. Cheers to those I met in the last 8 years here in Padova, but also to the homies from Telgate. Wish you all the best!

In the end, I want to reserve my last heartfelt words of gratitude to my family, including all my numerous relatives. Indeed, the selfless love coming from your family is something that often is taken for granted, but I'd like to spent a moment to say an huge thanks to you, especially to my mum, dad and brothers. I'd have never achieved this milestone without your priceless support. I want you to know this.

Now this journey has finally come to an end and I'm curious to see what the future holds for me. After all, sky is the limit, am I right?

Contents

Chapter 1

Thesis Introduction

1.1 Historical remarks on population dynamics

Ecological systems have been attracting the interest of scientists since long time in the past. This curiosity was not relegated simply to empirical investigations, which indeed led to ground-breaking revolutions in the way with which Nature is interpreted (to cite maybe the most innovative one, we could think of the Darwinian theory of species evolution), but efforts have been directed also to build mathematical models in order to gain quantitative predictions on these systems.

One of the most studied aspects of ecosystems is for sure the temporal dynamics of populations sizes, i.e., how the number of individuals belonging to a given species grows and changes with the elapsing of time. In fact being able to predict the future number of individuals is of crucial importance, for example, if one is interested in sustainability problems or conservation.

The first documented work dealing with this topic goes back around the year 1200 and it has to be attributed to Leonardo Fibonacci [1]. He aimed to mathematically describe the evolution of the number of rabbits belonging to a colony and to accomplish such a task he modelled the mating habits of the species assuming that the population of new rabbits born in each generation is equal to the sum of the numbers of individuals present in the previous two generations. If we call N_k the population size of the k-th generation we can express such idea in the following mathematical form

$$N_{k+2} = N_{k+1} + N_k, \tag{1.1}$$

where we impose the initial conditions $N_0 = 0$ and $N_1 = 1$. It is easy to see that Eq. (1.1) gives the celebrated Fibonacci' sequence.

Although it has the merit to be the first attempt tackling population evolution, this early work is very naïve since it simplifies the problem into a mere additive dynamics. A new description for the evolution of a single-species population was later proposed by Thomas Malthus in 1798 in his book "*An Essay on the Principle of Population*" [2], which turned out to be a cornerstone for the future developments of population dynamics. In this seminal work, Malthus stated that the population size of a given species, including the human kind, would grow with a speed proportional to the current size itself, in the absence of external constraints. Employing the concept of derivative

(which was not conceived yet at Fibonacci's era), we can mathematically express this idea in terms of a simple differential equation of the form

$$\dot{N}(t) = rN(t), \tag{1.2}$$

where $N(t)$ is the population size at time t and r is what has been called the *intrinsic growth rate*. Eq. (1.2) is known as *Malthusian growth model*.

If the initial condition is $N(0) = N_0$, the solution of Eq. (1.2) takes the simple form of an exponential function, i.e.,

$$N(t) = N_0 e^{rt}. \tag{1.3}$$

This is famous with the name of *Exponential Law* of population growth and due to its historic relevance is sometimes referred as the first principle of population dynamics.

It is immediate to see that if $r > 0$, Eq. (1.3) predicts that the population would diverge with the elapsing of the time. For this reason, this led to the so called *Malthusian catastrophe*: at a certain moment the population growth would outpace the supply of food and the other necessary resources, hence part of the individuals would be inevitably doomed and simultaneously the surviving population would go back to lower but more sustainable sizes.

However, the rationale behind such scaring prediction is not completely correct: indeed the exponential growth can capture pretty well the evolution in the early stages when the initial size is small, meaning that the population can grow without being limited by the finite availability of resources. But in real-world situations the growth rate has to start decreasing sensibly when the number of individuals grows too much since, sooner or later, the lack of resources and other environmental restrictions will start to be faced by the increasing population. In other words, an unbounded growth of any population is not feasible since it has to be subjected to the fact that environmental resources are limited.

This more realistic concept was properly formalized by Pierre-François Verhulst in 1838 [3]. He proposed to substitute the constant growth rate of the Malthusian growth model with one that depends on the population size such that it decreases linearly when the number of individuals goes up. To do this it is necessary to modify Eq. (1.2) with the substitution

$$r \longrightarrow r\left(1 - N(t)/K\right), \tag{1.4}$$

where the inverse of the parameters K quantifies the strength of the crowding effect that leads to the reduction of speed of the growth. Now it is clear that when $N(t)$ is larger than K the growth rate becomes negative. This means that the population size starts to decay until it reaches the equilibrium value K. For this reason, the parameter K has been called *carrying capacity*.

Because of this modification, the differential equation describing the population evolution is nonlinear and takes the form

$$\dot{N}(t) = r\, N(t)\left[1 - N(t)/K\right], \tag{1.5}$$

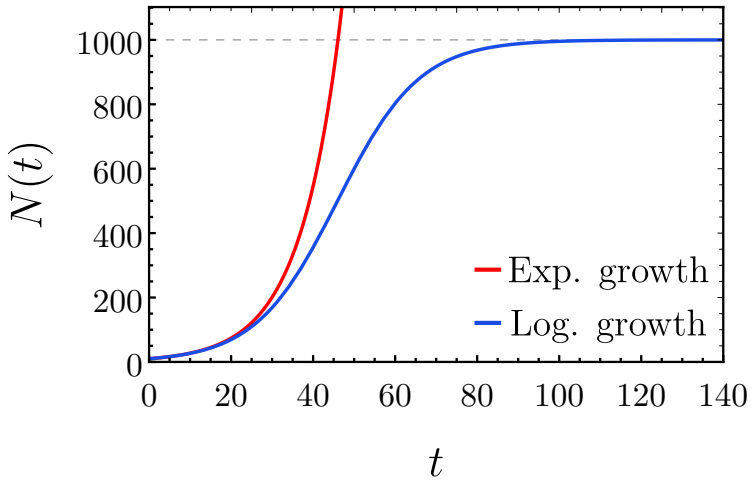

FIGURE 1.1: Exponential growth [Eq. (1.3)] (red line) versus logistic growth [Eq. (1.6)] (blue line). We can see that the two at a certain moment start to deviate one from the other. In particular, the red curves keeps on increasing indefinitely, whereas the blue one saturates up to the value of the carrying capacity $Kr = 1000$, as hinted by the horizontal gray dashed line. For both the curves we took the initial value $N_0 = 10$ and the intrinsic growth rate $r = 0.1$.

which is known as *logistic equation*. Given that $N(0) = N_0$, the solution of this dynamics, named *logistic growth*, can be found to be

$$N(t) = \frac{K}{1 + (K/N_0 - 1)\, e^{-rt}}. \tag{1.6}$$

It is possible to see that when the population is much smaller than the carrying capacity, the growth is still captured by an exponential, but when $N(t)$ becomes significantly big it starts to deviate from such behavior until it saturate reaching the value Kr. In Figure 1.1 we compare an exponential growth against a logistic one so that the deviation of the latter from the former with the elapsing of time is clear.

The introduction of a density-dependent growth rate can be seen as the first and simple attempt to model competition among the population individuals due to the finite availability of environmental resources. Indeed, detrimental competitive interactions for the resources become relevant when the population size grows and it therefore starts to affect negatively the population expansion. This means that while increasing in number, the competition among the individuals becomes stronger and stronger, reducing the speed of growth up to the moment in which such competitive interactions become so intense that it is not possible anymore to have a net increment in the population size.

If we limit ourselves to consider the expansion of a single-species population, the interactions are among individuals of the same type. However, in real ecosystems many species are observed to coexist together. This means

that realistic dynamics aiming to model such ecological settings should account for interactions occurring among different species. Therefore the extension to the co-evolution of multiple species interacting among each others was naturally the following conceptual revolution in the class of population dynamics models.

Mathematically, this can be achieved by introducing systems of coupled differential equations, one for each population taken into account. The coupling between the evolution dynamics is the key feature to model in a simple and yet realistic way the interactions that each species experience due to the presence of the others within the same habitat.

Such innovation was proposed for the first time by Alfred Lotka [4] and Vito Volterra in 1920 and 1926 [5], respectively. They independently came up with the same model to describe predator-prey systems in a simple and yet elegant form. Calling $x(t)$ the prey population size at time t and $y(t)$ the corresponding quantity for the predators, they wrote

$$\dot{x}(t) = ax(t) - bx(t)y(t) = x(t)\left[a - by(t)\right], \tag{1.7a}$$
$$\dot{y}(t) = -cy(t) + dx(t)y(t) = y(t)\left[-c + dx(t)\right], \tag{1.7b}$$

where all the model parameters are positive. The main ideas behind such a model, that for obvious reasons is also known as *Lotka-Volterra predator-prey model*, are quite easy to understand. The population of preys alone, i.e., in absence of predators, would grow because of an intrinsic birth rate, but when predators interact strongly with the preys by hunting, their population growth is negatively affected and so they must start to decrease. This is captured by the nonlinear term that couples the number of predators and prey. On the other hand, such an interaction must lead to an increment of predators number, that however decays in time, due to a mortality rate, when they are not able to predate because of the lack of preys.

In other words, the two populations have growth rates that depend linearly on the other one modeling a feedback mechanism: when predators are too abundant, preys will have a negative growth rate because predation has become too intense, whereas if there are few individuals of the prey species predators will start not to be able to maintain the population and hence decaying in number. In this way the model given by Eqs. (1.7a)-(1.7b) predicts oscillations in time where $x(t)$ and $y(t)$ go from high to low values and viceversa. We can either prove this using standard tools of dynamical systems or we can see it directly by plotting the numerical solutions of the dynamics, as we did in Figure 1.2. In particular, this cyclic behavior is tied to the existence of a the conserved quantity, which takes the form [6]

$$H(x, y) = a \ln y + d \ln x - cx - by. \tag{1.8}$$

Once the initial condition (x_0, y_0) is given, the predator and prey populations evolve in time such that $H\left(x(t), y(t)\right) = H(x_0, y_0)$ at any moment. Hence, with the elapse of time $x(t)$ and $y(t)$ will go back to the initial values x_0 and y_0 and the dynamics will start all over, repeating itself again and again.

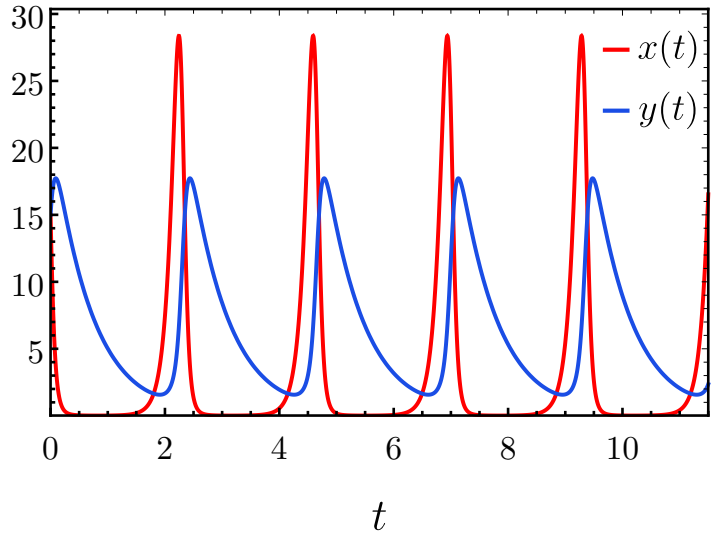

FIGURE 1.2: Solutions of the Lotka-Volterra predator-prey model (1.7a)-(1.7b) where $a = 10$, $b = 1.5$, $c = 1.5$ and $d = 0.4$. We used the initial conditions $x(0) = y(0) = 15$. We can see that both the population of preys $x(t)$ (red line) and of predators $y(t)$ (blue line) display regular oscillations.

To conclude, we must mention how it is possible to generalize Eqs. (1.7a)-(1.7b) to describe an arbitrary number of species $n \geq 2$ present in the same environment. In fact calling $\vec{x}(t)$ the vector whose components $x_i(t)$ (i goes from 1 to n) represent the population sizes of the different species, we have n coupled differential equations of the form

$$\dot{x}_i(t) = x_i(t) f_i\left(\vec{x}(t)\right), \tag{1.9}$$

where $f_i\left(\vec{x}(t)\right)$ can be seen as the components of the vectorial field

$$\vec{f}\left(\vec{x}\right) = \vec{r} + A\vec{x}, \tag{1.10}$$

with r_i being the intrinsic growth rate of the i-th species and the matrix A is called community matrix, since it contains information regarding the type of relationships among the species. In fact $a_{ij} < 0$ means that species i is negatively affected by the presence of species j in the ecosystem, whereas if $a_{ij} > 0$ we have the former benefits from the interaction with the latter. Such dynamics takes the name of *generalized Lotka-Volterra* model [7], [8].

1.2 The era of complex systems

As it emerged from this brief historic digression, theoretical models evolved in order to account in a more and more realistic way for the interactions occurring within the individuals of the same species, but also with the ones of a different kind. The generalized Lotka-Volterra model pushed this idea as further as it could while keeping the modeling in the simplest form possible.

Thus the role of interactions has started to be recognized as more and more crucial in shaping the dynamics and the features of ecological systems [9]–[11]. Nowadays in fact when studying such systems, but more in general living systems, we start by acknowledging they are affected by an huge degree of *complexity* [12]–[14]: these systems are made up by dozens of elementary components interacting in a very heterogeneous and intricate way among themselves. One could expect that such dynamics would display messy outcomes. Nevertheless, surprisingly we observe coherent behaviors emerging from the interactions among the myriads of components. Finding an answer regarding how such harmony arise a very interesting challenge in modern science [15].

In principle, one could start by following the behavior of each elementary units. Unfortunately this would not be feasible given the huge number of degrees of freedom required to describe the whole system. Also, in this way it could be hard to unveil the origin of systematic behaviors simply studying the dynamics of the single building-blocks [16], [17]. So we need an alternative to a reductionist standpoint, which aims to explain the entire system behavior starting from its smallest constituents.

This suggests that it would be more beneficial to use a holistic perspective, moving the focus of the description from the microscopic details in order to gain an overall description of the entire system [18].

Therefore the modern way to look at ecological but also biological systems is the same one employed for the study of the so called *complex systems* [19], [20]. Broadly speaking, systems whose components are correlated one to the other through dense and various interactions networks are said to be complex. Also, the systems could receive external disturbance from the environment, making them even more unpredictable at first glance. Because of this strong and articulated entwining featuring the system, it is not trivial at all to infer a priori from a microscopic picture the outcome of the system dynamics or the emergence of non-trivial properties at global scales [21]–[23]. Just to list some of these curious features, complex systems might display nonlinear response to external inputs and in general nonlinear dynamics (the change of the state of the system to an alteration is not proportional to the perturbation itself), self-organization (the system displays peculiar properties that can be observed only in suitable conditions, however the system rearranges itself and reaches such conditions without any required external tuning) and adaptation through feedback loops.

To sum up clearly the concept of complexity, often the long-standing quote "the whole is more than the sum of its parts" is employed: to understand the system in its wholeness it is not enough to frame it as a mere sum of elementary units. So, the core idea behind the formulation of complex systems is the possibility to describe collective phenomena and evidences regarding the behavior of the global systems emerging at different spatio-temporal scales which can not be obtained starting from the understanding of the elementary units on an individual basis [24], [25].

With this being said, it is clear why ecological and biological systems

should be regarded as complex [26], [27]. If one thinks of ecological communities, neural networks or fundamental cellular processes, just to make some remarkable examples, one can immediately identify the small constituents, i.e., the individuals of the coexisting species, the neurons in brain or protein, DNA molecules and so on in the case of cell machinery. Also it is evident that such units are strongly intertwined through an rich set of different interactions, leading in this way to complexity.

The field of complex systems is intrinsically interdisciplinary since within this broad framework we can naturally describe topics coming from different research fields. So the study of complex systems borrows several ideas and techniques from different disciplines, ranging from Mathematics to Computer and Network Science. However, for us it is very intriguing the possibility to employ Physics and in particular Statistical Physics with its powerful tools. Not only this, but applying a physics approach to the investigation of living complex systems might stimulate the development of frameworks and the discovery of new phenomena that might not be found when studying purely physical settings [28]. The application of Statistical Mechanics to the study of complex systems can indeed lead to remarkable scientific results that are able to fascinate and be acknowledged by the whole Physics community. As a culmination of this, in the present year (2021) the Nobel prize for Physics was awarded to the italian physicist Giorgio Parisi "for the discovery of the interplay of disorder and fluctuations in phyisical systems from atomic to planetary scales".

The concepts born with the seminal studies of Statistical Mechanics, such as order/disorder, phase transitions [29], scale-invariance and criticality [16], [30], [31], are indeed appealing to be exploited when trying to describe ecological and biological systems [32]–[34]. As we said, complex systems science always tries to treat the system as a whole and not simply made up by the summation of its units. This is exactly the core of statistical physics where we renounce to search for a microscopic description in favor of an ensemble treatment of the system under study. Therefore its standard techniques look suitable for a quantitative investigations of the living systems [25]. In this way the system behavior can be understood from simple laws emerging from the overall description of the dynamics that in principle can be compare with data to see if they have empirical confirmations.

As we stressed so far, interactions are strongly present and crucially shape the system's evolution, introducing non-trivial spatial and/or temporal correlations. Hence a proper theoretical modeling of the dynamics can not disregard these. Taking into account this naturally leads to the formulations of coupled and nonlinear dynamical systems (the generalized Lotka-Volterra is once again the archetypal of this type of models). As we will see in the next chapters of this Thesis when we will tackle three different ecological and biological topics, we will always start with models considering nonlinear equations in order to account for the correlations among the system components. Indeed, acknowledging the effects of these correlations in the systems' evolution will be crucial to retrieve results replicating the empirical evidences and to avoid that models might predict structureless and unrealistic outcomes.

A second recurrent motif of the Thesis is given by the generality of the theoretical frameworks we will develop in the following Chapters. In fact, consistently with the complex systems approach we discussed above, we will formulate fairly general models without the need of specifying the entire set of microscopic details that characterizes concrete case studies. However, the broad settings we will provide can still be employed to capture concrete relevant scenarios and retrieve insightful descriptions on the systems behavior.

At this point, we are ready to sketch the themes we are going to investigate in the next-coming chapters. Among the many features of living systems one might be interested in, we will focus on the followings. First we will investigate the long-standing puzzle of species coexistence and the maintenance of the huge biodiversity empirically encountered in many real-world ecosystems. The second topic will deal with the research of universality in the emergence of regular spatial structure, i.e., pattern formation, from nonlocal dynamical systems, which is a wide spread feature of many ecosystems (and not only). In latest, we will study how cyclic dynamics and seasonal behaviors, observed across many research fields, can arise just combining temporal delays effects with the intrinsic stochastic contributions affecting biological dynamics.

1.2.1 The puzzle of species coexistence

The species richness we can observe in many real-world ecosystems, whose scales range from microscopic to macroscopic ones, is a striking feature of our planet [35]. Examples include microbial organisms [36]–[38], birds [39], snakes [40]–[42], coral reefs [43]–[45] and trees communities [46], [47].

Sharing the same environment, we expect the species to be entwined one to the others via a network of trophic interactions that defines the food-web of the ecosystem under consideration [48], [49].

It might seem obvious that when the different species are not in contact with each other, they can survive, since the inter-specific interactions, which might be harmful for their survival, are not at play. However, as soon as species interface with each other, such damaging mechanisms might alter extensively the ecological panorama. In particular, more similar two species are, more intensely they are expected to compete [50] since they will have, for example, similar diets. Hence, observing such a richness in the species biodiversity featuring so many real scenarios seems surprising and unexpected a priori. Empirical evidences, in fact, tell us that several microbial species seem to coexist in close-by regions [51]–[53]. The same counter-intuitive scenario was noticed for the first time while studying plankton communities and therefore such puzzling outcome in these competitive ecological dynamics has been called the *paradox of plankton* [54].

So the large biodiversity, that on an intuitive level is hardly explained, is a property that frames ecological systems as complex. Trying to shed light on what makes species-rich ecosystems stable is still an open and very intriguing challenge.

The first theoretical attempt trying to investigate the stability of large ecosystems came from the Robert May' seminal work [55], which for this reason has to be undoubtedly regarded as one of the most influential works in theoretical ecology.

May started by considering an ecological community made by M different species. The evolution of their populations is subjected to a set of nonlinear coupled differential equations of a certain form [for example the generalized Lotka-Volterra model Eq. (1.9)]. To study the stability of the system, we search for its feasible equilibrium point, where for feasible we mean that the stationary values of the populations sizes have to be non-negative. Then we linearize the dynamics around such an equilibrium, obtaining a set of linear equations of the form

$$\dot{\vec{x}} = A\vec{x}, \tag{1.11}$$

where now $\vec{x}$ is the deviation from the stationary state, A is the Jacobian of the full set of equations evaluated at the equilibrium and it has the form of an $M \times M$ matrix. Employing the results of linear stability analysis, we can state whether the dynamics is (linearly) stable or not by searching for the eigenvalues of A. In particular, to ensure the stability we need that all its eigenvalues have negative real parts.

At this point, here May's revolutionary idea came. Instead of computing A from a concrete ecological model, which indeed must be very intricate for large ecosystems, he proposed to model directly the matrix A as a random matrix, i.e., a matrix whose entries are sampled from a certain probability distribution. We can see that an advantage of this would be that the stability we will find will not depend crucially on the structure of the system, on the contrary if we are able to find a criterion in this broad setting the results would have a larger applicability.

May postulated the A matrix to be a random matrix with connectance C. This means that each non-diagonal entry is zero with probability $1 - C$, whereas with probability C each A_{ij} is sampled from a probability distribution with zero mean and variance σ^2, i.e., $A_{ij} \sim P(0, \sigma)$.

Instead, the diagonal elements are taken as negative constants, i.e., $A_{ii} = -d < 0$ to ensure that each population size, when the species are isolated from the others, would not diverge. For clarity, such a contribution can be thought to model a carrying capacity binding the maximal value for the populations.

To infer the stability of the dynamics, now it is enough to compute the eigenvalues of A and search if all of them have a negative real part. This is equivalent to studying the sign of the eigenvalue having the largest real part. Employing results obtained from the theory of random matrices [56], [57] in the limit of large M, May (and later developments of his first proposal) was able to show that the system described by a matrix A drawn from the ensemble of matrices one can construct in such a way would be unstable with probability going to one in the limit of large M [58], i.e.,

$$P(M, C, \sigma) \to 1 \iff \sigma\sqrt{MC} < d. \tag{1.12}$$

From this we can immediately say that species-rich ecosystems, i.e., ecological communities with a large number M of interacting species, are likely to be unstable: small perturbation to the equilibrium population size would depart the system from it and so ecosystems with many coexisting populations should be hard to be observe. Using this simple mathematical formulation, May gave rise to the Diversity-Stability debate [59]: an increase on the complexity and diversity of the ecosystem, which is related to an increase of M, C and σ, leads to a resulting decrease of stability. But recalling what we presented at the very beginning of the section, this is in stark contrast with the empirical evidence, where large ecosystems seem to not be the exception, but rather the rule.

Although it has been enlightening and a very brilliant starting point to discuss the stability of biodiversity, May's work is limited by the fact that linear stability analysis gives a criterion only about the local stability, i.e., when the dynamics takes place in a neighbourhood of the equilibrium point [58]. Thus, May's criterion has limited application when describing out-of-equilibrium populations. Additionally, instability does not necessarily imply lack of persistence of the populations, which can be achieved through limit cycles or chaotic attractors emerging typically from unstable equilibrium points.

From an ecological standpoint instead, this way of thinking ecological communities is focusing on the interactions occurring between the coexisting species, regardless of the food resources and nutrients for which the different species are in competition for. Indeed, the availability of them will affect how the populations evolve themselves. If the concentrations of resources are too low, they would not be enough to sustain the expansion of the populations. Similarly, while growing the population uptake the nutrients, making them not available for the other individuals. Hence, correlations between the consumer populations' evolution and the availability of the nutrients they require to growth are indeed present and they should not be neglected.

For this reason, a more realistic description of species competing for a shared set of resources would consist in a framework describing the evolution of the species population along with the temporal changes in the levels of resource concentrations present in the environment. Going in this direction, Robert MacArthur was one of the first who developed such an approach [60], [61] that eventually led to the introduction of the so called *consumer-resource model* [62], [63].

As we said, the novel aspect of this model has to be searched in the fact that it does not limit only to describe the evolution of the species populations, but it aims also to take into account explicitly the dynamics determining the resources concentrations. To accomplish this, the consumer-resource model is made of two coupled systems of differential equations, one for the M species and the other for the R different types of resources consumed. In other words, the full dynamics takes the following form:

$$\dot{n}_\sigma = f_\sigma\left(n_\sigma, \{c_i\}\right), \qquad \sigma = 1, \cdots, M \tag{1.13a}$$

$$\dot{c}_i = g_i\left(\{n_\sigma\}, c_i\right), \qquad i = 1, \cdots, R \tag{1.13b}$$

where the right-hand sides depend on the assumptions we use to model the uptake, the consumption of the resources by the consumers along with how new quantities of resources get generated in the system. The state-of-the-art way of modeling these is given by

$$\dot{n}_\sigma = n_\sigma \left[\sum_{i=1}^{R} \alpha_{\sigma i} r_i(c_i) - \beta_\sigma \right], \qquad \sigma = 1, \cdots, M \tag{1.14a}$$

$$\dot{c}_i = \mu_i(\Lambda_i - c_i) - r_i(c_i) \sum_{\sigma=1}^{M} \alpha_{\sigma i} n_\sigma, \qquad i = 1, \cdots, R \tag{1.14b}$$

The first equation tells that the net growth rate of the population of species σ is given by the balance between an intrinsic mortality rate, β_σ, and a growth rate determined by the consumption of the resources. This contribution is modeled as the sum over all the R nutrients of the rates, quantified by the set of parameters $\alpha_{\sigma i}$ named *metabolic strategies*, with which the resources are consumed by the individuals of species σ times the rate with which the resources can be uptaken from the environment, modeled by the functions $r_i(c_i)$. It makes sense to assume that the uptake rate of a given resource i, when the concentration is small, varies linearly with the nutrient concentration itself. However, when the resource becomes abundant such contribution has to saturate, since it is biologically unrealistic to have individuals uptaking the resource in an unlimited fashion. Because of these arguments, commonly the $r_i(c_i)$ functions are assumed to take the so called *Monod form* [64], i.e.,

$$r_i(c_i) = \frac{c_i}{c_i + K_i}, \tag{1.15}$$

with the parameter K_i called the *half-saturation constant*. The same term determining the populations growth describes also the resources depletion. However, new resource is constantly added into the system through the supply rate $s_i = \mu_i \Lambda_i$, whereas there is an additional loss term due to resource degradation taking place with rate μ_i, which is thus called *degradation rate*. In some setting instead, it might be more appropriate to substitute such term with a logistic growth contribution. In the former case we say to deal with *abiotic* resource, in the latter with *biotic* ones.

At this point we can search for the stationary state of Eqs. (1.14a)-(1.14b). Asking that the stationary population sizes are all non-zero for all the M starting species, i.e., $n^*_\sigma > 0 \; \forall \sigma$, we end up with

$$\sum_{i=1}^{R} \alpha_{\sigma i} r_i\left(c_i^*\right) = \beta_\sigma \qquad \forall \sigma. \tag{1.16}$$

This gives us a set of M equations in R unknowns. When the number of species is larger than the number of resources, i.e., $M > R$, such system does not admit a solution (unless some tuning of the model parameters is assumed).

This implies that at least $M - R$ species necessarily go to extinction and

we have an upper bound on the total biodiversity the consumer-resource model can predict. In particular, we can conclude that the maximum number of different species that can coexist while competing for the consumption of the same resources is limited by the number of resources itself. This principle is famous under the name of *Competitive Exclusion Principle* (CEP) [65].

Once again, this theoretical result is manifestly in disagreement with the evidences provided by the empirical observation listed at the beginning. In fact, for the sake of clarity, there are ecosystems, whose extensions range from microscopic scales to macroscopic scales, where an huge biodiversity is maintained over a restricted, even a handful of different resources.

The irreconcilability between the unquestionable existence of so many biodiversity-rich ecosystems around the globe and the dramatic theoretical predictions of CEP is still an open question. In particular, why CEP in real-world ecosystems does not hold is an hot topic at the center of a vibrant scientific debate nowadays.

1.2.2 Pattern formation in complex systems

As we said, one of the possible signatures of complexity in systems is the possibility to observe spatial correlations, translating into spatial order, at the system scale without any external drive.

Maybe the most remarkable example of patterns breaking the translational invariance can be seen in the self-emergence of non-trivial spatial structures on very large scales. In this case, the system elementary constituents are heterogeneously distributed across space in an almost periodic fashion. Such ordered spatial structures are known in the literature as *spatial patterns* and for this reason when discussing their emergence we speak about *pattern formation*.

The basic mechanisms underpinning pattern formation [66]–[70] is commonly searched in the instability under small disturbances of the stationary and spatially uniform states emerging from the nonlinear dynamics modeling the interactions among the atomic system components under study.

Besides being an interesting phenomenon to be understood if one would like to properly describe a system displaying patterns, the self-emergence of spatial structures has captured the attention of a huge part of the scientific research since long time due to its wide-spread observations across many different scientific fields. To list some examples, one could cite chemical species undergoing reaction-diffusion mechanism [71]–[76], the convection and flow of fluids [77]–[80], the organization of nematic liquid crystals [81], [82] or the surfaces formed during the growth of a crystal [83].

Biological systems are no exception when it comes to provide clear evidences of pattern formation dynamics [84]. The interfaces between bacteria swarms [85] or auto- and cross-catalysis mechanism inducing patterns in cellular tissues [86] are just two examples. However, the archetypes of biological patterns are those observed in animals coats and skin [87], [88] or on seashells [89]. Mathematically, the emergence is related to the instability of the homogeneous stationary state of reaction-diffusion systems, whose

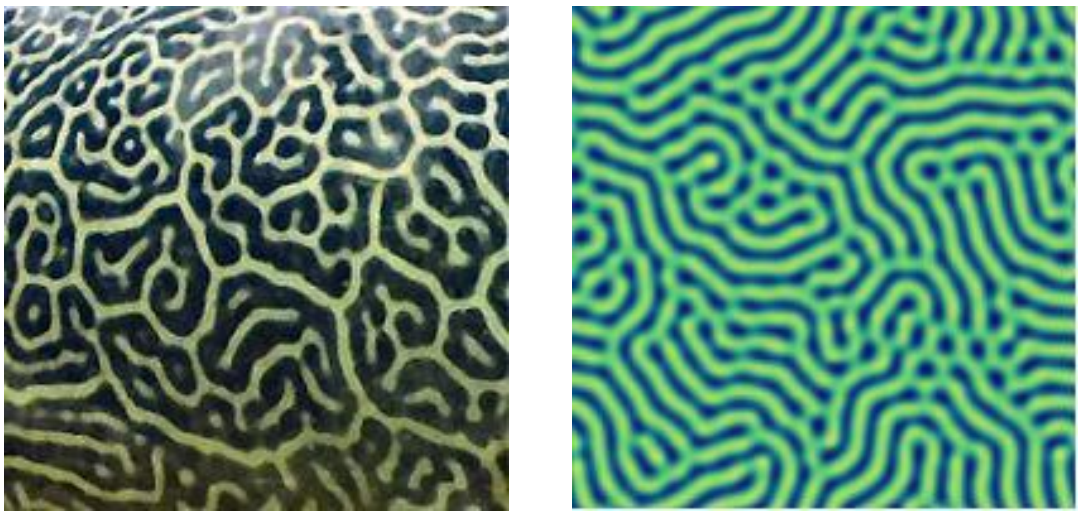

FIGURE 1.3: Left panel: pattern on the skin of a giant pufferfish (figure taken from [90]). Right panel: Turing pattern obtained from Eq. (1.17) using the set of chemical reactions of the Brusselator model [91].

dynamics is given by

$$\dot{\vec{\phi}}(\vec{x},t) = \mathbf{D}\nabla^2\vec{\phi}(\vec{x},t) + \mathbf{R}\left(\vec{\phi}(\vec{x},t)\right), \tag{1.17}$$

where $\vec{\phi}(\vec{x},t)$ is an $n-$ dimensional vector whose components are the densities of the n different chemical species at time t and position $\vec{x}$ (for example the pigments of the coat of an animal), $\mathbf{D}$ is an $n \times n$ diagonal matrix of the diffusion coefficients and $\mathbf{R}\left(\vec{\phi}(\vec{x},t)\right)$ is a nonlinear function accounting for all the interactions among the elementary units occurring at the location $\vec{x}$ and at time t. This framework was first proposed by Alan Turing in 1952 [71] and for this reason this class of patterns is commonly known as *Turing patterns*. From Eq. (1.17) patterns displaying spots, striped, hexagons or even spirals arise, which resemble closely regular motifs one could encounter in nature. In Figure 1.3 we display the skin of a pufferfish (left panel) and a Turing pattern emerging from Eq. (1.17) so that it is possible to notice how similar are one to the other.

In the system evolution equations, an essential role is played by the nonlinear terms that are able to stabilise the initial growth of perturbations and eventually select the spatial pattern. In many examples of interest, including those we have alluded to above, nonlinearities are assumed to be local, as in Eq. (1.17), albeit spatial patterns can be generated by more general forms of nonlinear terms. For instance, the Phase Field Crystal (PFC) theory incorporates crystalline details on length and time scales of experimental relevance and is used to model the structure of several materials [92], [93]. The connection to the microscopic details is achieved via the Dynamic Density Functional (DDF) theory, from which it can be derived [94]. In the DDF theory the pairwise and higher order spatial correlation functions are responsible for the nonlocal (and nonlinear) contributions, which govern the evolution of the conserved order parameter.

More relevant for the focus of this Thesis, ecology provides several other examples of systems displaying regular spatial structures on large scales from nonlocal dynamics. The first ones have to be searched in the vegetation landscapes of many different areas around the Earth characterized by a regular alternation of colonized regions and bare soil by plants, bush or grass [95]–[99]. Interestingly, models describing plant-species dynamics [100]–[108] provide, to some extent, the physical insights about the origin of such observations. To account for the interactions within the system in the most realistic way possible, these models use nonlocal contributions in the evolution equations. Such an idea can be mathematically expressed in the following form:

$$\dot{\phi}(\vec{x},t) = D\nabla^2\phi(\vec{x},t) + \phi(\vec{x},t)\left[r - \int_\Omega G\left(|\vec{x}-\vec{x}'|\right)\phi(\vec{x}',t)\,d\vec{x}'\right], \qquad (1.18)$$

where now $\phi(\vec{x},t)$ has the meaning of the vegetation density at position $\vec{x}$ at time t. The nonlinear interaction term is modeled with a convolution over the space domain of the landscape Ω between the density field and a kernel weighting the strength of interactions as a function of the distance. Therefore, to model the nonlocality of the interactions occurring in the system, the evolution in a fixed position $\vec{x}$ of the space domain Ω is affected by all the other positions with a weight given by the kernel $G\left(|\vec{x}-\vec{x}'|\right)$, as expressed through the convolution term. This naturally introduces correlations in space at the system' size scales.

Using the class of models given in Eq. (1.18), we can shed light on the empirical observations interpreting them as pattern formation phenomena. Therefore, in light of this, we predict regular structures over long scales to emerge on their own, even in the absence of any environmental perturbation.

Further, the nonlocal features also play an important role while modelling population dynamics. Herein, the intertwining combination of competition and environmental effects is usually modelled by assuming that species undergo a diffusion process and interact nonlocally in space. Such contributions play a vital role in describing the aggregation and distribution of individuals or species in terms of emerging patterns [109]–[111].

Similar settings also enhance our understanding of species origination [65]. In particular, the competition can indeed lead to formation of species by limiting their similarity and partitioning environmental resources [50]. In this case the diffusive process and inter-species interactions occur in the space of species traits, and the eventual patterns obtained from such models are a hallmark of the surviving species [112]–[114].

Given that emergence of patterns is a wide-spread phenomenon across many scientific fields, the research for universal behaviors in their formation could be of great interest since it may indicate that the key features of their evolution are common, despite of the details at the microscopic level that differ across many pattern-forming dynamics. Having ecological applications in mind, it might be relevant in this sense to search for universalities in models affected by nonlocal contributions.

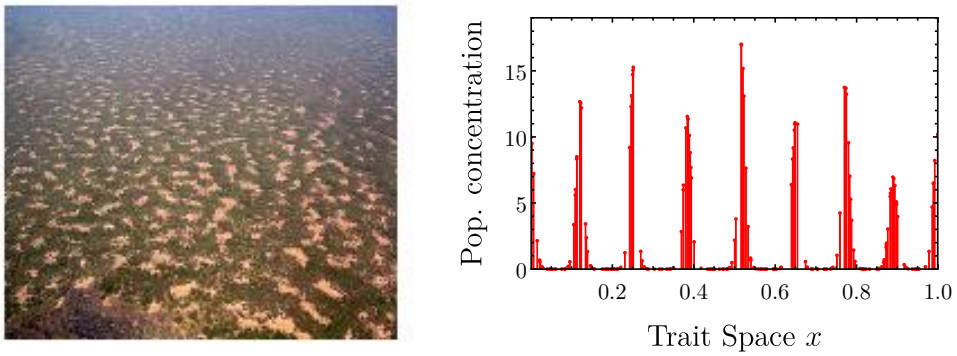

FIGURE 1.4: Examples of patterns emerging from nonlocal dynamics in ecology. Left panel: Aerial view of a vegetation landscaped with gapped bush in Niger where it is clear the alternation of occupied and occupied spots by the vegetation (figure taken from [115]). Right panel: Species formation as emerged pattern in the trait space with the dynamics described in [112] modified by the addition of a diffusion term. The lumpy peaks can be regarded as the possible phenotypes for the species, which have been selected by the competitive pressure occurring in the trait space among the continuous of possible phenotype allowed a priori.

1.2.3 Seasonality in complex systems temporal evolution

Besides from the self-organized spatial order discussed in the previous section, it is common in complex systems dynamics to observe also regularities on long timescales in the temporal evolution of the system key quantities. In this case, the temporal order acquires the form of (almost) periodic behaviors featured by oscillations typical of seasonal phenomena.

Living systems dynamics are deeply affected by this. Examples are provided by host-pathogen systems [116], where the concentrations of infected and healthy individuals keep on alternating regularly between high and low values. For the sake of concreteness, one could think of seasonality characterizing the spread of diseases, like measles [117], which has been studied for many years.

Experimental results also show that emergence of oscillations in the concentration of the chemical reactants in biochemical systems is a quite diffuse process. Circadian rhythms in microorganisms [118], [119] and the oscillation of ATP and ADP concentrations during glycolysis [120], [121] are just two well known instances in this field. Oscillations in proteins concentration within the cells also are crucial in ruling cellular cycles. For instance, this is well documented for the cyclin protein [122], [123].

Thinking of ecological settings instead, interacting populations in natural environments oftentimes display cycles in the evolution of their densities. The food web architecture is frequently responsible for the cyclic dynamics, even though the recognition of a general biological mechanism which induces oscillations is usually a hard task [124].

It is relatively easier, instead, to generate oscillatory dynamics with a model for biological interactions. The Lotka-Volterra (LV) model we already

presented in Eqs. (1.7a)-(1.7b) is probably the best known model which produces oscillations. We also briefly discussed from an ecological standpoint how the continuous feedback due to the predation interaction entwining the predators and prey populations leads to a seasonal temporal evolution.

However, the cyclic behavior in the LV equations depends on the existence of a conserved quantity which has no biological motivation, and this makes the model quite unrealistic. Simple, and more realistic, modifications of the equations actually do not have cyclic dynamics [125]. It is therefore bewildering that in order to predict oscillatory behaviors we require a very specific model, which is not robust in describing this feature against slight modifications.

At this point it is worth noting that when the LV model as well as the models describing the biological and epidemiological examples we listed above are formulated as a set of deterministic equations, sustained oscillations can emerge if and only if such dynamics predict limit cycles [126]. Of course, this is a quite limiting conditions to observe a feature that seems to appear to be fairly general and diffuse across so many different dynamics. Hence, employing a complex system approach to investigate these dynamics, we expect a more general mechanism, which is less dependent of the peculiarities of the evolution equations of the model, able to explain how the emerging seasonality.

The deterministic approach neglects completely the stochasticity that intrinsically affects biochemical reactions or predator-prey interactions [127]. In fact, such processes, given the system state, do not take place in a fully determined fashion, but more properly they have a propensity to occur or not to occur in time. Therefore, we must be cautious when modeling such dynamics and understand whether we can or can not neglect this intrinsic stochastic behavior.

It is known that the deterministic limit is correct when the systems are large enough, i.e., when the number of elementary units becomes formally infinite [128]. However, in the case of small systems where the number of components is quite restricted, stochasticity can play a major role and neglecting completely stochasticity might lead to erroneous descriptions of the system. Interestingly, this latter scenario is the one we most often observe in biological settings, where the concentrations levels can acquire usually low values.

It has been shown that the stochastic generalization of the LV equations introduces substantial new features. A paradigmatic example is the phenomenon of *stochastic amplification*, where the intrinsic demographic noise generated by the birth and death processes of a coupled predator-prey system can generate a persistent oscillating behavior, when the deterministic limit predicts damped oscillations [129].

Although being originally obtained for a predator-prey system, stochastic amplification turned out to be appropriate for explaining the emergence of non-trivial cycling dynamics and seasonal behaviors in a broad range of situations [129]–[131]. Applications can be found in biology [132], economics

[133] and epidemiology [134]. Due to the pure stochastic nature of the phenomenon, it is common to find that in the such oscillatory behaviors are also referred as *noise-induced cycles*.

On a mathematical ground, stochastic amplification occurs when the deterministic system approaches the stationary state with damped oscillations, i.e., the Jacobian calculated at the stationary state has complex eigenvalues with a negative real part, albeit this is only a necessary condition. In this situation the intrinsic noise excites all frequencies and, in resonating the system, sustains oscillations indefinitely. This reflects into the appearance of non-trivial peaks in the stationary power-spectrum, which, roughly speaking, gives information regarding the weight of each frequency components composing the fluctuations. It is therefore clear that the presence of an absolute maximum at a non-zero frequency implies that on average the signal is dominated and well described by an almost harmonic oscillation with characteristic frequency. As a clarification, we show in Figure 1.5 the results obtained in the seminal work by Alan McKane and Thea Newmann dealing with a predator-prey system [129]. In the left panels we see two typical time-series describing the prey and the predator populations evolution, respectively, according to the stochastic dynamics. As it is possible to see, these trajectories keep on oscillating almost regularly, even when the deterministic solutions have reached the stationary values via damped oscillations. Instead the right panel and its inset display the two power-spectra (one for the predator population and the other for the prey population) that capture the spectral properties of the predator-prey time-series. There, two peaks located at non-zero frequencies are clearly visible, confirming the emergence of the regular oscillatory behavior in the predator-prey system evolution. In particular, the two peaks correspond to the characteristic frequencies, one describing the predator and the other the prey population temporal oscillations observed in the stochastic trajectories, as displayed in the panels on the left.

The mathematical framework that originally led to the prediction of stochastic amplification is based on a Master Equation (ME) description of the system dynamics [127]. In order to achieve some analytical results, Van Kampen' system size expansion is then employed [128]. At the leading order of such expansion of the ME we obtain the mean-field dynamics which describe the behavior of the system in the deterministic limit, i.e., in the limit of infinite system size. The next-to-leading order instead gives the Fokker-Planck equation for the fluctuations around the deterministic solution. Equivalently, this can be translated into linear Langevin equations where the stochastic contributions appear explicitly in the form of white Gaussian noises [136]. To infer the spectral properties of these, it is enough to take the Fourier transform of the set of Langevin equations which eventually gives back the power-spectra. In this way, once the transition rates of the ME describing the microscopic dynamics of the systems are fixed, it is immediate to see if the power-spectra present a non-trivial peak, confirming the occurrence of the resonance between the asymptotic deterministic damped oscillations and the demographic noise (the detailed derivation can be found in [129],

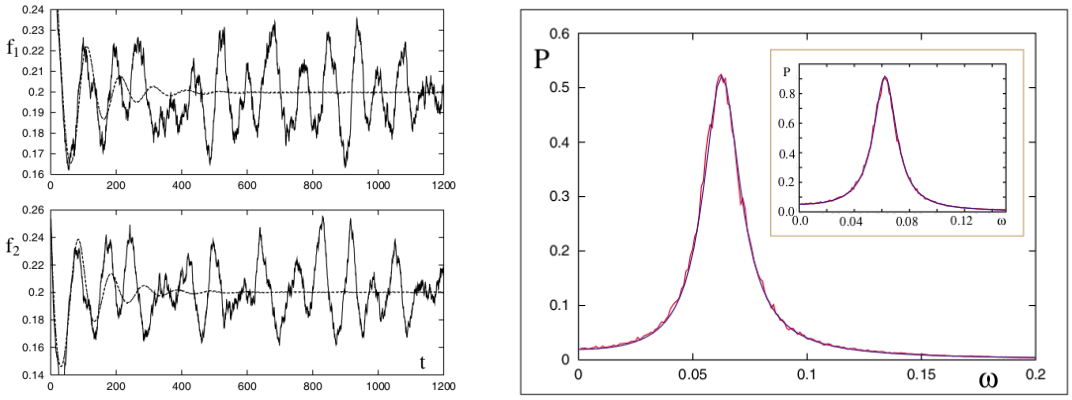

FIGURE 1.5: Figures taken from [129] where all the details to replicate them are provided. The noisy lines in the left panels represent two typical time-series, one for the prey density (f_1) and the second describing the predators density (f_2), numerically obtained using the Gillespie algorithm [135] against the deterministic solutions (dashed lines). As we can see, the stochastic time-series present an almost regular oscillatory behavior also when the deterministic solution reached the stationary state. In the right panel instead we can find the numerical power-spectra (noisy lines) compared to the theoretical ones. In both, the agreement is excellent and we can clearly state the presence of two peaks, which are the hallmarks that stochastic amplification took place.

[130]). We have to remark that in the scientific literature stochastic amplification is treated as a qualitatively different phenomenon from what is referred with the name of *stochastic resonance* [137], [138], acknowledged for the first time in meteorological models [139], [140]. Indeed, the two display a similar phenomenology since both of them rely on a resonance mechanism of deterministic oscillations with a stochastic component. Nevertheless, the key difference has to be searched in the origin of the forcing that makes the resonance possible: in the latter the forcing is provided by an external perturbation acting on the system, whereas when one deals with the former the resonance source is inherent to the system and it is the intrinsic stochasticity due to underlying dynamics.

However, besides the stochastic origin of the fluctuating dynamics, it is also known that in deterministic systems temporal delays, even small ones, may generate oscillations which could not be observed without delay [141]. In particular, this may happen even in one-dimensional first-order differential equations, which could not display oscillations otherwise. In fact, temporal delays introduce correlations in time, which can materialize into temporal cycles.

Gene expression networks are a crystal clear example of biological dynamics affected by delays induced by the underlying biochemical reactions [142]–[145]. Indeed, the key processes taking place in the cellular machinery involved, such as transcription and translation, are not instantaneous, but the effects of the reaction become manifest only well after the reaction has been triggered, especially in eukaryotes.

At the same time, empirical studies have shown that in the zebrafish gene expression network responsible for the production of Hes1 proteins the numbers of proteins and the associated coding mRNA sequences undergo an oscillatory evolution in time [146].

When the delayed deterministic equation predicts oscillations, generally their amplitude decays with time. As before, indefinitely lasting cycles are only captured by models for a fine-tuned choice of the parameters [142]–[144]. Even small deviations from the tuned values would dramatically alter the outcome of the predicted dynamics, leading to quickly vanishing oscillations. Biologically, this does not make sense, unless one accepts that natural evolution has selected such a peculiar set of parameters in the whole parameter space. Instead, it would seem more reasonable to search for the existence of an underlying more general physical mechanism that does not depend so crucially on the system intrinsic parameters, making the cyclic behavior robust against perturbations and noisy disturbances in the system setting, which strongly affect biochemical reactions inside cells.

Of course, in such biological processes stochasticity again is at play. Therefore, it is indeed appealing to investigate whether cycles in delayed and noisy systems can still be explained within the theoretical framework provided by stochastic amplification. Additionally, one might study if and how the delay modifies the main features of such phenomenon.

1.3 Thesis plan

We presented three behaviors emerging from the complex nature of ecological and biological systems. Aim of this Thesis is to investigate each of these with the broad framework of complex systems. By properly accounting for the spatial or temporal correlations among the systems' degrees of freedom, we will study the three topics introduced above to obtain new insights on their features and the possible mechanisms originating them.

In Chapter 2 we will deal with the problem of species coexistence. In particular, we will extent the consumer-resource framework to account for spatial terms, thus modeling other ecological mechanisms, apart from the indirect competition for nutrients consumption. We will achieve this by employing an effective description of such contributions after having performed a coarse-graining procedure on the starting spatial degrees of freedom, resulting in the addition in the mean-field dynamics of a new term with respect to the state-of-art model. We will argue that this modification can arise also from the incorporation within a consumer-resource model of other relevant ecological mechanisms, such as the noxious effect caused by host-specific pathogens. Then we will show that this modified setting is able to violate the CEP. On top of that, we will also be able to obtain analytical conditions on the model parameters with which we can predict if and which species would face extinction and be outcompeted by the surviving ones. With the same rationale, we will argue how it is possible to predict if an invading species could successfully colonize an environment and how this would affect the previous pool of coexisting species. Lastly, we will be able to get

quantitative predictions on important ecological patterns, such as the species abundance distribution describing how the species population sizes are distributed, which we will compare with empirical datasets.

At this point, we will study pattern-forming dynamics in Chapter 3. There we will be interested in searching for universal properties of patterns due to their wide-spread diffusion in complex systems dynamics. We already acknowledged that spatially regular structures emerge from homogeneous states if they are linearly unstable under small perturbations, either the nonlinear interactions terms are local or nonlocal. This can be seen as a first universal aspect shared by pattern-forming systems. Beside this, we will show that, in an appropriate system regime, also the evolution of patterns on long temporal and large spatial scales is ruled by a model-independent dynamics. After having discussed the necessary conditions required to develop our theory, we will provide a mathematical framework capable of obtaining such evolution equation. In particular, due to what we said about the role of nonlinearity in ecological applications, we will start from a general nonlinear and nonlocal model. Thanks to this generic starting point, we will be able to conclude that the result we find is universal. We will see that by universal we mean that the shape of this equation does not depend on the underlying system dynamics, as its details enter only through the specific form of the equation coefficients. In order to check the validity of the mathematical framework, we will perform some tests comparing the theoretical predictions with the patterns coming from numerical integration of a model dynamics.

Later, we will move our attention on the emergence of temporal cycles in noisy and delayed dynamics. In fact, in Chapter 4 we provide a simple setting, in the form of a Langevin dynamics, that naturally accounts for temporal delays effects and stochastic contribution. We will see that noise-induced cycles might emerge and we will demonstrate how this can be explained in term of stochastic amplification phenomenon. Moreover, we will argue how the addition of delay to the original formulation of the phenomenon leads to new features that can not be seen otherwise. For sure, the most remarkable one is the possibility to observe stochastic amplification in one-dimensional systems. Moving on, we will show analytically that the presence of asymptotic damped oscillation does not imply that, as soon as noise is taken into account, that the resonance leading to non-trivial peaks in the power-spectra necessarily occur. On the contrary, we will identify a region of the parameter space where the deterministic dynamics approach the stationary state via damped oscillations, however the stochastic description does not predict stochastic amplification and hence no cycles are observed. Going even further, surprisingly we will find scenarios in which the power-spectra of the fluctuations display non-trivial peaks even if in the asymptotic deterministic limit the dynamics reaches stationarity through an exponential decay. Finally, we will employ the framework unifying delays effects and noisy contributions to study a gene expression network. In this way we will argue how the empirical observations can be understood in terms of noise-induced cycles predicted by the resonance phenomenon of noise with the deterministic oscillations.

Chapter 2

Effective Resource-Competition Model for Species Coexistence

Chapter abstract: Local coexistence of species in large ecosystems is traditionally explained within the broad framework of niche theory, whose rationale however hardly justifies the rich biodiversity observed in nearly homogeneous environments. Here, we consider a consumer-resource model in which effective spatial effects, induced by a coarse-graining procedure, exhibit stabilization of species competition. We find that such interactions are crucial to maintain biodiversity. Herein, we provide conditions for several species to live in an environment with very few resources. In fact, the model displays two different phases depending on whether the number of surviving species is larger or smaller than the number of resources. We obtain conditions whereby a species can successfully colonize a pool of coexisting species. Finally, we analytically compute the distribution of the population sizes of coexisting species. Numerical simulations as well as empirical distributions of population sizes support our analytical findings.

2.1 Introduction

Herein, we deal with the long-standing puzzle of species coexistence. Our aim is to provide a theoretical framework, based on both ecological and physical arguments, that accounts for the most fundamental mechanisms at play in ecological competitive communities and that yet is capable of replicating the astonishing biodiversity empirically observed in many real-world ecosystems.

As mentioned in Section 1.2.1, our planet hosts an enormous number of species [35], which thrive within a variety of environmental conditions. The coexistence of this enormous biological diversity is traditionally explained in terms of local adaptation [148], [149], environmental heterogeneity [150], [151], species' abilities to aptly respond to the distribution of resources [152], [153], and other abiotic factors which broadly define a niche [154]. When species are geographically separated, they may survive because they match

a specific environmental condition and inter-specific competition is not detrimental.

However, several microbial or plankton species seem to coexist despite they occupy very similar niches in close-by regions [51]–[54], leaving the scientific community puzzled attempting to search for explanations able to dissolve this paradox. Now, on timescales that are larger than one generation but smaller than speciation timescales, the fittest species should outcompete all the others. Then, why do we still observe coexistence?

Consistent with this rationale, in Section 1.2.1 we showed how the theoretical work of MacArthur's consumer-resource model [62], [63] leads inevitably to observe the CEP: the number of coexisting species competing for the same resources is bounded by the number of resources themselves [155]–[161]. Despite numerous attempts [162]–[165], no definitive answer has yet been achieved for explaining such stark contrast between the predictions of CEP and species' coexistence.

In the scientific literature the role of space and how it might affect ecological interactions is at the center of a vivid debate. In fact it has been argued that spatial effects might promote the coexistence of species [166]–[169]. Nevertheless, spatial effect have been neglected so far, both in the classical formulation of the consumer-resource model and in its modified versions mentioned early on.

For these reasons, in this Chapter we propose a generalization of the aforementioned MacArthur's consumer-resource model capable of accounting for spatial effects in an ecological community made up by different species of consumers competing for the same resources. The key feature of this new framework is the emergence, from the inclusion of the spatial contributions, of new terms which stabilize species interactions and affect the dynamics on top of the traditional inter-species couplings, which account for the indirect resource consumption. Indeed, by coarse-graining the spatial degrees of freedom, we show that a density-dependent inhibition term forms and stabilizes the dynamics. Thus, these stabilizing factors emerge naturally in all ecosystems when spatial effects are not negligible.

More generally, such a term is not solely due to spatial contributions, but it might emerge whenever other mechanisms preventing overcrowding are crucially involved in the ecosystems dynamics. For the sake of concreteness, in tree communities, this term may model the *Janzen-Connell effect* (JCE) [170]–[172], that describes the inhospitability for the seedlings in the proximity of parent trees due to host-specific pathogens. This leads to a penalization of their growth and inhibits the local crowding of individuals belonging to the same species [173]–[175]. Apart from this, the new density-dependent inhibition term could be thought to capture crowding effects of species competing for resources in limited areas or species-induced modification of the environment for a competitive advantage. Clear examples are provided by microbial colonies, where certain strains produce toxins dangerous for the others or even themselves [176]–[180].

The rest of the Chapter is organized as follows. In Section 2.2 we introduce the generalized consumer-resource model including spatial terms from

which, after having performed a coarse-graining procedure of some spatial degrees of freedom, we get the effective model, as discussed in Section 2.3, used in the following investigation. We then show in Section 2.4 that this new formulation explains why a large number of species can coexist even in the presence of a limited number of resources. In particular we provide clear numerical examples and analytical criteria from which we can conclude that CEP can be openly violated. After this, in Section 2.5 we predict how many species will survive depending on the amount of resource present in the habitat and we also provide the conditions under which an invading species outcompetes a pool of coexisting species. Finally, we analytically obtain the species abundance distribution (SAD), i.e., the probability distribution of the population sizes of the species in Section 2.6, where we also show that it justifies the empirical SAD calculated from the plankton data presented in [181]. Finally, we conclude the discussion in Section 2.7 The full analytical derivations and the details of the numerical studies are presented in Appendix A. In particular, Appendices A.1 and A.2 contain the calculations showing how the new stabilizing inter-specific interaction term can emerge both from the spatial coarse-graining or by incorporating a host-pathogen mechanism, such as JCE, in a consumer-resource framework, respectively. We also provide in Appendix A.3 the details under some model conditions used to perform numerical simulations when we consider multiple different resources. We then discuss how to compute the SAD curve in the case of a large number of resources in Appendix A.4, whereas in Appendix A.5 we search for the same pattern when the dynamics present some extinctions. In the end, the behavior of the SAD tail, described by a power-law decay of which we can predict the range of values for the exponent, is studied in Appendix A.6.

2.2 Spatially extended model

Herein, we consider an ecological community composed by M different species competing for R resources. To do so, we start from MacArthur's consumer-resource model Eqs. (1.14a)-(1.14b), which we already described in Section 1.2.1. Motivated by what we said in the previous section about the potential key role played by spatial effects in promoting the biodiversity, we extend such classical framework to account for spatial degrees of freedom. Hence, we promote both the population densities n_σ and the resource concentrations c_i to depend on time (which in the following we do not make it explicit) and space. In this way we write a dynamics of the form

$$\dot{n}_\sigma(\vec{x}) = n_\sigma(\vec{x}) \left[\sum_{i=1}^{R} \alpha_{\sigma i} r_i \left(c_i(\vec{x}) \right) - \beta_\sigma \right] - \vec{\nabla} \cdot \vec{J}_\sigma(\vec{x}), \tag{2.1a}$$

$$\dot{c}_i(\vec{x}) = \mu_i(\Lambda_i - c_i(\vec{x})) - r_i(c_i(\vec{x})) \sum_{\sigma=1}^{M} n_\sigma(\vec{x}) \alpha_{\sigma i}, \tag{2.1b}$$

where for ease we do not explicit the time-dependencies, whereas $\vec{x}$ indicates the position in space, hence it indicates the spatial degrees of freedom of the

dynamical quantities and finally $\vec{J}_\sigma(\vec{x})$ is the flux describing the motion in space of the individuals of species σ.

In particular, inspired by the seminal work done by Keller and Segel [182], the motion of the individuals described by the flux $\vec{J}_\sigma(\vec{x})$ can be thought as the sum of two separate contributions. The former accounts for the diffusive random motion, whereas the latter models a motion of the organisms towards areas with more abundant resource concentrations due to their ability to trace resource gradients in the environment. In ecological context such effect is called *foraging*, whereas we speak about *chemotaxis* when considering microbial communities. In Appendix A.1 more details on these are given. We can notice that in Eq. (2.1b) no diffusive contribution for the resources is considered, which is equivalent to assume that the temporal scales, on which the resources diffusion takes place, are much longer than the corresponding ones for the consumers motion. In other words, the individuals of the different species populations are assumed to be more motile than the nutrients present in the environment.

2.3 Emergence of the quadratic competitive term

Analyzing the evolution of the ecosystem from the dynamics expressed in Eqs. (2.1a)-(2.1b) might be very complicated. An alternative way to study such dynamics would be to deal with a mean-field description of the dynamics which however takes into account spatial effects in an effective way. This is achieved by properly integrating the spatial degrees of freedom. Such procedure is called *spatial coarse-graining* and it is often employed in Physics, especially in Field Theory [183], [184].

Therefore, if we perform the spatial coarse-graining procedure on Eqs. (2.1a)-(2.1b) (the detailed steps and calculations are presented in Appendix A.1), we eventually end up with the following effective consumer-resource model:

$$\dot{n}_\sigma = n_\sigma \left[\sum_{i=1}^{R} \alpha_{\sigma i} r_i(c_i) - \beta_\sigma - \sum_{\rho=1}^{M} \epsilon_{\sigma\rho} n_\rho \right], \tag{2.2a}$$

$$\dot{c}_i = \mu_i(\Lambda_i - c_i) - r_i(c_i) \sum_{\sigma=1}^{M} n_\sigma \alpha_{\sigma i}, \tag{2.2b}$$

where now the spatial dependencies are washed away and the term $\epsilon_{\sigma\rho} n_\sigma n_\rho$ in Eq. (2.2a), emerged from the spatial coarse-graining, represents the competitive interaction of species ρ with species σ (notice the minus sign).

The emergence of this new quadratic term in the effective theory can be intuitively explained using the following argument: individuals head preferentially towards areas of high resource concentration due to the foraging strategy, but this also attracts other individuals of other species, leading in the coarse-grained model to this additional competition term. Moreover, $\epsilon_{\sigma\sigma}^{-1}$, coming from the self-inhibiting term $\epsilon_{\sigma\sigma} n_\sigma^2$ that quantifies the strength of interactions among the individuals of the same species, may be regarded as the carrying capacity for species σ.

Of course, the proposed coarse-graining approach is meaningful only when applied to those systems whose spatial extension results to be larger that the typical spatial scales characterizing the consumers motions. However, as we mentioned in the Introduction, the coarse-graining procedure is not the only mechanism leading to the emergence of the quadratic competitive term. Interestingly, the inhibition term in Eq. (2.2a) can also arise when studying ecosystems where the consumers evolution is also affected by the presence of pathogens. In the case of tree communities, for example, such a novel term can be thought to model effectively JCE. In Appendix A.2 we present a mathematical argument in favor of this statement.

We remark that in Eq. (2.2b), the quantity $\mu_i \Lambda_i$ is the rate of supplying *abiotic* resources. The modeling of biotic resources scenario is achieved by substituting μ_i with $\mu_i c_i$. In what follows, for simplicity, we report the results for the case of abiotic resources with degradation rates of all resources to be the same, i.e, $\mu_i = \mu$ because it is analytically treatable. The cases dealing with biotic resources and/or heterogeneous degradation rates μ_i do not display qualitative differences.

2.4 CEP violation

Given the dynamics Eqs. (2.2a)-(2.2b), we are ready to start exploring the model predictions. The first and maybe the most remarkable one consists in the possibility to overcome CEP, which instead was inevitably pictured by the classical formulation of the consumer-resource model independently of the choice of the model parameters, as we showed in Section 1.2.1. In fact, as we are going to see first numerically and then analytically, the framework with the modification due to the coarse-graining procedure is able to sustain a large number of different coexisting species even if the pool of nutrients is made up by a small number of different resources.

So let us start with some numerical exploration of the stationary values of the model dynamics Eqs. (2.2a)-(2.2b). In Figure 2.1 we plot the fraction of survived species out of the initial $M = 200$ as a function of the (rescaled) resource supply Λ in the presence of one resource, i.e., $R = 1$ after having let the dynamics Eqs. (2.2a)-(2.2b) evolve till the stationarity. At this point we can count the number of species which have survived, i.e., those that have a non-vanishing stationary population size. Here we vary the ratio, $a = \epsilon_{\sigma\rho}/\epsilon_{\sigma\sigma}$, of inter- to intra-species interaction. The different markers refers to different choices for the value of the ratio. In concrete, when choosing the parameters we decided to draw them from some probability distributions. Therefore, if the distribution of $\epsilon_{\sigma\sigma}$ is $P_{\text{diag}}(\epsilon)$, then the distribution of $\epsilon_{\sigma\rho}$ (with $\sigma \neq \rho$) is taken as $P_{\text{off-diag}}(\epsilon) = a^{-1} P_{\text{diag}}(\epsilon/a)$.

First we notice that when the ratio a increases, the fraction of survived species decreases. However from such preliminary numerical investigations, we can immediately see how CEP is violated: since we are considering $R = 1$, if CEP holds, we would expect only one species at stationarity. Instead we find higher values for the fraction of the surviving species. Interestingly,

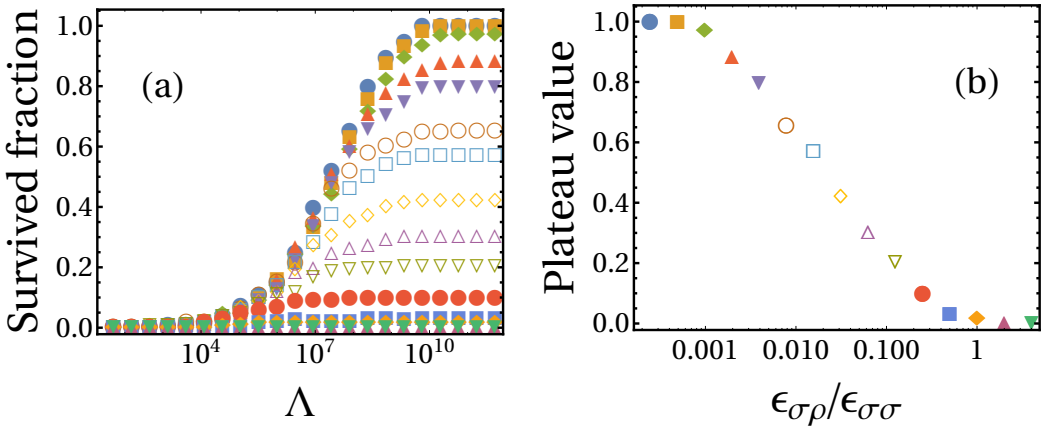

FIGURE 2.1: Panel (a): We numerically evolve dynamics (2.2a)-(2.2b) up stationarity and compute the fraction of survived species as a function of Λ. The ratio of inter- to intra-species interaction, i.e., $\epsilon_{\sigma\rho}/\epsilon_{\sigma\sigma}$, is increased by a power of 2 as we go from the top saturating curve ($\epsilon_{\sigma\rho}/\epsilon_{\sigma\sigma} = 2^{-12}$) to the bottom one ($\epsilon_{\sigma\rho}/\epsilon_{\sigma\sigma} = 2^{2}$). Here we take the initial number of species $M = 200$ and $R = 1$. The parameters $\epsilon_{\sigma\sigma}$ are sampled from a uniform distribution whose support is on the positive real axis, in the case of this numerical study $\epsilon_{\sigma\sigma} \sim \mathcal{U}(0.0001, 0.0005)$, whereas the parameters $\epsilon_{\sigma\rho}$ with $\sigma \neq \rho$ instead are sampled from the rescaled uniform distribution, where the current value of the ratio $\epsilon_{\sigma\rho}/\epsilon_{\sigma\sigma}$ is the scaling factor. Hence, also the support of the uniform distribution, from which $\epsilon_{\sigma\rho}$ with $\sigma \neq \rho$ are sampled, is on the positive real numbers, i.e, $\epsilon_{\sigma\rho} > 0$ The other parameters are $\mu = 0.001$, $k = 5$, $\beta_\sigma = 1\ \forall\sigma$ and the metabolic strategies are also drawn from an uniform distribution, i.e., $\alpha_\sigma \sim \mathcal{U}[5, 50]$. Panel (b): Plot for the saturation values, i.e., corresponding to $\Lambda = 10^{12}$, of the curves displayed in panel(a) (with same color coding) as a function of the ratio $\epsilon_{\sigma\rho}/\epsilon_{\sigma\sigma}$.

all initial species survive when the inter-species interactions are relatively weaker, and an increasing number of species coexists competing for one resource when the resource supply Λ is correspondingly larger. This is manifestly shown in Figure 2.2, which refers to the limiting case $\epsilon_{\sigma\rho} \to 0$ for $(\sigma \neq \rho)$. It turns out that such limit is analytically tractable and, therefore, we will focus on this case in the following to find explicit conditions on the model parameters to ensure species coexistence and CEP violation.

As the time progresses, we expect this system to reach a stationary state. If all species have survived (later we will discuss the case when a sub-set of them go extinct) at a large time $(n^*_\sigma > 0\ \forall\ \sigma)$, then the following equations in the matrix form can be obtained by setting the left-hand side of Eqs. (2.2a)-(2.2b) equal to zero:

$$\vec{\mathcal{N}} = E^{-1}(QG\,\vec{\mathcal{U}} - \vec{\mathcal{B}}), \tag{2.3a}$$

$$\mu(\vec{L} - \vec{\chi}) = GQ^T\vec{\mathcal{N}}, \tag{2.3b}$$

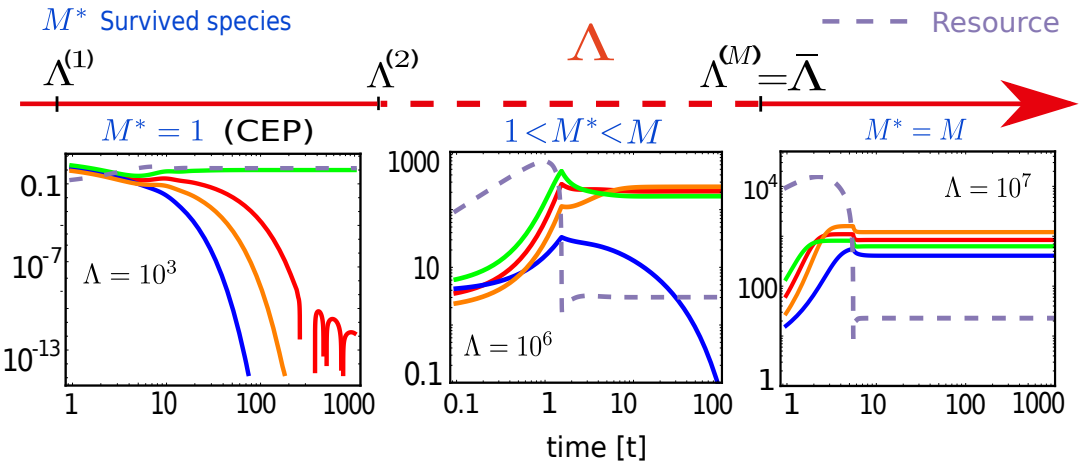

FIGURE 2.2: Coexistence of species competing for 1 resource. Horizontal arrow indicates a schematic for Λ such that l number of species coexist if $\Lambda^{(l)} < \Lambda < \Lambda^{(l+1)}$ with $\Lambda^{(M+1)} = \infty$. We verify these results by numerically evolving dynamics Eqs. (2.2a)-(2.2b) for 4 species ($M = 4$, solid lines) competing for one resource ($R = 1$, dashed line). Clearly, for $\Lambda < \bar{\Lambda}$, the number of survived species M^* is smaller than M. The other parameters are chosen to be $k = 5$, $\beta_\sigma = 1\ \forall\sigma$, $\mu = 0.001$, $\{\alpha_\sigma\}_{\sigma=1,\cdots,4} = (4.3, 2.5, 3.8, 4.7)$ and $\{\epsilon_{\sigma\sigma}\}_{\sigma=1,\cdots,4} = \{\epsilon_\sigma\}_{\sigma=1,\cdots,4} = (0.003, 0.00258, 0.00175, 0.00454)$, while $\epsilon_{\sigma\rho} = 0$ if $\sigma \neq \rho$.

where $\vec{\mathcal{N}} = (n_1^*, n_2^*, \ldots, n_M^*)^\top$ is the vector whose components are the stationary values of the population sizes, while

$$\vec{\mathcal{B}} = (\beta_1, \beta_2, \ldots, \beta_M)^\top, \tag{2.4}$$
$$\vec{L} = (\Lambda_1, \Lambda_2, \ldots, \Lambda_R)^\top, \tag{2.5}$$
$$\vec{\chi} = (c_1^*, c_2^*, \ldots, c_R^*)^\top, \tag{2.6}$$
$$E = \mathrm{diag}[\epsilon_1, \epsilon_2, \ldots, \epsilon_M], \tag{2.7}$$
$$G = \mathrm{diag}[r_1(c_1^*), r_2(c_2^*), \ldots, r_R(c_R^*)], \tag{2.8}$$
$$\vec{\mathcal{U}} = \underbrace{(1, 1, \ldots, 1)^\top}_{R \text{ components}} \tag{2.9}$$

and Q is a $M \times R$ matrix whose elements are the metabolic strategies ($[Q]_{\sigma i}$=$\alpha_{\sigma i}$). We remark that Eqs. (2.3a)-(2.3b) still hold in the case of a non-diagonal E matrix, as long as it is invertible, however it is not possible anymore to carry out analytical calculations. Substituting Eq. (2.3a) in Eq. (2.3b) gives R coupled equations:

$$GQ^T E^{-1} QG\vec{\mathcal{U}} - GQ^T E^{-1}\vec{\mathcal{B}} = \mu(\vec{L} - \vec{\chi}), \tag{2.10}$$

that can be solved for $r_i(c_i^*)$ as a function of the other parameters. Further, the condition for all species to survive, using Eq. (2.3a), is

$$(QG\,\vec{\mathcal{U}})_\sigma > \vec{\mathcal{B}}_\sigma\ \forall\,\sigma, \tag{2.11}$$

which gives the coexistence region in the R-dimensional space whose axes are $r_1(c_1^*), r_2(c_2^*), \ldots, r_R(c_R^*)$. Thus, we found a necessary condition for all initial species to coexist that is the solution of Eq. (2.10) lying within this coexistence region defined by Eq. (2.11); otherwise, some of them must go extinct.

In the following we will illuminate the above result by first showing $M = 3$ species coexisting while consuming only $R = 2$ and hence violating the CEP once the condition obtained above are fulfilled. Later, we will consider a case when several species are competing for one resource.

2.4.1 Example: coexistence of $M = 3$ species in the presence of $R = 2$ resources

Herein, we present the calculations to obtain the condition that ensures the coexistence of all initial species competing for two resources ($R = 2$). For convenience, we show the calculations for three species ($M = 3$). Nonetheless, for large number of species, one can follow the procedure given below.

As discussed in the previous section, the condition for all species to coexist is that the solutions $r_i \equiv r_i(c_i^*)$ of Eq. (2.10), which written explicitly are

$$r_1\left[\frac{\alpha_{21}\left(r_1\alpha_{21}+r_2\alpha_{22}-\beta_2\right)}{\epsilon_2}+\frac{\alpha_{31}\left(r_1\alpha_{31}+r_2\alpha_{32}-\beta_3\right)}{\epsilon_3}-\frac{\beta_1\alpha_{11}}{\epsilon_1}+\frac{\alpha_{11}\left(r_1\alpha_{11}+r_2\alpha_{12}\right)}{\epsilon_1}\right]=\mu\left(\Lambda_1-\frac{r_1k_1}{1-r_1}\right), \tag{2.12a}$$

$$r_2\left[\frac{\alpha_{22}\left(r_1\alpha_{21}+r_2\alpha_{22}-\beta_2\right)}{\epsilon_2}+\frac{\alpha_{32}\left(r_1\alpha_{31}+r_2\alpha_{32}-\beta_3\right)}{\epsilon_3}-\frac{\beta_1\alpha_{12}}{\epsilon_1}+\frac{\alpha_{12}\left(r_1\alpha_{11}+r_2\alpha_{12}\right)}{\epsilon_1}\right]=\mu\left(\Lambda_2-\frac{r_2k_2}{1-r_2}\right), \tag{2.12b}$$

should lie inside the region given by Eq. (2.11), i.e.,

$$\alpha_{11}r_1(c_1^*)+\alpha_{12}r_2(c_2^*)>\beta_1, \tag{2.13a}$$
$$\alpha_{21}r_1(c_1^*)+\alpha_{22}r_2(c_2^*)>\beta_2, \tag{2.13b}$$
$$\alpha_{31}r_1(c_1^*)+\alpha_{32}r_2(c_2^*)>\beta_3. \tag{2.13c}$$

In Eqs. (2.12a)-(2.12b) we substitute $c_i^* = \frac{r_ik_i}{1-r_i}$ as we inverte the Monod function.

To advance, numerics are required. Therefore, we first fix the model parameters as $\beta_\sigma = 1\ \forall\sigma$, $\mu = 0.001$, $k_i = 5$, $E = \mathrm{diag}(0.001, 0.002, 0.003)$ and

$$Q = \begin{pmatrix} 1.5 & 2.8 \\ 3.1 & 5.2 \\ 1.7 & 2.5 \end{pmatrix}. \tag{2.14}$$

Notice that in the following, we consider Λ as a tuning parameter.

Now using Eqs. (2.13a)-(2.13c), we show the coexistence region where all initial species survive in Figure 2.3 (a). For $\Lambda_1 = 3 \times 10^5$, we plot the equation of contour (2.12a), whereas we plot Eq. (2.12b) for two different values of Λ_2. In the first case we take $\Lambda_2 = 10^6$ and we can see that the solution of Eqs. (2.12a)-(2.12b) lies inside the shaded region. Instead in the second case we consider $\Lambda_2 = 10^5$ giving that the solution now is located outside of coexistence region. Thus, for the first case all the species coexist, as also proved by Figure 2.3 (b) where, displaying the temporal evolution of the population sizes given by the corresponding choice of the model parameters, we can see that all the three reach non-vanishing stationary values. In the second case instead two species go extinct, as shown by Figure 2.3 (c). In Figs. 2.3 (b) and (c), the solid lines indicate the evolution of species while the dashed ones are for resources.

2.4.2 Condition for the coexistence with $R = 1$

If we now consider a system with only one resource, we can obtain an explicit condition on the model parameters ensuring the survival of all M starting species. Clearly, the case of only one resource is a limit case, nevertheless it is interesting since it helps us to show our framework can picture a huge biodiversity even in presence of a reduced number of resources, openly violating CEP and thus retrieving prediction which look more similar to the empirical observations of natural systems.

Given $R = 1$, we can drop the immaterial index i. Thus, Eq. (2.3a) becomes

$$n_\sigma^* = [\alpha_\sigma r(c^*) - \beta_\sigma]/\epsilon_\sigma \quad \forall\sigma. \tag{2.15}$$

Since we need $n_\sigma^* > 0$, we find

$$r(c^*) > \beta_\sigma/\alpha_\sigma. \tag{2.16}$$

Moreover, we can write

$$r(c^*) > r(\bar{c}) \equiv \max_\sigma\{\beta_\sigma/\alpha_\sigma\}, \tag{2.17}$$

where $r(c^*)$ is the solution of Eq. (2.10):

$$Ar^2(c^*) - Br(c^*) - \mu(\Lambda - c^*) = 0, \tag{2.18}$$

in which the coefficients A and B are defined as

$$A = \sum_\sigma \alpha_\sigma^2/\epsilon_\sigma, \tag{2.19}$$

$$B = \sum_\sigma \alpha_\sigma\beta_\sigma/\epsilon_\sigma. \tag{2.20}$$

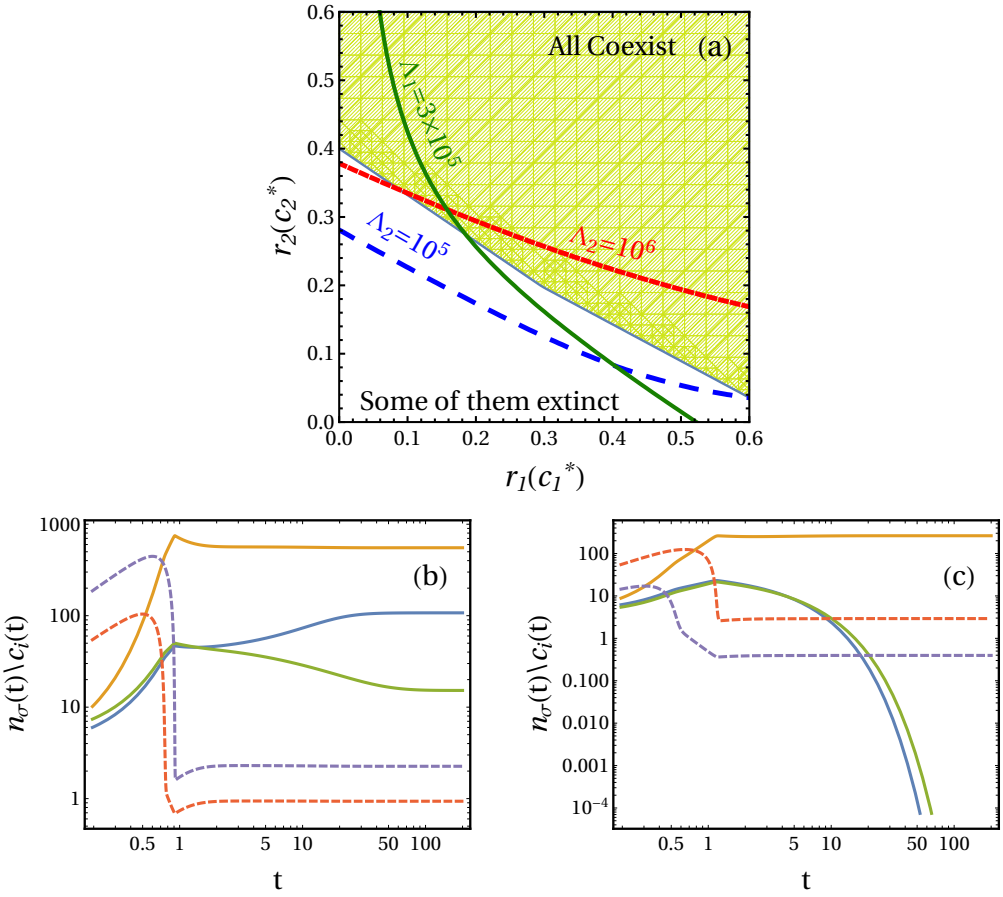

FIGURE 2.3: Coexistence of $M = 3$ species in the presence of $R = 2$ resources. Panel (a): The shaded region is obtained from Eqs. (2.13a)–(2.13c). Eq. (2.12a) is plotted for $\Lambda_1 = 3 \times 10^5$ (green curve), while Eq. (2.12b) is shown for two different Λ_2, where for $\Lambda_2 = 10^6$ (red curve) the intersection giving the solution of Eqs. (2.12a)-(2.12b) is inside the coexistence region, whereas for $\Lambda_2 = 10^5$ (blue curve), the solution is outside of shaded region. Panels (b) and (c): Numerical integration of the dynamics with two different Λ_2 as discussed for Panel (a). In all plots, the parameters are the ones presented in the text. In Panel (b) and (c), the solid lines indicate the evolution of species population sizes $n_\sigma(t)$, while the dashed ones refer to the resources concentrations $c_i(t)$.

Note that $r(c^*) \leq 1$, therefore, the metabolic strategies, in order to guarantee a coexistence of all species, should be greater than the death rates, i.e.,

$$\alpha_\sigma > \beta_\sigma \quad \forall\sigma. \tag{2.21}$$

Thus, for fixed parameters that characterize the species, i.e., $\{\alpha_\sigma, \beta_\sigma, \epsilon_\sigma\}$, coexistence of all species is achieved when tuning the resource supply rate by varying Λ at a fixed μ in such a way that the condition $r(c^*) > r(\bar{c})$ is satisfied. Such a critical value of Λ is given by

$$\bar{\Lambda} = r(\bar{c})[Ar(\bar{c}) - B]/\mu + \bar{c}. \tag{2.22}$$

In Figure 2.2, we consider an example of ecosystem having 4 species competing for 1 resource. Clearly, when $\Lambda > \bar{\Lambda}$, all initial species survive (shown by solid lines), while some of them go extinct in the contrasting case.

2.5 Extinction and invasibility conditions

As we saw, we can have that all the species survive for $\Lambda > \bar{\Lambda}$. However, if this is not true, the system will face some extinctions but still the CEP could be violated. We expect that the number of the extinct species depends on the choice of Λ once all the other parameters are fixed. In the following we will search for a condition within our theoretical framework with which we can state how many and which species go extinct when competing for a single resource when $\Lambda < \bar{\Lambda}$.

2.5.1 Threshold $\Lambda^{(l)}$ for the coexistence of $l < M$ species

For simplicity, in what follows, we consider $\beta_\sigma = 1\ \forall\sigma$. Nevertheless, the analysis can also be done along the same line for generic β_σ's. Since now each species is characterized by a set of parameters, one can define an array $\{\alpha_1, \epsilon_1; \alpha_2, \epsilon_2; \ldots; \alpha_M, \epsilon_M\}$, where species are arranged according to decreasing metabolic strategies.

Because of what we said, when $\Lambda < \bar{\Lambda}$ some extinctions will necessarily occur. For this reason the stationary state of Eqs. (2.2a)-(2.2b) can be expressed as

$$n_\sigma^* = \frac{\alpha_\sigma \tilde{r}(c^*) - 1}{\epsilon_\sigma} U(\alpha_\sigma - \tilde{\alpha}), \tag{2.23}$$

$$\tilde{r}(c^*) = \frac{\mu(\Lambda - c^*)}{\sum_\sigma n_\sigma^* \alpha_\sigma}. \tag{2.24}$$

Note that the sum in Eq. (2.24) is restricted because some n_σ-s are equal to zero (when $\alpha_\sigma < \tilde{\alpha}$) as shown in (2.23). Also the number $\tilde{\alpha}$ is yet to be obtained. In the above Eq. (2.23) $U(x)$ is the Unit-step function with $U(x \geq 0) = 1$ and 0 otherwise.

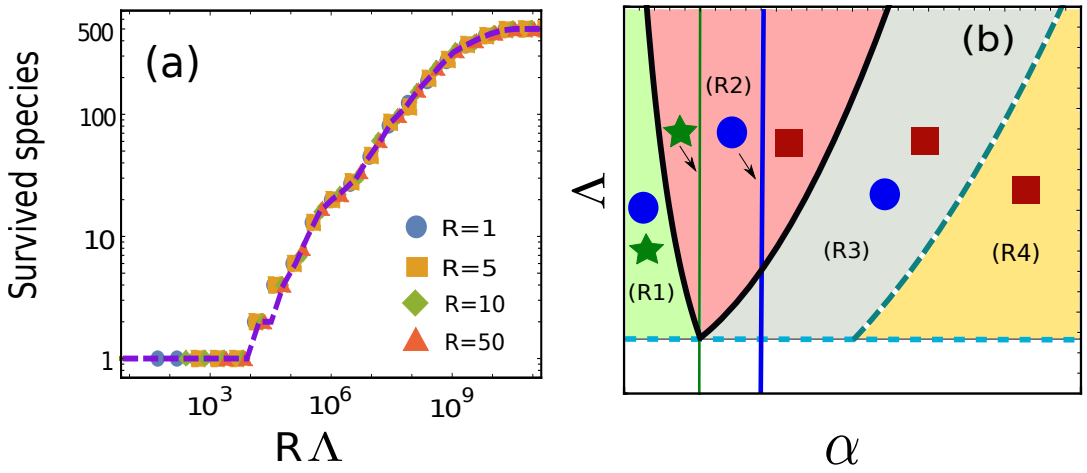

FIGURE 2.4: Survival of species with Λ. Panel (a): We compare the number of survived species obtained from numerical simulation (circles) of dynamics (2.2a)-(2.2b) for $R = 1$ with theoretical prediction (dashed curve) for initial 500 species. Moreover, we compare the simulations results of $R = 1$ with $R > 1$ (square, diamond, and triangle). Clearly, all these curves collapse to each other when one rescales Λ with R (simulation details for $R > 1$ are relegated to Appendix A.3). The model parameters are taken as follows: $\beta_\sigma = 1\ \forall\sigma$, $\mu_i = 0.001$ and $k_i = 5\ \forall i$, $\epsilon_\sigma \sim \mathcal{U}(0.0001, 0.0005)$ and $\alpha_{\sigma i} \sim \mathcal{U}(1.5, 10.0)$. Panel (b): Schematic of invasion by a third species (square) in a pool of two coexisting species (star and circle) competing for one resource. Two vertical lines correspond to metabolic strategies of two species (blue and thicker refers to the fitter one, i.e., the circle). We plot $\bar{\Lambda}_{(3)}$ given in Eq. (2.22), shown by a black solid curve [enclosing the region (R2)], that gives the critical resource supply for all of them to coexist as a function of metabolic strategy α of the invader for other fixed parameters. The dashed curve separating (R3) and (R4) corresponds to $\Lambda^{(2)}$ above which square and circle can coexist. The horizontal dashed line is the threshold $\bar{\Lambda}_{(2)}$ above which circle and star coexist in the absence of invader. Four different regions (R1)–(R4) are shown depending on the survival of species. For this Figure, the parameters are $\beta_{\text{circle}} = \beta_{\text{star}} = \beta_{\text{square}} = 1$, $\epsilon_{\text{circle}} = 0.0015$, $\epsilon_{\text{star}} = 0.0025$, $\epsilon_{\text{square}} = 0.0017$, $k = 5$ and $\mu = 0.001$.

Substituting Eq. (2.23) in Eq. (2.24), we find

$$\tilde{A}\tilde{r}^2(c^*) - \tilde{B}\tilde{r}(c^*) - \mu(\Lambda - c^*) = 0, \tag{2.25}$$

where we defined

$$\tilde{A} = \sum_{\sigma} \frac{\alpha_\sigma^2}{\epsilon_\sigma} U(\alpha_\sigma - \tilde{\alpha}), \tag{2.26}$$

$$\tilde{B} = \sum_{\sigma} \frac{\alpha_\sigma}{\epsilon_\sigma} U(\alpha_\sigma - \tilde{\alpha}). \tag{2.27}$$

With this reasoning, we can find the fraction of surviving species as

$$f_s = \frac{1}{M} \sum_{\sigma=1}^{M} U(\alpha_\sigma - \tilde{\alpha}), \tag{2.28}$$

implying the fraction of extinct ones to be $f_e = 1 - f_s$.

Now we need to find the cut-off $\tilde{\alpha}$. This depends on the value of Λ and the choice of α-s and ϵ-s. To do so, we first introduce two conditional sums $A_l^{(c)}$ and $B_l^{(c)}$:

$$A_l^{(c)} = \sum_{j=1}^{l} \frac{\alpha_j^2}{\epsilon_j}, \tag{2.29}$$

$$B_l^{(c)} = \sum_{j=1}^{l} \frac{\alpha_j}{\epsilon_j}, \tag{2.30}$$

in which $1 \leq l \leq M$.

Now if a number l of species survive starting from M, it follows from Eq. (2.23) that

$$\tilde{r}(c^*) > \alpha_l^{-1} = \tilde{r}(\bar{c}) = \max\{\alpha_\sigma^{-1} \mid 1 \leq \sigma \leq l\}. \tag{2.31}$$

In this way we find, similarly to what we did to obtain $\bar{\Lambda}$ before, the critical supply for first l species to survive to be

$$\Lambda^{(l)} = \frac{\tilde{r}(\bar{c})}{\mu}\left[A_l^{(c)}\tilde{r}(\bar{c}) - B_l^{(c)}\right] + \frac{k\tilde{r}(\bar{c})}{1 - \tilde{r}(\bar{c})}. \tag{2.32}$$

Thus, if $\Lambda^{(l)} < \Lambda < \Lambda^{(l+1)}$ then l species survive, $l = 1, 2, \ldots, M$, where we have defined $\Lambda^{(M+1)} \equiv \infty$. In Figure 2.2, we show both $\Lambda^{(1)}$ and $\Lambda^{(2)}$ (left markers) within which only the fittest species survives. We verify this result in Figure 2.2 by numerically evolving the dynamics (2.2a)-(2.2b) for 4 species competing for one resource.

In Figure 2.4 (a), we compare the theoretical prediction using $\Lambda^{(l)}$ for the number of coexisting species (dashed curve) with numerical simulations (circles) of Eqs. (2.2a) and (2.2b) for initial 500 species, and they have an excellent match. Moreover, we show the comparison for number of survived species

as R increases, where we relegate the detailed discussion of such cases in Appendix A.3. Interestingly, we find that the simulation data for $R > 1$ collapse on the theoretical prediction for $R = 1$ when the resource supply is scaled with the number of resources. This is because for the same number of species to coexist a smaller resource supply for each resource is required, as expected.

2.5.2 Outcome of an ecosystem invasion by an external species

The conditions found ensuring the survival of all the initial species or a fraction of those can be employed also to answer another question, which has a great interest from an ecological standpoint.

In fact, let us consider a pool of coexisting species and let us assume a new species enters the community. One could wonder if the invading species will ever be able to colonize successfully the environment and/or coexist with the other species and, when the answer is affirmative, under which conditions on the model parameters this could happen.

To answer this question, for convenience, we consider a system of two coexisting species consuming one resource. The coexistence is crucially determined, once all the other parameters are fixed, by the value of Λ with respect to the different thresholds identified in the previous discussions. In particular, to grant the coexistence of these first two species in absence of the invader, we need the value of Λ to be greater than the critical value $\bar{\Lambda}_{(2)}$ for the system composed by the initial two species, as we discussed before (the subscript is introduced to make clear that we are referring to the system with the first two species).

Let us assume that now a third one arrives. In Figure 2.4 (b) we show a schematic of the experiment. Here, on the axes we have the metabolic strategy α of the invading species and the rescaled supply rate of the resource Λ, while all the other model parameters are supposed to be fixed. In the scheme, the first two species are indicated by a circle and a star, whereas the square is used for the invader. Additionally, the horizontal dashed lines represents the value $\bar{\Lambda}_{(2)}$, while the green and blue vertical lines correspond to the values of the metabolic strategy of species star and circle. Finally, the black solid line shows the critical value $\bar{\Lambda}_{(3)}$ (the subscript now refers to the system in which we are considering the three species together) as a function of α. Hence for a fixed value of the metabolic strategy of the invader, α, the survival of all three species depends whether the considered Λ is above or below the point of the black curve corresponding to α.

Four different regimes, that we will call (R1)–(R4), can be identified in Figure 2.4 (b), depending on the different possible survival scenarios. Let us start analyzing them. For a given Λ above the horizontal dashed line $\bar{\Lambda}_{(2)}$, only species star and circle could survive in region (R1). In fact, in such region Λ is lower than the black solid curve and the invader has a weaker metabolic strategy with respect to initial two species, hence it will be outcompeted when facing them. In (R2) Λ is higher than the black curve and therefore we can see coexistence of all the three. In (R3) $\Lambda^{(2)} < \Lambda < \bar{\Lambda}_{(3)}$,

where we recall that $\Lambda^{(2)}$ is the critical values above which the two fittest species out of the three (the initial two plus the invader) can coexist. Such value, which depends indeed on α, is represented by the blue dashed curve at the boundary of (R3) and (R4). Hence the less fit species, which is species star, is outcompeted by the invader and the second initial one. Finally, in (R4) the invader is so much fit, i.e., its metabolic strategy is so high. Therefore, not only it can successfully colonize the system, but it also leads the previous coexisting two to extinction. This because in such region $\Lambda^{(1)} < \Lambda < \Lambda^{(2)}$, ensuring the survival only of the fittest.

In Figure 2.5 we show explicitly the outcomes of the model dynamics in the four different regimes we identified. In the end, we stress that it is not mandatory for the initial two species (circle and star) to reach a stationary state and then for the invader to arrive. Even if the system of these two species does not reach stationary state and the invader participates in the competition, the results do not change.

2.6 SAD pattern and comparison with data

In addition to the prediction of the critical values for Λ ensuring the coexistence of a certain number $l \leq M$ of species and the related invasibility problem, our framework also allows us to determine the species abundance distribution (SAD), an important ecological pattern which tells how many different species have a certain population size. If such distribution is normalized to one, it can be regarded as the probability density function $P(z)$ of observing a given population size z.

Such distribution $P(z)$ can be easily computed numerically for any number R of resource. However, in the case of one resource we can obtain the exact $P(z)$. Another case that is analytically treatable is the case of large number of resources R, as shown in Appendix A.4.

2.6.1 Calculations for the SAD pattern

Let us start from the case in which all initial M species survive. Herein, from Eq. (2.3a) we have

$$n_\sigma^* = \frac{\alpha_\sigma r(c^*) - \beta_\sigma}{\epsilon_\sigma}, \tag{2.33}$$

where we remember that $r(c^*)$ is the solution of Eq. (2.18), once all the parameters have been fixed. In what follows, for simplicity, we fix $\beta_\sigma = 1$.

Now, for a large number of species, one can think the parameters α_σ and ϵ_σ as random variables to incorporate the species variability and their differences. The stochasticity of these variables hinges on the way these are distributed among species. Since α-s and ϵ-s are distributed, this means that also n-s are distributed randomly. Our aim is to obtain the distribution describing the stationary population sizes, once the distributions of α-s and ϵ-s are known.

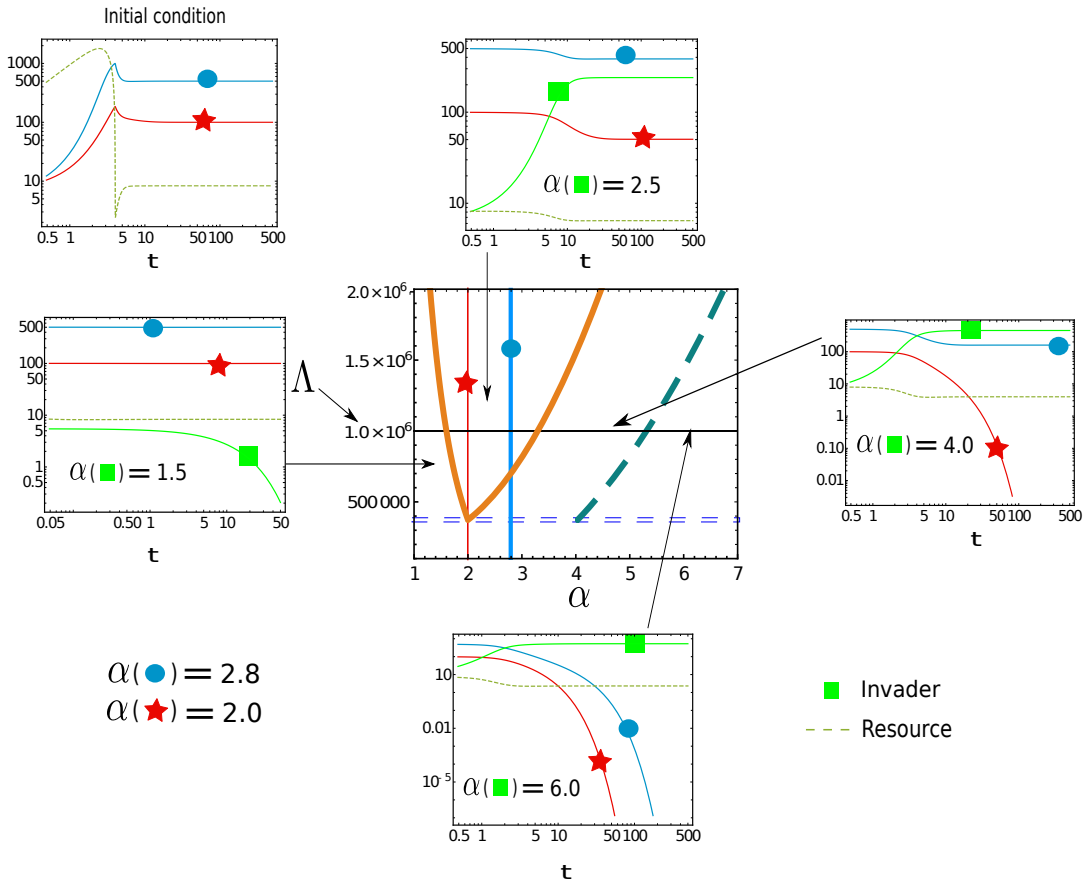

FIGURE 2.5: Discussion on Figure 2.4 (b). We begin (see top left corner) with two species (star and circle) at a given Λ (solid horizontal black line in the central panel) greater than the dashed line (critical value for both these species to survive in absence of the invader). Once the system reaches steady state, an invader arrives (shown by square) and, depending on its metabolic strategies, four possibilities can be seen. These are displayed in the central figure, similarly to Figure 2.4 (b). In the central panel, the solid orange curve indicates critical resource supply $\bar{\Lambda}$ for all three species to survive and dashed green curve (right side) is the critical resource supply $\bar{\Lambda}$ for invader and circle to survive. The parameters are taken as in Figure 2.4 (b) with $\Lambda = 10^6$. The metabolic strategies are displayed in the Figure. The top, bottom, left and right panels refer to the outcome of the system evolution in the four regimes, depending on the metabolic strategy of the invader, whose value is shown in each panel.

In other words, α and ϵ are random variables and, once a concrete ecosystem is considered, the sets $\{\alpha_\sigma\}_{\sigma=1,\cdots,M}$ and $\{\epsilon_\sigma\}_{\sigma=1,\cdots,M}$ are drawn from their distributions, corresponding to possible realizations of the α and ϵ random variables. Now, let us define $z = \frac{x}{y}$, where $x = \alpha r(c^*) - 1$ and $y = \epsilon$. Thus, we have $z \in \{n_1^*, n_2^*, \ldots, n_M^*\}$ and we want to find the distribution describing the histogram one could construct from $\{n_1^*, n_2^*, \ldots, n_M^*\}$.

Let $Q_1(\alpha)$ and $Q_2(\epsilon)$, respectively, be the distributions for α and ϵ. At this point one can compute the distribution of $z = x/y$ in full generality as follows:

$$\begin{aligned} P(z) &= \int dx \int dy\, Q_1(x)Q_2(y)\, \delta\left(z - \frac{x}{y}\right) \\ &= \frac{1}{z^2} \int dx \int dy\, |x| Q_1(x)Q_2(y)\, \delta\left(y - \frac{x}{z}\right) = \qquad (2.34) \\ &= \frac{1}{z^2} f(z), \qquad (2.35) \end{aligned}$$

where $Q_1(x) = Q_1(\alpha)\left|\frac{d\alpha}{dx}\right|$. In the above equation, the integrations are performed over the supports in which the distributions $Q_1(x)$ and $Q_2(y)$ are defined.

For the sake of concreteness, we can investigate three different scenarios. In the first one we have α distributed according to a non-trivial $Q_1(\alpha)$ and $Q_2(\epsilon) = \delta(\epsilon - \hat{\epsilon})$, which describes a scenario in which the species differs one to the others only because of the metabolic strategies, whereas the carrying-capacity term is the same for all of them. In this way it is easy to see that from Eq. (2.34) we would get

$$\begin{aligned} P(z) &= Q_1(\alpha)\left|\frac{d\alpha}{dx}\right|\left|\frac{dx}{dz}\right| \\ &= \frac{\hat{\epsilon}}{r(c^*)} Q_1\left(\frac{\hat{\epsilon}z + 1}{r(c^*)}\right), \qquad (2.36) \end{aligned}$$

where $Q_1(\alpha)$ is the distribution with which the α-s are distributed.

Similarly, one could consider the case in which $Q_1(\alpha) = \delta(\alpha - \hat{\alpha})$ and ϵ distributed as a non-trivial $Q_2(\epsilon)$. Plugging these into Eq. (2.34) we have

$$\begin{aligned} P(z) &= Q_2(y)\left|\frac{dy}{dz}\right| \\ &= \frac{\hat{\alpha}r(c^*) - 1}{z^2} Q_2\left(\frac{\hat{\alpha}r(c^*) - 1}{z}\right). \qquad (2.37) \end{aligned}$$

The final and most general case is obtained when both are non-trivial random variables. Here, the distribution is found from Eq. (2.34) once both $Q_1(\alpha)$ and $Q_2(\epsilon)$ are known. To show an explicit case in which analytical predictions are possible, we restrict to consider the case when α-s and ϵ-s are distributed uniformly such that $\alpha \in (a, b)$ and $\epsilon \in (c, d)$. Therefore, it follows that x takes values in (p, q), with $p \equiv a\, r(c^*) - 1$ and $q \equiv b\, r(c^*) - 1$. We

remark that $0 < p < q$ since we assumed all the species survive. Of course, y takes values in the interval (c, d).

Therefore, plugging all of this in Eq. (2.34) we find

$$P(z) = \frac{1}{(q-p)(d-c)z^2} \int_p^q dx|x| \overbrace{[\Theta(x-p) - \Theta(x-q)]}^{=1 \text{ since } 0<p<q} [\Theta(x/z - c) - \Theta(x/z - d)]$$
$$= \frac{1}{(q-p)(d-c)z^2} \int_p^q dx\, x\, [\Theta(x/z - c) - \Theta(x/z - d)]\,, \tag{2.38}$$

where $\Theta(\cdot)$ is the Heaviside theta function.

Now we change integration variable, replacing x/z with t. In this way we get

$$P(z) = \frac{1}{(q-p)(d-c)} \int_{p/z}^{q/z} dt\, t[\Theta(t-c) - \Theta(t-d)]$$
$$= \frac{1}{(q-p)(d-c)} \big[I_1(c,z) - I_1(d,z)\big]. \tag{2.39}$$

Finally, carrying out the integration, we end up with

$$I_1(\kappa, z) = \int_{p/z}^{q/z} dt\, t[\Theta(t-\kappa)] = \begin{cases} 0 & \kappa > q/z, \\ \dfrac{1}{2z^2}(q^2 - \kappa^2 z^2) & p/z < \kappa < q/z, \\ \dfrac{1}{2z^2}(q^2 - p^2) & \kappa < p/z < q/z, \end{cases} \tag{2.40}$$

and substituting it in Eq. (2.39), we obtain

$$P(z) = \frac{1}{2z^2(q-p)(d-c)} \big[J_1(c,z) - J_1(d,z)\big], \tag{2.41}$$

where

$$J_1(\kappa, z) = 2z^2 I_1(\kappa, z). \tag{2.42}$$

With a similar procedure, one can obtain the distribution of species' population sizes when only some of the initial ones survive. This case is presented in Appendix A.5.

In Figure 2.6, we plot the complementary cumulative distribution function (CCDF) of the population sizes of the coexisting species, defined as

$$F(z) = \int_z^\infty dy\, P(y). \tag{2.43}$$

The exact prediction from Eq. (2.34) is shown for the case of a single resource. From such Figure, we can see our theoretical predictions are confirmed by the numerical evidences, proving the validity of our derivation. Moreover,

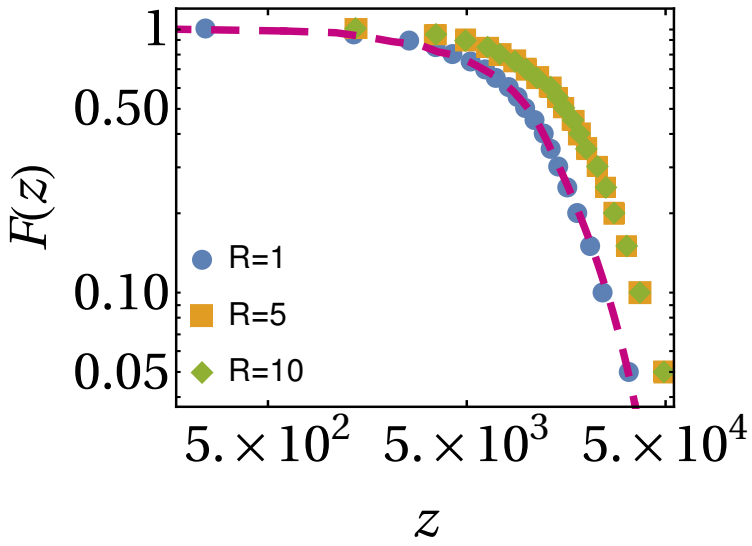

FIGURE 2.6: Complementary cumulative distribution function (CCDF), $F(z)$, is shown when all species coexist in the effective consumer-resource model. Circles are obtained by numerically integrating Eqs. (2.2a)-(2.2b) up to stationarity for $M = 500$ and one resource, where the parameters are taken as in Figure 2.4 (a), i.e., α-s and ϵ-s are uniformly distributed, with $\Lambda = 3 \times 10^{10}$. The dashed line is the analytical prediction of CCDF obtained within our framework. Since we consider uniform distributions for the species parameters, the analytical prediction of CCDF can be found from Eq. (2.41). Squares and diamonds, respectively, are the numerical CCDF curves obtained from numerical integration of the model dynamics when the number of resources is $R = 5$ or 10. All cases exhibit a similar trend.

we can see that the CCDFs obtained in the case $R > 1$ do not show qualitative differences with respect to the case of $R = 1$.

We emphasize that starting from Eq. (2.34), we predict the distribution $P(z)$ to have a power-law tail. This is mathematically shown in Appendix A.6. In particular, we find that the power-law tail z^{-2} for SAD is inevitable if $Q_2(\epsilon)$ is bounded in a neighbourhood of $\epsilon = 0$ with $Q_2(0) > 0$. In fact, by looking at Eq. (2.34), when $z \to \infty$ we have

$$f(z) \sim \overbrace{\left(\int dx\, |x| Q_1(x)\right)}^{\text{assuming it is finite}} \left(\int dy Q_2(y)\delta(y)\right) \propto Q_2(0) < \infty, \tag{2.44}$$

implying that $P(z)$ behaves like z^{-2} when z becomes larger and larger.

Finally, the population sizes distribution $P(z)$ seems to display a similar behavior when the matrix E is non-diagonal with off-diagonal entries relatively smaller with respect to the diagonal ones. Of course, in such case we do not have any theoretical prediction, Nevertheless, by letting the dynamics evolve we can find numerical estimates for this pattern. In Figure 2.7, we plot the complementary cumulative distribution function $F(z)$ as a function

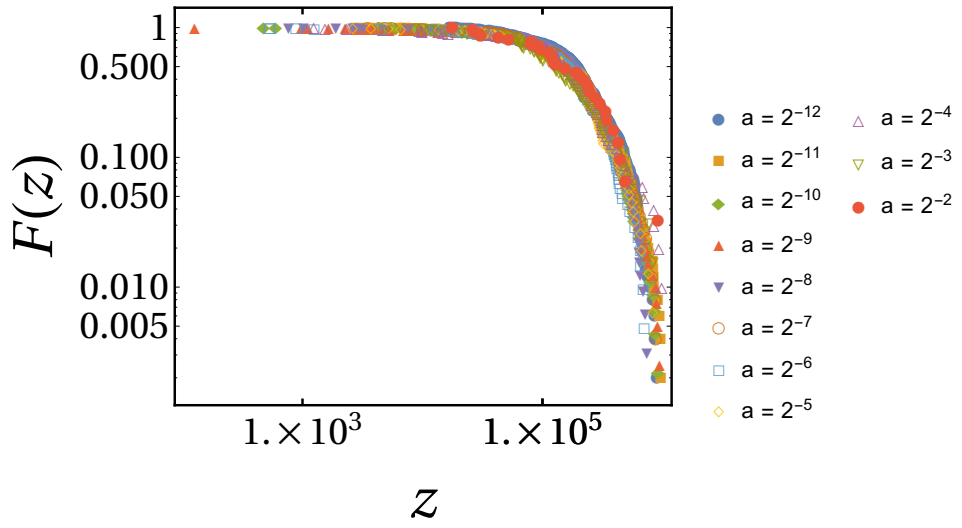

FIGURE 2.7: CCDF for the population sizes of surviving species of initial 500 species competing for one resource. The symbols are obtained from numerically integrating the model dynamics Eqs. (2.2a)-(2.2b) up to stationarity. The parameters are $\beta_\sigma = 1\ \forall\sigma$, $\mu = 0.001$, $k = 5$ and $\Lambda = 10^{12}$. The species parameters are instead drawn from the following uniform distributions: $\alpha_\sigma \sim \mathcal{U}(10, 50)$, diagonal entries $\epsilon_{\sigma\sigma} \sim \mathcal{U}(10^{-5}, 5. \times 10^{-5})$ and off-diagonal entries $\epsilon_{\sigma\rho} \sim a\ \mathcal{U}(10^{-5}, 5. \times 10^{-5})$ of E matrix, where the value of a, which is the ratio of the inter- to intra-species interaction strength, is given for each symbol in the Figure.

of the population sizes for different ratio for off-diagonal and diagonal elements of E, where the metabolic strategies $\{\alpha_\sigma\}$, the diagonal entries $\{\epsilon_{\sigma\sigma}\}$ and off-diagonal ones $\{\epsilon_{\sigma\rho}\}_{\sigma\neq\rho}$ are drawn from uniform distributions. We can see that the trend of $F(z)$ resembles closely to CCDF shown in Figure 2.6, obtained using a purely diagonal matrix E.

2.6.2 Plankton data

As mentioned above, ocean plankton communities are among the most famous and studied examples where several species coexist even in the presence of an handful of resources [54]. Recently, it has also been observed that in such communities we can observe population sizes distributions, as estimated by metagenomic studies, that decay as a steep power-law [181], [185].

Here we consider data on microplankton (20-180 μm in body size) from the Tara ocean expedition [186] (for more details, see [181], from which the data have been taken). In Figure 2.8, we compare the CCFDs obtained from the empirical SADs (color-coded points) constructed from 134 surface seawater samples distributed over all the oceans [181] (each point corresponds to one station) to the ones obtained from the stationary solution of our extended consumer-resource model (solid and dashed lines): $F(z) = \int_z^\infty P(x)dx \propto z^{-\gamma+1}$ for two "extreme" slopes $\gamma = 1.5$ and $\gamma = 1.75$. This was obtained from our model by considering a simple setting in which all species have the same α, whereas the ϵ-s follow a power-law distribution $Q_2(\epsilon) \sim \epsilon^{\gamma-2}$, for

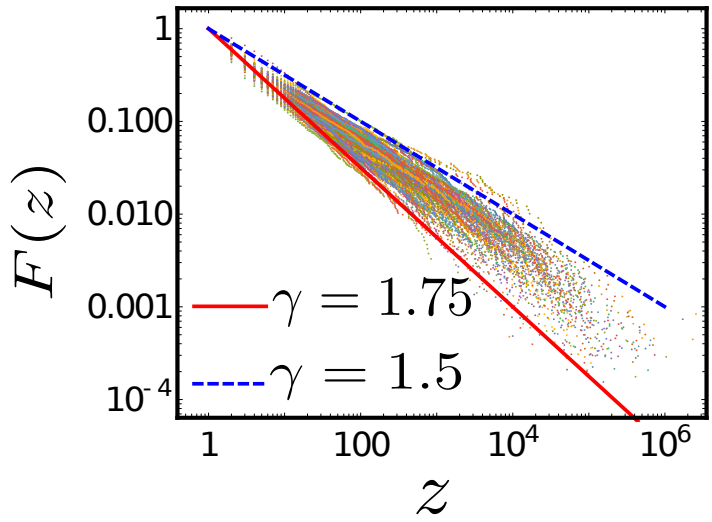

FIGURE 2.8: Empirical CCDF for 134 surface seawater samples of microplankton obtained from the Tara ocean expedition [181], [186] (each color-code indicates one station). The solid lines are the theoretical predictions of the power-law decay $F(z) \propto z^{-\gamma+1}$ with exponents between $\gamma = 1.5$ (blue dashed line) and $\gamma = 1.75$ (red solid line).

small ϵ, with $\gamma \in (1, 2]$, as we show in Appendix A.6. We point out that a range of exponents emerging from the data, i.e., $[1.5, 1.75]$, can be reproduced by an appropriate tuning of parameter γ in $Q_2(\epsilon)$.

2.7 Conclusions and future perspectives

In summary, we have extended the consumer-resource model by incorporating explicit inter- and intra-species competitive interactions term, on top of the indirect inter-specific competition for the resource consumption encoded also in the classical formulation of the model. We argued how such terms may arise from the coarse-graining of the spatial degrees of freedom and/or due to the presence of species-specific pathogens. Hence, these new terms, since are reminiscences of spatial effects, capture in an effective way the role of space and crowding effects in a mean-field dynamics.

This new version of the consumer-resource model is able to predict how several species can coexist even in the presence of relatively small number of resources, thus violating the CEP.

We were then able to obtain conditions ensuring the survival of the all species present at the beginning of the dynamics. If instead such condition is not met, we then shown how we can predict how many and which species would face extinction. Using a similar approach, we could also deal with invasibility problems and understand whether an invasion would be successful or not depending on the parameters.

Further, we obtained analytically the distribution of the population sizes for one and a large number of resources. Our results are supported by numerical simulations as well as the empirical SAD for plankton communities.

One of the first analysis we could perform to additionally check our results is indeed to consider new datasets, such as the ones obtained from experiments on microbial communities [187]. Testing our theoretical predictions, we could conclude whether they are still suited to capture such new data or not.

It could be indeed interesting to search for other predictions coming from the model dynamics to be tested against the outcomes of experimental results. For example, one could be interested in extracting the extinction rates from the model dynamics to compare them with the one measured in laboratory experiments.

Finally, another possibly interesting direction could be to study how SAD pattern might change after taking into account demographic stochasticity [188] in Eq. (2.2a). In particular, we could investigate if the inclusion of such an effect within our framework would lead to different behaviour as compared to those obtained in a neutral theory framework [189]. However, more careful and rigorous analysis, in which we need to perform statistical comparisons, would be required to make precise statements. For this reasons, this is left for further investigations.

Chapter 3

Ginzburg-Landau amplitude equation for nonlinear nonlocal models

Chapter abstract: Regular spatial structures emerge in a wide range of different dynamics characterized by local and/or nonlocal coupling terms. In several research fields this has spurred the study of many models, which can explain pattern formation. The modulations of patterns, occurring on long spatial and temporal scales, can not be captured by linear approximation analysis. Here, we start by considering a general model displaying patterns in presence of long range couplings. We then show that the spatio-temporal evolution of large scale modulations at the onset of instability is ruled by the well-known Ginzburg-Landau equation, independently of the details of the dynamics. Hence, we demonstrate the validity of such equation in the description of the behavior of a wide class of systems. We introduce a novel mathematical framework that is also able to retrieve the analytical expressions of the coefficients appearing in the Ginzburg-Landau equation as functions of the model parameters. Such a framework can also accounts for higher order nonlocal interactions, extending its applicability to even more general models with very different physical features.

3.1 Introduction

Now we move our attention on pattern forming systems. In Section 1.2.2 we presented what spatial patterns are and how they can be observed in a broad class of scenarios studied by different research fields. We also discuss the role played by the nonlinear contributions in the systems dynamics in stabilizing the perturbations on the homogeneous state and so how they are crucial in leading to the formation of such regular spatial structures. Later, we considered also patterns emerging from dynamics in which the evolution of the quantity of interest in a given position of the space is influenced and

determined by the current state of the system in all the other locations. Several examples worth to be mentioned of this latter scenario are provided by both empirical and theoretical ecology.

With all of this being said, it is of natural interest the research for possible universal mechanisms at play that determine and govern the emergence the eventual evolution of such spatial patterns. In particular, provided the homogeneous and stationary state to be unstable under small random perturbations, it would be engaging to find universal, i.e., model-independent, frameworks able to give back information on the spatial and temporal scales involved in the formation and stabilization of such ordered structures.

Indeed, the simplest method to have an insight into pattern formation is the linear stability analysis. Within this framework, we gain understanding of the modes which drive instability, and therefore, determine length and time scales that characterize the spatial structures. Typically these structures are distorted over either large length or large temporal scales, and these slow changes unfortunately cannot be determined by a simple linear analysis. However, near the onset of a supercritical instability [79] and in the weakly nonlinear regime, it is possible to deduce the evolution equation of the amplitude of the most unstable modes, which captures the basic information about those distortions and their relative scales.

Such equation known as the *Ginzburg-Landau* (GL) amplitude equation has been obtained first in simple settings like the Rayleigh-Bénard convection [191], [192] or the celebrated *Swift-Hohenberg* model [79]. In the following, those results have been extended to others models generating patterns from local dynamics [193]–[197]. However, the majority of studies taking into account nonlocal features were limited to particular cases, such as the generalizations of the aforementioned Swift-Hohenberg model [198], [199] or the paradigmatic Fisher-KPP equation [200], [201]. In these studies, the authors considered specific settings in order to derive the amplitude equation with nonlocal interaction terms. Thus, to the best of our knowledge, the validity of the amplitude equation in describing the large-scale properties of patterns emerging from a general nonlinear and nonlocal model has still not been explored. In other words, it has still to be demonstrated whether the spatio-temporal evolution of the patterns over large length or large temporal scales predicted by the GL amplitude equation can be regarded as an universal feature shared by pattern-forming systems, regardless the fact that the underlying dynamics might be local or nonlocal.

In this Chapter, we focus on this latter problem for systems with nonlinear dynamics in the presence of non-local interactions exhibiting supercritical instability [79]. Moreover, we assume that the nonlocal couplings are even functions and can be expanded in Taylor series. In this case, we first obtain the criterion for pattern formation in a general model. Then, we obtain the equation that takes the form of the GL equation using a novel mathematical approach based on the expansion of nonlocal operators in the parameter space around the onset of instability. We also show that, near the supercritical onset of instability, where stable pattern solutions emerge continuously from the homogeneous state, the amplitude equation does not depend on

the details of the specific model. In other words, we show that the amplitude equation is independent of the form of the nonlinearity and the interaction kernel as long as its Fourier transform exists. Finally, we emphasize that the GL equation depends on the model only through its coefficients. These latter are obtained analytically from the general setting we adopted in our derivation.

The rest of the Chapter is organized as follows. We first present our general setting, that will be used in the next-coming, in Section 3.2. From this in Section 3.3 we uncover the mechanism describing the emergence of patterns. Hence we obtain an explicit criterion, identifying two different phases of the system, with which we can divide the parameters space into two separated regions, depending on whether the translational invariance characterizing the general evolution equation is broken or not. Section 3.4 contains the information of the model that we use to illustrate concretely our general theoretical formalism. In Section 3.5, we introduce the main ideas underlying our mathematical formulation and we then derive the amplitude equation. We then compare the predicted evolution with numerical simulations in Section 3.6. Finally, we conclude the discussion in Section 3.7. The details of all the derivations required in Section 3.5 are relegated in Appendix B.1, Appendix B.2, and Appendix B.3. Also, we obtain some particular solutions of the amplitude equation in Appendix B.4, that are used to benchmark the theory with the amplitudes coming from numerical integration. The methods to obtains these are discussed in Appendix B.5.

3.2 Problem Setup

Herein, we investigate pattern formation in systems whose evolution is characterized by a nonlocal and nonlinear dynamics in the supercritical regime [79]. For the sake of simplicity, we study the dynamics of a real field $\phi(x,t)$, which is governed by the following equation in one spatial dimension

$$\partial_t \phi(x,t) = F_{\mathbf{q}}\left[\phi(x,t), \left(G_{\mathbf{q}} * \phi\right)(x,t)\right] + D\partial_x^2 \phi(x,t), \tag{3.1}$$

where $F_{\mathbf{q}}(\cdot,\cdot)$ is an analytic nonlinear function, $\mathbf{q}$ indicates a set of parameters and D a diffusion constant. In the above Eq. (3.1), for convenience, we write ∂_y for a partial derivative with respect to y. Notice that the nonlocal contribution to the equation comes from the convolution of the field with a smooth function $G_{\mathbf{q}}(\cdot)$, that plays the role of a kernel, defined as

$$(G_{\mathbf{q}} * \phi)(x,t) = \int_{-\infty}^{+\infty} G_{\mathbf{q}}(x-y)\, \phi(y,t)\, dy. \tag{3.2}$$

Moreover, we assume that $G_{\mathbf{q}}(\cdot)$ is even, and this function and its Fourier transform can be expanded using the Taylor series. We stress that in our formulation, we are not considering the contribution from the spatial boundaries. Therefore, we can perform the integral over the x-variable from $-\infty$ to $+\infty$. The generalization to spatial higher dimensions is straightforward,

as long as the kernel maintains the same symmetry properties, e.g., $G(\vec{\mathbf{x}}) = G(|\vec{\mathbf{x}}|)$. Further, we emphasize that Eq. (3.1) generalizes several models, including the competitive Lotka-Volterra equation [112], [202], [203] and some reaction-diffusion models [71], [204], [205].

3.3 Mechanism of the emergence of patterns

As stated in the Introduction, patterns start emerging due to the instability of the homogeneous and stationary solution $\phi_{\mathbf{q}}^{(0)}$. From Eq. (3.1) we can see that such solution satisfies

$$F_{\mathbf{q}}[\phi_{\mathbf{q}}^{(0)}, \tilde{G}_{\mathbf{q}}(k=0)\ \phi_{\mathbf{q}}^{(0)}] = 0, \tag{3.3}$$

where $\tilde{G}_{\mathbf{q}}(k) = \int_{-\infty}^{+\infty} dz\ G_{\mathbf{q}}(z)\ e^{ikz}$ is the Fourier transform of $G_{\mathbf{q}}$, and k being the wavenumber. Spatial patterns that form in the weakly nonlinear regime can be investigated in the region of instability around $\phi_{\mathbf{q}}^{(0)}$. To find such a region, we perform linear stability analysis. Therefore, we substitute

$$\phi_k(x,t) = \phi_{\mathbf{q}}^{(0)} + \delta\ e^{\lambda_{\mathbf{p}}(k)t + ikx} + c.c.$$

into Eq. (3.1), where we perturb the homogeneous solution with an harmonic perturbation of mode k. Now we assume that the spatially harmonic perturbation is uniformly small; namely, $0 < \delta \ll 1$. However, the amplitude of the perturbation will evolve in time as described by the term $e^{\lambda_{\mathbf{p}}(k)t}$. The quantity $\lambda_{\mathbf{p}}(k)$ is called the growth rate of the perturbation, since it gives the rate with which the amplitude of the harmonic perturbation of mode k evolves exponentially in time. Performing a linearization of Eq. (3.1) around $\phi_{\mathbf{q}}^{(0)}$ we can obtain, up to first order in δ, the growth rate $\lambda_{\mathbf{p}}(k)$ as a function of wave number k. Carrying out the calculations, we find that this reads

$$\lambda_{\mathbf{p}}(k) = (1, \tilde{G}_{\mathbf{q}}(k)) \cdot \nabla F_{\mathbf{q}}\big|_{\left(\phi_{\mathbf{q}}^{(0)}, \tilde{G}_{\mathbf{q}}(0)\phi_{\mathbf{q}}^{(0)}\right)} - D\,k^2, \tag{3.4}$$

where $\mathbf{p} \equiv \{\mathbf{q}, D\}$ refers to the set of all parameters of the model and

$$\nabla F_{\mathbf{q}}\big|_{(x^*,y^*)} = \left[\partial_x F_{\mathbf{q}}(x,y)|_{(x^*,y^*)}, \partial_y F_{\mathbf{q}}(x,y)|_{(x^*,y^*)}\right]^\top. \tag{3.5}$$

Since we assume that $G_{\mathbf{q}}(x)$ is an even function, $\lambda_{\mathbf{p}}(k)$ is a real function of k.

The sign of $\lambda_{\mathbf{p}}(k)$ tells us if the amplitude of the harmonic perturbation will increase or vanish in time. The former case occurs when $\lambda_{\mathbf{p}}(k) > 0$, the latter when $\lambda_{\mathbf{p}}(k) < 0$. Thus, $\phi_{\mathbf{q}}^{(0)}$ is stable if and only if all the modes will die out with the elapsing of time, i.e., $\lambda_{\mathbf{p}}(k) < 0$ for all k; otherwise, $\phi_{\mathbf{q}}^{(0)}$ is an unstable solution. Which one of these two scenarios is observed depends on

the system parameters $\mathbf{p}$. In fact, let us call $k_M(\mathbf{p})$, defined as a solution of

$$\left.\frac{\partial \lambda_{\mathbf{p}}(k)}{\partial k}\right|_{k=k_M(\mathbf{p})} = 0,$$

the point where the growth rate achieves maximum i.e., $\lambda_M(\mathbf{p}) = \lambda_{\mathbf{p}}(k_M(\mathbf{p}))$, where the subscript M refers to the maximum. Notice that both $\lambda_{\mathbf{p}}(k)$ and $k_M(\mathbf{p})$ are parameterized by system parameters $\mathbf{p}$. Thus, a sufficient condition that the parameters have to fulfill in order to observe instability and hence pattern formation is $\lambda_M(\mathbf{p}) > 0$. Therefore, in the parameter space a *critical hypersurface* $\mathcal{M}$ can be obtained by setting $\lambda_M \equiv \lambda_{\mathbf{p}_0}(k_M(\mathbf{p}_0)) = 0$ where $\mathbf{p}_0 \equiv \{\mathbf{q}_0, D_0\}$ belongs to $\mathcal{M}$, and this hypersurface distinguishes the regions depending on the stability of $\phi^{(0)}_{\mathbf{q}}$.

3.4 Example: the nonlocal Fisher-KPP equation

In order to make our formalism more transparent, we consider the Fisher equation, also known as Kolmogorov–Petrovsky–Piskunov equation and thus often called in the literature as Fisher-KPP (F-KPP) equation [204], [205], where we extend it introducing also a nonlocal contribution [206]–[208]. We refer to such equation as the nonlocal F-KPP equation. Notice that this latter is known as nonlocal Lotka-Volterra equation in the ecological literature [112]. Within this context, the model describes population dynamics characterized by the presence of nonlocal couplings, which can be interpreted as nonlocal interactions of individuals with those that are far away in space or that have different phenotypic traits.

We choose this particular model because it is amenable to analytical calculations and it exhibits pattern forming dynamics in the presence of nonlocal couplings [200], [201]. Therefore, in this example, the first term on the right-hand side of Eq. (3.1) has the following form:

$$F_{\mathbf{q}}[u, v] := u[1 - av], \tag{3.6}$$

where a is a dimensionless parameter. Explicitly, plugging Eq. (3.6) into Eq. (3.1), the nonlocal F-KPP equation used as a clarification example of the formalism reads

$$\partial_t \phi(x,t) = \phi(x,t)\left[1 - a\int_{-\infty}^{+\infty} G_{\mathbf{q}}(x-y)\,\phi(y,t)\,dy.\right] \tag{3.7}$$

Herein, we consider the functional form of the kernel as following:

$$G_{\mathbf{q}}(z) = \exp\left(-\frac{|z|}{R}\right) - b\,\exp\left(-\frac{|z|}{\beta R}\right). \tag{3.8}$$

This form has been chosen mainly because it illuminates the main steps of our calculations for the general model. In Eq. (3.8), R is the range of the interaction, β and b are dimensionless parameters such that $0 < b, \beta < 1$.

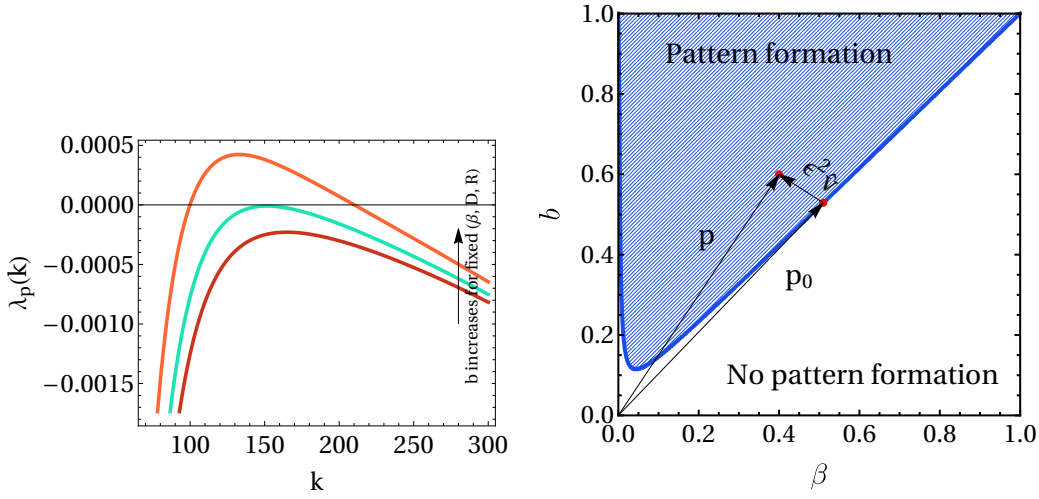

FIGURE 3.1: Left panel: The dispersion relation given in Eq. (3.11) $\lambda_{\mathbf{p}}(k)$ as a function of k for the nonlocal F-KPP equation at three different values of b. The remaining parameters for the plots are $\beta = 0.2$, $D = 10^{-8}$, and $R = 0.1$. Right panel: Phase diagram in the (β, b) space for the nonlocal F-KPP equation given in Eqs. (3.1) and (3.8) with $F_{\mathbf{q}}[u, v] := u[1 - av]$. In this case $\mathbf{p} \equiv \{\beta, b, R, a, D\}$ and the critical hyper-surface $\mathcal{M}$ does not depend on a. The phase diagram is shown for two fixed parameters $D = 10^{-8}$ and $R = 0.1$, where the solid contour $\mathcal{M}$ [defined by $\lambda_{\mathbf{p}_0}(k_M(\mathbf{p}_0)) = 0$] divides the parameter space depending on whether or not there is pattern formation. A vector $\mathbf{p} = \mathbf{p}_0 + \epsilon^2 \hat{v}$ indicates a point in the pattern forming region, where $\mathbf{p}_0$ sits on $\mathcal{M}$.

Following Section 3.2, we obtain the the homogeneous and stationary solution as

$$\phi_{\mathbf{q}}^{(0)} = [a\tilde{G}_{\mathbf{q}}(0)]^{-1}, \tag{3.9}$$

where

$$\tilde{G}_{\mathbf{q}}(k) = 2R\left(\frac{1}{1+k^2R^2} - \frac{b\beta}{1+k^2R^2\beta^2}\right). \tag{3.10}$$

Similarly, the dispersion relation using Eq. (3.4) can be obtained as

$$\lambda_{\mathbf{p}}(k) = \frac{1}{1-b\beta}\left(\frac{b\beta}{1+\beta^2k^2R^2} - \frac{1}{1+k^2R^2}\right) - D\,k^2, \tag{3.11}$$

in which $\mathbf{p} = \{b, \beta, a, R, D\}$ is the set of parameters as discussed in Section 3.2 and $\lambda_{\mathbf{p}}(k)$ does not depend on a. We plot $\lambda_{\mathbf{p}}(k)$ *vs.* k in the left panel of Figure 3.1 for three different values of b, while the other parameters are kept fixed.

In order to obtain the phase diagram that identifies the region of stability, we study the sign of maximum of $\lambda_{\mathbf{p}}(k)$ by varying the parameters $\mathbf{p}$. Specifically, the critical hypersurface, that divides the parameters space, we obtain by setting such maximum equal to zero. The analytical computation

to find this phase boundary is difficult. Nevertheless, we numerically obtain the phase diagram in the (β, b) plane for other fixed parameters, and it is shown in Figure 3.1 (right panel), where the blue shaded region indicates the region of instability of the homogeneous and stationary solution. Thus, we name that region as pattern forming region.

3.5 Amplitude equation

This section is dedicated to the derivation of the amplitude of the pattern near the contour of instability in the general case of which Figure 3.1 (right panel) is a particular case.

In order to make analytical progress, we use the Taylor series expansion of the right-hand side of Eq. (3.1) around the homogeneous and stationary solution $\phi_{\mathbf{q}}^{(0)}$, i.e., we expand the nonlinear function $F_{\mathbf{q}}(\cdot,\cdot)$ around $\left(\phi_{\mathbf{q}}^{(0)}, \tilde{G}_{\mathbf{q}}(0)\, \phi_{\mathbf{q}}^{(0)}\right)$. This allows to set up equations that hold in the weakly nonlinear regime and finally obtain the amplitude equation. We express the field as $\phi(x,t) = \phi_{\mathbf{q}}^{(0)} + \varphi(x,t)$. The evolution equation for $\varphi(x,t)$ can then be cast in the form:

$$\dot{\varphi} = \mathcal{L}_{\mathbf{p}}\varphi + \mathcal{N}_{\mathbf{q}}\varphi, \tag{3.12}$$

where the first and second term, respectively, on the right-hand side correspond to linear and nonlinear contributions in φ. In the above equation (3.12), the linear operator has the following structure

$$\begin{aligned}\mathcal{L}_{\mathbf{p}}\varphi &= \left(\varphi, G_{\mathbf{q}} * \varphi\right) \cdot \nabla F_{\mathbf{q}}\big|_{\left(\phi_{\mathbf{q}}^{(0)} \tilde{G}_{\mathbf{q}}(0) \phi_{\mathbf{q}}^{(0)}\right)} + D\partial_x^2\varphi \\ &= C_{\mathbf{q}}^{(1,0)}\varphi + C_{\mathbf{q}}^{(0,1)}\left(G_{\mathbf{q}} * \varphi\right) + D\partial_x^2\varphi,\end{aligned} \tag{3.13}$$

while the nonlinear operator is

$$\mathcal{N}_{\mathbf{q}}\varphi = \sum_{\substack{n,m=0 \\ \text{with } n+m\geq 2}}^{+\infty} C_{\mathbf{q}}^{(n,m)} \varphi^n \left(G_{\mathbf{q}} * \varphi\right)^m, \tag{3.14}$$

where $C_{\mathbf{q}}^{(n,m)}$ are the coefficients obtained from the Taylor series expansion.

We notice that Eq. (3.1) is translational invariant. Therefore, the eigenfunctions of the linear nonlocal operator $\mathcal{L}_{\mathbf{p}}$ are the simple wavefunctions e^{ikx}, and then, the eigenvalue equation reads

$$\mathcal{L}_{\mathbf{p}} e^{ikx} = \lambda_{\mathbf{p}}(k)\, e^{ikx}, \tag{3.15}$$

where the spectrum is defined in Eq. (3.4). The general solution of the linear part of Eq. (3.12), i.e., $\partial_t\varphi(x,t) = \mathcal{L}_{\mathbf{p}}\varphi$, is a linear combinations of functions

$e^{\lambda_{\mathbf{p}}(k)t+ikx}$ with k dependent coefficients. In this case, Eq. (3.4) becomes

$$\lambda_{\mathbf{p}}(k) = C_{\mathbf{q}}^{(1,0)} + C^{(0,1)}\tilde{G}_{\mathbf{q}}(k) - Dk^2. \tag{3.16}$$

To better understand the meaning of Eq. (3.12), we again consider our model discussed in Section 3.4. Herein, the linear operator acting on the perturbation field φ has the following form:

$$\mathcal{L}_{\mathbf{p}}\varphi = -[\tilde{G}_{\mathbf{q}}(0)]^{-1}(G_{\mathbf{q}} * \varphi) + D\partial_x^2\varphi, \tag{3.17}$$

and the second term on the right-hand side of Eq. (3.12) can be shown as

$$\mathcal{N}_{\mathbf{q}}\varphi = -a\ \varphi(G_{\mathbf{q}} * \varphi). \tag{3.18}$$

In what follows, unless specified, we focus on our general setting described in Eq. (3.1).

To obtain the equation that describes the evolution (whose form will be discussed later) of the patterns near the bifurcation contour, we investigate the behavior of the system close to the onset of instability, namely near the critical hyper-surface $\mathcal{M}$. Thus, we consider parameters $\mathbf{p}$ in the neighborhood of $\mathbf{p}_0 \equiv \{\mathbf{q}_0, D_0\}$, i.e.,

$$\mathbf{p} = \mathbf{p}_0 + \epsilon^2\hat{v}, \tag{3.19}$$

where $\mathbf{p}_0 \in \mathcal{M}$, $\hat{v}$ is a unit vector pointing toward the region of pattern formation, and $0 < \epsilon^2 \ll 1$. An example of such point $\mathbf{p}$ for nonlocal F-KPP equation (see Section 3.4) is indicated in the left panel of Figure 3.1.

In addition, we assume that the growth rate $\lambda_{\mathbf{p}}(k)$ exhibits a quadratic scaling in the wave-number k close to the point of maximum $k_M(\mathbf{p}) > 0$, which is satisfied if $\lambda_{\mathbf{p}}(k)$ admits continuous second derivative with respect to k.

With a set of parameters $\mathbf{p}$ that can be expressed as in Eq. (3.19) with ϵ small, we can expand the growth rate around $\mathbf{p}_0$ as

$$\lambda_{\mathbf{p}}(k) = \lambda_{\mathbf{p}_0}(k) + \epsilon^2\hat{v}\cdot\nabla_{\mathbf{p}}\lambda_{\mathbf{p}}(k)|_{\mathbf{p}=\mathbf{p}_0} + \mathcal{O}\left(\epsilon^4\right), \tag{3.20}$$

where we assume that the second term on the right-hand side is non-zero.

We know that the above function achieves the maximum at $k = k_M(\mathbf{p})$, and that $k_M(\mathbf{p})$ can also be expanded about $\mathbf{p}_0$

$$k_M(\mathbf{p}) = k_M(\mathbf{p}_0) + \epsilon^2\hat{v}\cdot\nabla_{\mathbf{p}}k_M|_{\mathbf{p}=\mathbf{p}_0} + \mathcal{O}\left(\epsilon^4\right). \tag{3.21}$$

Substituting Eq. (3.21) in Eq. (3.20) at $k = k_M(\mathbf{p})$, we get

$$\begin{aligned}\lambda_M &\equiv \lambda_{\mathbf{p}}(k_M(\mathbf{p})) \\ &= \lambda_{\mathbf{p}_0}(k_M(\mathbf{p})) + \epsilon^2 \hat{v}\cdot\nabla_{\mathbf{p}}\lambda_{\mathbf{p}}(k_M(\mathbf{p}))|_{\mathbf{p}=\mathbf{p}_0} \; + \; \mathcal{O}\left(\epsilon^4\right) \\ &= \underbrace{\lambda_{\mathbf{p}_0}(k_M(\mathbf{p}_0))}_{=0} \; + \epsilon^2 \hat{v}\cdot\nabla_{\mathbf{p}} k_M|_{\mathbf{p}=\mathbf{p}_0} \underbrace{\lambda'_{\mathbf{p}_0}(k_M(\mathbf{p}_0))}_{=0} \\ &+ \epsilon^2 \underbrace{\hat{v}\cdot\nabla_{\mathbf{p}}\lambda_{\mathbf{p}}(k_M(\mathbf{p}_0))|_{\mathbf{p}=\mathbf{p}_0}}_{\bar{\lambda}_M} + \mathcal{O}\left(\epsilon^4\right). \end{aligned} \tag{3.22}$$

Therefore, we find that the maximum scales like ϵ^2 as $\epsilon \to 0^+$, i.e.,

$$\lambda_M \to \epsilon^2 \bar{\lambda}_M \quad \text{as} \qquad \epsilon \to 0^+, \tag{3.23}$$

where we introduce the re-scaled quantity $\bar{\lambda}_M$, which is $\mathcal{O}(1)$.

Owing to this scaling property, we can introduce a temporal- and spatial-scale separation which simplifies Eq. (3.12). The long time modulations of the fast oscillations evolve on scales determined by the slower time variable $\tau = \epsilon^2 t$. A similar spatial-scale separation for the perturbation field $\varphi(x,t,\epsilon)$ occurs with a spatial scale given by the slower variable $\xi = \epsilon x$. Therefore we make the educated guess that the ϵ dependence is as follows: $\varphi(x,\xi,t) = \sum_{j\geq 1}\epsilon^j \varphi_j(x,\xi,\tau)$ where the time dependence in each mode on the right-hand side is through τ. Similarly the spatial dependence appears both through the x and the slower variable ξ [67].

Due to these separation of scales, the time derivative transforms as

$$\partial_t \to \epsilon^2 \partial_\tau, \tag{3.24}$$

while the spatial derivative encoded in the linear operator becomes

$$\partial_x \to \partial_x + \epsilon \partial_\xi. \tag{3.25}$$

As discussed above, $\varphi(x,\xi,\tau)$ can be written as a power series in ϵ, i.e.,

$$\varphi(x,\xi,\tau) = \sum_{i\geq 1} \epsilon^i \varphi_i(x,\xi,\tau), \tag{3.26}$$

From the above expression (3.26), we see that close to the bifurcation, only first terms will be dominant and that will determine the growth of the patterns.

Similar to Eqs. (3.20) and (3.21), we also expand the linear and nonlinear operators appearing in Eqs. (3.13) and (3.14):

$$\mathcal{L}_{\mathbf{p}} = \mathcal{L}_{\mathbf{p}_0} + \epsilon^2 \overbrace{\hat{v}\cdot\left(\nabla_{\mathbf{p}}\mathcal{L}_{\mathbf{p}}\right)|_{\mathbf{p}=\mathbf{p}_0}}^{\delta\mathcal{L}_{\mathbf{p}_0}} + \mathcal{O}\left(\epsilon^4\right), \tag{3.27}$$

$$\mathcal{N}_{\mathbf{q}} = \mathcal{N}_{\mathbf{q}_0} + \epsilon^2 \hat{v}\cdot\left(\nabla_{\mathbf{p}}\mathcal{N}_{\mathbf{q}}\right)|_{\mathbf{p}=\mathbf{p}_0} + \mathcal{O}\left(\epsilon^4\right). \tag{3.28}$$

Next, we proceed as follows. We first substitute Eqs. (3.24)–(3.28) into Eq. (3.12), and then we introduce the spatial scale separation in $\mathcal{L}_{\mathbf{p}_0}$ and in the nonlocal terms of $\mathcal{N}_{\mathbf{q}_0}$. The detailed procedure can be found in Appendix B.1. Finally, we arrive at

$$\epsilon^3\dot{\varphi}_1 + o\left(\epsilon^3\right) = \epsilon H_1(\mathbf{p}_0, \varphi_1) + \epsilon^2 H_2(\mathbf{p}_0, \varphi_1, \varphi_2) + \epsilon^3 H_3(\mathbf{p}_0, \varphi_1, \varphi_2), \quad (3.29)$$

where the functional forms of H_i are given in Appendix B.1, and we remind that $\mathbf{p}_0 \equiv \{\mathbf{q}_0, D_0\}$.

The above equation (3.29) is the starting point to obtain the amplitude equation. To proceed further, as a standard approach, we will compare the coefficients on the left and right-hand side of the equation at same order in ϵ. Let us first begin with the first order contribution. At the lowest order in ϵ, we find from Eq. (3.29) that

$$H_1(\mathbf{p}_0, \varphi_1) = 0. \quad (3.30)$$

Thus, from the expression of $H_1(\mathbf{p}_0, \varphi_1)$ shown in Appendix B.1 one can easily write the solution of this equation as:

$$\varphi_1(x, \xi, \tau) = A(\xi, \tau)\, e^{ik_M(\mathbf{p}_0)x} + \bar{A}(\xi, \tau)\, e^{-ik_M(\mathbf{p}_0)x}. \quad (3.31)$$

The functional form of $\varphi_1(x, \xi, \tau)$ suggests that it has harmonic oscillation with the mode characterized by $k_M(\mathbf{p}_0)$. We further notice that, the temporal dependence is only present through the amplitude of this harmonic oscillation on a slower scale defined by τ. Moreover, such amplitude may display a spatial evolution, but on the longer scale given by ξ. Near criticality, we expect that this is the relevant contribution to the pattern formation. Thus, to understand the growth of the patterns near bifurcation, we aim to obtain the equation for that amplitude.

Next, we compare the second order contribution $\mathcal{O}(\epsilon^2)$ in Eq. (3.29), and then, use the first order solution (3.31), we obtain (see Appendix B.2 for details)

$$\varphi_2(x, \xi, \tau) = \overbrace{B(\xi, \tau)e^{ik_M(\mathbf{p}_0)x} + \bar{B}(\xi, \tau)e^{-ik_M(\mathbf{p}_0)x}}^{\Lambda(x,\xi,\tau)} + \Sigma_{\mathbf{p}_0}\Bigg[\frac{A^2(\xi, \tau)e^{2ik_M(\mathbf{p}_0)x}}{\lambda_{\mathbf{p}_0}(2k_M(\mathbf{p}_0))} + 2\frac{|A|^2(\xi, \tau)}{\lambda_{\mathbf{p}_0}(0)} + \frac{\bar{A}^2(\xi, \tau)e^{-2ik_M(\mathbf{p}_0)x}}{\lambda_{\mathbf{p}_0}(2k_M(\mathbf{p}_0))}\Bigg], \quad (3.32)$$

Note that the system is at the onset of bifurcation, and we have

$$|\epsilon^2\varphi_2(x, \xi, \tau)| \ll |\epsilon\varphi_1(x, \xi, \tau)| \quad (3.33)$$

Therefore, due to the choice of the parameters, $\varphi_2(x, \xi, \tau)$ does not play any significant role in shaping the patterns. Hence, Eq. (3.31) would be sufficient to predict the patterns characterized by the amplitude $A(\xi, \tau)$.

Finally, on comparing third order contributions, as shown in Appendix B.3,

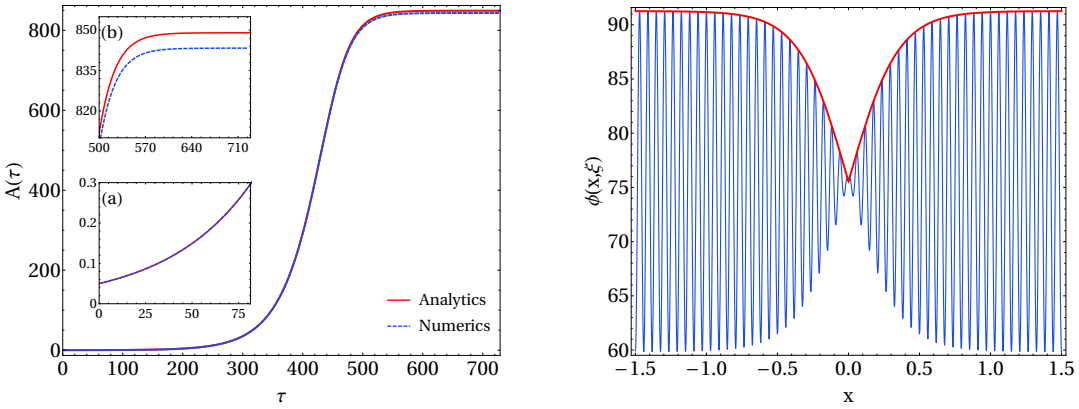

FIGURE 3.2: Left panel: Comparison between the growth in time of the amplitude predicted by Eq. (3.34) from the initial condition $A(\xi, \tau = 0) = A_0 = 0.05$ (solid red line) and the corresponding numerical evaluation (blue dashed line) from the integration of the nonlocal F-KPP equation using $\phi(x, \xi, 0) = \phi_{\mathbf{q}}^{(0)} + 2\epsilon A_0 \cos(k_M(\mathbf{p}_0)x)$ as an initial condition (see Appendix B.5). Owing to this choice, the amplitude remains space-independent at any time, displaying only temporal changes (see Appendix B.4). We refer to Appendix B.5 for the details of the parameters $\mathbf{p}$ and $\mathbf{p}_0$ used in both analytics and numerical simulation. The insets show the zoom on the initial growth (a) and the saturation observed at large time (b). We can notice a remarkable agreement between two curves at all times. Right panel: Comparison between the spatially-dependent stationary solution of Eq. (3.34), $A_{\text{st}}(\xi)$, presented in Appendix B.4 (the red solid line is the envelope curve $\phi_{\mathbf{q}}^{(0)} + 2\epsilon A_{\text{st}}(\xi)$, where $\xi = \epsilon x$) and the solution obtained from the numerical integration of the nonlocal F-KPP equation using $\phi(x, \xi, 0) = \phi_{\mathbf{q}}^{(0)} + 2\epsilon A_{\text{st}}(\xi) \cos(k_M(\mathbf{p}_0)x)$ as initial condition (see Appendix B.5). This plot is obtained at time $t = 10^2$ (time steps). The parameters $\mathbf{p}$ and $\mathbf{p}_0$ along with a discussion of this solution are included in Appendix B.5. We can appreciate how the carrier wave obtained from the numerical integration shows a remarkable agreement with the analytical solution calculated in the weakly nonlinear regime. This suggests that our framework is able to describe also the spatial modulations of the envelope of the emerging patterns.

and utilizing the solutions given in Eqs. (3.31) and (3.32), we obtain the growth equation for $A(\xi, \tau)$:

$$\frac{\partial A}{\partial \tau} = \bar{\lambda}_M A - \alpha |A|^2 A + \frac{1}{2} |\lambda''_{\mathbf{p}_0}(k_M(\mathbf{p}_0))| \frac{\partial^2 A}{\partial \xi^2}, \tag{3.34}$$

where we have dropped the dependence ξ and τ from $A(\xi, \tau)$. We stress that the above equation (3.34) is obtained by ensuring that the higher-order terms in the expansion of Eq. (3.12) are well defined. In the above equation (3.34), all coefficients on the right-hand side depend on $\mathbf{p}_0$, and the detailed expression of the constant α in terms of model details is given in Appendix B.3. Eq. (3.34) represents our main result, and interestingly, it is the celebrated GL equation for a complex field $A(\xi, \tau)$.

Since the interaction kernel $G_{\mathbf{q}}(\cdot)$ is even, the resulting amplitude equation (3.34) has real coefficients. Relaxing such constraint in the nonlocal coupling term, one may end up with a complex amplitude equation that can generate more complicated behaviors, including spatio-temporal intermittency and phase turbulence [209]. In our analysis, we have considered systems whose interaction kernel is smooth in the weakly nonlinear regime. Should the coupling be strong, those expansions were not valid [210], [211] and a different approach is necessary. We leave this study for a future investigation.

In our framework that includes the expansion of nonlocal operators in the parameters space at the onset of instability, we explicitly demonstrate that the GL equation emerges from a larger class of models, irrespective of whether systems have nonlocal interactions or not. In particular, we show that this equation is universal, namely only the three coefficients of Eq. (3.34) are affected by the specific form of the model defined by Eq. (3.1), as pointed by the derivation displayed in Appendix B.3.

For example, when Eq. (3.1) defines a nonlocal F-KPP equation, we retrieve the amplitude equation obtained in [200], in which, however, a slow spatial variable was not included. Instead, if we use the explicit forms of F and G in Eq. (3.1) as the one given in [201], we exactly end up with Eq. (3.34).

3.6 Numerical simulation

We confirm Eq. (3.34) with the numerical integration of the model discussed in Section 3.4, i.e., the nonlocal F-KPP equation, obtained inserting Eqs. (3.8) and (3.6) into Eq. (3.1). For fixed parameters $\mathbf{p}$ and $\mathbf{p}_0$, we consider two cases, which differ by the choice of the initial conditions used in the amplitude equation as well as for the evolution of the nonlocal F-KPP equation. In the first one, we take a homogeneous initial condition for the amplitude, while in the second we set the initial condition to be a particular stationary solution of Eq. (3.34). These two cases are discussed in Appendix B.4. The comparison between analytical predictions and numerical results are shown in Figs. 3.2 (left panel) and 3.2 (right panel). In both figures a remarkable agreement can be observed, suggesting the validity of our findings for temporally and spatially modulated patterns. The numerical amplitude and the

predicted envelope displayed in Figure 3.2 are obtained by taking into account only the first order term (3.31) of the perturbative expansion. In Appendix B.5 we present the results for the numerical evaluation of the amplitude when considering the next-to-leading order terms and compare with the numerical simulation, and they also have a very good agreement.

3.7 Conclusions and future perspectives

In this Chapter, we have considered a general model which can describe pattern formation in several physical systems. We have combined nonlocal coupling terms and nonlinear interactions, which may possibly include many-body terms. From this dynamics, the patterns can emerge when the homogeneous stationary solution becomes unstable. As an example, we can think of an ecological model defined on the abstract niche space, where species emerge as a trade-off between nonlocal interactions and their tendency to scour the space for better evolutionary solutions. In this case, we find regularly spaced lumps, showing a general tendency of species to coexist when they are either sufficiently similar or sufficiently different, with typical distance of lumps $\mathcal{O}(k_M^{-1}(\mathbf{p}_0))$ along a niche axis.

The amplitude of the patterns emerging from dynamics described by Eq. (3.1) is dictated by the universality which operates near the instability. The aforementioned universality is particularly interesting for the implications. The key steps in our derivations – e.g., the introduction of the nonlocal linear operator $\mathcal{L}_{\mathbf{p}}$, the expansion close to the boundaries of the critical hyper-surface $\mathcal{M}$ where a quadratic scaling occurs – could equally well be applied to models with different physical features. For instance, nonlocal higher-order interactions may play an important role in shaping patterns of many physical systems, e.g., ecological communities, and may also help to stabilize their dynamics [212]. The inclusion of such contributions in our framework is straightforward. One just need to insert in the function $F_{\mathbf{q}}$ in Eq. (3.1) terms with the form

$$\int G_{\mathbf{q}}(x-y_1, x-y_2, \ldots, x-y_n) \prod_{i=1}^{n} \left[\phi(y_i,t)\, dy_i\right]. \tag{3.35}$$

Close to instability, those terms will affect only the coefficients of the GL equation (3.34). Further, by replacing $F_{\mathbf{q}}$ with $\partial_x^2(\delta\mathcal{F}_{\mathbf{q}}/\delta\phi)$ in Eq. (3.1), we could also describe the dynamics of a conserved order parameter as we have alluded to in the Introduction. Large scale modulation of patterns of such fields may still be described by GL equations. Finally, generalized GL equations for many amplitudes could be derived for systems with many interacting fields/species $\phi_m(x,t)$, with m being a discrete index. We expect that, even in the presence of long range coupling terms, the number of components in the amplitude equation is determined by the symmetries and the conservation laws of the system [79]. This is an interesting aspect which we leave for future investigations.

Chapter 4

Stochastic amplification in delayed and noisy systems

The corresponding manuscript is currently under preparation.

Chapter abstract: The emergence of oscillations which persist indefinitely in time is a common feature of many natural systems, including cyclic dynamics in gene expression, neural oscillations or interacting species. Here we investigate how delay feedback along with stochastic perturbations to deterministic dynamics lead to sustained oscillations with a non-trivial power spectrum. Starting from a simple general setting, we show that the noise and the temporal delay are able to generate stochastic amplifications in a region of the parameter space where they are forbidden without delay. We demonstrate that systems with one dynamic variable may produce a power spectrum with multiple maxima, unlike the case without delay. As an application, we consider the coupled dynamics of protein and mRNA molecules in the gene expression, and show that our framework provides a general and robust prediction of the stochastic oscillations which are observed in the experiments.

4.1 Introduction

In this Chapter of the Thesis we study systems affected by seasonal behaviors, i.e., systems which display periodic cycles in their temporal evolution. In such systems, the time-series describing the dynamical quantities are characterized by almost regular and persistent oscillations which alternate regularly between high and low values [116]–[121].

As discussed in Section 1.2.3, stochastic models are able to predict and explain this feature in a more natural way thanks the phenomenon of *stochastic amplification* [129]–[131]. In fact it has been shown that such a result can be promptly applied to explain empirical evidences coming from natural and social sciences [132]–[134].

From a physical standpoint, the roots of stochastic amplification can be found in terms of a resonance phenomenon. In fact the noisy contributions arise from the demographic stochasticity. For this reason we deal with white noise terms, which can excite all frequencies. In resonating the system, the oscillations, which in the deterministic limit are predicted to be damped,

are sustained indefinitely. The smoking gun of this resonance process can be found by looking for the presence of non-trivial peaks of the stationary power-spectrum describing the spectral properties of such fluctuations.

Another possible mechanism leading to dynamics with oscillating behaviors is the presence of memory effects in the evolution equations. Mathematically this is modeled with the introduction of delayed terms so that the evolution of the system is not only determined by the current state of the system but also by its past history [141].

However, in many cases both memory effects and stochastic contributions are at play and therefore it might be worth to study their combined effect in producing cyclic dynamics.

Theoretical studies accounting for temporal delay within stochastic models have been proposed. In particular, a formalism has been developed that, starting from a microscopical description of the delayed and stochastic system, leads to a Langevin description of the dynamics [213], [214], that subsequently can be cast into a linear equation using the linear-noise approximation.

Computational works instead focus on developing numerical algorithms [145], [215] for integrating the delayed version of a chemical Master equation [216], which provide a recipe to generate faithfully the time-series associated to the process. Both the theoretical and numerical investigations showed the stochastic trajectory might be characterized by noise-induced cycle.

Therefore we aim to search for conditions on the dynamics ensuring the emergence of rhythmic behavior when we combine temporal delays with stochastic dynamics. In other words, we would like to understand which is the region of the model parameters describing a given delayed stochastic dynamics for which we can say affirmatively that stochastic amplification takes place. Moreover, since combing two effects that are said to generate oscillations, we are also interested in seeing if the combination of the two would modify the phenomenon with respect to its original formulation [129].

For these purposes, in this Chapter we build a general, yet simple, framework where delay contributions and random perturbations can be naturally taken into account. Given the theoretical results available in the literature, our starting point is cast into the form of a Langevin equation. From this, we show how delayed terms make an oscillatory dynamics to emerge and then we provide the conditions for which the noise is able to induce stochastic amplification. To this end, we analytically calculate the power-spectrum of the time series and compare it against the one obtained from numerical simulations. As we will see, temporal delays along with a generic stochastic dynamics indeed allow systems to display stochastic amplification with new features when compared to the original formulation [129]. For instance, a one-dimensional system may sustain oscillating fluctuations even though that would be impossible without delay. The framework which we define here captures the main oscillatory features of systems with noise and temporal delayed feedback. As an example, we will discuss the dynamics of a model for gene expression for which our results provide general theoretical insights on some remarkable empirical behaviors.

The rest of the Chapter is organized as follows. Section 4.2 introduces the stochastic and delayed equation we use as our general theoretical framework. We then study in Section 4.3 when the solution in the deterministic limit display asymptotic damped oscillation. We uncover the presence of a threshold mechanism, i.e., the delay has to be larger than a critical values for the system to start oscillating. Moving on, we analyze the spectral properties of the stochastic time-series obtained within our framework in Section 4.4. Herein, we compute analytically the power-spectrum and we obtain an explicit condition on the model parameters to ensure the presence of a non-trivial peak, uncovering once again a threshold mechanism. We then extend in Section 4.5 the starting model to take into account a more complex and general form of delay contributions, i.e., the distributed delay. As an application of the theoretical framework developed, we study gene expression in regulatory networks, as discussed in Section 4.6. Finally, we sum up the conclusions in Section 4.7. In Appendix C.1 we study the same setting and the presence of damped oscillations but with parameters taken in a different region with respect to the one used in the following. More generally, we also obtain the full solution of the deterministic delayed equation in Appendix C.2. In Appendix C.3 we also discuss the occurrence of stochastic amplification in the same region of parameters used in Appendix C.1. Having identified different threshold which determine the behavior of the system, we discussed their order in Appendix C.4. We then study in detail the case if distributed delay, uncovering a new and surprising feature in Appendix C.5. Appendices C.6 and C.7 contain two straightforward extensions of the framework. In particular, we discussed a multi-dimensional system in Appendix C.7, showing that the inclusion of delay enlarges the region the parameters providing the stochastic amplification with respect to non-delayed case.

4.2 Theoretical framework

Thanks to the results found in [213], [214], we can start from a delayed Ornstein-Uhlenbeck process, which can be seen as a paradigmatic example of delayed stochastic equation since it contains both noise and delay contributions in a simple form. Thus we consider a model defined by the following generalized Langevin equation

$$\frac{dx(t)}{dt} = -ax(t) - bx(t-\tau) + \sqrt{D}\xi(t), \tag{4.1}$$

where a, b are constant and $\xi(t)$ is a Gaussian white noise of strength D (which we made explicit for future purposes), i.e.,

$$\langle \xi(t) \rangle = 0 \tag{4.2}$$

$$\langle \xi(t)\xi(t') \rangle = \delta(t-t'). \tag{4.3}$$

Finally, the parameter $\tau > 0$, called *discrete delay*, selects the state at time $t - \tau$ in the past which affects the current state at time t. The delayed dynamics defined in Eq. (4.1) is well defined if we introduce initial conditions for all times $t \in [-\tau, 0]$.

Notice that Eq. (4.1) can be thought of as the linearization around a (deterministic) stationary state z^* of a nonlinear one-dimensional model, i.e.,

$$\frac{dz(t)}{dt} = f\left(z(t), z(t-\tau)\right) + \sqrt{D}\xi(t), \tag{4.4}$$

where $f(z^*, z^*) = 0$ is a minimum of f when the solutions of Eq. (4.1) are stable. Thus the linear Eq. (4.1) can be used a good approximation of the nonlinear model as long as the fluctuations $x(t) = z(t) - z^*$ away from the deterministic stationary state are small.

The properties of the solutions of Eq. (4.1) have been extensively studied [217]–[219]. In the following, we will investigate the stability of the deterministic solution of Eq. (4.1), which can be achieved by setting $D = 0$. Later, we investigate the spectral properties of the stochastic and delayed equation and the possibility of stochastic amplification to emerge [213], [214]. In particular, we will search for conditions on the model parameters so that we can find criteria to state whether noise-induced cycle can or cannot be detected.

4.3 Asymptotic damped oscillations in the deterministic Eq. (4.1)

Herein, we will consider $a > b > 0$. The results for other choices of a and b are presented in Appendix C.1. In this case, independently of τ, the asymptotic stability of the stationary state $\bar{x} = 0$ of the deterministic Eq. (4.1) ($D = 0$), i.e.,

$$\frac{dx(t)}{dt} = -ax(t) - bx(t-\tau), \tag{4.5}$$

is guaranteed [141].

This region of stability may be divided into two different sub-regions, according to whether the dynamics reaches asymptotically the stationary state through damped oscillations or not. Indeed, when seeking solutions of the form

$$x(t) = Ce^{\lambda(\tau)t} \tag{4.6}$$

and defining

$$\beta(\tau) = \mathrm{Im}(\lambda(\tau)), \tag{4.7}$$

one can identify a critical delay τ_c such that, for fixed values of a and b parameters,

$$\beta(\tau) = \begin{cases} 0 & \text{if } \tau \leq \tau_c \\ \neq 0 & \text{if } \tau > \tau_c \end{cases} \tag{4.8}$$

When substituting the exponential *ansatz* for the asymptotic behavior of the solution into the deterministic Eq. (4.5), one obtains the so called *characteristic*

equation, which reads

$$\lambda = -a - be^{-\lambda\tau}. \tag{4.9}$$

Employing Lambert W function, defined as the function satisfying the following identity $W(z)e^{W(z)} = z$ [220], we can obtain analytical solution of Eq. (4.9) as a function of the three parameters. In fact, multiplying both sides of Eq. (4.9) by $\tau e^{\tau a}$ we obtain

$$\tau(\lambda + a) = W\left(-\tau e^{\tau a} b\right). \tag{4.10}$$

At this point we can find the explicit expression of λ as

$$\lambda = \lambda(a, b, \tau) = \frac{W\left(-\tau e^{\tau a} b\right)}{\tau} - a. \tag{4.11}$$

When $z < -e^{-1}\, W(z)$, λ becomes complex. Therefore we can use such property to calculate τ_c. In concrete, we have that the solution of Eq. (4.5) starts to display an oscillatory behavior, i.e., when $\mathrm{Im}\,(\lambda) \neq 0$, if

$$-b\tau e^{\tau a} < -e^{-1} \Longrightarrow b\tau e^{\tau a} > e^{-1}. \tag{4.12}$$

Thus, τ_c can be found as the value for τ satisfying the equality and so we get

$$\tau_c = \frac{1}{a} \cdot W\left(\frac{a}{eb}\right). \tag{4.13}$$

Thus, for $\tau > \tau_c$ and sufficiently large times, the solutions decay with a frequency $\beta(\tau) \neq 0$. We can show that $\beta(\tau = \tau_c + \delta\tau) \sim \sqrt{\delta\tau}$ close to the critical delay τ_c, i.e., $0 < \delta\tau \ll \tau_c$.

In fact, if we call $\alpha = \mathrm{Re}(\lambda)$ and $\beta = \mathrm{Im}(\lambda)$ from Eq. (4.9) we get

$$\alpha = -a - be^{\tau\alpha}\cos(\beta\tau), \tag{4.14}$$

$$\beta = be^{\tau\alpha}\sin(\beta\tau) \tag{4.15}$$

by equating the real and imaginary parts of the two sides of the equation.

Close to the critical threshold τ_c, we expect β to be small. Hence we can expand the right-hand side of Eq. (4.15) in β finding

$$1 = b\tau e^{\tau\alpha}\left(1 - \frac{\tau^2\beta^3}{6}\right) + o\left(\beta^5\right), \tag{4.16}$$

that leads to

$$\beta^2 = \frac{6}{b\tau^3}\left(b\tau - e^{\tau\alpha}\right) + o\left(\beta^3\right). \tag{4.17}$$

At this point we insert $\tau = \tau_c + \delta\tau$ into Eq. (4.17) and we expand in $\delta\tau$ assuming it is small. This procedure gives us

$$\beta^2 = \frac{6}{b\tau_c^3}\left[b\tau_c - e^{\tau_c\alpha(\tau_c)}\right] + \delta\tau \cdot \frac{6}{b\tau_c^3} \cdot \left(-2b + \frac{3e^{\tau_c\alpha(\tau_c)}}{\tau_c} - \rho\right) + o\left(\delta\tau^2\right), \tag{4.18}$$

where

$$\rho = \left.\frac{de^{\tau\alpha(\tau)}}{d\tau}\right|_{\tau=\tau_c}. \tag{4.19}$$

Now we recall that

$$\alpha(\tau_c) = \lambda\left(\tau_c\right) = \frac{1}{\tau_c} - a, \tag{4.20}$$

since by definition $\beta\left(\tau_c\right) = 0$. Consequently we have that

$$b\tau_c - e^{\tau_c\alpha(\tau_c)} = 0. \tag{4.21}$$

In fact, assuming this is true we get

$$b\tau_c = e^{1-a\tau_c}, \tag{4.22}$$

which, after some manipulations, gives

$$\tau_c(a,b) = \frac{W\left(\frac{a}{eb}\right)}{a}, \tag{4.23}$$

consistently with the starting point.

Hence, the first contribution in the right-hand side of Eq.(4.18) is zero and so we get that

$$\beta \sim \sqrt{\delta\tau}. \tag{4.24}$$

We test this analytical result against numerical evidences in Figure 4.1, where the agreement is found to be remarkable.

Interestingly, although for our purposes for the moment it is enough to have studied the asymptotic stability of the deterministic system, using the solutions of characteristic equation it is possible to compute the exact solution of Eq. (4.5), as we show in Appendix C.2.

4.4 Spectral properties of Eq. (4.1)

We now consider the stochastic contribution to the solutions of Eq. (4.1) with $D \neq 0$. Figure 4.2 displays a typical time series of the process for $\tau > \tau_c$. The fluctuations around the stationary state show sustained stochastic oscillations whose amplitude does not decay with time.

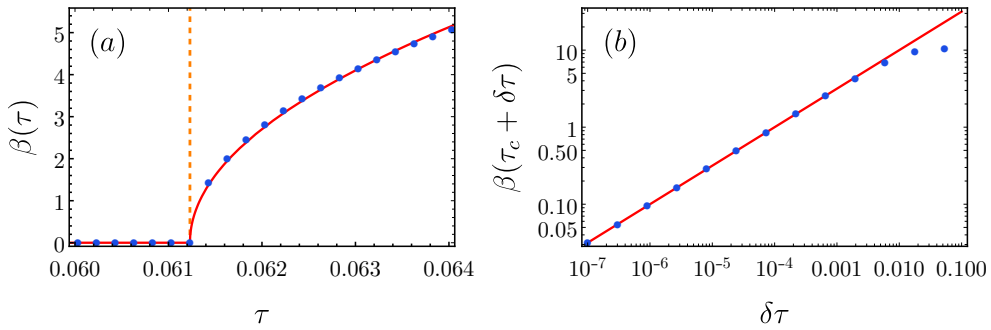

FIGURE 4.1: Numerical check for the scaling of the frequency of the oscillating solution of Eq. (4.5) after having fixed $a = 3$ and $b = 5$. In both panels the blue dots are obtained by taking the imaginary part of the solution of Eq. (4.9) obtained numerically, while the red line is the square root behavior we analytically found in Eq. (4.24). Panel (a): We use linear-linear scale with $\beta(\tau)$ evaluated for τ smaller and greater than τ_c. The vertical orange dashed lines indicates such critical threshold. For values of the delay greater than this, it is clear that the frequency grows as a square root. Panel (b): Here we use a double logarithmic scale. On the horizontal axis we show $\delta\tau = \tau - \tau_c$, whereas on the vertical axis we show $\beta(\tau = \tau_c + \delta\tau)$. In both cases, for small values of $\delta\tau$ the agreement is excellent, confirming the theoretical findings.

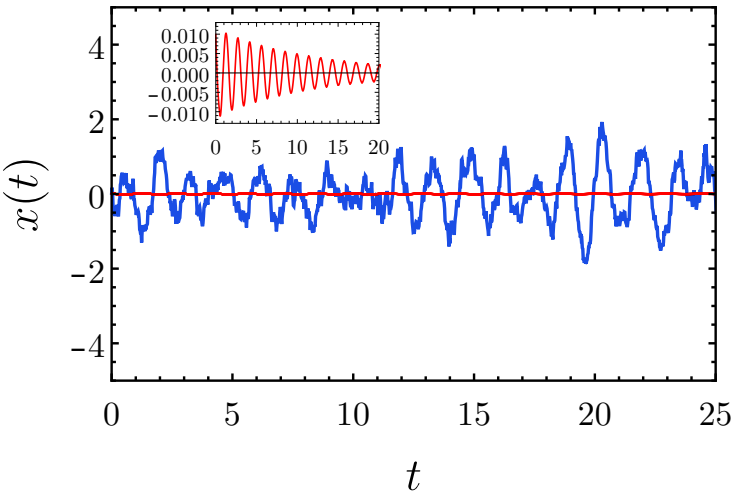

FIGURE 4.2: The blue noisy line shows a typical time series for $x(t)$ generated numerically from Eq. (4.1) with $D = 1$ in the time interval $t \in [0, 25]$; the solid red line in the inset shows the deterministic solution ($D = 0$) of the delayed process given by Eq. (4.1). In both cases the parameters are $a = 3$, $b = 5$ and $\tau = 0.5$, whereas the time increment is $dt = 10^{-3}$ and $x(t) = x_0 = 10^{-2}$ for $t \in [-\tau, 0]$. A deterministic trajectory relaxes to the stationary state with damped oscillations (inset), whilst the corresponding stochastic solution fluctuates with sustained random oscillations.

This behaviour can be analytically investigated by looking at the spectral properties of $x(t)$. We consider the Fourier transform of Eq. (4.1) and find

$$i\omega\hat{x}(\omega) = -a\hat{x}(\omega) - b\hat{x}(\omega)e^{-i\omega\tau} + \sqrt{D}\hat{\xi}(\omega), \tag{4.25}$$

where $\hat{x}(\omega)$ and $\hat{\xi}(\omega)$ indicate the Fourier components of frequency ω of $x(t)$ and $\xi(t)$, respectively. Given that $\xi(t)$ is a Gaussian white noise, it follows that $\langle\hat{\xi}(\omega)\rangle = 0$ and $\langle\hat{\xi}(\omega)\hat{\xi}(\omega')\rangle = \frac{\delta(\omega+\omega')}{2\pi}$. From Eq. (4.25) we can express the Fourier component of $x(t)$ of a given given frequency ω in terms of the relative component of the noise $\xi(t)$, i.e., we get

$$\hat{x}(\omega) = \frac{\sqrt{D}}{[a + b\cos(\omega\tau)] + i\,[\omega - b\sin(\omega\tau)]}\hat{\xi}(\omega). \tag{4.26}$$

Following [127], the power-spectrum $P(\omega)$ can be obtained from the relation $\langle\hat{x}(\omega)\hat{x}^*(\omega')\rangle = \delta(\omega - \omega')P(\omega)$. A direct computation from Eq. (4.26) yields

$$P(\omega) = \frac{D}{[a + b\cos(\omega\tau)]^2 + [\omega - b\sin(\omega\tau)]^2}. \tag{4.27}$$

Let us comment on this result. Because of the sinusoidal functions in the denominator, which are caused by the discrete delay, the power-spectrum is not reminiscent of the one of a simple damped harmonic oscillator as it is for the original stochastic amplification [129]. The first new feature is that $P(\omega)$ itself may oscillate, thus displaying multiple local maxima, even though the deterministic system has only one characteristic frequency. This is different from the stochastic amplification without delay, in which multiple peaks are not possible with only two degrees of freedom [129].

To get an analytical insight about this, we can set to zero the first derivative with respect to ω of $P(\omega)$, obtaining

$$\omega = \frac{(a\tau + 1)b\sin(\omega\tau)}{1 - b\tau\cos(\omega\tau)}. \tag{4.28}$$

Asymptotically, if $b\tau > 1$, this equations is solved by

$$\omega \approx 2\pi n \pm \arccos\left(\frac{1}{b\tau}\right) \quad \text{with } n \text{ a large integer.} \tag{4.29}$$

Hence in this case the power-spectrum has multiple local maxima and minima.

In Figure 4.3 we benchmark the theoretical power-spectrum of Eq. (4.27) against the one obtained from an ensemble of independent realizations of Eq. (4.1) showing the absolute maximum, while the inset includes local maxima occurring at higher frequencies.

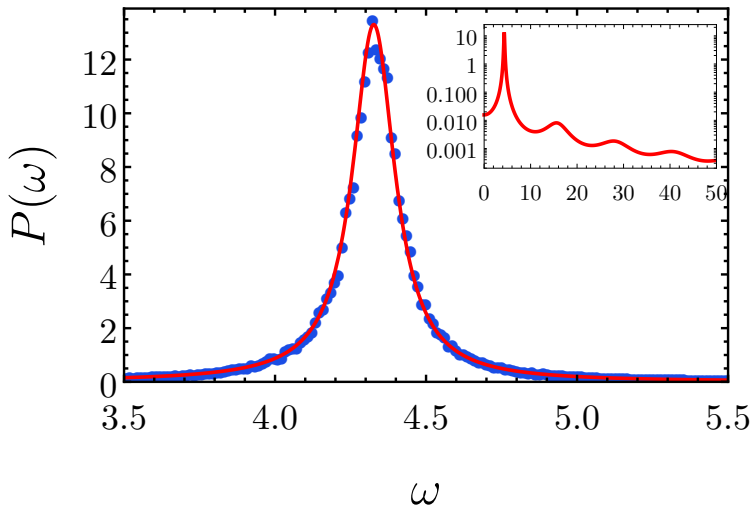

FIGURE 4.3: Comparison between the predicted power-spectrum in Eq. (4.27) (solid red line) and the numerical one (blue dots) obtained from 500 independent realizations of the process defined in Eq. (4.1). The parameters and the initial conditions are those in Figure 4.2. The main panel includes a range of frequencies where $P(\omega)$ contains only its absolute maximum; this identifies the characteristic frequency ω_{max} of stochastic oscillations (similarly to Figure 4.2). The inset instead shows the power-spectrum on a larger interval of frequencies in which other local maxima are reached (notice that $b\tau > 1$).

In addition, Eq. (4.27) shows that peaks may emerge at $\omega > 0$ only for $\tau > 0$. Indeed, if we set $\tau = 0$, the power-spectrum becomes

$$P_{\tau=0}(\omega) = \frac{D}{(a+b)^2 + \omega^2}, \tag{4.30}$$

which has an absolute maximum at $\omega_{max} = 0$ and $P(\omega)$ decays as $P(\omega) \sim \omega^{-2}$ for $\omega \gg a$. Hence, stochastic amplification can not take place with only one degree of freedom if there are no delay effects.

More interestingly, as we saw from Figure 4.3, when $\tau > 0$ non-trivial peaks might appear. In this case, the time series for $x(t)$ generated via Eq. (4.1) are characterized by a dominant frequency corresponding to ω_{max}. Therefore, the stationary solutions of the process fluctuate with a characteristic frequency ω_{max} and the random oscillations are persistent in time. The amplitude of the noise D simply changes the size of the fluctuations, but does not alter the characteristic frequency of the resonance.

4.4.1 Emergence of stochastic amplification

At this point, given that the introduction of a discrete delay might guarantee the onset of stochastic amplification, we search for a condition for the power spectrum to display a peak at $\omega > 0$. This is readily found by studying the nature of the stationary point $\omega = 0$. Indeed, the first derivative of

the power-spectrum with respect to ω computed in $\omega = 0$ is always zero, independently of the parameters, i.e.,

$$\left.\frac{dP}{d\omega}\right|_{\omega=0} = 0. \tag{4.31}$$

From the expression shown in Eq. (4.27) we can see that $P(\omega)$ is an even positive function that decays to zero at infinity, i.e., $P(\omega) > 0\ \forall\omega$ with $P(\omega) \to 0$ for $\omega \to \pm\infty$. Thus, if $\omega = 0$ is a point of minimum, it must be that such function displays a point of (absolute) maximum for $\omega_{max} > 0$. For this reason, we evaluate the second derivative of $P(\omega)$ in $\omega = 0$ finding

$$\left.\frac{d^2P}{d\omega^2}\right|_{\omega=0} = 2D\frac{[b\tau(2+a\tau)-1]}{(a+b)^4}. \tag{4.32}$$

Therefore $\omega = 0$ is a local minimum if and only if

$$b\tau(2+a\tau) - 1 > 0. \tag{4.33}$$

Given that we are considering $a > 0$, we get

$$\tau > \tau_a = \frac{-1+\sqrt{1+\frac{a}{b}}}{a}. \tag{4.34}$$

Given this result, we can see that stochastic amplification does not occur for delays that are too small, i.e., if $0 < \tau \leq \tau_a$, whereas it requires $\omega_{max}(\tau) > 0$ for $\tau > \tau_a$.

Furthermore, if we consider a delay greater than the critical threshold, we can find that the position of the maximum ω_{max} of the power-spectrum grows as the square root of the increment of τ from the critical threshold τ_a, i.e., $\omega_{max}(\tau_a + \delta\tau) \sim \sqrt{\delta\tau}$ as $0 < \delta\tau \ll \tau_a$.

To prove this, we need to evaluate the first derivative of Eq. (4.27) with respect to ω and, setting it to be equal to zero, we obtain

$$\omega_{max} = b\omega_{max}\tau\cos(\omega_{max}\tau) + b(1+a\tau)\sin(\omega_{max}\tau) \tag{4.35}$$

When $\tau = \tau_a + \delta\tau$ with $0 < \delta\tau \ll 1$ we expect ω_{max} to be small. Hence we can expand the above equation to get

$$1 = b\tau(2+a\tau) - \omega_{max}^2\tau^3 b\left(\frac{4+a\tau}{6}\right) + o\left(\omega_{max}^4\right). \tag{4.36}$$

Neglecting the higher order in ω_{max} we find

$$\omega_{max}^2 = \frac{6[b\tau(2+a\tau)-1]}{b\tau^3(4+a\tau)}. \tag{4.37}$$

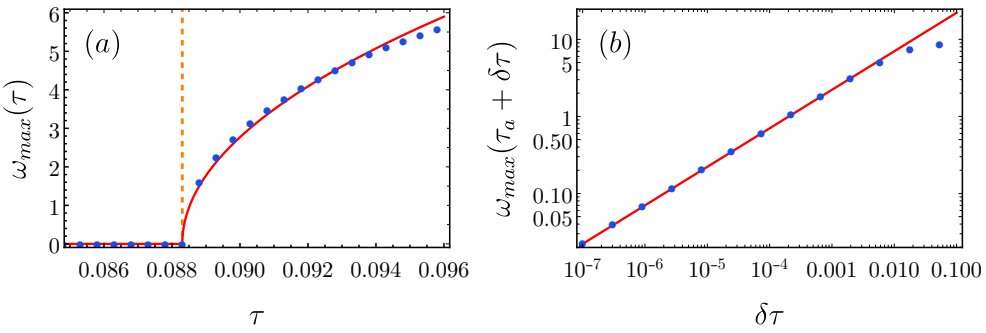

FIGURE 4.4: Numerical check for the scaling of the characteristic frequency of the stochastic fluctuations describing the time series generated with Eq. (4.1) after having fixed $a = 3$ and $b = 5$. In both panels the blue dots are obtained numerically by searching numerically the absolute maximum of Eq. (4.27) while changing $\tau = \tau_a + \delta\tau$ numerically, while the red line is the square root behavior we analytically found in Eq. (4.38). Panel (a): We use linear-linear scale with $\omega_{max}(\tau)$ evaluated for τ smaller and greater than τ_a. The vertical orange dashed lines indicates such critical threshold. For values of the delay greater than this, it is clear that the frequency grows as a square root. Panel (b): Here we use a double logarithmic scale. On the horizontal axis we show $\delta\tau = \tau - \tau_a$, whereas on the vertical axis we show $\omega_{max}(\tau = \tau_a + \delta\tau)$. For small values of $\delta\tau$ the agreement is excellent, confirming the theoretical findings.

Now we can insert $\tau = \tau_a + \delta\tau$ and expand in $\delta\tau$. Since by definition we have that $b\tau_a\,(2 + a\tau_a) - 1 = 0$, it is easy to see that we get

$$\omega_{max} \sim \sqrt{\delta\tau}. \tag{4.38}$$

We numerically check the scaling in Eq. (4.38). We show this in Figure 4.4, noticing the excellent agreement between the numerical outcome and the theoretical findings.

Interestingly, in the discrete delay case we considered so far we can prove that $\tau_c < \tau_a$, as shown in Appendix C.4. This means that, if we take any delay larger than τ_c but smaller than τ_a, the asymptotic deterministic dynamics displays damped oscillations, but the noise in the stochastic equation is not sufficient to sustain random oscillations. Figure 4.5 confirms that, for $\tau = 1$ (without any loss of generality), the region providing damped oscillations in the deterministic regime and the one where stochastic amplification occurs are nested.

4.5 Distributed delay case

The analysis carried out so far can be further developed in several directions. For example, one may consider the effect of a distributed delay in the dynamics defined by Eq. (4.1), whereby multiple states of the past contribute with

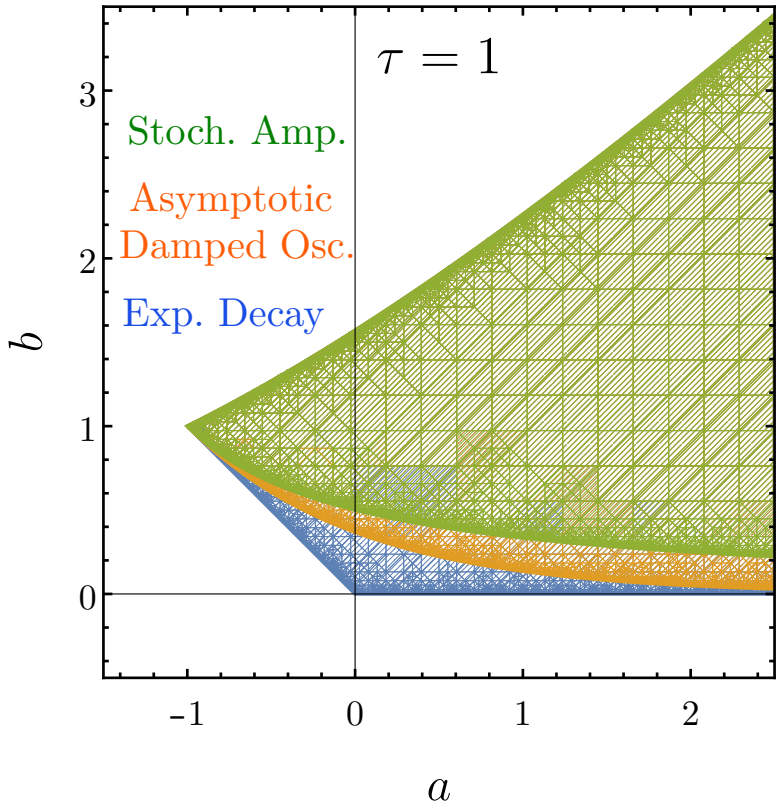

FIGURE 4.5: Phase diagram in the $a - b$ plane for a fixed delay ($\tau = 1$) characterizing the behavior of the dynamics Eq. (4.1). Within the white area the system is unstable, whereas inside the colored one, $\bar{x} = 0$ is asymptotically stable in the deterministic dynamics. In the blue region the system approaches asymptotically $\bar{x}$ via exponential decay, while the orange one indicates an asymptotic decay with damped oscillations. Finally, the green area shows the region where stochastic amplification occurs.

different weights to the current state . The dynamics in this case is given by

$$\frac{dx(t)}{dt} = -ax(t) - bI(t) + \sqrt{D}\xi(t), \tag{4.39}$$

where

$$I(t) = \int_0^{+\infty} dz\, G(z)x(t-z), \tag{4.40}$$

with $G(z)$ being a normalized memory kernel. Starting from Eq. (4.39), we can gain analytical insight by following the same steps we presented above.

We can now replicate the same steps presented in Section 4.4 to test if oscillations occur in the deterministic limit and then study what happens when noisy contributions are taken into account.

So, inserting $x(t) = Ce^{\lambda t}$ in Eq. (4.39) in which we set $D = 0$ (deterministic limit), we get

$$\lambda = -a - b\int_0^{+\infty} dz\, G(z)e^{-\lambda z} = -a - b\tilde{G}(\lambda), \tag{4.41}$$

where $\tilde{G}(\lambda)$ indicates the Laplace transform of the kernel. Given a functional form for the kernel $G(z)$, we can search whether the above equation admits complex solutions. If so, the system will display oscillations. In particular writing $\lambda = \alpha + i\beta$ Eq. (4.41) can be split to obtain the following coupled equations for the real and imaginary part of λ

$$\alpha = -a - b\int_0^{+\infty} dz\, G(z)e^{-\alpha z}\cos(\beta z), \tag{4.42}$$

$$\beta = b\int_0^{+\infty} dz\, G(z)e^{-\alpha z}\sin(\beta z). \tag{4.43}$$

From the first equation we can see that in order to have $\alpha < 0$, i.e., a stable dynamics, we need that the kernel $G(z)$ has to decay faster than e^{-cz} with $c \in \mathbb{R}$ and $c > |\alpha|$, otherwise the integral would diverge. This implies that the all moments of $G(z)$, in particular the first and second ones, are finite. This observation would be useful later in the discussion.

When noise is taken into account we know stochastic amplification might occur. To see this, we study the spectral properties of the dynamics by computing the Fourier transform of Eq. (4.39). In this way we find

$$i\omega\hat{x}(\omega) = -a\hat{x}(\omega) - b\hat{I}(\omega) + \sqrt{D}\hat{\xi}(\omega), \tag{4.44}$$

where again $\hat{\xi}(\omega)$ is such that $\langle\hat{\xi}(\omega)\rangle = 0$ and $\langle\hat{\xi}(\omega)\hat{\xi}(\omega')\rangle = \frac{\delta(\omega+\omega')}{2\pi}$, while

$$\hat{I}(\omega) = \hat{\bar{G}}(\omega)\hat{x}(\omega), \tag{4.45}$$

with $\hat{\bar{G}}(\omega)$ being the Fourier transform of $\bar{G}(z) = G(z)\Theta(z)$. This because

$$\hat{I}(\omega) = \int_{-\infty}^{+\infty} dt\, I(t)e^{-i\omega t}$$

$$
\begin{aligned}
&= \int_{-\infty}^{+\infty} dt \int_{0}^{+\infty} dz\, G(z) x(t-z) e^{-i\omega t} \\
&= \int_{-\infty}^{+\infty} dt \int_{-\infty}^{+\infty} dz\, \overbrace{G(z)\Theta(z)}^{:=\bar{G}(z)} x(\overbrace{t-z}^{:=s}) e^{-i\omega t} \\
&= \int_{-\infty}^{+\infty} ds\, x(s) e^{-i\omega s} \int_{-\infty}^{+\infty} dz\, \bar{G}(z) e^{-i\omega z} = \hat{\bar{G}}(\omega)\hat{x}(\omega). \qquad (4.46)
\end{aligned}
$$

Thus we end up with

$$
\hat{x}(\omega) = \frac{\sqrt{D}}{a + b\hat{\bar{G}}(\omega) + i\omega}\hat{\xi}(\omega) = \frac{\sqrt{D}}{a + b\,\mathrm{Re}\left[\hat{\bar{G}}(\omega)\right] + i\left(\omega + b\,\mathrm{Im}\left[\hat{\bar{G}}(\omega)\right]\right)}\hat{\xi}(\omega). \qquad (4.47)
$$

From this we can obtain easily the power-spectrum which takes the form

$$
P(\omega) = \frac{D}{\left(a + b\,\mathrm{Re}\left[\hat{\bar{G}}(\omega)\right]\right)^2 + \left(\omega + b\,\mathrm{Im}\left[\hat{\bar{G}}(\omega)\right]\right)^2}. \qquad (4.48)
$$

To confirm the occurrence of stochastic amplification, the power-spectrum has to present a non-trivial peak. Therefore, as we did for the discrete delay case, we investigate the nature of the point $\omega = 0$. From a direct calculation of the first derivative, but also for symmetry arguments, we can see that it is always a stationary point of Eq. (4.48).

By computing the second derivative of Eq. (4.48) in $\omega = 0$, we can see that the condition for which such point is a local minimum, i.e., stochastic amplification takes place, now reads

$$
(1 - b\mu_1)^2 - b(b+a)\mu_2 < 0, \qquad (4.49)
$$

where μ_n is the n-th moment of $G(z)$, i.e.,

$$
\mu_n = \int_{-\infty}^{+\infty} dz\, z^n \bar{G}(z) = \int_{0}^{+\infty} dz\, z^n G(z). \qquad (4.50)
$$

From what we said above about the stability of the deterministic solution, it follows that all the moments are finite.

The condition displayed in Eq. (4.49) can be found by noticing that

$$
\frac{d^n}{d\omega^n}\hat{\bar{G}}(\omega) = \frac{d^n}{d\omega^n}\left(\mathrm{Re}\left[\hat{\bar{G}}(\omega)\right]\right) + i\frac{d^n}{d\omega^n}\left(\mathrm{Im}\left[\hat{\bar{G}}(\omega)\right]\right). \qquad (4.51)
$$

From the definition of $\bar{G}(z)$ we see that

$$
\left.\frac{d^n}{d\omega^n}\hat{\bar{G}}(\omega)\right|_{\omega=0} = (-i)^n \mu_n. \qquad (4.52)
$$

Therefore we can see that

$$\text{Re}\left[\hat{\tilde{G}}(\omega)\right]\Big|_{\omega=0} = 1 \quad \text{and} \quad \text{Im}\left[\hat{\tilde{G}}(\omega)\right]\Big|_{\omega=0} = 0, \tag{4.53}$$

$$\frac{d}{d\omega}\text{Re}\left[\hat{\tilde{G}}(\omega)\right]\Big|_{\omega=0} = 0 \quad \text{and} \quad \frac{d}{d\omega}\text{Im}\left[\hat{\tilde{G}}(\omega)\right]\Big|_{\omega=0} = -\mu_1, \tag{4.54}$$

$$\frac{d^2}{d\omega^2}\text{Re}\left[\hat{\tilde{G}}(\omega)\right]\Big|_{\omega=0} = -\mu_2 \quad \text{and} \quad \frac{d^2}{d\omega^2}\text{Im}\left[\hat{\tilde{G}}(\omega)\right]\Big|_{\omega=0} = 0. \tag{4.55}$$

Hence, performing some algebra and using these results, we can easily obtain the condition in Eq. (4.49).

To test the validity of Eq. (4.48), we perform numerical simulation in which we consider a kernel with the shape of a Gamma distribution, i.e.,

$$G(z) = \frac{e^{-z/\tau}}{\tau\Gamma(k)}\left(\frac{z}{\tau}\right)^{k-1}. \tag{4.56}$$

From this choice it follows that

$$\hat{\tilde{G}}(\omega) = \frac{1}{\tau^k}\left(\frac{1}{\tau} + i\omega\right)^{-k}. \tag{4.57}$$

and so the power-spectrum explicitly reads

$$P(\omega) = D\Bigg\{\left[a + \frac{b}{\tau^k}\left(\frac{1}{\tau^2}+\omega^2\right)^{-\frac{k}{2}}\cos\left(k\arctan(\omega\tau)\right)\right]^2 + \\ + \left[\omega - \frac{b}{\tau^k}\left(\frac{1}{\tau^2}+\omega^2\right)^{-\frac{k}{2}}\sin\left(k\arctan(\omega\tau)\right)\right]^2\Bigg\}^{-1}. \tag{4.58}$$

In Figure 4.6 we present the comparison of Eq. (4.58) with the power-spectrum numerically found from an ensemble of trajectories obtained simulating the dynamics Eq. (4.39). As we can see the agreement is excellent.

The phenomenology of the asymptotic analysis is similar to the one we found with the discrete delay. Also, it is immediate to see that Eq. (4.1) is recovered when considering $G(z) = \delta(z - \tau)$. With such kernel, we obtain the same condition on the model parameters to have stochastic amplification we found before.

Interestingly, however, in the distributed delay case there exists a region of the model parameters where one can observe a non-trivial peak in the power-spectrum even when the asymptotic dynamics does not display damped oscillations. In Appendix C.5 we show this surprising behavior in the case of an exponential memory kernel. By studying the deterministic behavior of the full solution of the exponentially distributed delay, we find a region of the parameters where the solution has a unique zero at finite times, as shown by analytical calculations provided in Appendix C.5 where we use the full solution of the linear delayed ordinary differential equation found in Appendix C.2. We show then, albeit in the absence of damped oscillations,

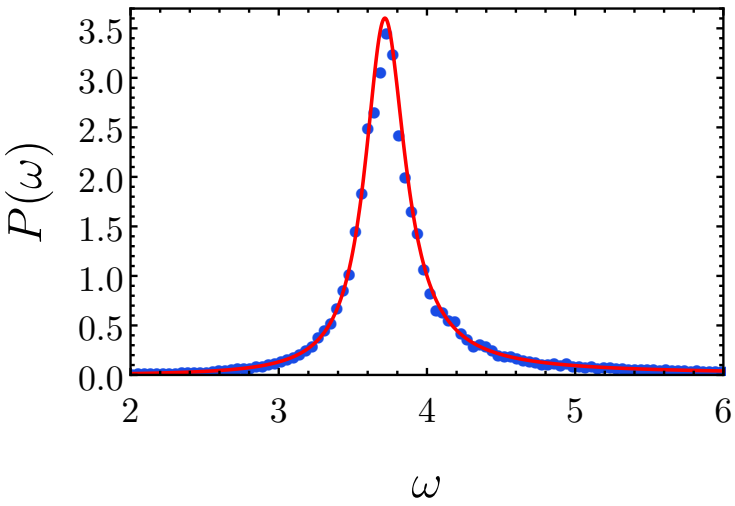

FIGURE 4.6: Comparison between the theoretical power-spectrum (solid red line) in the case of distributed delay with a Gamma distribution kernel Eq. (4.58) and the one numerically obtained as an average from 250 independent realizations (blue dots). We used the prescription $x(t) = x_0 = 10^{-2}$ for $t \leq 0$. Additionally, the integral in Eq. (4.40) is computed integrating from 0 to 10τ and the time increment used is $dt = 5 \cdot 10^{-4}$. The other parameters are $a = 3$, $b = 20$, $\tau = 0.5$, $k = 2$ and $D = 1$. The clear presence of a peak is the signature that also in this case the stochastic amplification phenomenon occurred.

this is still a necessary condition for the occurrence of stochastic amplification when introducing noise. This new feature can be generalized to distributed delays whose solutions have only a finite number of zeros.

4.6 Application: gene expression in regulatory networks

The results obtained so far offer theoretical insights and more natural explanations for the oscillatory behavior observed in real world systems, which often need relatively more complicated nonlinear dynamics for explaining oscillations. The gene expression in regulatory networks provides an interesting example. Experimental evidence supports oscillatory behavior in the concentrations of mRNA, $m(t)$, as well as protein molecules, $p(t)$, as a function of the time, t, within cells on long time-scales due to negative autoregulation mechanisms [146].

The coupled stochastic dynamics between mRNA and protein species has been described by several models [130], [221] and time delay effects intrinsic to transcription, translation and export processes have been considered to gain insight in the regulatory processes [142]–[144]. For instance, a simple formulation of the delayed dynamics of transcription and translation may

take the form

$$\frac{dm(t)}{dt} = \alpha_m f(p(t-\tau_m)) - \mu_m m(t), \tag{4.59a}$$

$$\frac{dp(t)}{dt} = \alpha_p m(t-\tau_p) - \mu_p p(t), \tag{4.59b}$$

where μ_m and μ_p are the degradation rates of the mRNA and proteins, respectively, α_m and α_p are the maximal rates of synthesis for the two components, τ_m and τ_p are the time delays, respectively, for the transcription and translation processes; finally we have

$$f(p) = \frac{1}{1+(p/p_0)^h}, \tag{4.60}$$

and it is the monotonically decreasing Hill function representing the suppression of the mRNA production when the concentration of proteins increases, and p_0 is such that $f(p_0) = 1/2$. This model and its variants are able to predict deterministic oscillations. However, the long-time persistence of the oscillatory dynamics is only reached for specific values of the model parameters and some of those (like the Hill factor h) cannot be empirically measured [215].

The evolution described by Eqs. (4.59a)-(4.59b) neglects the effects of intrinsic noise, which may play a major role at times, when the numbers of mRNA and protein molecules within a cell are small. Thus, in order to capture the essential features of noise in the system, we add two independent white Gaussian noises to Eqs. (4.59a)-(4.59b) with small strength, respectively, D_m and D_p. So we now have to consider the following stochastic dynamics

$$\frac{dm(t)}{dt} = \alpha_m f(p(t-\tau_m)) - \mu_m m(t) + \sqrt{D_m}\xi_m(t), \tag{4.61a}$$

$$\frac{dp(t)}{dt} = \alpha_p m(t-\tau_p) - \mu_p p(t) + \sqrt{D_p}\xi_p(t). \tag{4.61b}$$

In order to study the fluctuations around the deterministic stationary state, we express $m(t)$ and $p(t)$ as

$$m(t) = m^* + x(t), \tag{4.62}$$

$$p(t) = p^* + y(t), \tag{4.63}$$

and we then linearize the deterministic part of the stochastic model around m^* and p^*. In this way we obtain a set of coupled Langevin equations akin to Eq. (4.1), which read

$$\frac{dx(t)}{dt} = \alpha_m \cdot \bar{f} \cdot y(t-\tau_m) - \mu_m \cdot x(t) + \sqrt{D_m}\xi_m(t), \tag{4.64a}$$

$$\frac{dy(t)}{dt} = \alpha_p \cdot x(t-\tau_p) - \mu_p \cdot y(t) + \sqrt{D_p}\xi_p(t), \tag{4.64b}$$

where

$$\bar{f} = \left.\frac{df(p)}{dp}\right|_{p=p^*}. \tag{4.65}$$

At this point we repeat the procedure we described in the previous sections. Hence taking the Fourier transform of Eqs. (4.64a)-(4.64b) we get

$$i\omega\hat{x}(\omega) = \alpha_m \cdot \bar{f} \cdot \hat{y}(\omega)e^{-i\omega\tau_m} - \mu_m \cdot \hat{x}(\omega) + \sqrt{D_m}\hat{\xi}_m(\omega), \tag{4.66a}$$

$$i\omega\hat{y}(\omega) = \alpha_p \cdot \hat{x}(\omega)e^{-i\omega\tau_p} - \mu_p \cdot \hat{y}(\omega) + \sqrt{D_p}\hat{\xi}_p(\omega). \tag{4.66b}$$

In this way we can easily get

$$\hat{x}(\omega) = \frac{\left(i\omega + \mu_p\right)\sqrt{D_m}\hat{\xi}_m(\omega) + \alpha_m \cdot \bar{f}\sqrt{D_p}\hat{\xi}_p(\omega)}{-\omega^2 + i\left(\mu_m + \mu_p\right)\omega + \mu_m \cdot \mu_p - \alpha_p\alpha_m \cdot \bar{f}e^{-i\omega(\tau_m+\tau_p)}}, \tag{4.67a}$$

$$\hat{y}(\omega) = \frac{\left(i\omega + \mu_m\right)\sqrt{D_p}\hat{\xi}_p(\omega) + \alpha_p\sqrt{D_m}\hat{\xi}_m(\omega)}{-\omega^2 + i\left(\mu_m + \mu_p\right)\omega + \mu_m \cdot \mu_p - \alpha_p\alpha_m \cdot \bar{f}e^{-i\omega(\tau_m+\tau_p)}}. \tag{4.67b}$$

From these it is straightforward to get the two power-spectra.

The numerical simulations of the full stochastic dynamics given by Eqs. (4.61a)-(4.61b) show sustained oscillations with a characteristic frequency, as we can see from the examples provided in panels (a)-(b) of Figure 4.7. From these, we can see that when the deterministic solution reaches a stationary state, the numerical time-series display a quite regular oscillating behavior. Hence in this case the deterministic model does not predict the presence of long-standing oscillations, whereas the stochastic formulation is able to provide such a picture. This is well captured by computing the power-spectrum. Panels (c)-(d) of Figure 4.7 show the power spectra for the stochastic formulation Eqs. (4.61a)-(4.61b) and the comparison with the corresponding analytical results as obtained from the linearization of the model. Two peaks at positive frequencies, one for each power-spectrum, emerge quite generally over a large region of the model parameters. Therefore within our setting the dependence on the model parameters of the time-persistence of the fluctuations is reduced, confirming the robustness of the oscillations.

4.7 Conclusions and future perspectives

In conclusion, we have studied the spectral properties of the solutions of linear stochastic equations with a delay contribution. We have shown that, under suitable conditions which we have aptly identified, the dynamics displays time-persistent stochastic oscillations, as confirmed by the peak of the power-spectrum for strictly positive frequencies. Although the spectrum is not reminiscent of a damped harmonic oscillator, the amplification mechanism may be intuitively understood in the following terms: the white noise, which covers all the frequencies, excites those that are naturally present in the

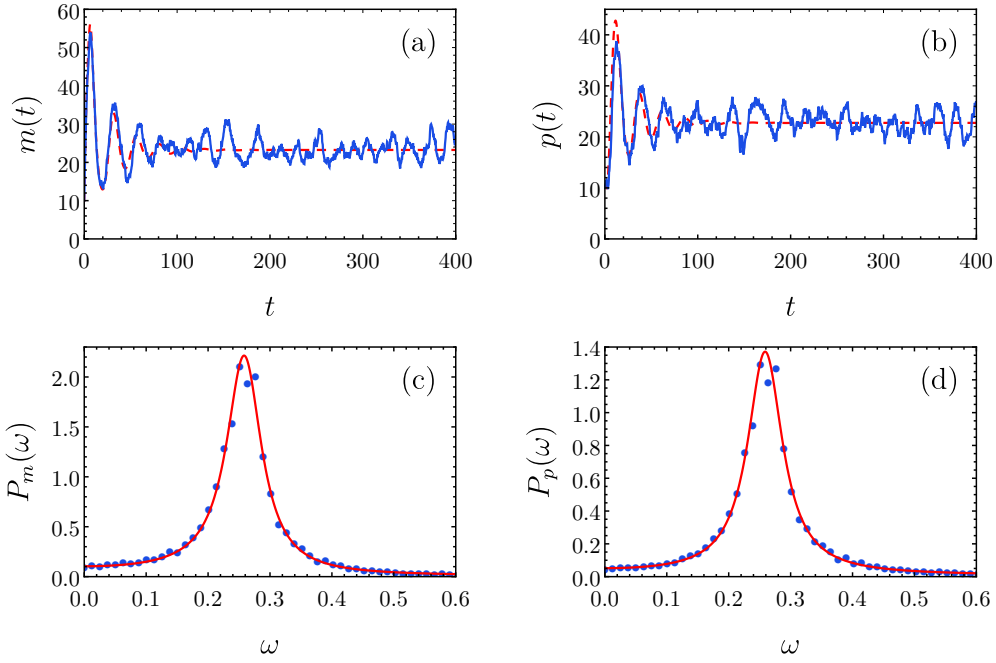

FIGURE 4.7: Solutions of the deterministic model Eqs. (4.59a)-(4.59b) (red dashed lines) versus two typical realizations obtained from the stochastic dynamics (noisy blue lines) for the mRNA molecules $m(t)$ [panel (a)] and proteins $p(t)$ [panel (b)] generated from the full process full process Eqs. (4.61a)-(4.61b). Power-spectra $P_m(\omega)$ and $P_p(\omega)$ for these fluctuations of mRNA molecules [panel (c)] and proteins [panel (d)]: each presents a maximum occurring at $\omega_{m,max,}, \omega_{p,max,} > 0$, respectively. Theoretical power-spectra (solid red lines), computed from Eqs. (4.67a)-(4.67b), are compared to the numerical ones (blue dots) obtained from 250 independent realization of the full process given by Eqs. (4.61a)-(4.61b). In all four panels the parameters are $\alpha_m = 33$, $\alpha_p = 0.225$, $\mu_m = \mu_p = 0.23$, $h = 2$, $p_0 = 10$, $\tau_m = 2$, $\tau_p = 3$, $D_m = D_p = 1$ and a time increment $dt = 10^{-3}$. The initial conditions are $m(t) = m_0 = 10$ for $t \in [-\tau_m, 0]$ and $p(t) = p_0 = 10$ for $t \in [-\tau_p, 0]$.

deterministic model because of the delay. Thus, without tuning the system, one or more characteristic frequencies are singled out in the power spectrum.

However, albeit damped oscillations caused by delay in the deterministic regime are necessary for the emergence of random oscillations, they are not sufficient to sustain them indefinitely. Indeed, the delay has to be larger than a threshold in order to guarantee stochastic amplification.

Moreover, in Appendix C.5 for the distributed delay case we have shown that it might be that noise-induced cycles, signature of the occurrence of the stochastic amplification mechanism, can be observed even if the deterministic dynamics does not approach the stationary state via damped oscillations. We argued by studying the exact solution of the deterministic delayed ordinary differential equation that such puzzling evidence can be interpreted as follows: although the deterministic solution does not oscillate, there exists a $\bar{t} > 0$ in which it intercepts once the stationary value, i.e., the fluctuations become zero. Hence this resembles a single oscillation. Thus the noise might resonate with this, providing time-persistent oscillations.

Our theoretical investigations can be straightforwardly applied to consider many modifications of the general framework we presented at the beginning in Section 4.2. A possible route of generalization can be pursued when substituting the white noise in Eq. (4.1) with colored noise with a stationary non-trivial temporal correlation. Also in this case the key-steps illustrated above lead to an analytic expression of the power-spectrum with internal peaks, thus confirming the existence of sustained stochastic oscillations. Such case is discussed in details in Appendix C.6.

Another interesting natural generalization includes the study of an $n-$ dimensional Ornstein-Uhlenbeck process, in which the coefficients of Eq. (4.1) are appropriate matrices. The spectral analysis of the fluctuations can be performed straightforwardly and confirms that the delay introduces new features with respect to the original formulation: terms with delayed contributions may lead to stochastic amplification even when it is forbidden in the non-delayed case. The detailed study of this scenario is relegated in Appendix C.7.

The oscillatory behavior found in the gene expression in regulatory networks provides a relevant example of the predictions based on the simple Eq. (4.1): general model systems where the dynamics is affected by states encountered in the past as well as noise perturbations, display persistent oscillatory behavior in a wide region of the parameter space. This has the potential ability to explain in a more natural way, avoiding any particular tuning of the model parameters, the emergence of sustained oscillations in empirical systems under quite general conditions.

In fact, it could be interesting to search for other systems for which the developed framework can be successfully employed to describe their dynamics. Examples might be found when tackling the diffusion of diseases. Here intrinsic stochasticity plays indeed an important role, since the contagious process, for instance, is certainly not deterministic. Additionally, when considering pathogens with an incubation period, the occurrence of an infection

in contributing to the spread of the disease starts to matter well after the moment in which the contagion took place. Hence it is clear that such dynamics possesses clear delay effects.

Chapter 5

Thesis Conclusions

Living systems are intrinsically affected by an huge degree of complexity: they are made by a large number of singular entities entangled one to the others via dense networks of interaction.

Due to this, ecological and biological systems display non-trivial behaviors, which have captured the interests of researchers since long time. Such peculiar features emerge from the intertwining of the several degrees of freedom involved in the dynamics. However, the mechanisms leading to their observation and the explanations shedding lights on their origins are not obvious neither clear a priori. Indeed, this makes the study of these type of systems very captivating.

In order to obtain mathematical descriptions of ecological phenomena, quantitative predictions on the systems behaviors to be compared with data and reliable clarifications about what leads to the origination of a given complex feature, tools and techniques common in physical sciences, especially those coming from Statistical Mechanics, are largely employed.

In this Thesis, as we argued in Chapter 1, we fully adopted a complex systems vision of ecological and biological scenarios. Herein, we exploited ideas, such as coarse-graining of spatial degrees of freedom or universality and scaling-properties near the transition point, to study three different problems attracting extensively the interests of the scientific community in the last decades.

So, in Chapter 2, we first focused on the study of species-rich ecosystems, such as tropical rain-forests, microbial colonies or plankton communities, where several different species coexists while competing for the consumption of the few resources present in the environment. In order to model quantitatively this type of systems, the phenomenological MacArthur's consumer-resource model was proposed and it soon started to take hold. However, such framework is not able to explain the origin of the huge biodiversity empirically observed in real natural systems. In fact, it inevitably predicts the so-called Competitive Exclusion Principle (CEP): the number of surviving species is bounded from above by the number of resources present in the environment, in stark contrast with empirical observations.

This implies that such a phenomenological model might be lacking in something crucial to describe in a reliable fashion competitive communities. An huge literature hints that such a missing factor could be provided by the

inclusion of spatial effects, which have been thought to might help in promoting biodiversity sustenance and which are completely neglected in the original formulation. Motivated by this, we extended the model including spatial terms. As an exemplification, we took such terms to describe the exploration of the environment by the individuals in the form of dispersal fluxes accounting for chemotaxis/foraging along with diffusive motion. Nonetheless, the approach is not limited to a specific spatial effect, but it can be generalized to possibly account other spatially originated mechanisms. Then, in order to deal with mean-field equations, which are amenable to perform analytical investigations, and attracted by the possibility of employing the tools of Statistical Mechanics, we performed a coarse-graining procedure on the spatial degrees of freedom we just introduced. In this way we obtained a new quadratic term,which takes into account spatial contributions in an effective way, with the meaning of inter- and intra-species interactions on top of the implicit resource competition.

However, we also argued that this newly added competitive contribution has more general and ecologically meaningful interpretations. In fact, it can possibly be employed to capture other ecological mechanisms affecting the ecosystem evolution, such as the presence of host-specific pathogens harmful for the consumers population. We explicitly showed this having in mind the concrete case of tree communities, hence modeling the so called Janzen-Connel effect. Also in this case, taking into account effectively the host-pathogens dynamics, the consumers evolution was modified by the emergence of a quadratic inter- and intra-specific interaction term.

Starting from the modified framework, we analytically showed that it is now possible to violate CEP. Performing numerical simulations, we saw that at stationarity the number of species with a non-vanishing population size could be larger that the number of resources itself. Moreover, under some conditions, we could obtained an explicit criterion that allows us to state whether all the starting species would survive or not. In the limit-case of one resource, we were able to get an analytical condition on the model parameters that, if fulfilled, grants the survival of an arbitrary number of species. This scenario fully demonstrate the power of the new framework and how it can openly violate CEP.

Later on, we showed also how it is possible to infer, depending on the parameters, if some species would go extinct and, if so, which ones. Again, we found an analytical criterion, which has been tested against numerical simulations of the model dynamics. The same result was employed to predict the outcome of an invasion experiment, in which a new species enters in a community in which others species already coexists together.

Finally, we retrieved illuminating insights on the shape of a remarkable statistical pattern, the Species Abundance Distribution (SAD), which describes how the population sizes of the surviving species are scattered. In particular, we could uncover the emergence of power-law tails of such distributions as well as the range of (negative) values acquired by their exponents. In other words, we discovered that the probability of observing a species with a large population size decreases as power-law with a certain negative exponent.

Such a result turned out to be correct when it was compared with some empirical plankton datasets.

The second ecological complex feature that captured our attention was the self-emergence of spatial order on large scales in ecological contexts. In fact, several landscapes around the globe amazingly display an almost regular alternation of colonized and empty spots by the vegetation. The same behavior is observed also in theoretical investigations studying a possible mechanism that might have led to proto-speciation. There, species emerge as regular lumpy distributions in an abstract continuum space where each position is thought to identify a possible characteristic identifying a species. Both the pictures can be understood in terms of pattern formation, where the main element of the underlying dynamics is given by the nonlocalilty of the nonlinear interaction terms among the microscopic constituents, which eventually shape the emerging spatial structures.

Of course pattern formation is a phenomenon which is not relegated to ecology, but it is widely observed in other research fields. For this reason, in Chapter 3 we devoted our efforts in the research of any universal behavior shared across pattern forming systems, independently of the specific details of the process under consideration. To do so we built a generic model accounting for nonlocal nonlinear terms displaying a supercritical bifurcation, which separates the pattern forming phase to the one in which self-organized structures can not emerge. In this way the model eventually leads to the breaking of the translational symmetry in the stationary state. We first showed that in this general framework the mechanism from which patterns emerge is the instability of the homogeneous and stationary solution of the dynamics under small perturbations, as well documented in the literature.

Subsequently, we developed a mathematical framework, based on multiple scales analysis, to uncover the spatio-temporal evolution on long and large scales of the envelope of the emerging patterns. We discovered that, at the onset of the supercritical bifurcation and in the weakly nonlinear regime, the initial formation and the following evolution is determined by an universal equation. Namely, the form of this equation is model independent, whereas the dynamics details enter in the expressions giving its coefficients, which are naturally obtained within the proposed framework. In particular, we predicted that such an equation acquires the well-known shape of the *Ginzburg-Landau* (GL) amplitude equation. This became famous from the studies on the local *Swift-Hohenberg* model, which is regarded as an archetypal of pattern-forming dynamics. We analytically showed that GL amplitude equation validity goes beyond such a simple model and it can be employed to study more general dynamics, accounting also for nonlocal nonlinear contributions, which have remarkable ecological (but not only) meanings. To double-checked the quality of the result, we tested the GL amplitude equation prediction against the outcomes of numerical simulations of nonlocal dynamics to find an excellent agreement between the two.

Thanks to this, we concluded that the behavior of patterns at the onset of the bifurcation is universal, regardless the local or nonlocal nature of the interaction terms. This is a result in full similarity with universality features

at the transition point in critical phenomena studied by Statistical Mechanics, where in such a regime the microscopic details do not play any role in determining the system behavior.

Lastly, in Chapter 4 we focused on the development of a framework naturally accounting for stochastic and temporal delay effects, aiming to investigate if the combination of these two contributions might lead to cyclic dynamics. Indeed, the evidences coming from experiments on gene expression in self-regulatory networks has spurred the investigation of noisy and delayed systems. In fact, data resulting from such experiments show that the time series of mRNA and protein molecules concentrations present long-standing and almost regular oscillations in time.

For this reason, we proposed a very simple model in the form of a Langevin dynamics accounting also for delayed contributions, on top of the explicit noise modeling the intrinsic stochastic source. To start, we described the evolution of a single dynamical variable in presence of a discrete delayed term, which couples the evolution of the current state to one observed in the past system history.

In the first place, we studied the asymptotic stability of the homogeneous stationary state of the corresponding deterministic dynamics, identifying in particular the region of the parameters space where the solution approaches the stationary state via damped oscillations.

Later on, we took into account also the stochastic contribution of the Langevin dynamics. We first observed numerically the emergence of almost rhythmic dynamics in the typical time series associated to the process. Motivated by these evidences, we studied the spectral properties of such time series and we computed the power-spectrum of the fluctuations around the homogeneous stationary state of the deterministic dynamics.

From such expression, we obtained a condition on the model parameters for which the power-spectrum displays a non-trivial peak, i.e., its maximum is located in a positive and finite value. In this way the cyclic dynamics observed can be interpreted as a stochastic amplification phenomenon and so the indefinitely lasting oscillations, whose characteristic frequency are given by the position of the peak, are explained as noise-induced cycles. We remark that the addition of the delay drastically modify the scenario with respect to the non-delayed version. For example, it made possible the occurrence of this resonance phenomenon also in the case of a single dynamical variable, which would have been impossible in non-delayed settings. All these prediction were confirmed by comparing them with the outcomes of numerical simulations.

Additionally, in the case of a discrete delay, we interestingly showed that the presence of deterministic asymptotic oscillations is a necessary but not sufficient condition to observed stochastic amplification, i.e., it exists a region in the parameters space where the deterministic dynamics displays damped oscillations, nonetheless the simple introduction of noise might be not enough to ensure their resonance.

Continuing with a more theoretical investigation, we extended the framework to account also for distributed delay contributions. They provide a

more general description of memory effect since the evolution in such scenarios is influenced by a weighted average, given by a kernel, of the history of past states. Replicating the same steps, we predicted the a similar phenomenology with respect to the discrete delay scenario. In particular, also in this case we found the conditions on the model to ensure the emergence of a non-trivial peak in the power-spectrum.

However, studying a scenario where the kernel has an exponential form, we uncovered that there is a region of the model parameters where the system deterministically approaches the stationarity without damped oscillations, but the stochastic counterpart allows to the emergence of stochastic amplification, i.e., a deterministic damped oscillatory behavior is not anymore a necessary condition to observe noise-induced cycles. This behavior, to the best of our knowledge, has never been predicted before and also it can not be observed in the discrete delay case. We argued, supported by analytical calculations, that this odd behavior is due to the fact that in such a region, the deterministic solution crossed the stationary value once, resembling in this way a single oscillation, which will resonate with the noisy term of the Langevin equation.

To conclude, we applied our theoretical framework to gain an insight on the empirical observations emerging about gene expression networks, which motivated from a biological standpoint this work. Starting from a stochastic and delayed model describing the coupled temporal evolution of mRNA and protein molecules, we shed light on the origin of oscillations empirically observed, interpreting them as noise-induced cycles due to stochastic amplification. Remarkably, with respect to the deterministic models proposed in the literature so far, our framework does not require any tuning of the parameters to predict rhythmic dynamics, making it more appealing and reliable.

Appendix A

Appendix for Effective Resource-Competition Model for Species Coexistence

The contents presented in this Appendix, including the displayed figures, are taken with permission from the Supplemental Material accompanying the published paper [147]. Copyright (2021) by the American Physical Society.

A.1 Emergence of the quadratic competitive interaction term via coarse-graining

In this section, we present an argument that justifies how the quadratic interaction term, emerges quite generally in the consumer-resource model although it has a clear ecological interpretation by itself. In order to do so, we apply a coarse graining procedure on a spatially extended consumer-resource model where we consider motility terms due to diffusive motion along with foraging or chemotactic strategies. In principle, we could also account for crowding effects which modify the motility of the consumers. Such contributions could be modeled through the introduction of a superdiffusive behavior at high consumers concentration.

Let us start by considering the MacArthur's model for many species consuming only one resource. Thus there is no need for sub-indices for species and resources. To include spatial contributions in the dynamics, we add flux-terms motivated by the seminal work of Keller and Segel [182] in which the flux of the motion of species in the environment of resources are expressed as

$$J_n(x,t) = -D_1(c(x,t))\,\nabla n(x,t) + D_2(c(x,t))\,n(x,t)\,\nabla c(x,t). \tag{A.1}$$

Later studies pointed that $D_2(c) \sim (c + K_d)^{-2}$ [222], where K_d is the *receptor-ligand binding dissociation constant* [223]. Hence in the limit of small resource concentration, i.e., $c \ll K_d$, Eq. (A.1) can be written (up to the leading order in c) as

$$J_n(x,t) = -(A_1 + A_2 c(x,t))\,\nabla n(x,t) + A_3\,n(x,t)\,\nabla c(x,t). \tag{A.2}$$

where A_1, A_2, and A_3 are constants.

Therefore, the systems' dynamics is given by

$$\dot{n}_\sigma(x,t) = n(x,t)(\alpha_\sigma c(x,t) - \beta_\sigma) - \nabla J_{n_\sigma}(x,t), \tag{A.3}$$
$$\dot{c}(x,t) = s - \mu c(x,t) - c(x,t)\sum_\rho \alpha_\rho n_\rho(x,t). \tag{A.4}$$

Notice that we replaced the Monod function with $c(x,t)$, which is the leading order in a small c expansion.

Substituting J_{n_σ} from Eq. (A.2), we rewrite Eqs (A.3) and (A.4) as

$$\dot{n}_\sigma(x,t) = n(x,t)(\alpha_\sigma c(x,t) - \beta) + \Big(A_{1,\sigma} + A_{2,\sigma}c(x,t)\Big)\,\nabla^2 n_\sigma(x,t) + \\ - A_{3,\sigma}\, n_\sigma(x,t)\,\nabla^2 c(x,t) + (A_{2,\sigma} - A_{3,\sigma})\nabla n_\sigma(x,t)\cdot\nabla c(x,t), \tag{A.5}$$
$$\dot{c}(x,t) = s - \mu c(x,t) - c(x,t)\sum_\rho \alpha_\rho n_\rho(x,t). \tag{A.6}$$

Next we consider the case in which the spatial variable is discrete in a one-dimensional lattice, where each site, i, represents a patch of linear size a with populations $n_\sigma^{(i)}$ and a resource concentration $c^{(i)}$. Notice that the super-indices refer to spatial position. Therefore, we have

$$\dot{n}_\sigma^{(i)}(t) = n_\sigma^{(i)}(t)[\alpha c^{(i)}(t) - \beta] + [A_1 + A_2 c^{(i)}(t)]\big[n_\sigma^{(i+1)}(t) + n_\sigma^{(i-1)}(t) - 2n_\sigma^{(i)}(t)\big] + \\ - A_3 n_\sigma^{(i)}(t)\big[c^{(i+1)}(t) + c^{(i-1)}(t) - 2c^{(i)}(t)\big] + \\ + (A_2 - A_3)\big[n_\sigma^{(i+1)}(t) - n_\sigma^{(i)}(t)\big]\big[c^{(i+1)}(t) - c^{(i)}(t)\big], \tag{A.7}$$
$$\dot{c}^{(i)}(t) = s - \mu c^{(i)}(t) - c^{(i)}(t)\sum_\rho \alpha_\rho n_\rho^{(i)}(t), \tag{A.8}$$

where $i \in \mathbb{Z}$ indicates the lattice site or the label for the patch. Thus, this model [Eqs. (A.7)-(A.8)] describes the migration of species from one patch to another for the consumption of the resource.

The coarse-graining consists in eliminating the dynamical variables $n_\sigma^{(i)}$ and $c^{(i)}$ corresponding to the odd positions in favour of the remaining ones in the even positions in the same spirit as in the first step of the renormalization group technique (see Refs. [183], [184]). The essence of the calculation can be exemplified by considering just one species of consumers colonizing two adjacent sites/patches $i = 1, 2$ with periodic boundary conditions. The complete calculation, besides being more cumbersome, does not present any technical difficulty and leads to the same result of inducing the quadratic competitive interaction term, $\sum_\rho \epsilon_{\sigma\rho} n_\sigma n_\rho$, in Eq. (2.2a). Hence, since we are considering a single population consuming only one resource, we can now drop the immaterial subscript for the species population. Thus the dynamics given in Eqs. (A.7) and (A.8) can be rewritten as

$$\dot{n}^{(1)} = n^{(1)}(\alpha c^{(1)} - \beta) + 2A_1\big(n^{(2)} - n^{(1)}\big) + (A_2 - A_3)\Big(n^{(2)}c^{(2)} - n^{(1)}c^{(1)}\Big) +$$

$$+ (A_2 + A_3)\left(n^{(2)}c^{(1)} - n^{(1)}c^{(2)}\right), \tag{A.9}$$

$$\dot{n}^{(2)} = n^{(2)}(\alpha c^{(2)} - \beta) + 2A_1\left(n^{(1)} - n^{(2)}\right) + (A_2 - A_3)\left(n^{(1)}c^{(1)} - n^{(2)}c^{(2)}\right) + + (A_2 + A_3)\left(n^{(1)}c^{(2)} - n^{(2)}c^{(1)}\right), \tag{A.10}$$

$$\dot{c}^{(1)} = s - \mu c^{(1)} - \alpha n^{(1)}c^{(1)}, \tag{A.11}$$

$$\dot{c}^{(2)} = s - \mu c^{(2)} - \alpha n_2 c^{(2)}, \tag{A.12}$$

where, for convenience, we are not writing explicitly the time dependence.

In order to proceed forward, let us first define Laplace transform and its inverse as follow

$$\tilde{\Omega}(\omega) = \mathcal{L}\left[\Omega(t)\right](\omega) = \int_0^{+\infty} dt\, e^{-\omega t}\, \Omega(t), \tag{A.13}$$

$$\Omega(t) = \mathcal{L}^{-1}\left[\tilde{\Omega}(\omega)\right](t) = \frac{1}{2\pi i}\lim_{\gamma\to\infty}\int_{a-i\gamma}^{a+i\gamma} d\omega\, e^{\omega t}\, \tilde{\Omega}(\omega), \tag{A.14}$$

where a is such that all singularities of $\tilde{\Omega}(\omega)$ are in the region $\Re(\omega) < a$.

Now Laplace transform of Eqs. (A.9)–(A.12) gives

$$\omega\tilde{n}^{(1)}(\omega) - n^{(1)}(0) = -\beta\tilde{n}^{(1)}(\omega) + \alpha\tilde{n}^{(1)}(\omega) * \tilde{c}^{(1)}(\omega) + 2A_1\left(\tilde{n}^{(2)}(\omega) - \tilde{n}^{(1)}(\omega)\right) + + (A_2 - A_3)\left(\tilde{n}^{(2)}(\omega) * \tilde{c}^{(2)}(\omega) - \tilde{n}^{(1)}(\omega) * \tilde{c}^{(1)}(\omega)\right) + + (A_2 + A_3)\left(\tilde{n}^{(2)}(\omega) * \tilde{c}^{(1)}(\omega) - \tilde{n}^{(1)}(\omega) * \tilde{c}^{(2)}(\omega)\right), \tag{A.15}$$

$$\omega\tilde{n}^{(2)}(\omega) - n^{(2)}(0) = -\beta\tilde{n}^{(2)}(\omega) + \alpha\tilde{n}^{(2)}(\omega) * \tilde{c}^{(2)}(\omega) + 2A_1\left(\tilde{n}^{(1)}(\omega) - \tilde{n}^{(2)}(\omega)\right) + + (A_2 - A_3)\left(\tilde{n}^{(1)}(\omega) * \tilde{c}^{(1)}(\omega) - \tilde{n}^{(2)}(\omega) * \tilde{c}^{(2)}(\omega)\right) + + (A_2 + A_3)\left(\tilde{n}^{(1)}(\omega) * \tilde{c}^{(2)}(\omega) - \tilde{n}^{(2)}(\omega) * \tilde{c}^{(1)}(\omega)\right), \tag{A.16}$$

$$\omega\tilde{c}^{(1)}(\omega) - c^{(1)}(0) = \tilde{s}(\omega) - \mu\tilde{c}^{(1)}(\omega) - \alpha\tilde{n}^{(1)}(\omega) * \tilde{c}^{(1)}(\omega), \tag{A.17}$$

$$\omega\tilde{c}^{(2)}(\omega) - c^{(2)}(0) = \tilde{s}(\omega) - \mu\tilde{c}^{(2)}(\omega) - \alpha\tilde{n}^{(2)}(\omega) * \tilde{c}^{(2)}(\omega), \tag{A.18}$$

where $n_i(0)$ and $c_i(0)$ are the initial conditions of the system and the symbol $*$ indicates the convolution of the functions in the complex plane defined as

$$\mathcal{L}\left[n^{(2)}(t)c^{(1)}(t)\right](\omega) = \tilde{n}^{(2)}(\omega) * \tilde{c}^{(1)}(\omega) = \frac{1}{2\pi i}\lim_{\gamma\to\infty}\int_{a-i\gamma}^{a+i\gamma} d\omega'\, \tilde{n}^{(2)}(\omega')c^{(1)}(\omega - \omega') \tag{A.19}$$

We can recast Eqs. (A.15)–(A.18) as follows:

$$(\omega + \beta + 2A_1)\,\tilde{n}^{(1)}(\omega) = n^{(1)}(0) + 2A_1\tilde{n}^{(2)}(\omega) + \Big[\alpha\tilde{n}^{(1)}(\omega) * \tilde{c}^{(1)}(\omega) + + (A_2 - A_3)\left(\tilde{n}^{(2)}(\omega) * \tilde{c}^{(2)}(\omega) - \tilde{n}^{(1)}(\omega) * \tilde{c}^{(1)}(\omega)\right) +$$

$$+ (A_2 + A_3)\left(\tilde{n}^{(2)}(\omega) * \tilde{c}^{(1)}(\omega) - \tilde{n}^{(1)}(\omega) * \tilde{c}^{(2)}(\omega)\right)\Big], \tag{A.20}$$

$$\begin{aligned}(\omega + \beta + 2A_1)\,\tilde{n}^{(2)}(\omega) = n^{(2)}(0) + 2A_1\tilde{n}^{(1)}(\omega) + \Big[&\alpha\tilde{n}^{(2)}(\omega) * \tilde{c}^{(2)}(\omega) + \\ &+ (A_2 - A_3)\big(\tilde{n}^{(1)}(\omega) * \tilde{c}^{(1)}(\omega) - \tilde{n}^{(2)}(\omega) * \tilde{c}^{(2)}(\omega)\big) + \\ &+ (A_2 + A_3)\left(\tilde{n}^{(1)}(\omega) * \tilde{c}^{(2)}(\omega) - \tilde{n}^{(2)}(\omega) * \tilde{c}^{(1)}(\omega)\right)\Big],\end{aligned} \tag{A.21}$$

$$(\omega + \mu)\,\tilde{c}^{(1)}(\omega) = c^{(1)}(0) + \tilde{s}(\omega) - \alpha\tilde{n}^{(1)}(\omega) * \tilde{c}^{(1)}(\omega), \tag{A.22}$$

$$(\omega + \mu)\,\tilde{c}^{(2)}(\omega) = c^{(2)}(0) + \tilde{s}(\omega) - \alpha\tilde{n}^{(2)}(\omega) * \tilde{c}^{(2)}(\omega). \tag{A.23}$$

Now to implement the coarse-graining procedure we employ a standard perturbative approach where the non-linear terms, i.e., terms containing the convolution $\tilde{n}^{(i)}(\omega) * \tilde{c}^{(j)}(\omega)$ with $i, j = 1, 2$, are treated as perturbation to the linear terms. This is a procedure largely employed in the renormalization group technique, where to advance analytically the non-linear terms are regarded as small with respect to the linear contributions [183], [184]. To help us in the implementation of the pertubative approach, it is convenient to formally substitute

$$\tilde{n}^{(i)}(\omega) \longrightarrow \delta\tilde{n}^{(i)}(\omega). \tag{A.24}$$

in terms of the form $\tilde{n}^{(i)}(\omega) * \tilde{c}^{(j)}(\omega)$ with $i, j = 1, 2$, where δ is an abstract parameter. In particular, we are now going to use it as the expansion parameter in order to express $\tilde{n}^{(1)}(\omega)$ and $\tilde{c}^{(1)}(\omega)$ in terms of $\tilde{n}^{(2)}(\omega)$ and $\tilde{c}^{(2)}(\omega)$ up to terms of order δ^2 performing in this way the desired coarse-graining. Additionally we assume $n^{(1)}(0) = c^{(1)}(0) = 0$. Once this procedure has been carried out (the calculations are straightforward and yet cumbersome, so we avoid the full presentation of all the intermediate steps), we can plug such expressions into Eq. (A.21). In this way we remove from the dynamics the patch 1 by taking into account its contribution in an effective way. Neglecting order δ^3 terms or higher, we obtain

$$\begin{aligned}\omega\tilde{n}^{(2)}(\omega) = n_2(0) - &\left(\beta + 2A_1 - \frac{4A_1^2}{\omega + \beta + 2A_1}\right)\tilde{n}^{(2)}(\omega) + \\ &+ \delta\Bigg\{\left(\alpha - A_2 + A_3 + \frac{2A_1(A_2 + A_3)}{\omega + \beta + 2A_1}\right)\tilde{n}^{(2)}(\omega) * \tilde{c}^{(2)}(\omega) + \\ &+ \frac{2A_1(A_2 + A_3)}{\omega + \beta + 2A_1}\left(\frac{\tilde{s}(\omega)}{\omega + \mu}\right) * \tilde{n}^{(2)}(\omega) - (A_2 + A_3)\tilde{n}^{(2)}(\omega) * \left(\frac{\tilde{s}(\omega)}{\omega + \mu}\right) + \\ &+ \frac{4A_1^2(\alpha - A_2 + A_3)}{\omega + \beta + 2A_1}\left(\frac{\tilde{n}^{(2)}(\omega)}{\omega + \beta + 2A_1}\right) * \left(\frac{\tilde{s}(\omega)}{\omega + \mu}\right) + \\ &- \frac{4A_1^2(A_2 + A_3)}{\omega + \beta + 2A_1}\left(\frac{\tilde{n}^{(2)}(\omega)}{\omega + \beta + 2A_1}\right) * \tilde{c}^{(2)}(\omega) - (A_2 + A_3)\tilde{n}^{(2)}(\omega) * \left(\frac{\tilde{s}(\omega)}{\omega + \mu}\right) +\end{aligned}$$

$$
\begin{aligned}
&+ 2A_1(A_2+A_3)\tilde{c}^{(2)}(\omega) * \left(\frac{\tilde{n}^{(2)}(\omega)}{\omega+\beta+2A_1}\right) + \\
&+ 2A_1(A_2-A_3)\left(\frac{\tilde{s}(\omega)}{\omega+\mu}\right) * \left(\frac{\tilde{n}^{(2)}(\omega)}{\omega+\beta+2A_1}\right)\Bigg\} + \\
&+ \delta^2\Bigg\{\frac{8A_1^3\alpha(\alpha-A_2+A_3)}{\omega+\beta+2A_1}\left[\left(\frac{\tilde{n}^{(2)}(\omega)}{\omega+\beta+2A_1}\right) * \left(\frac{\left(\frac{\tilde{n}^{(2)}(\omega)}{\omega+\beta+2A_1}\right) * \left(\frac{\tilde{s}(\omega)}{\omega+\mu}\right)}{\omega+\mu}\right)\right] + \\
&- \frac{2A_1(A_2-A_3)(A_2+A_3)}{\omega+\beta+2A_1}\left[\left(\frac{\tilde{n}^{(2)}(\omega)*\tilde{c}^{(2)}(\omega)}{\omega+\beta+2A_1}\right) * \tilde{c}^{(2)}(\omega)\right] + \\
&- \frac{4A_1^2\alpha(A_2+A_3)}{\omega+\beta+2A_1}\left[\left(\frac{\left(\frac{\tilde{s}(\omega)}{\omega+\mu}\right) * \left(\frac{\tilde{n}^{(2)}(\omega)}{\omega+\beta+2A_1}\right)}{\omega+\mu}\right) * \tilde{n}^{(2)}(\omega)\right] + \\
&+ \frac{4A_1^2(\alpha-A_2+A_3)^2}{\omega+\beta+2A_1}\left[\left(\frac{\tilde{s}(\omega)}{\omega+\mu}\right) * \left(\frac{\left(\frac{\tilde{s}(\omega)}{\omega+\mu}\right) * \left(\frac{\tilde{n}^{(2)}(\omega)}{\omega+\beta+2A_1}\right)}{\omega+\beta+2A_1}\right)\right] + \\
&+ \frac{2A_1(A_2-A_3)(\alpha-A_2+A_3)}{\omega+\beta+2A_1}\left[\left(\frac{\tilde{s}(\omega)}{\omega+\mu}\right) * \left(\frac{\tilde{n}^{(2)}(\omega)*\tilde{c}^{(2)}(\omega)}{\omega+\beta+2A_1}\right)\right] + \\
&+ \frac{2A_1(A_2+A_3)(\alpha-A_2+A_3)}{\omega+\beta+2A_1}\left[\left(\frac{\tilde{s}(\omega)}{\omega+\mu}\right) * \left(\frac{\tilde{n}^{(2)}(\omega)*\left(\frac{\tilde{s}(\omega)}{\omega+\mu}\right)}{\omega+\beta+2A_1}\right)\right] + \\
&- \frac{4A_1^2(A_2+A_3)(\alpha-A_2+A_3)}{\omega+\beta+2A_1}\left[\left(\frac{\tilde{s}(\omega)}{\omega+\mu}\right) * \left(\frac{\tilde{c}^{(2)}(\omega)*\left(\frac{\tilde{n}^{(2)}(\omega)*\tilde{c}^{(2)}(\omega)}{\omega+\beta+2A_1}\right)}{\omega+\beta+2A_1}\right)\right] + \\
&- \frac{4A_1^2(A_2+A_3)(\alpha-A_2+A_3)}{\omega+\beta+2A_1}\left[\tilde{c}^{(2)}(\omega) * \left(\frac{\left(\frac{\tilde{s}(\omega)}{\omega+\mu}\right) * \left(\frac{\tilde{n}^{(2)}(\omega)*\tilde{c}^{(2)}(\omega)}{\omega+\beta+2A_1}\right)}{\omega+\beta+2A_1}\right)\right] + \\
&- \frac{2A_1(A_2+A_3)^2}{\omega+\beta+2A_1}\left[\tilde{c}^{(2)}(\omega) * \left(\frac{\tilde{n}^{(2)}(\omega)*\left(\frac{\tilde{s}(\omega)}{\omega+\mu}\right)}{\omega+\beta+2A_1}\right)\right] + \\
&+ \frac{4A_1^2(A_2+A_3)^2}{\omega+\beta+2A_1}\left[\tilde{c}^{(2)}(\omega) * \left(\frac{\tilde{c}^{(2)}(\omega)*\left(\frac{\tilde{n}^{(2)}(\omega)}{\omega+\beta+2A_1}\right)}{\omega+\beta+2A_1}\right)\right] + \\
&+ 2A_1\alpha(A_2+A_3)\left[\tilde{n}^{(2)}(\omega) * \left(\frac{\left(\frac{\tilde{s}(\omega)}{\omega+\mu}\right) * \left(\frac{\tilde{n}^{(2)}(\omega)}{\omega+\beta+2A_1}\right)}{\omega+\mu}\right)\right] + \\
&+ 2A_1(A_2+A_3)(\alpha-A_2+A_3)\left[\tilde{c}^{(2)}(\omega) * \left(\frac{\left(\frac{\tilde{s}(\omega)}{\omega+\mu}\right) * \left(\frac{\tilde{n}^{(2)}(\omega)}{\omega+\beta+2A_1}\right)}{\omega+\mu}\right)\right] +
\end{aligned}
$$

$$
\begin{aligned}
&+ (A_2 + A_3)(A_2 - A_3)\left[\tilde{c}^{(2)}(\omega) * \left(\frac{\tilde{n}^{(2)}(\omega) * \tilde{c}^{(2)}(\omega)}{\omega + \beta + 2A_1}\right)\right] + \\
&+ (A_2 + A_3)^2\left[\tilde{c}^{(2)}(\omega) * \left(\frac{\tilde{n}^{(2)}(\omega) * \left(\frac{\tilde{s}(\omega)}{\omega+\mu}\right)}{\omega + \beta + 2A_1}\right)\right] + \\
&- 2A_1(A_2 + A_3)^2\left[\tilde{c}^{(2)}(\omega) * \left(\frac{\tilde{c}^{(2)}(\omega) * \left(\frac{\tilde{n}^{(2)}(\omega)}{\omega+\beta+2A_1}\right)}{\omega + \beta + 2A_1}\right)\right] + \\
&- 4A_1^2\alpha(A_2 - A_3)\left[\left(\frac{\tilde{n}^{(2)}(\omega)}{\omega + \beta + 2A_1}\right) * \left(\frac{\left(\frac{\tilde{s}(\omega)}{\omega+\mu}\right) * \left(\frac{\tilde{n}^{(2)}(\omega)}{\omega+\beta+2A_1}\right)}{\omega + \mu}\right)\right] + \\
&+ 2A_1(A_2 - A_3)(\alpha - A_2 + A_3)\left[\left(\frac{\tilde{s}(\omega)}{\omega + \mu}\right) * \left(\frac{\left(\frac{\tilde{s}(\omega)}{\omega+\mu}\right) * \left(\frac{\tilde{n}^{(2)}(\omega)}{\omega+\beta+2A_1}\right)}{\omega + \mu}\right)\right] + \\
&+ (A_2 - A_3)(A_2 + A_3)\left[\left(\frac{\tilde{s}(\omega)}{\omega + \mu}\right) * \left(\frac{\tilde{n}^{(2)}(\omega) * \left(\frac{\tilde{s}(\omega)}{\omega+\mu}\right)}{\omega + \beta + 2A_1}\right)\right] + \\
&- 2A_1(A_2 - A_3)(A_2 + A_3)\left[\left(\frac{\tilde{s}(\omega)}{\omega + \mu}\right) * \left(\frac{\tilde{c}^{(2)}(\omega) * \left(\frac{\tilde{n}^{(2)}(\omega)}{\omega+\beta+2A_1}\right)}{\omega + \beta + 2A_1}\right)\right] + \\
&+ (A_2 - A_3)^2\left[\left(\frac{\tilde{s}(\omega)}{\omega + \mu}\right) * \left(\frac{\tilde{n}^{(2)}(\omega) * \tilde{c}^{(2)}(\omega)}{\omega + \beta + 2A_1}\right)\right]\Bigg\} + \mathcal{O}(\delta^3)
\end{aligned}
\tag{A.25}
$$

Since we are interested in the large-time limit, where both $\dot{n}^{(2)}$ and $\dot{c}^{(2)}$ are small, the above formula can be simplified as follows. For example, the inverse Laplace transform of $\tilde{n}^{(2)}(\omega)/(\omega + \omega_0)$, with $\beta + 2A_1 \equiv \omega_0 > 0$, is:

$$
\mathcal{L}^{-1}\left[\frac{\tilde{n}^{(2)}(\omega)}{\omega + \omega_0}\right](t) = \int_0^t dt'\, n^{(2)}(t') e^{-\omega_0(t-t')} \tag{A.26}
$$

$$
= \frac{1}{\omega_0}\left(n^{(2)}(t) - n^{(2)}(0)e^{-t\omega_0} - \int_0^t dt'\, \dot{n}^{(2)}(t') e^{-\omega_0(t-t')}\right) \tag{A.27}
$$

$$
\approx \frac{n^{(2)}(t)}{\omega_0} \tag{A.28}
$$

when $t \gg \omega_0^{-1}$. Notice that we use integration by parts to reach Eq. (A.27) from Eq. (A.26). In order to make this more formal we simply introduce a parameter τ multiplying the time derivatives in Eqs. (A.9)–(A.12). This leads to a simple modification of the Eq. (A.25) where all ω's are multiplied by τ except for the ω's appearing as arguments of the functions $\tilde{n}^{(2)}(\omega)$, $\tilde{c}^{(2)}(\omega)$

and $\tilde{s}(\omega)$. In the small τ limit, and redefining $\tilde{n}^{(2)}(\omega)$ as

$$\tilde{n}'^{(2)}(\omega) \equiv \left[1+\left(\frac{2A_1}{\beta+2A_1}\right)^2\right]\tilde{n}^{(2)}(\omega), \tag{A.29}$$

we get (now we drop the super-indices)

$$\tau\dot{n}'(t) = n'(t)\left(\alpha'[c(t)]c(t)-\beta'\right)-\epsilon' n'^2(t), \tag{A.30}$$

with

$$\begin{aligned}
\beta' &= \left(C_1+\delta\, s\, C_2+\delta^2\, s^2\, C_3\right)\left[1+\left(\frac{2A_1}{\beta+2A_1}\right)^2\right]^{-1}+\mathcal{O}(\tau\delta),\\
\alpha'[c(t)] &= \left(\delta\, C_4+\delta^2\, s\, C_5+\delta^2\, C_6\, c(t)\right)\left[1+\left(\frac{2A_1}{\beta+2A_1}\right)^2\right]^{-1}+\mathcal{O}(\tau\delta),\\
\epsilon' &= \delta^2 s\, C_7\left[1+\left(\frac{2A_1}{\beta+2A_1}\right)^2\right]^{-2}+\mathcal{O}(\tau\delta^2),
\end{aligned} \tag{A.31}$$

where

$$\begin{aligned}
C_1 &= \beta\left(\frac{\beta+4A_1}{\beta+2A_1}\right),\\
C_2 &= -\frac{1}{\mu}\left(\frac{4A_1A_2}{\beta+2A_1}+\frac{4A_1^2(\alpha-A_2+A_3)}{(\beta+2A_1)}-(A_2+A_3)\right),\\
C_3 &= -\frac{1}{\mu^2(\beta+2A_1)}\left(\frac{4A_1^2(\alpha-A_2+A_3)^2}{(\beta+2A_1)^2}+\frac{4A_1A_2(\alpha-A_2+A_3)}{\beta+2A_1}+A_2^2-A_3^2\right),\\
C_4 &= \left(\alpha-A_2+A_3+\frac{4A_1A_2}{\beta+2A_1}-\frac{4A_1^2(A_2+A_3)}{(\beta+2A_1)^2}\right),\\
C_5 &= \frac{2}{\mu(\beta+2A_1)}\left(-\frac{4A_1^2(\alpha-A_2+A_3)(A_2+A_3)}{(\beta+2A_1)^2}+A_2^2+A_3^2+\frac{2A_1A_2(\alpha-2A_2)}{\beta+2A_1}\right),\\
C_6 &= \frac{1}{\beta+2A_1}\left(-\frac{4A_1A_2(A_2+A_3)}{\beta+2A_1}+\frac{4A_1^2(A_2+A_3)^2}{(\beta+2A_1)^2}+A_2^2-A_3^2\right),\\
C_7 &= \frac{2A_1\alpha}{\mu^2(\beta+2A_1)}\left(\frac{4A_1^2(\alpha-A_2+A_3)}{(\beta+2A_1)^2}+\frac{4A_1A_2}{\beta+2A_1}-(A_2+A_3)\right).
\end{aligned} \tag{A.32}$$

Hence, we can see from Eq. (A.30) that we ended up with a mean-field equation for the consumer population that, on top of the classical growth and death terms of the MacArthur's model, contains also a quadratic competitive contribution. This is exactly the term we aimed to get for our model shown in Eqs. (2.2a)-(2.2b), here for the particular case of one species and one

resource. Notice also that the quantity $n'(t)$ in Eq. (A.30) is a rescaled population density with respect to $n^{(2)}(t)$, as shown in Eq. (A.29), which becomes the effective consumer concentration due to the coarse-graining procedure, the one studied in Chapter 2.

Summarizing the main steps that led us to obtain this result, we first discretized the space assuming that the dynamics takes place in two separated patches where locally the evolution is given by the classical MacArthur's consumer-resource model and, in addition to this, consumers are free to move from one patch to the other according to the fluxes terms presented at the beginning of this Section. Then, we explicitly implemented the coarse-graining procedure as follows: we expressed the quantities, i.e., the consumer density and the resource concentration, of patch one solely as functions of the same quantities of patch two using a perturbative approach to handle the non-linear terms. Later, we plugged the expressions for the densities of consumers and resource of patch one just found into the equations describing the evolution of the quantities at patch two. In this way, we integrated the spatial degrees of freedom of patch one and we remained with the evolution equation of consumers at patch two that depends only on resource concentration and consumers density in the same position.

The new term in Eq. (A.30) emerged from the coarse-graining procedure and hence it is a reminiscence of the spatial effects, capturing them in an effective way. As a confirmation, we can see that such term vanishes when the space does not play any significant role, for example when the system is either well-mixed or it has a spatial extension much smaller than the spatial scale of the diffusion. In fact, in the limit $A_1 \approx 0$, i.e., no diffusion, the coefficient C_7 shown in Eq. (A.32) vanishes and so, from Eq. (A.31) we have that $\epsilon' \approx 0$.

Finally, notice that the effect of the coarse-graining leads to a "renormalization" of the growth, the term linear in n, which is an expansion in the resource concentration, c, and in the resource supply, s.

Similarly, one can extend the above derivation considering many species competing for a single resource. The same steps can be repeated, minding the subscripts indicating the different species. Without displaying the full calculations, again in the small τ limit we need to redefine

$$\tilde{n}'_\sigma(\omega) \equiv \left[1 + \left(\frac{2A_{1,\sigma}}{\beta_\sigma + 2A_{1,\sigma}}\right)^2\right] \tilde{n}_\sigma(\omega), \tag{A.33}$$

and so we get

$$\tau \dot{n}'_\sigma(t) = n'_\sigma(t)\left(\alpha'_\sigma[c(t)]c(t) - \beta'_\sigma\right) - \sum_\rho \epsilon'_{\sigma\rho} n'_\sigma(t) n'_\rho(t), \tag{A.34}$$

with

$$\beta'_\sigma = \left(C_{1,\sigma} + \delta\, s\, C_{2,\sigma} + \delta^2\, s^2\, C_{3,\sigma}\right)\left[1 + \left(\frac{2A_{1,\sigma}}{\beta_\sigma + 2A_{1,\sigma}}\right)^2\right]^{-1} + \mathcal{O}(\tau\delta),$$

$$\alpha'_\sigma[c(t)] = \left(\delta\, C_{4,\sigma} + \delta^2\, s\, C_{5,\sigma} + \delta^2\, C_{6,\sigma}\, c(t)\right)\left[1+\left(\frac{2A_{1,\sigma}}{\beta_\sigma+2A_{1,\sigma}}\right)^2\right]^{-1} + \mathcal{O}(\tau\delta),$$
$$\epsilon'_{\sigma\rho} = \delta^2\, s\, C_{7,\sigma\rho}\left[1+\left(\frac{2A_{1,\sigma}}{\beta_\sigma+2A_{1,\sigma}}\right)^2\right]^{-1}\left[1+\left(\frac{2A_{1,\rho}}{\beta_\rho+2A_{1,\rho}}\right)^2\right]^{-1} + \mathcal{O}(\tau\delta^2), \tag{A.35}$$

where

$$C_{1,\sigma} = \beta_\sigma\left(\frac{\beta_\sigma+4A_{1,\sigma}}{\beta_\sigma+2A_{1,\sigma}}\right),$$
$$C_{2,\sigma} = -\frac{1}{\mu}\left(\frac{4A_{1,\sigma}A_{2,\sigma}}{(\beta_\sigma+2A_{1,\sigma})}+\frac{4A_{1,\sigma}^2(\alpha_\sigma-A_{2,\sigma}+A_{3,\sigma})}{(\beta_\sigma+2A_{1,\sigma})^2}-(A_{2,\sigma}+A_{3,\sigma})\right),$$
$$C_{3,\sigma} = -\frac{1}{\mu^2(\beta_\sigma+2A_{1,\sigma})}\left(\frac{4A_{1,\sigma}^2(\alpha_\sigma-A_{2,\sigma}+A_{3,\sigma})^2}{(\beta_\sigma+2A_{1,\sigma})^2}+A_{2,\sigma}^2-A_{3,\sigma}^2+\right.$$
$$\left.+\frac{4A_{1,\sigma}A_{2,\sigma}(\alpha_\sigma-A_{2,\sigma}+A_{3,\sigma})}{\beta_\sigma+2A_{1,\sigma}}\right),$$
$$C_{4,\sigma} = \left(\alpha_\sigma-A_{2,\sigma}+A_{3,\sigma}+\frac{4A_{1,\sigma}A_{2,\sigma}}{\beta_\sigma+2A_{1,\sigma}}-\frac{4A_{1,\sigma}^2(A_{2,\sigma}+A_{3,\sigma})}{(\beta_\sigma+2A_{1,\sigma})^2}\right),$$
$$C_{5,\sigma} = \frac{2}{\mu(\beta_\sigma+2A_{1,\sigma})}\left(-\frac{4A_{1,\sigma}^2(\alpha_\sigma-A_{2,\sigma}+A_{3,\sigma})(A_{2,\sigma}+A_{3,\sigma})}{(\beta_\sigma+2A_{2,\sigma})^2}+A_{2,\sigma}^2+A_{3,\sigma}^2+\right.$$
$$\left.+\frac{2A_{1,\sigma}A_{2,\sigma}(\alpha_\sigma-2A_{2,\sigma})}{\beta_\sigma+2A_{1,\sigma}}\right),$$
$$C_{6,\sigma} = \frac{1}{\beta_\sigma+2A_{1,\sigma}}\left(-\frac{4A_{1,\sigma}A_{2,\sigma}(A_{2,\sigma}+A_{3,\sigma})}{\beta_\sigma+2A_{1,\sigma}}+\frac{4A_{1,\sigma}^2(A_{2,\sigma}+A_{3,\sigma})^2}{(\beta_\sigma+2A_{1,\sigma})^2}+A_{2,\sigma}^2-A_{3,\sigma}^2\right),$$
$$C_{7,\sigma\rho} = \frac{2A_{1,\rho}\alpha_\rho}{\mu^2\left(\beta_\rho+2A_{1,\rho}\right)}\left(\frac{4A_{1,\sigma}^2(\alpha_\sigma-A_{2,\sigma}+A_{3,\sigma})}{(\beta_\sigma+2A_{1,\sigma})^2}+\frac{4A_{1,\sigma}A_{2,\sigma}\alpha_\sigma}{\beta_\sigma+2A_{1,\sigma}}-(A_{2,\sigma}+A_{3,\sigma})\right). \tag{A.36}$$

A.2 Emergence of the quadratic competitive interaction via Janzen-Connell effect

In this section, we derive our effective consumer-resource model Eqs. (2.2a)-(2.2b) by incorporating the Janzen-Connell effect into the classical MacArthur's model. In this setting, the population of the species and pathogens (where

latter survive on the species population) along with the resource concentration co-evolve according to following coupled differential equations:

$$\dot{n}_\sigma = n_\sigma \left[\sum_{i=1}^{R} \alpha_{\sigma i} r_i(c_i) - \beta_\sigma \right] - n_\sigma \sum_{a=1}^{M_P} A_{\sigma a}^{(p)} p_a, \tag{A.37}$$

$$\dot{c}_i = \mu_i(\Lambda_i - c_i) - r_i(c_i) \sum_{\sigma=1}^{M} n_\sigma \alpha_{\sigma i}, \tag{A.38}$$

$$\dot{p}_a = p_a \sum_{\rho=1}^{M} B_{a\rho}^{(p)} n_\rho - k_a^{(p)} p_a^2, \tag{A.39}$$

where p_a denotes the population of the pathogens at time t, and M_P is the number of kinds of pathogens. Due to the presence of the pathogens, the populations of the species degrade and such effect can be written as the last term in Eq. (A.37), where the matrix $A^{(p)}$ describes the degradation rate of each species population due to interaction with the surrounding pathogens. Similarly, these interactions benefits the pathogens and are encoded in the benefit matrix $B^{(p)}$ in Eq. (A.39), where each elements of this matrix corresponds to the benefit rate for the pathogens. The last term in Eq. (A.39) limits the growth of the pathogens' population (i.e., the carrying capacity term), where $1/k_a^{(p)}$ is the carrying capacity for pathogen a.

Evidently the time-scale associated with the growth of the pathogens is much faster than that of n_σ and c_i. Therefore, the pathogen dynamics (A.39) reaches stationary state much sooner than the species and resource dynamics (A.37) and (A.38), respectively. So by employing such time-scale separations, the stationary solution of Eq (A.39) is given by

$$p_a(t) \sum_{\rho=1}^{M} B_{a\rho}^{(p)} n_\rho(t) - k_a^{(p)} p_a^2(t) = 0, \tag{A.40}$$

where $p_a(t)$ is the instantaneous stationary values of pathogen for the actual species population $n_\sigma(t)$.

The non-trivial solution of the above equation is

$$\vec{P}(t) = [K^{(p)}]^{-1} B^{(p)} \vec{\mathcal{N}}(t), \tag{A.41}$$

where $K^{(p)} = \text{diag}\left[k_1^{(p)}, k_2^{(p)}, \ldots, k_{M_P}^{(p)}\right]$ is a diagonal matrix. Substituting the instantaneous values of the pathogen populations in Eq. (A.37), we get Eqs. (2.2a)-(2.2b) where the matrix elements $\epsilon_{\sigma\rho}$ can be identified as

$$\epsilon_{\sigma\rho} \equiv \sum_{a=1}^{M_P} \frac{A_{\sigma a}^{(p)} B_{a\rho}^{(p)}}{k_a^{(p)}}. \tag{A.42}$$

Notice that when there are pathogens which are specific to each species in the environment, and so $M_P = M$, the benefit matrix $B^{(p)}$ and degradation

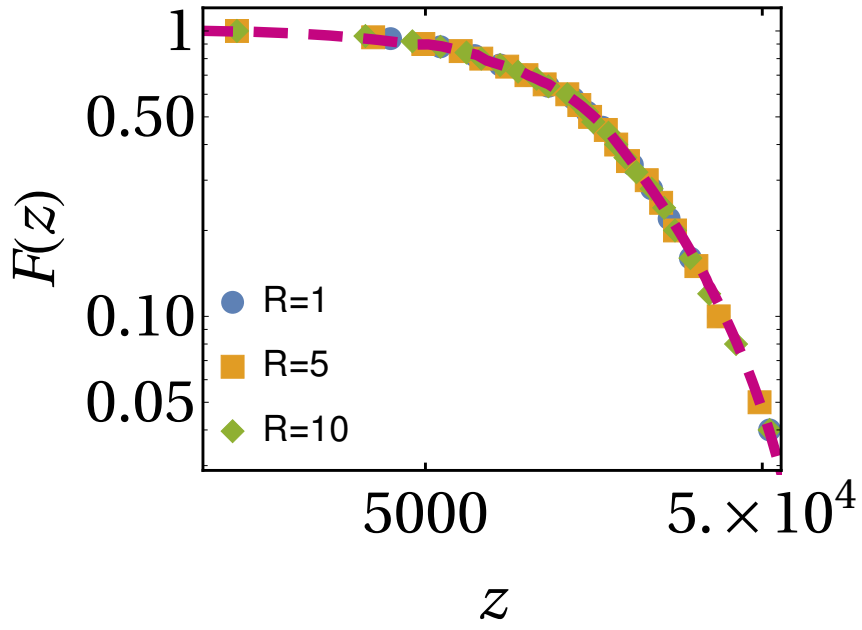

FIGURE A.1: CCDF for the population sizes of 500 species competing for 1, 5, and 10 resources. The symbols are obtained from numerically integrating Eqs. (A.43)-(A.44). The solid line is the analytical result for $R = 1$ given in Eq. (2.41). Clearly, we can see that there is no dependence on the number of resources. Other parameters are $\alpha_\sigma \sim \mathcal{U}(1.5, 10.0)$, $\beta_\sigma = 1$, $\mu = 0.001$, $\epsilon_\sigma \sim \mathcal{U}(0.0001, 0.0005)$, $k_i = 5$ and $\Lambda = 10^{12}$.

matrix $A^{(p)}$ become diagonal which eventually leads to a diagonal form of matrix E.

A.3 Discussion for the cases with $R > 1$

In this section, we give the details on the simulation for $R > 1$ shown in Figures 2.4 (a), 2.6 (a) and A.3. As already mentioned in Chapter 2 that we can compute the exact curve for surviving species when these are competing one resource. However, such exact computation for $R > 1$ is not illuminating to us. Nevertheless, one can count the number of surviving species for a given Λ_i, where $1 \leq i \leq R$ by numerically integrating Eqs. (2.2a)-(2.2b).

To compare the result for $R = 1$ and $R > 1$, we do a slight modification in our model, where we consider that all resources have same supply, i.e., $\Lambda_i = \Lambda$ for all i. Further, we assume that the metabolic strategies $\alpha_{\sigma i} = \alpha_\sigma q_i$, where $q_i \sim \mathcal{U}[0, 1]$ is a resource dependent uniform random variable such that $\sum_i q_i = 1$. Using this, Eqs. (2.2a)-(2.2b) ($\epsilon_{\sigma\rho} \to 0$ for $\sigma \neq \rho$, and $\epsilon_\sigma \equiv \epsilon_{\sigma\sigma}$)

can be rewritten as follows:

$$\dot{n}_\sigma = n_\sigma \left[\alpha_\sigma \sum_{i=1}^{R} q_i r_i(c_i) - \beta_\sigma - \epsilon_\sigma n_\sigma \right], \tag{A.43}$$

$$\dot{c}_i = \mu_i(\Lambda - c_i) - r_i(c_i) q_i \sum_{\sigma=1}^{M} \alpha_\sigma n_\sigma, \tag{A.44}$$

where M and R, respectively, are the number of species and resources. For convenience, we set $\mu_i = \mu$ and $\beta_\sigma = 1$ for all σ. Now we fix α_σ for M species, and numerically integrate the coupled dynamics (A.43)-(A.44), and count the number of species surviving as a function for Λ for different number of resources and this result is shown in Figure 2.4 (a).

Similarly, we compute the distribution of the population in Figures 2.6 (a) and A.3 for a large number of resources. As we can see from Figure 2.4 (a) that when Λ is sufficiently large, all initial species survive. In that case, the population of the species in the stationary state can be written using Eq. (A.43):

$$n_\sigma^* = \frac{\alpha_\sigma \sum_i q_i r_i(c_i^*) - 1}{\epsilon_\sigma}. \tag{A.45}$$

We have checked numerically that when Λ is sufficiently large, $r_i(c_i^*) \to 1$. In that case,

$$n_\sigma^* \approx \frac{\alpha_\sigma - 1}{\epsilon_\sigma}, \tag{A.46}$$

since $\sum_i q_i = 1$. Therefore, the distribution of the population is independent of the number of resources, and in the case when α and ϵ are distributed uniformly, the distribution is given by Eq. (2.41). In Figure A.1, we show the comparison of the numerical simulation for different number of resources for $\Lambda = 10^{12}$ and the analytical prediction given in Eq. (2.41) and we find an excellent match between them.

A.4 SAD pattern for large number of resources

In this section, we compute the distribution of population of species when the number of resources are very large $R \gg 1$. For large number of resources, it is difficult to obtain the exact distribution for the population. Nonetheless, it is possible obtain the approximate distribution when we consider the case $\epsilon_{\sigma\rho} \to 0$ for $\sigma \neq \rho$ in Eq. (2.2a).

In this case, the equation for the non-zero population sizes of M^* surviving species in the stationary state can be obtained from Eq. (2.2a):

$$n_\rho^* = \frac{1}{\epsilon_\rho} \left(\sum_{i=1}^{R} \alpha_{\rho i} r_i(c_i^*) - 1 \right), \tag{A.47}$$

where $1 \leq \rho \leq M^*$ are the species with non-zero population. Again, for simplicity, we asume that $\beta_\sigma = 1$.

In the above Eq. (A.47), we have to first find the distribution according to which the numerator is distributed. We again stress that once $\alpha_{\rho i}$ are drawn, $r(c_i^*)$-s are fixed numbers that only depend on the surviving species ($n_\rho^* > 0$).

Let us first discuss the numerator of the above equation. We define $w = h - 1$, where

$$h = \sum_{j=1}^{R} x_j a_j. \tag{A.48}$$

We can write the mean and the variance of x_j, respectively, as $\theta = \langle x_j \rangle$ and $\phi^2 = \langle x_j^2 \rangle - \theta^2$ in which the angular brackets represent the average with respect to the distribution with which α-s are distributed. Herein, x_j-s and a_j, respectively, play the role of $\alpha_{\rho i}$ and $r_i(c_i)$ for a given ρ.

From Eq. (A.48), we can see the mean of $\langle h \rangle = \theta \sum_j a_j$. Therefore, the quantity $v = \sum_j a_j (x_j - \theta)$ has zero mean zero and variance given by

$$\begin{aligned}
\langle v^2 \rangle &= \sum_j a_j^2 \langle (x_j - \theta)^2 \rangle + \sum_{i \neq j} a_i a_j \langle (x_i - \theta)(x_j - \theta) \rangle \\
&= \sum_j a_j^2 \langle (x_j - \theta)^2 \rangle + \sum_{i \neq j} a_i a_j \langle x_i x_j + \theta^2 - \theta x_j - \theta x_i \rangle, \\
&= \phi^2 \sum_j a_j^2,
\end{aligned} \tag{A.49}$$

where the last term in the second equality is zero since x_i-s are independent.

Now, we define the rescaled sum as

$$S = \sum_j b_j m_j, \tag{A.50}$$

where $b_j = \frac{a_j}{\sqrt{\sum_j a_j^2}}$, and $m_j = (x_j - \theta)/\phi$. In the following, we also assume that $b_j \sim 1/\sqrt{R}$.

Now the probability density function for S is

$$\begin{aligned} P_1(S) &= \frac{1}{2\pi}\int dk\, e^{ikS}\prod_{j=1}^{R}\left(\int dm_j\, e^{-ikb_jm_j}p(m_j)\right) \\ &= \frac{1}{2\pi}\int dk\, e^{ikS}\prod_{j=1}^{R}\left\langle e^{-ikb_jm_j}\right\rangle \\ &\approx \frac{1}{2\pi}\int dk\, e^{ikS}\prod_{j=1}^{R}\left[1-k^2\frac{b_j^2}{2}+\dots\right] \\ &\approx \frac{1}{2\pi}\int dk\, e^{ikS}\left[1-k^2\frac{\sum_{j=1}^{R}b_j^2}{2}+\dots\right] \\ &\approx \frac{1}{2\pi}\int dk\, e^{ikS}e^{-k^2/2} \\ &\approx \frac{1}{\sqrt{2\pi}}e^{-\frac{S^2}{2}}, \end{aligned} \tag{A.51}$$

where $\sum_j b_j^2 = 1$, and each m has zero and unit variance, and also $R \gg 1$.

Since $h = S\phi\sqrt{\sum_j a_j^2} + \theta\sum_j a_j$, the probability density function for z is

$$p_1(h) \approx \frac{1}{\sqrt{2\pi(\sum_j a_j^2)\phi^2}}\exp\left[-\frac{(h-\theta\sum_j a_j)^2}{2(\sum_j a_j^2)\phi^2}\right] \tag{A.52}$$

Therefore,

$$p_2(w) \approx \frac{1}{\sqrt{2\pi(\sum_j a_j^2)\phi^2}}\exp\left[-\frac{[w-(\theta\sum_j a_j-1)]^2}{2(\sum_j a_j^2)\phi^2}\right]. \tag{A.53}$$

Thus, the numerator of (A.47) is typically distributed according to the above shown Gaussian distribution. In Figure A.2 (a), we compare the distribution given in Eq. (A.53) with proper rescaling where the rescaled variable is $\xi = \frac{w-\langle w\rangle}{\sqrt{\mathrm{Var}[w]}}$, with the numerical simulation of the dynamics given in Eqs. (2.2a)-(2.2b), where the solid curve is the analytical prediction and the circles are obtained from numerical simulation. We can see that there is a good agreement between theory and numerical simulation.

Now, we aim to find the ratio $z = w/y$ assuming the denominator to be uniformly distributed such that $y \in \mathcal{U}(c,d)$ this distribution, we have

$$\begin{aligned}
P(z) &= \int dw \int dy\; p_2(w)Q_2(y)\delta\left(z-\frac{w}{y}\right) \\
&= \frac{1}{z^2}\int dw \int dy\; |w|\; p_2(w)Q_2(y)\delta\left(y-\frac{w}{z}\right) \\
&\approx \frac{1}{z^2\sqrt{2\pi\Sigma^2}}\int_{-\infty}^{\infty} dw\; |w|\; \exp\left[-\frac{(w-\mathcal{M})^2}{2\Sigma^2}\right] Q_2(w/z) \\
&\approx \frac{1}{\sqrt{2\pi\Sigma^2}}\int_{-\infty}^{\infty} dt\; |t|\; \exp\left[-z^2\frac{(t-\mathcal{M}/z)^2}{2\Sigma^2}\right][\Theta(t-c)-\Theta(t-d)] \\
&\approx \frac{1}{(d-c)\sqrt{2\pi\Sigma^2}}\int_{c}^{d} dt\; t\; \exp\left[-z^2\frac{(t-\mathcal{M}/z)^2}{2\Sigma^2}\right] \\
&\approx \frac{1}{\sqrt{2\pi}(d-c)z^2}\left[\Sigma\left(e^{-\frac{(\mathcal{M}-cz)^2}{2\Sigma^2}}-e^{-\frac{(\mathcal{M}-dz)^2}{2\Sigma^2}}\right)\right. \\
&\qquad \left. +\sqrt{\frac{\pi}{2}}\mathcal{M}\left\{\mathrm{Erf}\left(\frac{\mathcal{M}-cz}{\sqrt{2}\Sigma}\right)-\mathrm{Erf}\left(\frac{\mathcal{M}-dz}{\sqrt{2}\Sigma}\right)\right\}\right], \qquad \text{(A.54)}
\end{aligned}$$

where $\mathcal{M} = \theta\sum_j a_j - 1$ and $\Sigma = \sqrt{\phi^2\sum_j a_j^2}$. Here $\theta = \int d\alpha\; p(\alpha)\; \alpha$, $\phi^2 = \int d\alpha\; p(\alpha)\; (\alpha-\theta)^2$ and $a_j = r_j(c_j^*)$.

In Figure A.2 (b), we compare the above Eq. (A.54) with the numerical simulation of the dynamics given in Eqs. (2.2a)-(2.2b), where the solid curve is the analytical prediction and the circles are obtained from numerical simulation. Finally, we stress that in this case, either exact or numerical value of $r_i(c_i^*)$ is difficult to obtain. Therefore, we have taken $r_i(c_i^*)$ from the numerical simulation of dynamics Eqs. (2.2a)-(2.2b).

A.5 SAD pattern with the occurrence of some species extinctions

In this section we compute the distribution of population sizes for surviving species starting from a pool of M species at a large-time. Here again, we consider the case when both α and ϵ are distributed uniformly.

Now the range of the numerator of (2.23) is $p = 0$, $q = b\tilde{r}(c^*) - 1$ where $\tilde{r}(c^*)$ is the solution of Eq. (2.25).

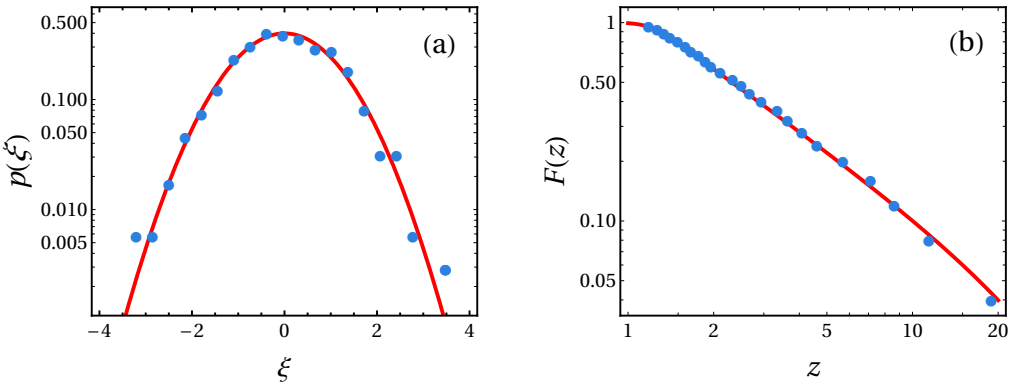

FIGURE A.2: Species in the presence of large number of resources. Panel (a): We numerically verified the Gaussian distribution given in Eq. (A.53) with proper rescaling where the rescaled variable $\xi = \frac{w-\langle w\rangle}{\sqrt{\mathrm{Var}[w]}}$. The solid curve is given by $p(\xi) = \frac{1}{\sqrt{2\pi}}\exp(-\xi^2/2)$ whereas the circles are obtained by numerically simulating the dynamics given in Eqs. (2.2a)-(2.2b). Panel (b): We compare the complementary cumulative function obtained from the analytical distribution given in Eq. (A.54) with the numerical simulation of the dynamics. We can see that there is a good agreement between theory and numerical simulation. For both panels, we consider $M = 1000$, $R = 50$, $\mu = 0.001$, $k = 5, \alpha_\sigma \sim \mathcal{U}(1.5, 5.0), \epsilon_\sigma \sim \mathcal{U}(0.01, 0.5), \beta_\sigma = 1, \Lambda_i = 1.5 \times 10^5$ for all i. As we can see from the log-scales, the SAD displays a power-law tail with exponent -2 (since $F(z) \sim z^{-1}$).

Thus, the probability distribution of population sizes of the coexisting species is given by

$$\begin{aligned}
P(z) &= \int_0^q dx \int_c^d dy\, Q_1(x)Q_2(y)\,\delta\left(z-\frac{x}{y}\right) \\
&= \frac{1}{q(d-c)}\int_0^q dx \int_c^d dy\,[\Theta(x)-\Theta(x-q)][\Theta(y-c)-\Theta(y-d)]\delta\left(z-\frac{x}{y}\right) \\
&= \frac{1}{q(d-c)z^2}\int_0^q dx|x|\overbrace{[\Theta(x)-\Theta(x-q)]}^{=1 \text{ since } 0<q}[\Theta(x/z-c)-\Theta(x/z-d)] \\
&= \frac{1}{q(d-c)z^2}\int_0^q dx\overbrace{|x|}^{x}[\Theta(x/z-c)-\Theta(x/z-d)]. \qquad \text{(A.55)}
\end{aligned}$$

Finally, we replace x/z by t and get

$$P(z) = \frac{1}{q(d-c)}[I_2(c,z) - I_2(d,z)], \quad \text{where} \qquad \text{(A.56)}$$

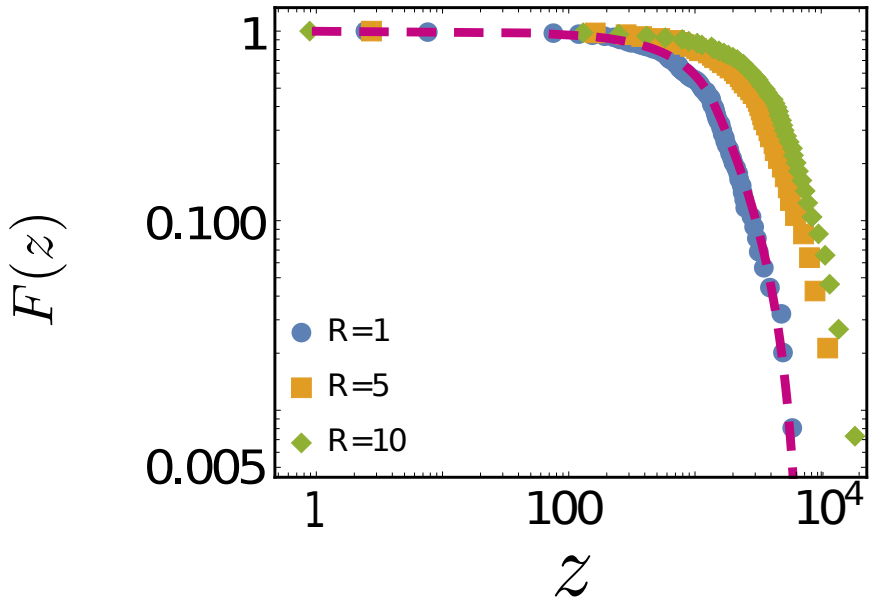

FIGURE A.3: Complementary cumulative distribution function (CCDF) for population of coexisting species. $F(z)$ is shown for surviving species starting from an initial number of species M. Circles are obtained by numerically integrating Eqs. (3) and (4) (see main text) for time $t = 10^8$ for $M = 500$ and one resource while dashed line is the analytical prediction of CCDF: $F(z) = \int_z^\infty dy\ P(y)$, from Eq. (A.58). Squares and diamonds, respectively, are the numerical simulations when the number of resources is $R = 5$ and 10. All cases exhibit a similar trend. The details of simulation for $R > 1$ are given in Appendix A.3. The parameters are $\alpha_\sigma \in \mathcal{U}(1.5, 10.0)$, $\beta_\sigma = 1$, $\mu = 0.001$, $\epsilon_\sigma \in \mathcal{U}(0.0001, 0.0005)$, $k_i = 5$, and $\Lambda = 5 \times 10^8$.

$$I_2(\kappa, z) = \int_0^{q/z} dt\ t[\Theta(t-\kappa)] = \begin{cases} 0 & \kappa > q/z, \\ \dfrac{1}{2z^2}(q^2 - \kappa^2 z^2) & 0 < \kappa < q/z, \end{cases} \tag{A.57}$$

which gives

$$P(z) = \frac{J_2(c,z) - J_2(d,z)}{2z^2 q(d-c)}, \tag{A.58}$$

where $J_2(\kappa, z) = (q^2 - \kappa^2 z^2)\Theta(q/z - \kappa)$.

In Figure A.3 we show the comparison of the analytical result (A.58) against the result obtained for CCDF by numerical evolving Eqs. (2.2a)-(2.2b) for a Λ such that some of the initial number of species survive. We also show the comparison for a large number of resource case. All these cases show the similar trend for the population distribution.

A.6 Power-law tail exponents of the SAD pattern

In this section, we present an analysis on our model to show it predicts fat-tail probability distribution for the population size. Herein, we show how power-law tails can be observed with a possible the range of variability of the exponent. We remark that this calculation will predict the tails of the empirical distribution of the Plankton data shown in the main text.

We recall the ratio $z = \frac{x}{y}$ and its distribution, shown also in Eq. (2.34), reads

$$P(z) = \frac{1}{z^2} \int dx \int dy \, |x| Q_1(x) Q_2(y) \, \delta\left(y - \frac{x}{z}\right). \tag{A.59}$$

In the following, we show that our extended consumer-resource model could retrieve a range of exponents for the power-law tail of the distribution. In order to make things transparent, let us begin our analysis from a simple setting: $Q_1(x) = \delta(x - \hat{x})$. Hence Eq. (A.59) reduces to

$$P(z) = \frac{\hat{x}}{z^2} Q_2(\hat{x}/z) \left[\Theta(\hat{x} - z y_-) - \Theta(\hat{x} - z y_+)\right], \tag{A.60}$$

where we have assumed that the random variable y takes values in the interval $[y_-, y_+]$ (consequentially $z \in \left[\frac{\hat{x}}{y_+}, \frac{\hat{x}}{y_-}\right]$). Suppose the distribution $Q_2(y)$ is

$$Q_2(y) = \frac{N}{y^\nu}, \tag{A.61}$$

where the normalization constant N is given by

$$1 = \frac{N}{1-\nu} [y^{-\nu+1}] \Big|_{y_-}^{y_+}. \tag{A.62}$$

Since we would like to deal with small y (i.e., small ϵ that gives large carrying capacity) we can consider the limit $y_- \to 0$. In this limit N diverges if $\nu \geq 1$. Therefore, we must consider $\nu < 1$. Moreover, on a physical ground, we expect the probability density function of y (or ϵ) to decrease monotonically as y increases. This is because of the fact that a large number of species might have a small value of ϵ (or y) that results in a large carrying capacity for those species. Thus, under such assumption, we get $0 \leq \nu < 1$. Therefore, Eq. (A.60) becomes

$$P(z) = \frac{B}{z^{2-\nu}} \left[\Theta(\hat{x}/y_- - z) - \Theta(\hat{x}/y_+ - z)\right]. \tag{A.63}$$

where $B = N\hat{x}^{1-\nu}$. Notice that the first Heaviside function gives the largest value of z above which the distribution vanishes. Therefore, we find that the distribution $P(z)$ is a power-law (with a prefactor):

$$P(z) \sim z^{-\gamma}. \tag{A.64}$$

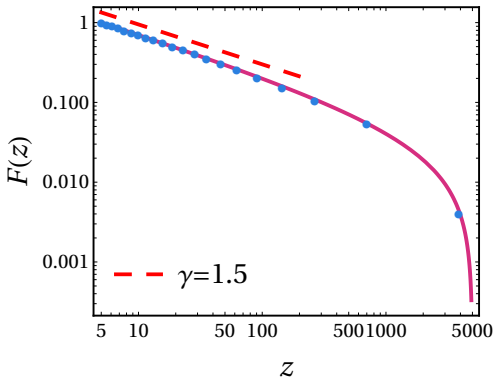

FIGURE A.4: Comparison of analytical result (A.64) with the numerical simulation. The solid curve is theoretical prediction of the complementary cumulative distribution $F(z) = \int_z^\infty dy\ P(y)$ obtained from Eq. (A.64), while the blue dots are obtained numerically after having sampled $M = 10^4$ independent draws from the distribution Eq. (A.61). The parameters for the plot are $\hat{x} = 5$, $y_- = 10^{-3}$, $y_+ = 1$ and $\nu = 0.5$. Clearly, we can see that there is an excellent match. In the plot, the dashed line is indicated for $F(z) \sim z^{-\gamma+1}$, where $\gamma = 1.5$. We remark that the deviation at a large z from the power-law is due to presence of Heaviside functions in the prefactor of Eq. (A.63), that introduce cut-off effects.

where $\gamma = 2 - \nu \in (1, 2]$. We stress that $\nu = 0$ corresponds to the uniform distribution that we have considered in the previous sections. In Figure A.4, we show the comparison of the complementary cumulative distribution function $F(z) = \int_z^\infty dy\ P(y)$ obtained from Eq. (A.64) with the numerical simulation (see caption of Figure A.4 for details).

We can extend this result to a broad class of distributions $Q_1(x)$ and $Q_2(y)$ using asymptotic analysis. Let us assume $y \in (0, y_+]$ and $x \in (0, x_+)$. This implies that $z \in (0, \infty)$. From Eq. (A.59) we have that

$$P(z) = \frac{1}{z^2} \int_0^{\min\{x_+, z y_+\}} dx\ x\ Q_1(x) Q_2(x/z). \tag{A.65}$$

At this point we can distinguish two cases:

1. $Q_2(y)$ is regular at $y = 0$ with

$$\frac{d^i}{dy^i} Q_2(y) \bigg|_{y=0} = 0 \quad \text{for } i = 0, \cdots, n-1. \tag{A.66}$$

Then, in the limit of large z we write the following expansion:

$$Q_2\left(\frac{x}{z}\right) = \frac{x^n}{z^n} Q_2^{(n)}(0) + o\left(\frac{1}{z^n}\right). \tag{A.67}$$

Finally, we find

$$P(z) \sim \frac{1}{z^{2+n}} \overbrace{\left(Q_2^{(n)}(0) \int_0^{x_+} dx\, x^{1+n}\, Q_1(x) \right)}^{<\infty}. \tag{A.68}$$

2. $Q_2(y)$ diverges at $y = 0$ like a power-law, i.e, $Q_2(y) = \frac{A}{y^\nu}$ with $\nu \in [0, 1)$. Therefore, we have ($\frac{x}{z} \to 0$ as $z \to \infty$)

$$P(z) \sim \frac{1}{z^{2-\nu}} \overbrace{\left(A \int_0^{x_+} dx\, x^{1-\nu}\, Q_1(x) \right)}^{<\infty}, \tag{A.69}$$

where in both Eqs. (A.68) and (A.69), the prefactors remain finite.

In all cases, the distribution $P(z)$ displays asymptotically a power-law tail, i.e.,

$$P(z) \sim \frac{1}{z^\gamma} \quad \text{for large } z, \tag{A.70}$$

with $\gamma \geq 2$ in the first case and $1 < \gamma \leq 2$ in the second one.

From an ecological point of view, the relevant case is the second one. Hence, the analysis we performed here indicates that the model presented in the main text predicts distributions of population size with power-law tails whose exponents ranges in an interval that we have shown above. In Figure A.5, we show the comparisons of the theoretical results for two concrete examples, one for each case discussed in Eqs. (A.68) and (A.69), with the reuslts of the corresponding numerical simulations. Clearly, we can see the theory and numerical evidences have a nice agreement.

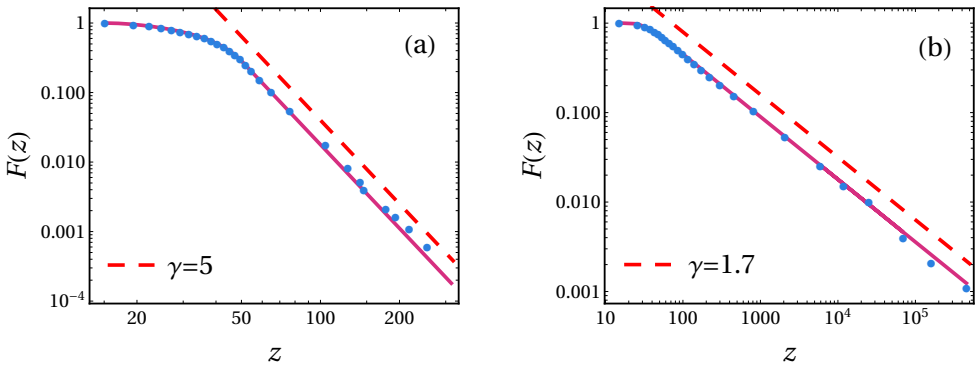

FIGURE A.5: Comparison of theoretical prediction of Eqs. (A.68) and (A.69) with the numerical simulations. The solid curves are the theoretical prediction of the complementary cumulative distribution $F(z) = \int_z^\infty dy\ P(y)$ obtained from Eq.(A.68) [for panel (a)] and Eq. (A.69) [for panel (b)], while blue dots are obtained from numerical simulation in which we generated $M = 10^4$ independent draws for the numerator and denominator by sampling the respective probability distributions (details are given below). Panel (a): We consider the case in which the denominator of the ratio $z = x/y$ is distributed according to a regular function at $y = 0$. In concrete, we take $Q_2(y) = Cy^3$ in the interval $[0, 0.1]$ (C is the normalization constant) while the numerator is assumed to be uniformly distributed in the interval $[1.5, 5]$, i.e., $Q_1(x) = \mathcal{U}(1.5, 5)$. Panel (b): $Q_2(y)$ is chosen to be a power-law distribution with exponent $\nu = 0.3$ on the same interval $[0, 0.1]$ while the numerator is again distributed uniformly in the interval $[1.5, 5]$. As expected, a power-law for large-z is observed. In both panels, we plot the dashed line corresponding to $F(z) \sim z^{-\gamma+1}$, where $\gamma = 5$ for panel (a) and for panel (b), we find $\gamma = 1.7$ as predicted by the theoretical investigation in Eqs. (A.68) and (A.69).

Appendix B

Appendix for Ginzburg-Landau amplitude equation for nonlinear nonlocal models

B.1 Derivation of Eq. (3.29)

In this section, we show the derivation to obtain the Eq. (3.29). We begin with substituting Eqs. (3.24)–(3.28) into Eq. (3.12) which gives

$$\begin{aligned}\epsilon^3\dot{\varphi}_1 + o\left(\epsilon^3\right) = \epsilon\left(\mathcal{L}_{\mathbf{p}_0}\varphi_1\right) + \epsilon^2\Big[\mathcal{L}_{\mathbf{p}_0}\varphi_2 + C^{(2,0)}_{\mathbf{q}_0}\varphi_1^2 + C^{(1,1)}_{\mathbf{q}_0}\varphi_1(G_{\mathbf{q}_0} * \varphi_1) + \\ + C^{(0,2)}_{\mathbf{q}_0}\left(G_{\mathbf{q}_0} * \varphi_1\right)^2\Big] + \epsilon^3\Big[\mathcal{L}_{\mathbf{p}_0}\varphi_3 + \delta\mathcal{L}_{\mathbf{p}_0}\varphi_1 + 2C^{(2,0)}_{\mathbf{q}_0}\varphi_1\varphi_2 + \\ + C^{(1,1)}_{\mathbf{q}_0}\left[\varphi_1(G_{\mathbf{q}_0} * \varphi_2) + \varphi_2(G_{\mathbf{q}_0} * \varphi_1)\right] + 2C^{(0,2)}_{\mathbf{q}_0}(G_{\mathbf{q}_0} * \varphi_1)(G_{\mathbf{q}_0} * \varphi_2) + \\ + C^{(3,0)}_{\mathbf{q}_0}\varphi_1^3 + C^{(2,1)}_{\mathbf{q}_0}\varphi_1^2(G_{\mathbf{q}_0} * \varphi_1) + C^{(1,2)}_{\mathbf{q}_0}\varphi_1(G_{\mathbf{q}_0} * \varphi_1)^2 + C^{(0,3)}_{\mathbf{q}_0}(G_{\mathbf{q}_0} * \varphi_1)^3\Big],\end{aligned} \tag{B.1}$$

where, for convenience, we have not written the x, ξ, t dependence in φ_i.

Note that the expansion of Eq. (3.12) should also include all the contributions at different orders of ϵ. Therefore, we have to also take into account the ones coming from the spatial scale separation. Using Eq. (3.25), we can see that

$$\partial_x^2 \to \left(\partial_x + \epsilon\partial_\xi\right)^2 = \partial_x^2 + 2\epsilon\partial_x\partial_\xi + \epsilon^2\partial_\xi^2, \tag{B.2}$$

and this indicates how the Laplacian operator in the $\mathcal{L}_{\mathbf{p}_0}$ given in Eq. (B.1), transforms and operates on both x and ξ variables.

Next ingredient we need in the following is the convolutions between the function $G_{\mathbf{q}_0}(x)$ and $\varphi_i(x, \xi, \tau)$ that appear in Eq. (B.1):

$$(G_{\mathbf{q}_0} * \varphi_i)(x, \xi, \tau) = \int_{-\infty}^{+\infty} dy\, G_{\mathbf{q}_0}(x - y)\varphi_i(y, \xi', \tau)\, dy, \tag{B.3}$$

where $\xi = \epsilon x$ and $\xi' = \epsilon y$. Following [199], we write the above integration (B.3) as

$$(G_{\mathbf{q}_0} * \varphi_i)(x, \xi, \tau) = \int_{-\infty}^{+\infty} dz\, G_{\mathbf{q}_0}(-z)\, \varphi_i(x + z, \xi + \epsilon z, \tau). \tag{B.4}$$

where we make a change in the integration variable from x to $z = y - x$.

Expanding the above equation (B.4) about the slow variable ξ, and integrating term by term yields

$$(G_{\mathbf{q}_0} * \varphi_i)(x, \xi, \tau) = \sum_{n=0}^{\infty} \frac{\epsilon^n}{n!} (G_{\mathbf{q}_0} * \varphi_i)_n, \tag{B.5}$$

where, for brevity, we define

$$(G_{\mathbf{q}_0} * \varphi_i)_n(x, \xi, \tau) = \int_{-\infty}^{+\infty} dz\, G_{\mathbf{q}_0}(-z) z^n \frac{\partial^n \varphi_i}{\partial \xi^n}(x + z, \xi, \tau). \tag{B.6}$$

With these considerations, the linear operator given in Eq. (3.27) can be rewritten as

$$\mathcal{L}_{\mathbf{p}_0} = \sum_{n=0}^{\infty} \epsilon^n \mathcal{L}_{\mathbf{p}_0}^{(n)}, \tag{B.7}$$

where

$$\mathcal{L}_{\mathbf{p}_0}^{(0)} \varphi_i(x, \xi, \tau) = D_0 \partial_x^2 \varphi_i(x, \xi, \tau) + C_{\mathbf{q}_0}^{(1,0)} \varphi_i(x, \xi, \tau) + C_{\mathbf{q}_0}^{(0,1)} \left(G_{\mathbf{q}_0} * \varphi_i\right)_0 (x, \xi, \tau), \tag{B.8}$$

$$\mathcal{L}_{\mathbf{p}_0}^{(1)} \varphi_i(x, \xi, \tau) = 2D_0 \partial_x \partial_\xi \varphi_i(x, \xi, \tau) + C_{\mathbf{q}_0}^{(0,1)} (G_{\mathbf{q}_0} * \varphi_i)_1(x, \xi, \tau), \tag{B.9}$$

$$\mathcal{L}_{\mathbf{p}_0}^{(2)} \varphi_i(x, \xi, \tau) = D_0 \partial_\xi^2 \varphi_i(x, \xi, \tau) + \frac{1}{2} C_{\mathbf{q}_0}^{(0,1)} (G_{\mathbf{q}_0} * \varphi_i)_2(x, \xi, \tau), \tag{B.10}$$

$$\mathcal{L}_{\mathbf{p}_0}^{(n \geq 3)} \varphi_i(x, \xi, \tau) = \frac{1}{n!} C_{\mathbf{q}_0}^{(0,1)} (G_{\mathbf{q}_0} * \varphi_i)_n(x, \xi, \tau). \tag{B.11}$$

Finally, we obtain Eq. (3.29) in which

$$H_1(\mathbf{p}_0, \varphi_1) = \mathcal{L}_{\mathbf{p}_0}^{(0)} \varphi_1, \tag{B.12}$$

$$\begin{aligned} H_2(\mathbf{p}_0, \varphi_1, \varphi_2) = {} & \mathcal{L}_{\mathbf{p}_0}^{(1)} \varphi_1 + \mathcal{L}_{\mathbf{p}_0}^{(0)} \varphi_2 + C_{\mathbf{q}_0}^{(2,0)} \varphi_1^2 + C_{\mathbf{q}_0}^{(1,1)} \varphi_1 (G_{\mathbf{q}_0} * \varphi_1)_0 + \\ & + C_{\mathbf{q}_0}^{(0,2)} \left(G_{\mathbf{q}_0} * \varphi_1\right)_0^2, \end{aligned} \tag{B.13}$$

$$
\begin{aligned}
H_3(\mathbf{p}_0,\varphi_1,\varphi_2) = {} & \mathcal{L}^{(0)}_{\mathbf{p}_0}\varphi_3 + \delta\mathcal{L}^{(0)}_{\mathbf{p}_0}\varphi_1 + \mathcal{L}^{(2)}_{\mathbf{p}_0}\varphi_1 + \mathcal{L}^{(1)}_{\mathbf{p}_0}\varphi_2 + 2C^{(2,0)}_{\mathbf{q}_0}\varphi_1\varphi_2 + \\
& + C^{(1,1)}_{\mathbf{q}_0}[\varphi_1(G_{\mathbf{q}_0} * \varphi_2)_0 + \varphi_2(G_{\mathbf{q}_0} * \varphi_1)_0] + C^{(3,0)}_{\mathbf{q}_0}\varphi_1^3 + \\
& + 2C^{(0,2)}_{\mathbf{q}_0}(G_{\mathbf{q}_0} * \varphi_1)_0(G_{\mathbf{q}_0} * \varphi_2)_0 + C^{(2,1)}_{\mathbf{q}_0}\varphi_1^2(G_{\mathbf{q}_0} * \varphi_1)_0 C^{(1,2)}_{\mathbf{q}_0} + \\
& + \varphi_1(G_{\mathbf{q}_0} * \varphi_1)_0^2 + C^{(0,3)}_{\mathbf{q}_0}(G_{\mathbf{q}_0} * \varphi_1)_0^3 + C^{(1,1)}_{\mathbf{q}_0}\varphi_1(G_{\mathbf{q}_0} * \varphi_1)_1 + \\
& + 2C^{(0,2)}_{\mathbf{q}_0}\left(G_{\mathbf{q}_0} * \varphi_1\right)_0\left(G_{\mathbf{q}_0} * \varphi_1\right)_1 . \qquad \text{(B.14)}
\end{aligned}
$$

B.2 Derivation of Eq. (3.32)

In this section, we present the detailed derivation to obtained the Eq. (3.32). To do so, we group the second order terms in Eq. (3.29) by comparing the left and right-hand side, and we obtain

$$H_2(\mathbf{p}_0,\varphi_1,\varphi_2) = 0 \qquad \text{(B.15)}$$

that can be rewritten extensively as

$$\mathcal{L}^{(0)}_{\mathbf{p}_0}\varphi_2 = -C^{(2,0)}_{\mathbf{q}_0}\varphi_1^2 - C^{(1,1)}_{\mathbf{q}_0}\varphi_1(G_{\mathbf{q}_0} * \varphi_1)_0 - C^{(0,2)}_{\mathbf{q}_0}\left(G_{\mathbf{q}_0} * \varphi_1\right)_0^2 - \mathcal{L}^{(1)}_{\mathbf{p}_0}\varphi_1. \qquad \text{(B.16)}$$

In order to find the solution φ_2 we need to evaluate $(G_{\mathbf{q}_0} * \varphi_1)_0$ and $\mathcal{L}^{(1)}_{\mathbf{p}_0}\varphi_1$. Using Eqs. (B.6) and (3.31), we get

$$(G_{\mathbf{q}_0} * \varphi_1)_0(x,\xi,\tau) = \int_{-\infty}^{+\infty} G_{\mathbf{q}_0}(-z)\left[A(\epsilon x,\tau)e^{ik_M(\mathbf{p}_0)(x+z)} + \bar{A}(\epsilon x,\tau)e^{-ik_M(\mathbf{p}_0)(x+z)}\right]dz. \qquad \text{(B.17)}$$

Thanks to the even nature of the function $G_{\mathbf{q}_0}(z)$, we find

$$
\begin{aligned}
(G_{\mathbf{q}_0} * \varphi_1)_0(x,\xi,\tau) &= \tilde{G}_{\mathbf{q}_0}(k_M(\mathbf{p}_0))\left[A(\xi,\tau)e^{ik_M(\mathbf{p}_0)x} + \bar{A}(\xi,\tau)e^{-ik_M(\mathbf{p}_0)x}\right] \\
&= \tilde{G}_{\mathbf{q}_0}(k_M(\mathbf{p}_0))\varphi_1(x,\xi,\tau). \qquad \text{(B.18)}
\end{aligned}
$$

Let us now evaluate $\mathcal{L}^{(1)}_{\mathbf{p}_0}\varphi_1$. Doing some algebra, we get

$$\mathcal{L}^{(1)}_{\mathbf{p}_0}\varphi_1 = C^{(0,1)}_{\mathbf{q}_0}(G_{\mathbf{q}_0} * \varphi_1)_1 + 2D_0\partial_x\partial_\xi\varphi_1, \qquad \text{(B.19)}$$

where

$$(G_{\mathbf{q}_0} * \varphi_1)_1(x,\xi,\tau) = (\partial_\xi A)(\epsilon x,\tau)e^{ik_M(\mathbf{p}_0)(x)}I + (\partial_\xi \bar{A})(\epsilon x,\tau)e^{-ik_M(\mathbf{p}_0)(x)}\bar{I}, \qquad \text{(B.20)}$$

in which the integral

$$I = \int_{-\infty}^{+\infty} G_{\mathbf{q}_0}(-z)ze^{ik_M(\mathbf{p}_0)z}dz = -i\tilde{G}'(k_M(\mathbf{p}_0)), \qquad \text{(B.21)}$$

and $\bar{I}$ is its complex conjugate. Therefore, $\mathcal{L}^{(1)}_{\mathbf{p}_0}\varphi_1$ becomes

$$\mathcal{L}^{(1)}_{\mathbf{p}_0}\varphi_1 = i\partial_{\tilde{\xi}}A(\xi,\tau)e^{ik_M(\mathbf{p}_0)x}\underbrace{\lambda'_{\mathbf{p}_0}(k_M(\mathbf{p}_0))}_{=0} + \\ + i\partial_{\tilde{\xi}}\bar{A}(\xi,\tau)e^{-ik_M(\mathbf{p}_0)x}\underbrace{\lambda'_{\mathbf{p}_0}(-k_M(\mathbf{p}_0))}_{=0} = 0. \tag{B.22}$$

Using Eqs. (B.18), (B.20), and (B.22) in Eq. (B.16), we finally get

$$\mathcal{L}^{(0)}_{\mathbf{p}_0}\varphi_2 = \Sigma_{\mathbf{p}_0}\varphi_1^2, \tag{B.23}$$

where we define the coefficient $\Sigma_{\mathbf{p}_0}$ as

$$\Sigma_{\mathbf{p}_0} = -C^{(2,0)}_{\mathbf{q}_0} - C^{(1,1)}_{\mathbf{q}_0}\tilde{G}_{\mathbf{q}_0}(k_M(\mathbf{p}_0)) - C^{(0,2)}_{\mathbf{q}_0}\tilde{G}_{\mathbf{q}_0}(k_M(\mathbf{p}_0))^2. \tag{B.24}$$

Clearly, Eq. (B.23) satisfies the Fredholm's alternative since $\varphi_1^2 \notin ker\left(\mathcal{L}^{(0)}_{\mathbf{p}_0}\right)$. In fact, the right-hand side of Eq. (B.23) is orthogonal to φ_1, and therefore, using Fredholm's alternative, Eq. (B.16) admits a bounded solution. Thus, using Eq. (3.31) in (B.23), we obtain the solution $\varphi_2(x,\xi,\tau)$ and it is shown in Eq. (3.32).

B.3 Derivation of Eq. (3.34): the GL amplitude equation

Here, we obtain the GL amplitude equation shown in Eq. (3.34). In the following, we compare the terms of third order in ϵ in the two sides of expansion (3.29). Therefore, we get

$$\dot{\varphi}_1 = H_3(\mathbf{p}_0,\varphi_1,\varphi_2) \tag{B.25}$$

that can be recast as

$$-\mathcal{L}^{(0)}_{\mathbf{p}_0}\varphi_3 = -\dot{\varphi}_1 + \delta\mathcal{L}^{(0)}_{\mathbf{p}_0}\varphi_1 + 2C^{(2,0)}_{\mathbf{q}_0}\varphi_1\varphi_2 + C^{(1,1)}_{\mathbf{q}_0}\left[\varphi_1(G_{\mathbf{q}_0}*\varphi_2)_0 + \right. \\ \left. + \varphi_2(G_{\mathbf{q}_0}*\varphi_1)_0\right] + 2C^{(0,2)}_{\mathbf{q}_0}(G_{\mathbf{q}_0}*\varphi_1)_0(G_{\mathbf{q}_0}*\varphi_2)_0 + C^{(3,0)}_{\mathbf{q}_0}\varphi_1^3 + \\ + C^{(2,1)}_{\mathbf{q}_0}\varphi_1^2(G_{\mathbf{q}_0}*\varphi_1)_0 + C^{(1,2)}_{\mathbf{q}_0}\varphi_1(G_{\mathbf{q}_0}*\varphi_1)_0^2 + C^{(0,3)}_{\mathbf{q}_0}(G_{\mathbf{q}_0}*\varphi_1)_0^3 + \\ + C^{(1,1)}_{\mathbf{q}_0}\varphi_1(G_{\mathbf{q}_0}*\varphi_1)_1 + 2C^{(0,2)}_{\mathbf{q}_0}\left(G_{\mathbf{q}_0}*\varphi_1\right)_0\left(G_{\mathbf{q}_0}*\varphi_1\right)_1 + \\ + \mathcal{L}^{(2)}_{\mathbf{p}_0}\varphi_1 + \mathcal{L}^{(1)}_{\mathbf{p}_0}\varphi_2. \tag{B.26}$$

We substitute the expression of $(G_{\mathbf{q}_0} * \varphi_2)_0$ [following Eqs. (B.6) and (3.32)], $\delta\mathcal{L}^{(0)}_{\mathbf{p}_0}\varphi_1$, and $\mathcal{L}^{(2)}_{\mathbf{p}_0}\varphi_1$:

$$(G_{\mathbf{q}_0} * \varphi_2)_0(x,\xi,\tau) = \Sigma_{\mathbf{p}_0}\Bigg\{\frac{\tilde{G}_{\mathbf{q}_0}(2k_M(\mathbf{p}_0))}{\lambda_{\mathbf{p}_0}(2k_M(\mathbf{p}_0))}\big[A^2(\xi,\tau)e^{2ik_M(\mathbf{p}_0)x}+ \\ + \bar{A}^2(\xi,\tau)e^{-2ik_M(\mathbf{p}_0)x}\big] + \frac{2\tilde{G}_{\mathbf{q}_0}(0)}{\lambda_{\mathbf{p}_0}(0)}|A(\xi,\tau)|^2\Bigg\}+ \\ + \tilde{G}_{\mathbf{q}_0}(k_M(\mathbf{p}_0))\Lambda(x,\xi,\tau), \tag{B.27}$$

$$\delta\mathcal{L}^{(0)}_{\mathbf{p}_0}\varphi_1 = \hat{v}\cdot\left(\vec{\nabla}_{\mathbf{p}}\mathcal{L}^{(0)}_{\mathbf{p}}\right)|_{\mathbf{p}=\mathbf{p}_0}\varphi_1 \equiv \bar{\lambda}_M\varphi_1, \tag{B.28}$$

$$\mathcal{L}^{(2)}_{\mathbf{p}_0}\varphi_1 = \frac{1}{2}C^{(0,1)}_{\mathbf{q}_0}(G_{\mathbf{q}_0} * \varphi_1)_2 + D_0\partial^2_\xi\varphi_1, \tag{B.29}$$

in Eq. (B.26), where

$$(G_{\mathbf{q}_0} * \varphi_1)_2(x,\xi,\tau) = -\tilde{G}''(k_M(\mathbf{p}_0))\partial^2_\xi A(\xi,\tau))e^{ik_M(\mathbf{p}_0)x}+ \\ - \tilde{G}''(-k_M(\mathbf{p}_0))\partial^2_\xi\bar{A}(\xi,\tau))e^{-ik_M(\mathbf{p}_0)x}. \tag{B.30}$$

Notice that in arriving the above form of $(G_{\mathbf{q}} * \varphi_1)_2(x,\xi,\tau)$ we have used the same strategy as in Eq. (B.20). Thus, Eq. (B.29) becomes

$$\mathcal{L}^{(2)}_{\mathbf{p}_0}\varphi_1 = -\frac{1}{2}\lambda''_{\mathbf{p}_0}(k_M(\mathbf{p}_0))\partial^2_\xi A(\xi,\tau))e^{ik_M(\mathbf{p}_0)x}+ \\ - \frac{1}{2}\lambda''_{\mathbf{p}_0}(-k_M(\mathbf{p}_0))\partial^2_\xi\bar{A}(\xi,\tau))e^{-ik_M(\mathbf{p}_0)x}. \tag{B.31}$$

Finally, we substitute Eqs. (B.27), (B.28), (B.31), and φ_1 from Eq. (3.31) in Eq. (B.26). Since φ_3 has to be bounded, the right-hand side of Eq. (B.26) must be orthogonal to φ_1 (Fredholm's alternative). Therefore, setting the coefficients of $e^{ik_M(\mathbf{p}_0)x}$ in Eq. (B.26) equal to zero while noticing that $\mathcal{L}^{(1)}_{\mathbf{p}_0}\varphi_2 + C^{(1,1)}_{\mathbf{q}_0}\varphi_1(G_{\mathbf{q}_0} * \varphi_1)_1 + 2C^{(0,2)}_{\mathbf{q}_0}\left(G_{\mathbf{q}_0} * \varphi_1\right)_0\left(G_{\mathbf{q}_0} * \varphi_1\right)_1$ does not have any term proportional to $e^{ik_M(\mathbf{p}_0)x}$, we obtain the GL amplitude equation as shown in Eq. (3.34), where $\bar{\lambda}_M$ is given in (3.22) and the coefficient α has the following form:

$$\alpha = -\Bigg\{2\Sigma_{\mathbf{p}_0}C^{(2,0)}_{\mathbf{q}_0}\left[\frac{2}{\lambda_{\mathbf{p}_0}(0)} + \frac{1}{\lambda_{\mathbf{p}_0}(2k_M(\mathbf{p}_0))}\right] + \Sigma_{\mathbf{p}_0}C^{(1,1)}_{\mathbf{q}_0}\Bigg[2\frac{\tilde{G}_{\mathbf{q}_0}(0)+\tilde{G}_{\mathbf{q}_0}(k_M(\mathbf{p}_0))}{\lambda_{\mathbf{p}_0}(0)}+ \\ + \frac{\tilde{G}_{\mathbf{q}_0}(k_M(\mathbf{p}_0))+\tilde{G}_{\mathbf{q}_0}(2k_M(\mathbf{p}_0))}{\lambda_{\mathbf{p}_0}(2k_M(\mathbf{p}_0))}\Bigg] + 2\Sigma_{\mathbf{p}_0}C^{(0,2)}_{\mathbf{q}_0}\tilde{G}_{\mathbf{q}_0}(k_M(\mathbf{p}_0))\Bigg[\frac{2\tilde{G}_{\mathbf{q}_0}(0)}{\lambda_{\mathbf{p}_0}(0)}+ \\ + \frac{\tilde{G}_{\mathbf{q}_0}(2k_M(\mathbf{p}_0))}{\lambda_{\mathbf{p}_0}(2k_M(\mathbf{p}_0))}\Bigg] + 3C^{(3,0)}_{\mathbf{q}_0} + 3C^{(2,1)}_{\mathbf{q}_0}\tilde{G}_{\mathbf{q}_0}(k_M(\mathbf{p}_0)) + 3C^{(1,2)}_{\mathbf{q}_0}(\tilde{G}_{\mathbf{q}_0}(k_M(\mathbf{p}_0)))^2+$$

$$+ 3C^{(0,3)}_{\mathbf{q}_0}(\tilde{G}_{\mathbf{q}_0}(k_M(\mathbf{p}_0)))^3 \Big\}. \tag{B.32}$$

B.4 Particular solutions of the GL amplitude equation

In this section, we present two interesting analytical solutions of the GL amplitude equation (3.34).

Let us substitute the complex amplitude $A(\xi,\tau)$:

$$A(\xi,\tau) = |A(\xi,\tau)|e^{i\theta(\xi,\tau)} \tag{B.33}$$

where both $|A(\xi,\tau)|$ and $\theta(\xi,\tau)$ are real functions of ξ and τ, in Eq. (3.34). Separating the real and imaginary parts, we obtain a set of coupled differential equations for the modulus $|A(\xi,\tau)|$ and the phase of the amplitude $\theta(\xi,\tau)$:

$$\begin{aligned}\partial_\tau|A| &= \bar{\lambda}_M|A| - \alpha|A|^3 + \\ &+ \frac{1}{2}|\lambda''_{\mathbf{p}_0}(k_M(\mathbf{p}_0))|\left[\partial^2_{\tilde{\xi}}|A| - |A|(\partial_{\tilde{\xi}}\theta)^2\right], \qquad \text{(B.34)}\\ |A|\partial_\tau\theta &= \frac{1}{2}|\lambda''_{\mathbf{p}_0}(k_M(\mathbf{p}_0))|\left[2(\partial_{\tilde{\xi}}|A|)(\partial_{\tilde{\xi}}\theta) + |A|\partial^2_{\tilde{\xi}}\theta\right], \qquad \text{(B.35)}\end{aligned}$$

where, for convenience, we have dropped the arguments in both $|A(\xi,\tau)|$ and $\theta(\xi,\tau)$.

It is difficult to obtain the solution of above coupled differential for a generic initial condition. Nonetheless, for some particular initial conditions, the exact solution can be obtained. As a first example, we consider an initial homogeneous condition, i.e.,

$$A(\xi,0) \equiv A_0 e^{i\theta_0}, \tag{B.36}$$

where both A_0 and θ_0 are independent of ξ. Therefore, the solution in this case can be obtained as

$$\begin{aligned}|A(\xi,\tau)| &= \frac{A_0\sqrt{\bar{\lambda}_M}\exp\left(\bar{\lambda}_M\tau\right)}{\sqrt{\bar{\lambda}_M + A_0^2\alpha\left[\exp\left(2\bar{\lambda}_M\tau\right) - 1\right]}}, \qquad \text{(B.37)}\\ \theta(\xi,\tau) &= \theta_0, \qquad \text{(B.38)}\end{aligned}$$

and they satisfy both Eq. (B.34) and (B.35) and the initial condition Eq. (B.36). Thus, for a given initial homogeneous condition, the GL amplitude equation predicts the amplitude to be homogeneous where only the modulus $|A|$ evolves with time τ.

To obtain a spatial solution of the amplitude equation, we again consider an initial homogeneous condition for the phase, i.e., $\theta(\xi,0) \equiv \theta_0$. Thus, the

equation for the modulus of the amplitude reduces to

$$\partial_\tau |A| = \bar{\lambda}_M |A| - \alpha |A|^3 + \frac{1}{2} |\lambda''_{\mathbf{p}_0}(k_M(\mathbf{p}_0))| \partial^2_\xi |A| \tag{B.39}$$

A steady solution $|A_{st}(\xi)|$ of above Eq. (B.39) can be obtained by setting the left hand side of Eq. (B.39) to 0, and we get

$$|A_{st}(\xi)| = \pm \sqrt{\frac{\bar{\lambda}_M}{\alpha}} \tanh \left[\xi \sqrt{\frac{\bar{\lambda}_M}{|\lambda''(k_M(\mathbf{p}_0))|}} \right]. \tag{B.40}$$

as one possible solution, as shown in Ref. [67].

Since $|A_{st}(\xi)|$ must be non-negative, a solution that satisfies this condition can be constructed as

$$|A_{st}(\xi)| = \sqrt{\frac{\bar{\lambda}_M}{\alpha}} \tanh \left[|\xi| \sqrt{\frac{\bar{\lambda}_M}{|\lambda''(k_M(\mathbf{p}_0))|}} \right]. \tag{B.41}$$

In the above solution, we consider both solutions (B.40) depending on the sign of the variable ξ and introduce a defect at $\xi = 0$, where the amplitude becomes zero. In fact, this solution also satisfies the amplitude equation everywhere except at the defect where it changes the behavior passing from one to the other solution displayed in Eq. (B.40).

It is possible to show analytically that the homogeneous solution of Eq. (3.34) is linearly stable while the steady spatial one (B.40) is locally linearly unstable. In other words, the numerical spatial solution is a good approximation of the analytical prediction only up to a finite observation time. Indeed, because of numerical inaccuracies, at larger time scales the profile will inevitably fall into the basin of attraction of the stationary stable solution.

B.5 Numerical Methods

In this section, we discuss the method of numerical simulation to verify the analytical prediction of the amplitude equation Eq. (3.34). As an example, we consider the discrete nonlocal Fisher equation. To do so we consider a one dimensional line where the spatial variable x ranges from $-L$ to L. Then we discretize the space creating a lattice introducing the discrete spatial variable x_i defined as follows

$$x_i = -L + i\, dx \quad \text{where} \quad i = 1, \ldots, N, \tag{B.42}$$

with $x_N = x_0$ [i.e., periodic boundary condition (PBC)]. In the above equation, $dx = 2L/N$ is the uniform spacing.

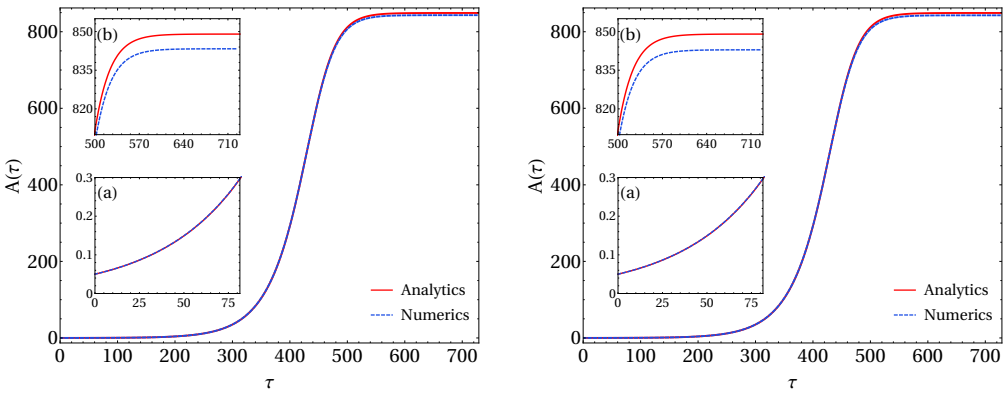

FIGURE B.1: Comparison between theoretical prediction of the GL amplitude equation (3.34) with the initial condition $A(\xi_i, 0) = |A(\xi_i, 0)| = A_0 = 0.05$ (solid red line) and the amplitude obtained from the numerical simulation (blue dashed line) for the discrete nonlocal F-KPP equation where the system is initialized in the state $\phi_i(\xi_i, 0) = \phi(x_i, \xi_i, 0) = \phi_{\mathbf{q}}^{(0)} + 2\epsilon A_0 \cos[k_M(\mathbf{p}_0)x_i]$. In the numerical implementation, we take $N = 3060$ species equispaced along a ring of length $2L = 3$, and these are interacting among each others with an interaction kernel given by $G_{\mathbf{q}}(z) = \exp\left(-\frac{|z|}{R}\right) - b \exp\left(-\frac{|z|}{\beta R}\right)$. In the left panel, the amplitude is extracted from the numerical simulation exploiting Eq. (B.48) whereas in the right panel, we employ the truncated series (3.26) up to second order to estimate the amplitude from the same numerical simulation. Insets in the two plots show the zooming of the curves up to a particular range of time τ. Both plots are shown for fixed sets of parameters $\mathbf{p}$ and $\mathbf{p}_0$. In particular, here we set $R = 0.1$, $\beta = 0.5851$, $b = 0.6$, $a = 10^{-4}$, and $D = 10^{-8}$. To compute the coefficients of Eq. (3.34) we used the set $\mathbf{p}_0$ in which we tuned β leaving the other parameters fixed.

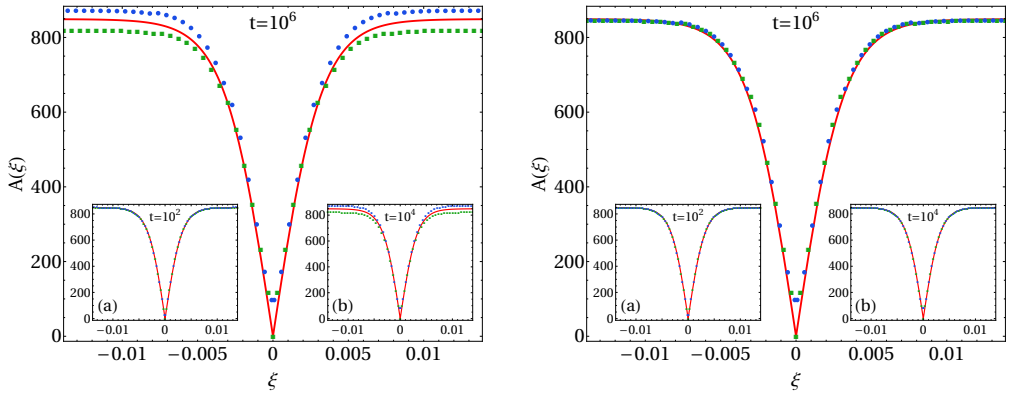

FIGURE B.2: Comparison of theoretical prediction of the GL amplitude equation (3.34) (solid red line) with the numerical simulation (blue circles and green squares) for the discrete nonlocal F-KPP equation using the defective steady solution $A_{st}(\xi)$ (B.41) and $\phi_i(\xi_i, 0) = \phi(x_i, \xi_i, 0) = \phi_{\mathbf{q}}^{(0)} + 2\epsilon A_{st}(\xi_i)\cos[k_M \mathbf{p}_0) x_i]$, respectively, as initial conditions. From the numerical integration of the discrete CLV dynamics, we extract the envelope of the pattern using its local maxima (circles) and minima (squares). In the left panel, the amplitude is extracted from the numerical simulation exploiting Eq. (B.48) whereas in the right panel, we use the truncated series (3.26) up to second order to estimate the amplitude from the same numerical simulation. We show in the main plots the comparison at $t = 10^6$ of the discrete nonlocal F-KPP equation, while in the insets the comparison is displayed at $t = 10^2$ (a) and $t = 10^4$ (b). Clearly, we can see that when we consider the higher-order contribution the agreement improves at larger time. The simulated dynamics, including the interaction kernel and the sets of parameter $\mathbf{p}$ and $\mathbf{p}_0$ used, is the same one presented in the caption of Figure B.1, where the initial condition has been changed.

The dynamics described by the discrete nonlocal Fisher-KPP equation reads as

$$\partial_t \phi_i(t) = \phi_i(t)\left[1 - a\sum_{j=1}^{N} G_{\mathbf{q}}\left(\min\{|i-j|dx, 2L - |i-j|dx\}\right)\phi_j(t)\right] + D\Delta\phi_i(t). \tag{B.43}$$

where the kernel respects PBC. The above equations (B.43) are supplemented with initial conditions $\phi_i(t=0)$ which we will discuss later.

In the above Eq. (B.43), the subscript i corresponds to i-th position along the lattice, $\phi_i(t)$ is the value of the field at that position at time t and the discrete Laplacian operator Δ acting on the field ϕ_i is defined as

$$\Delta\phi_i = \frac{\phi_{i-1} - 2\phi_i + \phi_{i+1}}{dx^2}.$$

The homogeneous and stationary solution corresponding to Eq. (B.43) is given by

$$\begin{aligned}\phi_{\mathbf{q}}^{(0)} &= \frac{1}{a\sum_{j=1}^{N} G_{\mathbf{q}}\left(\min\{|i-j|\,dx, 2L - |i-j|\,dx\}\right)} \\ &= \frac{1}{2a\sum_{j=1}^{\frac{N}{2}-1} G_{\mathbf{q}}(j\,dx) + a\,G_{\mathbf{q}}(L) + a\,G_{\mathbf{q}}(0)}.\end{aligned} \tag{B.44}$$

Now, to understand the stability of $\phi_{\mathbf{q}}^{(0)}$, we substitute $\phi_j(t) \equiv \phi_{\mathbf{p}}^{(0)} + \delta e^{\lambda_{\mathbf{p}}(k_n)t + ik_n x_j} + c.c.$, where $0 < \delta \ll 1$ and $k_n = n\frac{\pi}{L}$ with n being an integer, in Eq. (B.43). Therefore, we obtain the following dispersion relation (up to a linear order in δ)

$$\lambda_{\mathbf{p}}(k_n) = -\frac{\tilde{g}_{\mathbf{q}}(k_n)}{\tilde{g}_{\mathbf{q}}(0)} + 2D\frac{\cos(k_n\,dx) - 1}{dx^2}, \tag{B.45}$$

where we have introduced the discrete Fourier transform as

$$\begin{aligned}\tilde{g}_{\mathbf{q}}(k_n) = 2\sum_{j=1}^{\frac{N}{2}-1} \cos(k_n\,j\,dx)\,G_{\mathbf{q}}(j\,dx) + \\ + (-1)^n G_{\mathbf{q}}(L) + G_{\mathbf{q}}(0).\end{aligned} \tag{B.46}$$

In the following, we describe the recipe to obtain the amplitude of the pattern formed near the critical hypersurface $\mathcal{M}$ (Figure 3.1) by numerical simulating Eq. (B.43). We stress that the theoretical prediction of amplitude equation [see Eq. (3.34)] does not get affected for the above discussed model. In this case, we just replace the Fourier transform with its discrete counterpart (B.46).

First, we consider a point $\mathbf{p}$ in the pattern forming region (See Figure 3.1) and find the value of λ_M using Eq. (B.45), where $\lambda_M = \max_{k_n}\{\lambda_{\mathbf{p}}(k_n)\}$. Then

we take the point $\mathbf{p}_0$, that lies on $\mathcal{M}$ around which we perform the expansion as discussed in Section 3.5, and we compute $k_M(\mathbf{p}_0)$ and the coefficients appearing in Eq. (3.34).

We note that in general for the continuous model shown in Eq. (3.1), the analytical solution of the dynamics [using solution of Eq. (3.34) given initial conditions, and Eq. (3.26)] can be written as (up to first order in ϵ)

$$\begin{aligned}\phi(x,\xi,\tau) &\approx \phi_{\mathbf{q}}^{(0)} + \epsilon\varphi_1(x,\xi,\tau) \\ &\approx \phi_{\mathbf{q}}^{(0)} + 2\epsilon|A(\xi,\tau)|\cos\left[k_M(\mathbf{p}_0)x + \theta(\xi,\tau)\right], \end{aligned} \tag{B.47}$$

where $A(\xi,\tau) = |A(\xi,\tau)|e^{i\theta(\xi,\tau)}$. Therefore, the analogous discrete version of the above solution is

$$\begin{aligned}\phi_i(\xi_i,\tau) &= \phi(x_i,\xi_i,\tau) \\ &\approx \phi_{\mathbf{q}}^{(0)} + 2\epsilon|A(\xi_i,\tau)|\cos\left[k_M(\mathbf{p}_0)x_i + \theta(\xi_i,\tau)\right], \end{aligned} \tag{B.48}$$

where x_i corresponds to discrete spatial location of the i-th species.

Here we aim to compare the amplitude given in the Eq. (B.48) with the numerical simulation. To do so, we use the same initial and boundary conditions imposed on the solution (B.48). Finally, we verify the analytical prediction for growth of the amplitude for two different initial conditions given in Eqs. (B.37), (B.38), and (B.41) in Figures B.1 and B.2.

Appendix C

Appendix for Stochastic amplification in delayed and noisy systems

C.1 Asymptotic stability and damped oscillations from when $a > -b$

In this section we provide some results regarding the solution of chap: amp-eq in the deterministic limit $D = 0$. Hence the dynamics is a linear delayed differential equation that reads

$$\frac{dx(t)}{dt} = -ax(t) - bx(t-\tau). \tag{C.1}$$

In all Chapter 4 we considered $a > b > 0$. Herein, we consider the most general case where with $a > -b$ and $\tau > 0$.

The asymptotic stability of the stationary state $\bar{x} = 0$ of Eq. (C.1) can be proved when $-b < a < b$ with $b > 0$ and $0 < \tau < \tau^* = \left(b^2 - a^2\right)^{-1/2} \cos^{-1}\left(-\frac{a}{b}\right)$ [141].

Of course, the characteristic equation and its solution, displayed in Eqs. (4.9) and (4.11), respectively, are left unchanged. Hence, the condition to observe asymptotic damped oscillations is still

$$-b\tau e^{\tau a} < -e^{-1} \Longrightarrow b\tau e^{\tau a} > e^{-1} \tag{C.2}$$

We can immediately see that if $b < 0$, the above inequality will never be satisfied. Therefore in the following we will always have $b > 0$.

Since $-b < a < 0$, when we multiply both sides of Eq. (C.2) by a we end up with

$$a\tau e^{a\tau} < \frac{a}{eb}, \tag{C.3}$$

that retrieves

$$\tau > \tau_c = \frac{W\left(\frac{a}{eb}\right)}{a}, \tag{C.4}$$

as in the case $a > b > 0$ discussed in the Chapter.

Therefore, to sum up, in order for the deterministic dynamics to display damped oscillations we need $a > -b$ with $b > 0$ and $\tau > \tau_c$.

C.2 Generic solution of a linear delayed ordinary differential equation

In this section we are going to show the full solution of a generalized version of the deterministic delayed equation Eq. (4.1) where the discrete delay term is substituted with a distributed counterpart. Such term is mathematically expressed as an average over the past states acquired during the evolution $x(t-z)$ weighted with a kernel function $G(z)$. So the deterministic version of the equation now becomes

$$\frac{dx(t)}{dt} = -ax(t) - bI(t) \tag{C.5}$$

where the functional $I(t)$ is the distributed delay taking the form

$$I(t) = \int_0^{+\infty} dz\, G(z)x(t-z) \tag{C.6}$$

where, without any loss of generality, we assume the kernel to be normalized, i.e., $\int_0^{+\infty} dz\, G(z) = 1$. We can easily notice that using $G(z) = \delta(z-\tau)$ we recover the deterministic Eq. (1) of the main text.

We start by taking the Laplace transform of Eq. (C.5) obtaining

$$\begin{aligned}
s\tilde{x}(s) - x(0) &= -a\tilde{x}(s) - b\int_0^{+\infty} dz \int_0^{+\infty} dt\, G(z)e^{-st}x(t-z) \\
&= -a\tilde{x}(s) - b\int_0^{+\infty} dz\, G(z)e^{-sz}\int_{-z}^{+\infty} du\, e^{-su}x(u) \\
&= -a\tilde{x}(s) - b\left(\int_0^{+\infty} dz\, G(z)e^{-sz}\right)\left(\int_0^{+\infty} du\, e^{-su}x(u)\right) + \\
&- b\int_0^{+\infty} dz\, G(z)e^{-sz}\int_{-z}^{0} du\, e^{-su}x(u) \\
&= -a\tilde{x}(s) - b\tilde{G}(s)\tilde{x}(s) - bJ(s)
\end{aligned} \tag{C.7}$$

where $\tilde{x}(s)$ and $\tilde{G}(s)$ indicate the Laplace transform of $x(t)$ and $G(t)$, respectively, $x(0) = x(t=0)$ is the state at time $t = 0$ and $J(s)$ is defined as

$$J(s) = \int_0^{+\infty} dz\, G(z)e^{-sz}\int_{-z}^{0} du\, e^{-su}x(u) \tag{C.8}$$

Notice that this is a functional of the past history we used as initial condition of the system for negative times. We use an initial condition $x(t)$ for $t \in (-\infty, 0]$ which is continuous and such that $J(s)$ exists and it is finite.

From Eq. (C.7) we find

$$\tilde{x}(s) = \frac{x(0) - bJ(s)}{s + a + b\tilde{G}(s)} \tag{C.9}$$

If $J(s)$ has no poles with negative real part and its zeros do not coincide with those of the denominator of Eq. (C.9), then the poles of Eq. (C.9) are the solutions of the characteristic equation of Eq. (C.5) obtained by inserting the ansatz $x(t) = Ce^{\lambda t}$ for the asymptotic solution, i.e.,

$$\lambda = -a - b\tilde{G}(\lambda) \tag{C.10}$$

As we argued in the main text, studying the solutions λ of this equation we can understand the asymptotic stability of the dynamics.

Finally the solution of Eq. (C.5) can be found from Eq. (C.9) by performing the inverse Laplace transform, i.e.,

$$\begin{aligned} x(t) &= \frac{1}{2\pi i} \lim_{\gamma\to\infty} \int_{c-i\gamma}^{c+i\gamma} ds\, \frac{x(0) - b\tilde{G}(s)J(s)}{s + a + b\tilde{G}(s)} e^{st} \\ &= \frac{1}{2\pi i} \lim_{\gamma\to\infty} \left[\int_{c-i\gamma}^{c+i\gamma} ds\, \frac{x(0)}{s + a + b\tilde{G}(s)} e^{st} - b \int_{d-i\gamma}^{d+i\gamma} ds\, \frac{\tilde{G}(s)J(s)}{s + a + b\tilde{G}(s)} e^{st} \right] \end{aligned} \tag{C.11}$$

where c and d are real numbers taken such the integration paths in the complex plane lie in the convergence region of the arguments of the two integrals.

In particular, to ensure the asymptotic stability of the dynamics we need to have that all the solutions of the characteristic equation have a negative real part, i.e., all the poles of Eq. (C.9) lie in the left half of the complex plane. We have also to consider that $J(s)$ could have poles lying in the convergence region.

If the poles are simple, we can compute Eq. (C.11) using Cauchy's integration with the residues. In this way we get (assuming for simplicity here that $J(s)$ does not have poles with negative real parts)

$$x(t) = \sum_i \frac{x(0) - bJ(\lambda_i)}{1 + b\tilde{G}'(\lambda_i)} e^{\lambda_i t} \tag{C.12}$$

where the summation is performed over the solutions of the characteristic equation Eq. (C.10). So we can see that the solution $x(t)$ is expressed as linear combination of exponential functions. In particular, asymptotically the stability is determined by the eigenvalue with the largest real part, which corresponds to the analysis we discussed in the main text.

C.3 Occurrence of stochastic amplification when $a > -b$

We hereby consider the case in which $-b < a < b$, opposite to the case $a > b > 0$ considered in Chapter 4. Here we find, independently of the region of the parameters considered, that the condition for which $\omega = 0$ is a local minimum of the power-spectrum Eq. (4.27) is

$$b\tau(2 + a\tau) - 1 > 0 \tag{C.13}$$

In the case $a > 0$ this requires

$$\tau > \tau_a = \frac{-1 + \sqrt{1 + \frac{a}{b}}}{a} \tag{C.14}$$

If instead we have $-b < a < 0 < b$ Eq. (C.13) gives us the condition

$$\tau_a = \frac{-1 + \sqrt{1 + \frac{a}{b}}}{a} < \tau < \frac{1 + \sqrt{1 + \frac{a}{b}}}{|a|} = \bar{\tau}_a \tag{C.15}$$

In this way, when $a > -b$ and $b > 0$ we need $\tau > \tau_a > 0$ to observe stochastic amplification, identifying in this way a new threshold. In the next section we will show that given a, b such that we need $\tau < \tau^*$ to ensure stability in the deterministic dynamics, we will have that $\tau_a < \tau^*$. Additionally, if $a < 0$ we also have $\tau^* > \bar{\tau}_a$

C.4 Order relation between the thresholds τ_c, τ_a and τ^*

So far we found three thresholds for the parameter τ once the other two other parameters of Eq. (4.1) are fixed with $a > -b$: one for the stationary deterministic solution to be stable, i.e., $\tau < \tau^*$ when either $-b < a < b$ with $b > 0$ (if $a > b > 0$ is always stable and so such threshold does not exist anymore), the second for the deterministic case to display oscillating solutions, i.e., $\tau > \tau_c$, and the last for the stochastic version to ensure stochastic amplification to occur, i.e., $\tau > \tau_a$.

It is natural to ask which is the order relation between these depending on a and b. It is possible to show that we always have that $\tau_c < \tau_a$ and $\tau_c < \tau_a < \tau^*$ when τ^* exists. When $a > 0$ we can also show that $\tau_a < \tau^* < \bar{\tau}_a$.

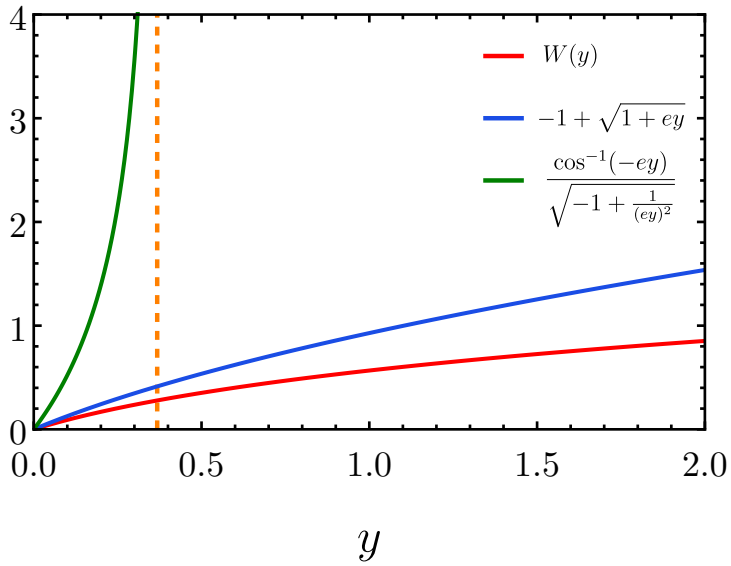

FIGURE C.1: Graphical proof that Eq. (C.17) is satisfied, where we used $y = \frac{a}{eb}$. In particular we can see that $W(y) > -1+\sqrt{1+ey}$ whenever $y > 0$, whereas the second inequality holds when $0 < y < e^{-1}$, i.e., when last term takes real values and so when τ^* exists. The orange dashed line correspond to $y = e^{-1}$ after which $\frac{\cos^{-1}\left(-\frac{a}{b}\right)}{|a|\sqrt{(b/a)^2-1}}$ (hence $*\tau^*$) does not exists anymore. Hence these comparisons would be enough to conclude that with $a > 0$ we have $\tau_c < \tau_a$ always, but also that $\tau_c < \tau_a < \tau^*$ in the region of the parameters in which the last threshold exists, i.e., when $0 < a < b$.

To do so, looking at the expression for τ_c, τ_a and τ^* we gave in the main text, we need to show

$$\underbrace{\frac{1}{a}\cdot W\left(\frac{a}{eb}\right)}_{\text{for } a>-b} < \overbrace{\frac{-1+\sqrt{1+\frac{a}{b}}}{a}}^{\text{for } |a/b|<1} < \frac{\cos^{-1}\left(-\frac{a}{b}\right)}{|a|\sqrt{(b/a)^2-1}} \tag{C.16}$$

Let us consider first the case $a > 0$. In this case Eq. (C.16) is equivalent to

$$\underbrace{W\left(\frac{a}{eb}\right)}_{\text{for } a/b>0} < \overbrace{-1+\sqrt{1+\frac{a}{b}}}^{\text{for } 0<a/b<1} < \frac{\cos^{-1}\left(-\frac{a}{b}\right)}{\sqrt{(b/a)^2-1}} \tag{C.17}$$

To start, we can show these comparisons by plotting the three functions after having defined $y = \frac{a}{eb}$. The result, which confirms that Eq. (C.16) holds for $a > 0$, is displayed in Figure C.1.

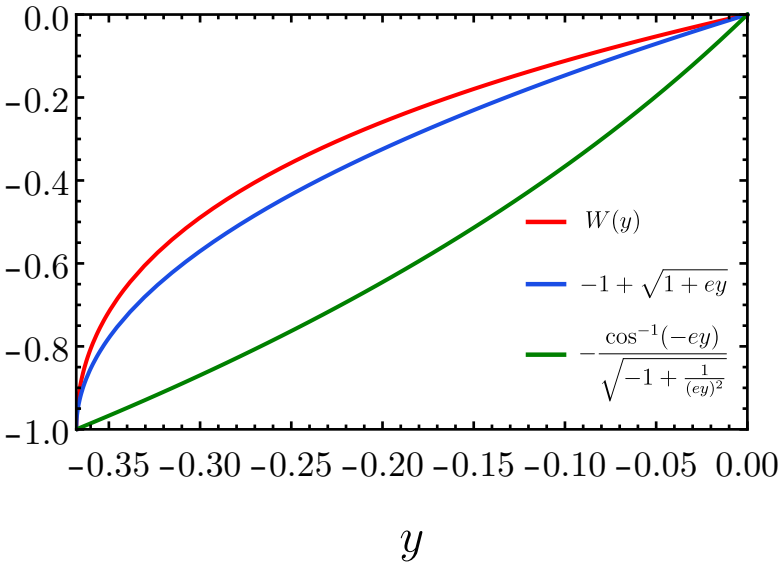

FIGURE C.2: Graphical proof that Eq. (C.17) is satisfied for $-e^{-1} < y < 0$, where $y = \frac{a}{eb}$. Thanks to this we can conclude that $\tau_c < \tau_a < \tau^*$ when $-b < a < 0 < b$.

If $a < 0$ instead, looking at Eq. (C.16) we need to show that

$$W\left(\frac{a}{eb}\right) > -1 + \sqrt{1 + \frac{a}{b}} > -\frac{\cos^{-1}\left(-\frac{a}{b}\right)}{\sqrt{(b/a)^2 - 1}} \tag{C.18}$$

Here we are going to show this again through the graphical comparison shown in Figure C.2. In this we defined again $y = \frac{a}{eb}$ with $-e^{-1} < y < 0$ (remember that in order to have stability when $a < 0$ we need $-b < a < 0 < b$).

In this way we shown that $\tau_c < \tau_a < \tau^*$, proving that for fixed a and b there is a range of values for the delay in which the mean-field limit of the dynamics displays damped oscillations, however the noise is not able to sustain them. Also in this regime the mean-field stationary solution is stable and hence everything is well-defined.

Last we can also show by graphical comparison that for $-b < a < 0 < b$ we always have $\tau^* < \bar{\tau}_a$. This is equivalent to

$$\frac{\cos^{-1}\left(-\frac{a}{b}\right)}{|a|\sqrt{(b/a)^2 - 1}} < \frac{1 + \sqrt{1 + \frac{a}{b}}}{|a|} \tag{C.19}$$

Calling $q = \frac{a}{b}$ where $-1 < q < 0$, Eq. (C.19) can be written as

$$\frac{\cos^{-1}\left(-q\right)}{\sqrt{\frac{1}{q^2} - 1}} < 1 + \sqrt{1 + q} \tag{C.20}$$

Figure C.3 shows that Eq. (C.20) holds, proving $\tau^* < \bar{\tau}_a$ as we wanted.

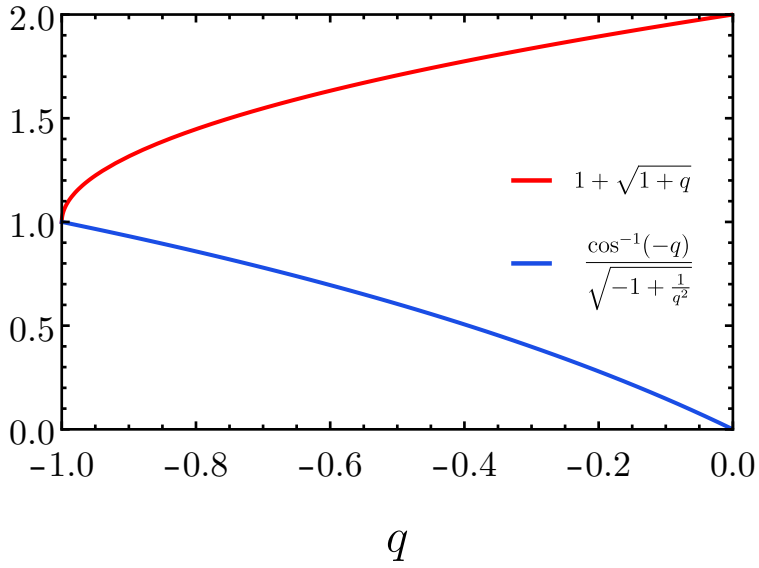

FIGURE C.3: Graphical proof that Eq. (C.20) is satisfied for $-1 < q < 0$, where $q = \frac{a}{b}$. Thanks to this we can conclude that $\tau^* < \bar{\tau}_a$ when $-b < a < 0 < b$.

C.5 Stochastic amplification without asymptotic damped oscillations

In this section we are going to show that the framework accounting for distributed delay can display non-trivial peaks in the power-spectrum even if the deterministic dynamics asymptotically does not oscillate.

To do so, for the sake of concreteness, we consider an exponential memory kernel, i.e.,

$$G(z) = \frac{e^{-t/\tau}}{\tau} \tag{C.21}$$

which of course it is the the Gamma distribution we presented in Eq. (4.56) for $k = 1$.

In this case, the characteristic equation Eq. (4.41) reduces to

$$\lambda + a + \frac{b}{1+\lambda\tau} = \frac{\tau\lambda^2 + (1+a\tau)\lambda + a + b}{1+\lambda\tau} = 0 \tag{C.22}$$

So the roots are found to be

$$\lambda_{1,2} = \frac{-(1+a\tau) \pm \sqrt{(1+a\tau)^2 - 4\tau(a+b)}}{2\tau} \tag{C.23}$$

From Eq. (4.58) we can see that in the exponential case we get

$$P(\omega) = \frac{D}{\left(a + \frac{b}{1+(\omega\tau)^2}\right)^2 + \left(\omega - \frac{b\omega}{1+(\omega\tau)^2}\right)^2} \tag{C.24}$$

with the general condition to have a non-trivial peak becoming

$$(1 - b\tau)^2 - 2\tau^2 b(b + a) < 0 \tag{C.25}$$

since $\mu_1 = \tau$ and $\mu_2 = 2\tau^2$.

For a fixed τ, we can search for the regions of the model parameters a and b for which the system is deterministically and asymptotically stable ($\mathrm{Re}\,[\lambda_{1,2}] < 0$), where the dynamics displays damped oscillations ($\mathrm{Re}\,[\lambda_{1,2}] < 0$ and $\mathrm{Im}\,[\lambda_{1,2}] \neq 0$) and when condition Eq. (C.25) is fulfilled. Doing this for $\tau = 1$, we obtain Figure C.4. Surprisingly, we find a region (indicated by the black star) in which the system does not display damped oscillations but we predict a non-trivial peak in the power-spectrum. We also check this by computing the numerical power-spectrum for a and b in such region and we show the result in Figure tot. As we can see a clear peak emerge in the theoretical power-spectrum and in the numerical one, which show an excellent agreement, emerges, although with the parameters we chose for the simulation we find real and negative values for $\lambda_{1,2}$.

Hence to understand what is happening, we have to go beyond the simple asymptotic analysis of the deterministic dynamics and look at the solution we obtained in Eq. (C.11). In the exponential kernel scenario, we can see that Eq. (C.9) becomes

$$\tilde{x}(s) = \frac{x(0) - bJ(s)}{\tau(s - \lambda_1)(s - \lambda_2)}(1 + s\tau) \tag{C.26}$$

since $\tilde{G}(s) = \frac{1}{1+s\tau}$. Assuming that the initial condition used are such that $J(s)$ does not have any pole with negative real part we get that

$$x(t) = \frac{1}{\tau\,(\lambda_1 - \lambda_2)}\left\{ (1 + \lambda_1\tau)\,[x(0) - bJ\,(\lambda_1)]\,e^{\lambda_1 t} - (1 + \lambda_2\tau)\,[x(0) - bJ\,(\lambda_2)]\,e^{\lambda_2 t}\right\} \tag{C.27}$$

Setting $t = 0$, we can see that for consistency this is a solution, i.e., we retrieve $x(t = 0) = x(0)$, if and only if we get

$$(1 + \lambda_1\tau)J(\lambda_1) = (1 + \lambda_2\tau)J(\lambda_2) \tag{C.28}$$

Hence Eq. (C.27) is a solution only if we consider initial condition satisfying Eq. (C.28). For example, if we assume that $x(t) = x(0)e^{kt}$ for $k > 0$, we get

$$J(s) = \frac{x(0)\tau}{(1 + k\tau)(1 + s\tau)} \tag{C.29}$$

and we can immediately see that Eq. (C.28) holds. So we get that

$$\tilde{x}(s) = \frac{x(0)(1 + s\tau) - b\frac{x(0)\tau}{1+k\tau}}{\tau(s - \lambda_1)(s - \lambda_2)} \tag{C.30}$$

and we see that all its poles come from the solutions of the characteristic equation. Thus, the solution in the time domain $x(t)$, shown in Eq. (C.27), is

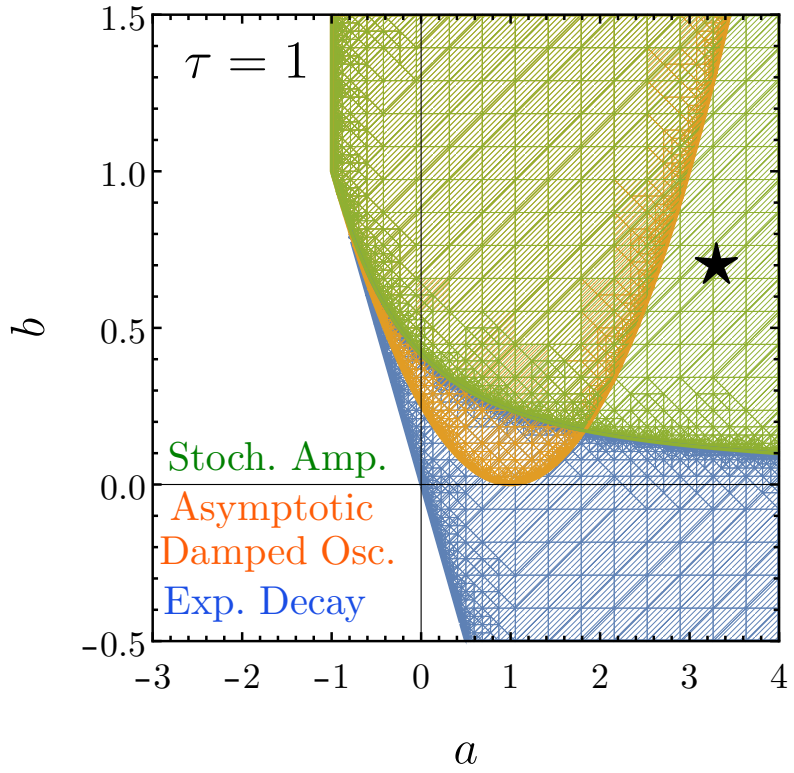

FIGURE C.4: Phase diagram in the $a - b$ plane characterizing the behavior of the dynamics Eq. (4.39) with the exponential kernel Eq. (C.21) ($\tau = 1$). Outside the colored area the system is unstable, whereas inside the colored area $\bar{x} = 0$ is asymptotically stable in the deterministic dynamics. In the blue sub-region the system approaches asymptotically $\bar{x}$ via exponential decay, while in the orange one damped oscillations can be observed. Finally the green tells us where power-spectrum of the random fluctuations presents a non-trivial peak. Interestingly, we can see that there is a region, indicated by the black star, where we have a non trivial peak in the power-spectrum, but the deterministic dynamics does not present oscillations, i.e., we have stochastic amplification even without damped oscillations.

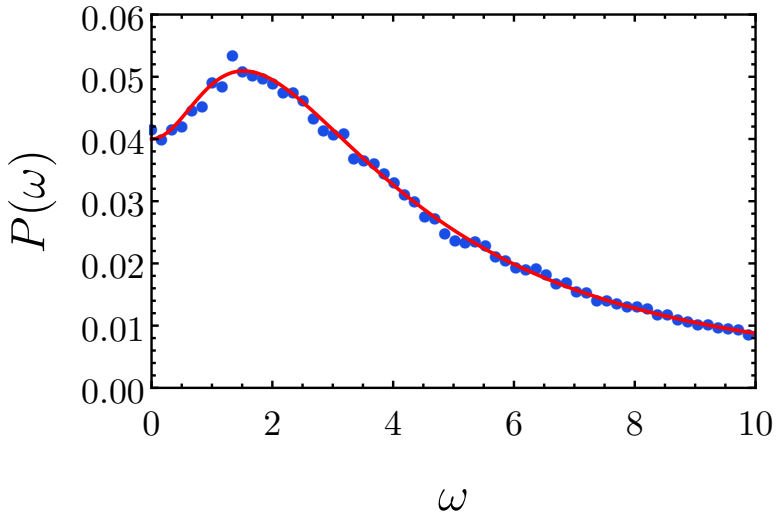

FIGURE C.5: Comparison between the theoretical power-spectrum (solid red line) in the case of distributed delay with an exponential kernel Eq. (C.21) and the one numerically obtained as an average from 1000 independent realizations (blue dots). The time increment used is $dt = 5 \cdot 10^{-4}$. The parameters are $a = 4$, $b = 2$, $\tau = 1$ and $D = 1$. The clear presence of a peak is the signature that also in this case the stochastic amplification phenomenon occurred, however we also have $\lambda_1 \approx -1.38$ and $\lambda_2 \approx -3.62$, so the system does not show damped oscillations.

given by the following expression

$$x(t) = \frac{x(0)}{\tau\left(\lambda_1 - \lambda_2\right)}\left\{\left[\left(1+\lambda_1\tau\right) - \frac{b\tau}{1+k\tau}\right]e^{\lambda_1 t} - \left[\left(1+\lambda_2\tau\right) - \frac{b\tau}{1+k\tau}\right]e^{\lambda_2 t}\right\} \tag{C.31}$$

Assuming the system does not display asymptotic damped oscillations, i.e., $\lambda_{1,2}$ are real and negative, we can search if Eq. (C.31) becomes zero for $t = t^* > 0$. This gives

$$t^* = \frac{1}{\lambda_1 - \lambda_2}\ln\left(\frac{x(0)\left(1+\lambda_2\tau\right) - b\left(1+\lambda_2\tau\right)J(\lambda_2)}{x(0)\left(1+\lambda_1\tau\right) - b\left(1+\lambda_1\tau\right)J(\lambda_1)}\right) > 0 \tag{C.32}$$

If we take $\lambda_1 > \lambda_2$ the above inequality reduces to

$$\frac{x(0)\left(1+\lambda_2\tau\right) + \Lambda}{x(0)\left(1+\lambda_1\tau\right) + \Lambda} > 1 \tag{C.33}$$

where $\Lambda = -b(1+\lambda_1\tau)J(\lambda_1) = -b(1+\lambda_2\tau)J(\lambda_2)$, as we employed the condition Eq. (C.28). We can still simplify the above inequality to obtain

$$\frac{1+\lambda_2\tau}{1+\lambda_1\tau} > 1 \tag{C.34}$$

In order to be true, numerator and the denominator need to have the same sign. Moreover, since we know that $\lambda_1 > \lambda_2$, finally we get that the condition

to have $t^* > 0$ reads

$$\lambda_2 < \lambda_1 < -\frac{1}{\tau} \tag{C.35}$$

independently of the initial condition we used. Searching the region of the parameters space where such condition is met, we obtain Figure C.6. This shows that the necessary condition to ensure the occurrence of stochastic amplification is the deterministic solution to cross the zero, even a finite number of times. Asymptotically this is granted in the case of damped oscillations. More in general, as we discussed in this section, one should be more careful and consider the full solution and not simply rely on the asymptotic predictions, which could cause the apparent surprising result of the presence of a non-trivial peak in the power-spectrum when the deterministic dynamics does not oscillate.

C.6 Dynamics affected by colored noise

In this section we investigate what happens when we substitute the white noise appearing in Eq. (4.1) with one having non-trivial temporal autocorrelation at the stationarity, i.e., a colored noise. So the starting equation now becomes

$$\frac{dx(t)}{dt} = -ax(t) - bx(t-\tau) + \zeta(t) \tag{C.36}$$

where the noise $\zeta(t)$ is such that it has zero mean, i.e., $\langle \zeta(t) \rangle = 0$, and correlation depending only on the temporal distance, i.e., $\langle \zeta(t)\zeta(t') \rangle = C(t-t')$.

To compute the power-spectrum we replicate the same procedure we have shown so far. So we start by taking the Fourier transform of Eq. (C.36). In this way one gets

$$i\omega\hat{x}(\omega) = -a\hat{x}(\omega) - b\hat{x}(\omega)e^{-i\omega\tau} + \hat{\zeta}(\omega) \tag{C.37}$$

where we have $\langle \hat{\zeta}(\omega) \rangle = 0$ and $\langle \hat{\zeta}(\omega)\hat{\zeta}(\omega') \rangle = \delta(\omega - \omega')\hat{C}(\omega)$, with $\hat{C}(\omega)$ being the Fourier transform of the correlation function $C(t)$.

At this point it is easy to obtain the power-spectrum, which now it has the form

$$P(\omega) = \frac{\hat{C}(\omega)}{\left[a + b\cos(\omega\tau)\right]^2 + \left[\omega - b\sin(\omega\tau)\right]^2} \tag{C.38}$$

Hence we can see that the power-spectrum is the same one obtained in Eq. (4.27) for the white noise case multiplied by the Fourier transform of the temporal correlation affecting now the noise term.

We test this result against numerical evidences for the case in which the correlation decays exponentially with the elapsing of the time, i.e.,

$$C(t) = \frac{D}{2\tau_{corr}} e^{-\frac{|t|}{\tau}} \tag{C.39}$$

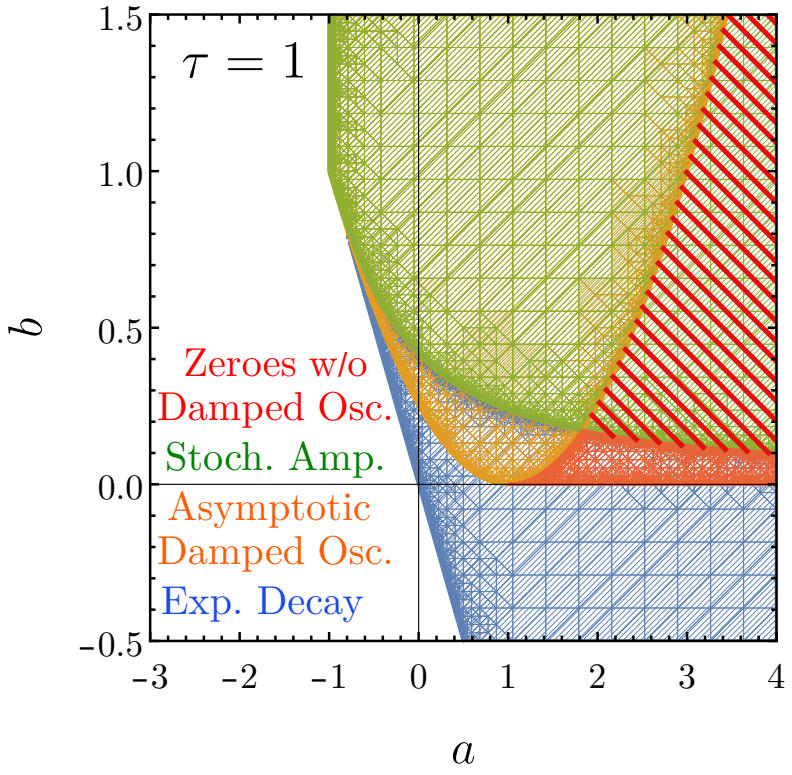

FIGURE C.6: Phase diagram in the $a - b$ plane characterizing the behavior of the dynamics Eq. (4.39) with the exponential kernel Eq. (C.21) ($\tau = 1$). With respect to the one shown in Figure C.4, we add the red region where the condition Eq. (C.35) is satisfied and hence the deterministic solution has a zero at a certain moment $t^* > 0$. The region striped red and green region (previously marked by the black star) corresponds to the region of the parameters where deterministically we do not observe damped oscillation but $x(t)$ touches the horizontal axes and at the same time the stochastic formulation predicts the emergence of a peak in the power-spectrum, hinting the presence of time persistent oscillations. Also in this case we see that there is a region where Eq. (C.35) holds but not Eq. (C.25), meaning that also the presence of zero in the deterministic evolution of the dynamics is a necessary but not a sufficient condition to observe stochastic amplification.

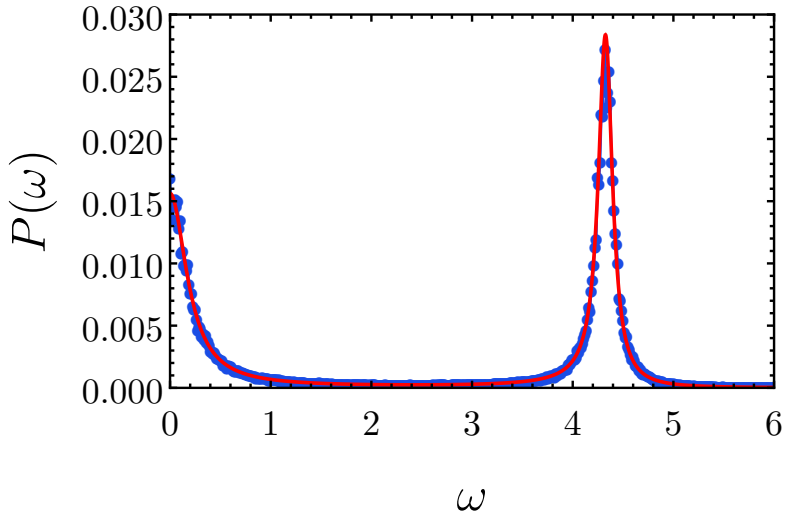

FIGURE C.7: Comparison between the theoretical power-spectrum shown in Eq. (C.38) (solid red line) and the one obtained numerically as an average of the single estimates obtained from 250 independent realizations of the process. In this case we consider a noise with correlation as the one displayed in Eq. (C.39). The parameters considered are $a = 3$, $b = 5$, $\tau = 0.5$, $\tau_{corr} = 0.1$ and $D = 1$. The simulations are performed using a time increment $dt = 10^{-3}$ with the prescription $x(t) = x_0 = 10^{-2}$ for $t \in [-\tau, 0]$.

and so we have

$$\hat{C}(\omega) = \frac{D}{1 + (\omega\tau_{corr})^2} \tag{C.40}$$

In Figure C.7 we show the agreement between analytical result and the simulation outcomes. We see that, again for the parameters choice we made, stochastic amplification took place, as supported by the presence of a peak in a non-zero value of ω.

C.7 Multi-dimensional delayed Ornstein-Uhlenbeck process

In this section we show that stochastic amplification in presence of delay takes place also in the case of multidimensional system. Of course this is not surprising since in the non-delayed scenario it is required to deal with more than two dynamical quantities in order to observed long-standing fluctuations around the deterministic solution. However, here we show by providing a numerical example that including delay contributions stochastic amplification is more likely to be observed.

For simplicity we discuss now a two-dimensional system, but the generalization to higher dimension is straightforward. So we will consider two

coupled equation of the type of Eq. (4.1) obtaining the following dynamics

$$\begin{pmatrix} \frac{dx(t)}{dt} \\ \frac{dy(t)}{dt} \end{pmatrix} = \mathbf{A} \begin{pmatrix} x(t) \\ y(t) \end{pmatrix} + \mathbf{B} \begin{pmatrix} x(t-\tau_1) \\ y(t-\tau_2) \end{pmatrix} + \overbrace{\begin{pmatrix} \sqrt{D_1} & 0 \\ 0 & \sqrt{D_2} \end{pmatrix}}^{\mathbf{D}} \begin{pmatrix} \xi_1(t) \\ \xi_2(t) \end{pmatrix} \tag{C.41}$$

where $\xi_{1,2}(t)$ are Gaussian white noises as usual.

For simplicity we assumed the noises to be uncorrelated, i.e., the matrix D to be diagonal. Also we could generalized even further the setting by letting the delayed terms to have different values of delays, i.e.,

$$\mathbf{B} \begin{pmatrix} x(t-\tau_1) \\ y(t-\tau_2) \end{pmatrix} \to \begin{pmatrix} b_{11} \cdot x(t-\tau_{11}) & b_{12} \cdot y(t-\tau_{12}) \\ b_{21} \cdot x(t-\tau_{21}) & b_{22} \cdot y(t-\tau_{22}) \end{pmatrix} \tag{C.42}$$

However, the steps of the derivation we are going to show can still be followed and similar results can be obtained.

Let us take $\mathbf{A}$ to be invertible and such that $x(t)$ and $y(t)$ do not display oscillations when the dynamics approach to the steady state. We also want that the stationary solution of

$$\begin{pmatrix} \frac{dx(t)}{dt} \\ \frac{dy(t)}{dt} \end{pmatrix} = \mathbf{A} \begin{pmatrix} x(t) \\ y(t) \end{pmatrix}, \tag{C.43}$$

which is $(x^*, y^*) = (0, 0)$, to be stable. To accomplish this we have therefore to consider a matrix $\mathbf{A}$ with real and negative eigenvalues. This requirements is made because now we add terms affected by time delay and the dynamics may display oscillations. Therefore we can be sure that the oscillations are caused by the delayed contribution described by $\mathbf{B} \begin{pmatrix} x(t-\tau_1) \\ y(t-\tau_2) \end{pmatrix}$ in Eq. (C.41). The dynamics now is

$$\begin{pmatrix} \frac{dx(t)}{dt} \\ \frac{dy(t)}{dt} \end{pmatrix} = \mathbf{A} \begin{pmatrix} x(t) \\ y(t) \end{pmatrix} + \mathbf{B} \begin{pmatrix} x(t-\tau_1) \\ y(t-\tau_2) \end{pmatrix} \tag{C.44}$$

To observe oscillations the roots of the characteristic equation

$$(\lambda - a_{11} - b_{11}e^{-\lambda\tau_1})(\lambda - a_{22} - b_{22}e^{-\lambda\tau_2}) - (-a_{12} - b_{12}e^{-\lambda\tau_2})(-a_{21} - b_{21}e^{-\lambda\tau_1}) = 0 \tag{C.45}$$

have to be complex, i.e., $\mathrm{Im}(\lambda) \neq 0$.

At this point we can compute the power-spectra for $x(t)$ and $y(t)$ with the same procedure. So considering the Fourier transform of Eq. (C.41) we get

$$i\omega \begin{pmatrix} \hat{x}(\omega) \\ \hat{y}(\omega) \end{pmatrix} = \mathbf{A} \begin{pmatrix} \hat{x}(\omega) \\ \hat{y}(\omega) \end{pmatrix} + \mathbf{B} \begin{pmatrix} \hat{x}(\omega)e^{-i\omega\tau_1} \\ \hat{y}(\omega)e^{-i\omega\tau_2} \end{pmatrix} + \begin{pmatrix} \sqrt{D_1} & 0 \\ 0 & \sqrt{D_2} \end{pmatrix} \begin{pmatrix} \hat{\xi}_1(\omega) \\ \hat{\xi}_2(\omega) \end{pmatrix} \tag{C.46}$$

Hence we find that

$$\hat{x}(\omega) = \frac{\sqrt{D_1}c_2 2(\omega)\hat{\xi}_1(\omega) + \sqrt{D_2}c_{12}(\omega)\hat{\xi}_2(\omega)}{c_{11}(\omega)c_{22}(\omega) - c_{12}(\omega)c_{21}(\omega)} \quad , \tag{C.47a}$$

$$\hat{y}(\omega) = \frac{\sqrt{D_1}c_{12}(\omega)c_{21}(\omega)\hat{\xi}_1(\omega) + \sqrt{D_2}c_{12}(\omega)c_{11}(\omega)\hat{\xi}_2(\omega)}{c_{12}(\omega)\{c_{11}(\omega)c_{22}(\omega) - c_{12}(\omega)c_{21}(\omega)\}} \quad , \tag{C.47b}$$

where

$$c_{11}(\omega) = i\omega - a_{11} - b_{11}e^{-i\omega\tau_1} \quad , \tag{C.48}$$

$$c_{12}(\omega) = a_{12} + b_{12}e^{-i\omega\tau_2} \quad , \tag{C.49}$$

$$c_{21}(\omega) = a_{21} + b_{21}e^{-i\omega\tau_1} \quad , \tag{C.50}$$

$$c_{22}(\omega) = i\omega - a_{22} - b_{22}e^{-i\omega\tau_2} \quad . \tag{C.51}$$

From Eqs. (C.47a)-(C.47b) it is easy to get the expressions of the two power-spectra.

To test the bounty of this results, we perform a comparison with the numerical outcomes where we take

$$\mathbf{A} = \begin{pmatrix} -0.01 & 0.001 \\ 0.001 & -0.02 \end{pmatrix} \qquad \mathbf{B} = \begin{pmatrix} -0.4 & 0 \\ 0 & -0.4 \end{pmatrix} \tag{C.52}$$

It is possible to proof that both the matrices A and $A + B$ have real eigenvalues. Hence, when introducing non-zero delays, we can state that the solutions of the characteristic equation Eq. (C.45) become complex because of them. In other words, we are sure that the oscillations we might observe will be due to the presence of the negative delayed feedback contribution.

Generating several independent time series for $x(t)$ and $y(t)$ by direct simulation of Eq. (C.41) can numerically evaluate the power-spectra of these two quantities. The comparison with the ones obtained from Eqs. (C.47a) and (C.47b) is shown in Figure C.8. In both the power-spectra we can clearly observe a peak, confirming stochastic amplification took place. For the choice we made, this was possible only because of the presence of the time-delays.

Hence we can conclude that the addition to the framework of delayed terms enlarge the region in the parameters space in which stochastic amplification is observed.

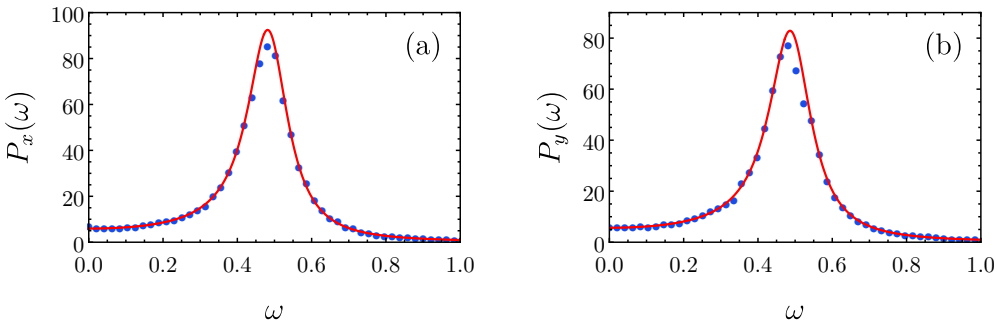

FIGURE C.8: Comparison between the theoretical power-spectra (solid red lines) with the ones obtained averaging over 250 independent time-series (blue dots). In panel (a) we present the result for the variable $x(t)$, while panel (b) refers to the component $y(t)$. In the simulations we used the matrices A and B presented in Eq. (C.52). The other parameters are $\tau_1 = \tau_2 = 3$ and $D_1 = D_2 = 1$. The time increment is $dt = 10^{-3}$ and the prescriptions are $x(t) = x_0 = 10^{-2}$ and $y(t) = y_0 = -10^{-2}$ for $t \in [-\tau_1, 0]$. The agreement between theory and numerical analysis is remarkable.

Bibliography

[1] AF Horadam. “" Fibonacci’s Liber Abaci": A Translation into Modern English of Leonardo Pisano’s Book of Calculation by LE Sigler”. In: *FIBONACCI QUARTERLY* 42.1 (2004), pp. 82–85.

[2] Thomas Robert Malthus. *An essay on the principle of population, as it affects the future imporvement of society, with remarks on the speculations of Mr. Godwin, M. Condorcet, and other writers*. The Lawbook Exchange, Ltd., 1798.

[3] Pieter Frans Verhulst. “Recherches mathématiques sur la loi d’accroissement de la population”. In: *Journal des économistes* 12 (1845), p. 276.

[4] Alfred J Lotka. “Analytical note on certain rhythmic relations in organic systems”. In: *Proceedings of the National Academy of Sciences* 6.7 (1920), pp. 410–415.

[5] Vito Volterra. “Variazioni e fluttuazioni del numero d’individui in specie animali conviventi”. In: (1926).

[6] Gerald Teschl. *Ordinary differential equations and dynamical systems*. Vol. 140. American Mathematical Soc., 2012.

[7] Johan AJ Metz, Stefan AH Geritz, Géza Meszéna, et al. “Adaptive dynamics: a geometrical study of the consequences of nearly faithful reproduction”. In: (1995).

[8] Josef Hofbauer, Karl Sigmund, et al. *Evolutionary games and population dynamics*. Cambridge university press, 1998.

[9] Robert M May. *Stability and complexity in model ecosystems*. Princeton university press, 2019.

[10] Richard L Olson and Ronaldo A Sequeira. “An emergent computational approach to the study of ecosystem dynamics”. In: *Ecological Modelling* 79.1-3 (1995), pp. 95–120.

[11] Nino Boccara. *Modeling complex systems*. Springer Science & Business Media, 2010.

[12] Simon A Levin. “Ecosystems and the biosphere as complex adaptive systems”. In: *Ecosystems* 1.5 (1998), pp. 431–436.

[13] Brian A Maurer. *Untangling ecological complexity: the macroscopic perspective*. University of Chicago Press, 1999.

[14] William K Michener, Thomas J Baerwald, Penelope Firth, et al. “Defining and unraveling biocomplexity”. In: *BioScience* 51.12 (2001), pp. 1018–1023.

[15] Erwin Schrödinger. *What is Life? The Physical Aspect of the Living Cell*. Cambridge University Press, 1944.

[16] Miguel A Munoz. "Colloquium: Criticality and dynamical scaling in living systems". In: *Reviews of Modern Physics* 90.3 (2018), p. 031001.

[17] Uwe Sauer, Matthias Heinemann, and Nicola Zamboni. "Getting closer to the whole picture". In: *Science(Washington)* 316.5824 (2007), pp. 550–551.

[18] Jay Odenbaugh. "Idealized, inaccurate but successful: A pragmatic approach to evaluating models in theoretical ecology". In: *Biology and Philosophy* 20.2-3 (2005), pp. 231–255.

[19] Robert M May. "Biological populations obeying difference equations: stable points, stable cycles, and chaos". In: *Journal of Theoretical Biology* 51.2 (1975), pp. 511–524.

[20] Ricard Solé and Brian Goodwin. "How complexity pervades biology". In: *Basic Books* (2000).

[21] Jordl Bascompte and Ricard V Solé. "Rethinking complexity: modelling spatiotemporal dynamics in ecology". In: *Trends in Ecology & Evolution* 10.9 (1995), pp. 361–366.

[22] David Storch and Kevin J Gaston. "Untangling ecological complexity on different scales of space and time". In: *Basic and Applied Ecology* 5.5 (2004), pp. 389–400.

[23] James P O'Dwyer and Jessica L Green. "Field theory for biogeography: a spatially explicit model for predicting patterns of biodiversity". In: *Ecology letters* 13.1 (2010), pp. 87–95.

[24] Simon A Levin. "The problem of pattern and scale in ecology: the Robert H. MacArthur award lecture". In: *Ecology* 73.6 (1992), pp. 1943–1967.

[25] William Bialek. "Perspectives on theory at the interface of physics and biology". In: *Reports on Progress in Physics* 81.1 (2017), p. 012601.

[26] Ricard V Sole and Ma Montoya. "Complexity and fragility in ecological networks". In: *Proceedings of the Royal Society of London. Series B: Biological Sciences* 268.1480 (2001), pp. 2039–2045.

[27] Elise Filotas, Lael Parrott, Philip J Burton, et al. "Viewing forests through the lens of complex systems science". In: *Ecosphere* 5.1 (2014), pp. 1–23.

[28] Hans Frauenfelder. "Ask not what physics can do for biology—ask what biology can do for physics". In: *Physical biology* 11.5 (2014), p. 053004.

[29] Gerald H Pollack and Wei-Chun Chin. *Phase transitions in cell biology*. Springer, 2008.

[30] Benoit B Mandelbrot. *The fractal geometry of nature*. Vol. 1. WH freeman New York, 1982.

[31] Manfred Schroeder. *Fractals, chaos, power laws: Minutes from an infinite paradise*. Courier Corporation, 2009.

[32] Uri Alon. *An introduction to systems biology: design principles of biological circuits*. CRC press, 2019.

[33] William Bialek, Andrea Cavagna, Irene Giardina, et al. "Statistical mechanics for natural flocks of birds". In: *Proceedings of the National Academy of Sciences* 109.13 (2012), pp. 4786–4791.

[34] William Bialek. *Biophysics: searching for principles*. Princeton University Press, 2012.

[35] A. Sher and M.C. Molles. *Ecology: Concepts and Applications*. McGraw-Hill Education, 2018.

[36] Rolf Daniel. "The metagenomics of soil". In: *Nature Reviews Microbiology* 3 (2005), pp. 470–478.

[37] Steven R. Gill, Mihai Pop, Robert T. DeBoy, et al. "Metagenomic Analysis of the Human Distal Gut Microbiome". In: *Science* 312.5778 (2006), pp. 1355–1359.

[38] Catherine A. Lozupone, Jesse I. Stombaugh, Jeffrey I. Gordon, et al. "Diversity, stability and resilience of the human gut microbiota". In: *Nature* 489 (2012), pp. 220–230.

[39] Robert H. MacArthur and John W. MacArthur. "On Bird Species Diversity". In: *Ecology* 42.3 (1961), pp. 594–598.

[40] Olivier S. G. Pauwels, Van Wallach, and Patrick David. "Global diversity of snakes (Serpentes; Reptilia) in freshwater". In: *Freshwater Animal Diversity Assessment*. Ed. by E. V. Balian, C. Lévêque, H. Segers, et al. Dordrecht: Springer Netherlands, 2008, pp. 599–605.

[41] Elise F. Zipkin, Graziella V. DiRenzo, Julie M. Ray, et al. "Tropical snake diversity collapses after widespread amphibian loss". In: *Science* 367.6479 (2020), pp. 814–816.

[42] Ricardo Lourenço-de Moraes, Fernando Miranda Lansac-Toha, Leilane Talita Fatoreto Schwind, et al. "Climate change will decrease the range size of snake species under negligible protection in the Brazilian Atlantic Forest hotspot". In: *Scientific Reports* 9 (2019), p. 8523.

[43] M A Huston. "Patterns of Species Diversity on Coral Reefs". In: *Annual Review of Ecology and Systematics* 16.1 (1985), pp. 149–177.

[44] Nancy Knowlton and Jeremy Jackson. "The Evolutionary Diversity and Ecological Complexity of Coral Reefs". In: *The Paleontological Society Papers* 17 (2011), 111–120.

[45] Laetitia Plaisance, M. Julian Caley, Russell E. Brainard, et al. "The Diversity of Coral Reefs: What Are We Missing?" In: *PLOS ONE* 6.10 (Oct. 2011), pp. 1–7.

[46] Michael Asigbaase, Sofie Sjogersten, Barry H. Lomax, et al. "Tree diversity and its ecological importance value in organic and conventional cocoa agroforests in Ghana". In: *PLOS ONE* 14.1 (Jan. 2019), pp. 1–19.

[47] AH Gentry. "Tree species richness of upper Amazonian forests". In: *Proceedings of the National Academy of Sciences of the United States of America* 85.1 (Jan. 1988), 156—159.

[48] R. May and A.R. McLean. *Theoretical Ecology: Principles and Applications*. OUP Oxford, 2007.

[49] DAVID TILMAN. *Resource Competition and Community Structure. (MPB-17), Volume 17*. Princeton University Press, 1982.

[50] Robert MacArthur and Richard Levins. "The limiting similarity, convergence, and divergence of coexisting species". In: *The american naturalist* 101.921 (1967), pp. 377–385.

[51] Francesco Carrara, Andrea Giometto, Mathew Seymour, et al. "Inferring species interactions in ecological communities: a comparison of methods at different levels of complexity". In: *Methods in Ecology and Evolution* 6.8 (2015), pp. 895–906.

[52] Aleksej Zelezniak, Sergej Andrejev, Olga Ponomarova, et al. "Metabolic dependencies drive species co-occurrence in diverse microbial communities". In: *Proceedings of the National Academy of Sciences* 112.20 (2015), pp. 6449–6454.

[53] Joshua E. Goldford, Nanxi Lu, Djordje Bajić, et al. "Emergent simplicity in microbial community assembly". In: *Science* 361.6401 (2018), pp. 469–474.

[54] G. E. Hutchinson. "The Paradox of the Plankton". In: *The American Naturalist* 95.882 (1961), pp. 137–145.

[55] Robert M May. "Will a large complex system be stable?" In: *Nature* 238.5364 (1972), pp. 413–414.

[56] Terence Tao, Van Vu, and Manjunath Krishnapur. "Random matrices: Universality of ESDs and the circular law". In: *The Annals of Probability* 38.5 (2010), pp. 2023–2065.

[57] Giacomo Livan, Marcel Novaes, and Pierpaolo Vivo. *Introduction to random matrices: theory and practice*. Vol. 26. Springer, 2018.

[58] Stefano Allesina and Si Tang. "The stability–complexity relationship at age 40: a random matrix perspective". In: *Population Ecology* 57.1 (2015), pp. 63–75.

[59] Kevin Shear McCann. "The diversity–stability debate". In: *Nature* 405.6783 (2000), pp. 228–233.

[60] Robert Mac Arthur. "Species packing, and what competition minimizes". In: *Proceedings of the National Academy of Sciences* 64.4 (1969), pp. 1369–1371.

[61] Robert MacArthur. "Species packing and competitive equilibrium for many species". In: *Theoretical population biology* 1.1 (1970), pp. 1–11.

[62] Robert Mac Arthur. "SPECIES PACKING, AND WHAT COMPETITION MINIMIZES". In: *Proceedings of the National Academy of Sciences* 64.4 (1969), pp. 1369–1371.

[63] Peter Chesson. "MacArthur's consumer-resource model". In: *Theoretical Population Biology* 37.1 (1990), pp. 26 –38.

[64] Jacques Monod. "The growth of bacterial cultures". In: *Annual review of microbiology* 3.1 (1949), pp. 371–394.

[65] Garrett Hardin. "The competitive exclusion principle". In: *science* 131.3409 (1960), pp. 1292–1297.

[66] Michael Cross and Henry Greenside. *Pattern formation and dynamics in nonequilibrium systems*. Cambridge University Press, 2009.

[67] Rebecca Hoyle and Rebecca B Hoyle. *Pattern formation: an introduction to methods*. Cambridge University Press, 2006.

[68] JD Murray. *Mathematical biology II: spatial models and biomedical applications*. Vol. 3. Springer-Verlag, 2001.

[69] Len M Pismen. *Patterns and interfaces in dissipative dynamics*. Springer Science & Business Media, 2006.

[70] Daniel Walgraef. *Spatio-temporal pattern formation: with examples from physics, chemistry, and materials science*. Springer Science & Business Media, 2012.

[71] Alan Mathison Turing. "The chemical basis of morphogenesis". In: *Bulletin of mathematical biology* 52.1 (1990), pp. 153–197.

[72] Tamás Bánsági, Vladimir K Vanag, and Irving R Epstein. "Tomography of reaction-diffusion microemulsions reveals three-dimensional Turing patterns". In: *Science* 331.6022 (2011), pp. 1309–1312.

[73] Vincent Castets, Etiennette Dulos, Jacques Boissonade, et al. "Experimental evidence of a sustained standing Turing-type nonequilibrium chemical pattern". In: *Physical review letters* 64.24 (1990), p. 2953.

[74] Qi Ouyang and Harry L Swinney. "Transition from a uniform state to hexagonal and striped Turing patterns". In: *Nature* 352.6336 (1991), pp. 610–612.

[75] John A Vastano, John E Pearson, W Horsthemke, et al. "Chemical pattern formation with equal diffusion coefficients". In: *Physics Letters A* 124.6-7 (1987), pp. 320–324.

[76] Hideki Nabika, Masaki Itatani, and István Lagzi. "Pattern formation in precipitation reactions: the Liesegang phenomenon". In: *Langmuir* 36.2 (2019), pp. 481–497.

[77] RC Di Prima and Harry L Swinney. "Instabilities and transition in flow between concentric rotating cylinders". In: *Hydrodynamic instabilities and the transition to turbulence*. Springer, 1981, pp. 139–180.

[78] Subrahmanyan Chandrasekhar. *Hydrodynamic and hydromagnetic stability*. Courier Corporation, 2013.

[79] Mark C Cross and Pierre C Hohenberg. "Pattern formation outside of equilibrium". In: *Reviews of modern physics* 65.3 (1993), p. 851.

[80] Jean Karl Platten and Jean Claude Legros. *Convection in liquids*. Springer Science & Business Media, 2012.

[81] Lorenz Kramer and Werner Pesch. "Convection instabilities in nematic liquid crystals". In: *Annual review of fluid mechanics* 27.1 (1995), pp. 515–539.

[82] E Dubois-Violette, G Durand, E Guyon, et al. "Instabilities in nematic liquid crystals". In: *1955-1999: Overview, Contents, and Authors* (1999), p. 122.

[83] James S Langer. "Instabilities and pattern formation in crystal growth". In: *Reviews of modern physics* 52.1 (1980), p. 1.

[84] AJ Koch and Hans Meinhardt. "Biological pattern formation: from basic mechanisms to complex structures". In: *Reviews of modern physics* 66.4 (1994), p. 1481.

[85] Alison E Patteson, Arvind Gopinath, and Paulo E Arratia. "The propagation of active-passive interfaces in bacterial swarms". In: *Nature communications* 9.1 (2018), pp. 1–10.

[86] Alfred Gierer and Hans Meinhardt. "A theory of biological pattern formation". In: *Kybernetik* 12.1 (1972), pp. 30–39.

[87] James D Murray. *Mathematical biology: I. An introduction*. Vol. 17. Springer Science & Business Media, 2007.

[88] Akiko Nakamasu, Go Takahashi, Akio Kanbe, et al. "Interactions between zebrafish pigment cells responsible for the generation of Turing patterns". In: *Proceedings of the National Academy of Sciences* 106.21 (2009), pp. 8429–8434.

[89] Hans Meinhardt and Martin Klingler. "A model for pattern formation on the shells of molluscs". In: *Journal of Theoretical Biology* 126.1 (1987), pp. 63–89.

[90] Chiswick Chap. *Giant Pufferfish skin pattern detail*. 2012. URL: https://en.wikipedia.org/wiki/File:Giant_Pufferfish_skin_pattern_detail.jpg.

[91] Shaun Ault and Erik Holmgreen. "Dynamics of the Brusselator". In: *Math* 715 (2003), p. 2.

[92] William J Boettinger, James A Warren, Christoph Beckermann, et al. "Phase-field simulation of solidification". In: *Annual review of materials research* 32.1 (2002), pp. 163–194.

[93] Zhi-Feng Huang, KR Elder, and Nikolas Provatas. "Phase-field-crystal dynamics for binary systems: Derivation from dynamical density functional theory, amplitude equation formalism, and applications to alloy heterostructures". In: *Physical Review E* 82.2 (2010), p. 021605.

[94] Andrew J Archer, Daniel J Ratliff, Alastair M Rucklidge, et al. "Deriving phase field crystal theory from dynamical density functional theory: consequences of the approximations". In: *Physical Review E* 100.2 (2019), p. 022140.

[95] Max Rietkerk and Johan Van de Koppel. "Regular pattern formation in real ecosystems". In: *Trends in ecology & evolution* 23.3 (2008), pp. 169–175.

[96] René Lefever and Olivier Lejeune. "On the origin of tiger bush". In: *Bulletin of Mathematical biology* 59.2 (1997), pp. 263–294.

[97] Olivier Lejeune and Mustapha Tlidi. "A model for the explanation of vegetation stripes (tiger bush)". In: *Journal of Vegetation science* 10.2 (1999), pp. 201–208.

[98] Jost von Hardenberg, Ehud Meron, Moshe Shachak, et al. "Diversity of vegetation patterns and desertification". In: *Physical Review Letters* 87.19 (2001), p. 198101.

[99] Mustapha Tlidi, René Lefever, and Andrei Vladimirov. "On vegetation clustering, localized bare soil spots and fairy circles". In: *Dissipative Solitons: From Optics to Biology and Medicine*. Springer, 2008, pp. 1–22.

[100] Nicolas Barbier, Pierre Couteron, René Lefever, et al. "Spatial decoupling of facilitation and competition at the origin of gapped vegetation patterns". In: *Ecology* 89.6 (2008), pp. 1521–1531.

[101] Erez Gilad, Jost von Hardenberg, Antonello Provenzale, et al. "Ecosystem engineers: from pattern formation to habitat creation". In: *Physical Review Letters* 93.9 (2004), p. 098105.

[102] Cristian Fernandez-Oto, Mustapha Tlidi, Daniel Escaff, et al. "Strong interaction between plants induces circular barren patches: fairy circles". In: *Philosophical Transactions of the Royal Society A: Mathematical, Physical and Engineering Sciences* 372.2027 (2014), p. 20140009.

[103] Pierre Couteron, Fabien Anthelme, Marcel Clerc, et al. "Plant clonal morphologies and spatial patterns as self-organized responses to resource-limited environments". In: *Philosophical Transactions of the Royal Society A: Mathematical, Physical and Engineering Sciences* 372.2027 (2014), p. 20140102.

[104] Daniel Ruiz-Reynés, Damià Gomila, Tomàs Sintes, et al. "Fairy circle landscapes under the sea". In: *Science advances* 3.8 (2017), e1603262.

[105] Ehud Meron. *Nonlinear physics of ecosystems*. CRC Press, 2015.

[106] F Borgogno, P D'Odorico, F Laio, et al. "Mathematical models of vegetation pattern formation in ecohydrology". In: *Reviews of Geophysics* 47.1 (2009).

[107] NM Shnerb, P Sarah, H Lavee, et al. "Reactive glass and vegetation patterns". In: *Physical Review Letters* 90.3 (2003), p. 038101.

[108] Alon Manor and Nadav M Shnerb. "Facilitation, competition, and vegetation patchiness: from scale free distribution to patterns". In: *Journal of theoretical biology* 253.4 (2008), pp. 838–842.

[109] MA Fuentes, MN Kuperman, and VM Kenkre. "Nonlocal interaction effects on pattern formation in population dynamics". In: *Physical review letters* 91.15 (2003), p. 158104.

[110] MG Clerc, D Escaff, and VM Kenkre. "Analytical studies of fronts, colonies, and patterns: combination of the Allee effect and nonlocal competition interactions". In: *Physical Review E* 82.3 (2010), p. 036210.

[111] Emilio Hernández-García and Cristóbal López. "Clustering, advection, and patterns in a model of population dynamics with neighborhood-dependent rates". In: *Physical Review E* 70.1 (2004), p. 016216.

[112] Simone Pigolotti, Cristóbal López, and Emilio Hernández-García. "Species clustering in competitive Lotka-Volterra models". In: *Physical review letters* 98.25 (2007), p. 258101.

[113] Marten Scheffer and Egbert H van Nes. "Self-organized similarity, the evolutionary emergence of groups of similar species". In: *Proceedings of the National Academy of Sciences* 103.16 (2006), pp. 6230–6235.

[114] Olof Leimar, Akira Sasaki, Michael Doebeli, et al. "Limiting similarity, species packing, and the shape of competition kernels". In: *Journal of Theoretical Biology* 339 (2013), pp. 3–13.

[115] Nicolas Barbier, Pierre Couteron, Jean Lejoly, et al. "Self-organized vegetation patterning as a fingerprint of climate and human impact on semi-arid ecosystems". In: *Journal of Ecology* 94.3 (2006), pp. 537–547.

[116] Roy Malcolm Anderson and Robert Mccredie May. "The invasion, persistence and spread of infectious diseases within animal and plant communities". In: *Philosophical Transactions of the Royal Society of London. B, Biological Sciences* 314.1167 (1986), pp. 533–570.

[117] Roy M Anderson and Robert M May. *Infectious diseases of humans: dynamics and control*. Oxford university press, 1992.

[118] Patricia L Lakin-Thomas and Stuart Brody. "Circadian rhythms in microorganisms: new complexities". In: *Annu. Rev. Microbiol.* 58 (2004), pp. 489–519.

[119] Masato Nakajima, Keiko Imai, Hiroshi Ito, et al. "Reconstitution of circadian oscillation of cyanobacterial KaiC phosphorylation in vitro". In: *science* 308.5720 (2005), pp. 414–415.

[120] Paul Smolen. "A model for glycolytic oscillations based on skeletal muscle phosphofructokinase kinetics". In: *Journal of theoretical biology* 174.2 (1995), pp. 137–148.

[121] James Keener and James Sneyd. "Mathematical physiology, volume 8 of Interdisciplinary applied mathematics". In: *Springer-Verlag, New York* 200 (1998), p. 400.

[122] Tom Evans, Eric T Rosenthal, Jim Youngblom, et al. "Cyclin: a protein specified by maternal mRNA in sea urchin eggs that is destroyed at each cleavage division". In: *Cell* 33.2 (1983), pp. 389–396.

[123] Peter K Jackson. "The hunt for cyclin". In: *Cell* 134.2 (2008), pp. 199–202.

[124] Alan Berryman. *Population cycles: the case for trophic interactions*. Oxford University Press, 2002.

[125] John Maynard-Smith. *Models in ecology*. CUP Archive, 1978.

[126] Steven H. Strogatz. *Nonlinear Dynamics and Chaos: With Applications to Physics, Biology, Chemistry and Engineering*. Westview Press, 2000.

[127] Crispin W Gardiner et al. *Handbook of stochastic methods*. Vol. 3. springer Berlin, 1985.

[128] Nicolaas Godfried Van Kampen. *Stochastic processes in physics and chemistry*. Vol. 1. Elsevier, 1992.

[129] Alan J McKane and Timothy J Newman. "Predator-prey cycles from resonant amplification of demographic stochasticity". In: *Physical review letters* 94.21 (2005), p. 218102.

[130] Alan J McKane, James D Nagy, Timothy J Newman, et al. "Amplified biochemical oscillations in cellular systems". In: *Journal of Statistical Physics* 128.1 (2007), pp. 165–191.

[131] David Alonso, Alan J McKane, and Mercedes Pascual. "Stochastic amplification in epidemics". In: *Journal of the Royal Society Interface* 4.14 (2007), pp. 575–582.

[132] Alexis B Webb, Nikhil Angelo, James E Huettner, et al. "Intrinsic, nondeterministic circadian rhythm generation in identified mammalian neurons". In: *Proceedings of the National Academy of Sciences* 106.38 (2009), pp. 16493–16498.

[133] Mustafa N Gultekin and N Bulent Gultekin. "Stock market seasonality: International evidence". In: *Journal of financial economics* 12.4 (1983), pp. 469–481.

[134] David JD Earn, Jonathan Dushoff, and Simon A Levin. "Ecology and evolution of the flu". In: *Trends in ecology & evolution* 17.7 (2002), pp. 334–340.

[135] Daniel T Gillespie. "Exact stochastic simulation of coupled chemical reactions". In: *The journal of physical chemistry* 81.25 (1977), pp. 2340–2361.

[136] Hannes Risken. "Fokker-planck equation". In: *The Fokker-Planck Equation*. Springer, 1996, pp. 63–95.

[137] Roberto Benzi, Alfonso Sutera, and Angelo Vulpiani. "The mechanism of stochastic resonance". In: *Journal of Physics A: mathematical and general* 14.11 (1981), p. L453.

[138] Luca Gammaitoni, Peter Hänggi, Peter Jung, et al. "Stochastic resonance". In: *Reviews of modern physics* 70.1 (1998), p. 223.

[139] Roberto Benzi, Giorgio Parisi, Alfonso Sutera, et al. "Stochastic resonance in climatic change". In: *Tellus* 34.1 (1982), pp. 10–16.

[140] Roberto Benzi, Giorgio Parisi, Alfonso Sutera, et al. "A theory of stochastic resonance in climatic change". In: *SIAM Journal on applied mathematics* 43.3 (1983), pp. 565–578.

[141] Hal L Smith. *An introduction to delay differential equations with applications to the life sciences*. Vol. 57. Springer New York, 2011.

[142] Nicholas AM Monk. "Oscillatory expression of Hes1, p53, and NF-κB driven by transcriptional time delays". In: *Current Biology* 13.16 (2003), pp. 1409–1413.

[143] Julian Lewis. "Autoinhibition with transcriptional delay: a simple mechanism for the zebrafish somitogenesis oscillator". In: *Current Biology* 13.16 (2003), pp. 1398–1408.

[144] MH Jensen, Kim Sneppen, and G Tiana. "Sustained oscillations and time delays in gene expression of protein Hes1". In: *Febs Letters* 541.1-3 (2003), pp. 176–177.

[145] Dmitri Bratsun, Dmitri Volfson, Lev S Tsimring, et al. "Delay-induced stochastic oscillations in gene regulation". In: *Proceedings of the National Academy of Sciences* 102.41 (2005), pp. 14593–14598.

[146] Hiromi Hirata, Shigeki Yoshiura, Toshiyuki Ohtsuka, et al. "Oscillatory expression of the bHLH factor Hes1 regulated by a negative feedback loop". In: *Science* 298.5594 (2002), pp. 840–843.

[147] Deepak Gupta, Stefano Garlaschi, Samir Suweis, et al. "Effective Resource Competition Model for Species Coexistence". In: *Phys. Rev. Lett.* 127 (20 2021), p. 208101.

[148] John N Thompson. *The coevolutionary process*. University of Chicago press, 1994.

[149] Dolph Schluter. *The ecology of adaptive radiation*. OUP Oxford, 2000.

[150] Peter Chesson and Nancy Huntly. "The roles of harsh and fluctuating conditions in the dynamics of ecological communities". In: *The American Naturalist* 150.5 (1997), pp. 519–553.

[151] Peter Chesson. "Mechanisms of maintenance of species diversity". In: *Annual review of Ecology and Systematics* 31.1 (2000), pp. 343–366.

[152] TLS Vincent, D Scheel, JS Brown, et al. "Trade-offs and coexistence in consumer-resource models: it all depends on what and where you eat". In: *The American Naturalist* 148.6 (1996), pp. 1038–1058.

[153] Kenneth A Schmidt, Sasha RX Dall, and Jan A Van Gils. "The ecology of information: an overview on the ecological significance of making informed decisions". In: *Oikos* 119.2 (2010), pp. 304–316.

[154] Jonathan M Chase and Mathew A Leibold. *Ecological niches: linking classical and contemporary approaches*. University of Chicago Press, 2003.

[155] Garrett Hardin. "The Competitive Exclusion Principle". In: *Science* 131.3409 (1960), pp. 1292–1297.

[156] Robert MacArthur and Richard Levins. "COMPETITION, HABITAT SELECTION, AND CHARACTER DISPLACEMENT IN A PATCHY ENVIRONMENT". In: *Proceedings of the National Academy of Sciences* 51.6 (1964), pp. 1207–1210.

[157] Simon A. Levin. "Community Equilibria and Stability, and an Extension of the Competitive Exclusion Principle". In: *The American Naturalist* 104.939 (1970), pp. 413–423.

[158] Richard McGehee and Robert A Armstrong. "Some mathematical problems concerning the ecological principle of competitive exclusion". In: *Journal of Differential Equations* 23.1 (1977), pp. 30–52.

[159] Robert A Armstrong and Richard McGehee. "Competitive exclusion". In: *The American Naturalist* 115.2 (1980), pp. 151–170.

[160] NF Britton. "Aggregation and the competitive exclusion principle". In: *Journal of Theoretical Biology* 136.1 (1989), pp. 57–66.

[161] Alexandru Hening and Dang H Nguyen. "The competitive exclusion principle in stochastic environments". In: *Journal of mathematical biology* 80.5 (2020), pp. 1323–1351.

[162] Jef Huisman and Franz J Weissing. "Biodiversity of plankton by species oscillations and chaos". In: *Nature* 402.6760 (1999), pp. 407–410.

[163] Anna Posfai, Thibaud Taillefumier, and Ned S. Wingreen. "Metabolic Trade-Offs Promote Diversity in a Model Ecosystem". In: *Phys. Rev. Lett.* 118 (2 Jan. 2017), p. 028103.

[164] Leonardo Pacciani-Mori, Andrea Giometto, Samir Suweis, et al. "Dynamic metabolic adaptation can promote species coexistence in competitive microbial communities". In: *PLOS Computational Biology* 16.5 (May 2020), pp. 1–18.

[165] Shovonlal Roy and J. Chattopadhyay. "The stability of ecosystems: A brief overview of the paradox of enrichment". In: *Journal of Biosciences* 32 (2007), pp. 421 –428.

[166] Stephen W Pacala and Simon A Levin. "9. Biologically Generated Spatial Pattern and the Coexistence of Competing Species". In: *Spatial ecology*. Princeton University Press, 2018, pp. 204–232.

[167] Richard Durrett and Simon Levin. "The importance of being discrete (and spatial)". In: *Theoretical population biology* 46.3 (1994), pp. 363–394.

[168] Simon A Levin. "Dispersion and population interactions". In: *The American Naturalist* 108.960 (1974), pp. 207–228.

[169] Simon P Hart, Jacob Usinowicz, and Jonathan M Levine. "The spatial scales of species coexistence". In: *Nature Ecology & Evolution* 1.8 (2017), pp. 1066–1073.

[170] Daniel H Janzen. "Herbivores and the number of tree species in tropical forests". In: *The American Naturalist* 104.940 (1970), pp. 501–528.

[171] Joseph H Connell. "On the role of natural enemies in preventing competitive exclusion in some marine animals and in rain forest trees". In: *Dynamics of populations* 298 (1971), p. 312.

[172] Eugene W. Schupp. "The Janzen-Connell Model for Tropical Tree Diversity: Population Implications and the Importance of Spatial Scale". In: *The American Naturalist* 140.3 (1992), pp. 526–530.

[173] Deborah A Clark and David B Clark. "Spacing dynamics of a tropical rain forest tree: evaluation of the Janzen-Connell model". In: *The American Naturalist* 124.6 (1984), pp. 769–788.

[174] Robert Bagchi, Tom Swinfield, Rachel E Gallery, et al. "Testing the Janzen-Connell mechanism: pathogens cause overcompensating density dependence in a tropical tree". In: *Ecology letters* 13.10 (2010), pp. 1262–1269.

[175] Robert Bagchi, Rachel E Gallery, Sofia Gripenberg, et al. "Pathogens and insect herbivores drive rainforest plant diversity and composition". In: *Nature* 506.7486 (2014), pp. 85–88.

[176] Sijmen E Schoustra, Jonathan Dench, Rola Dali, et al. "Antagonistic interactions peak at intermediate genetic distance in clinical and laboratory strains of Pseudomonas aeruginosa". In: *BMC microbiology* 12.1 (2012), pp. 1–9.

[177] Leonor García-Bayona and Laurie E Comstock. "Bacterial antagonism in host-associated microbial communities". In: *Science* 361.6408 (2018).

[178] Elisa T Granato, Thomas A Meiller-Legrand, and Kevin R Foster. "The evolution and ecology of bacterial warfare". In: *Current biology* 29.11 (2019), R521–R537.

[179] Primrose J Boynton. "The ecology of killer yeasts: Interference competition in natural habitats". In: *Yeast* 36.8 (2019), pp. 473–485.

[180] Andrea Giometto, David R Nelson, and Andrew W Murray. "Antagonism between killer yeast strains as an experimental model for biological nucleation dynamics". In: *bioRxiv* (2020).

[181] Enrico Ser-Giacomi, Lucie Zinger, Shruti Malviya, et al. "Ubiquitous abundance distribution of non-dominant plankton across the global ocean". In: *Nature Ecology & Evolution* 2 (Aug. 2018), pp. 1243–1249.

[182] Evelyn F. Keller and Lee A. Segel. "Model for chemotaxis". In: *Journal of Theoretical Biology* 30.2 (1971), pp. 225–234.

[183] Kenneth G. Wilson. "The renormalization group: Critical phenomena and the Kondo problem". In: *Rev. Mod. Phys.* 47 (4 Oct. 1975), pp. 773–840.

[184] Shang-keng Ma and Gene F. Mazenko. "Critical dynamics of ferromagnets in $6 - \epsilon$ dimensions: General discussion and detailed calculation". In: *Phys. Rev. B* 11 (11 June 1975), pp. 4077–4100.

[185] Paula Villa Martin, Ales Bucek, Tom Bourguignon, et al. "Ocean currents promote rare species diversity in protists". In: *bioRxiv* (2020).

[186] Colomban De Vargas, Stéphane Audic, Nicolas Henry, et al. "Eukaryotic plankton diversity in the sunlit ocean". In: *Science* 348.6237 (2015).

[187] Jacopo Grilli. "Macroecological laws describe variation and diversity in microbial communities". In: *Nature communications* 11.1 (2020), pp. 1–11.

[188] Russell Lande, Steinar Engen, Bernt-Erik Saether, et al. *Stochastic population dynamics in ecology and conservation*. Oxford University Press on Demand, 2003.

[189] Rafael D'Andrea, Theo Gibbs, and James P O'Dwyer. "Emergent neutrality in consumer-resource dynamics". In: *PLoS computational biology* 16.7 (2020), e1008102.

[190] Stefano Garlaschi, Deepak Gupta, Amos Maritan, et al. "Ginzburg-Landau amplitude equation for nonlinear nonlocal models". In: *Physical Review E* 103.2 (2021), p. 022210. DOI: https://doi.org/10.1103/PhysRevE.103.022210.

[191] Lee A Segel. "Distant side-walls cause slow amplitude modulation of cellular convection". In: *Journal of Fluid Mechanics* 38.1 (1969), pp. 203–224.

[192] Alan C Newell and John A Whitehead. "Finite bandwidth, finite amplitude convection". In: *Journal of Fluid Mechanics* 38.2 (1969), pp. 279–303.

[193] EA Kuznetsov, AA Nepomnyashchy, and LM Pismen. "New amplitude equation for Boussinesq convection and nonequilateral hexagonal patterns". In: *Physics Letters A* 205.4 (1995), pp. 261–265.

[194] Peilong Chen and Jorge Vinals. "Amplitude equation and pattern selection in Faraday waves". In: *Physical Review E* 60.1 (1999), p. 559.

[195] G Gambino, MC Lombardo, Mml Sammartino, et al. "Turing pattern formation in the Brusselator system with nonlinear diffusion". In: *Physical Review E* 88.4 (2013), p. 042925.

[196] G Gambino, MC Lombardo, and Mml Sammartino. "Turing instability and pattern formation for the Lengyel–Epstein system with nonlinear diffusion". In: *Acta Applicandae Mathematicae* 132.1 (2014), pp. 283–294.

[197] Arjen Doelman. "Pattern formation in reaction-diffusion systems–an explicit approach". In: *Complexity science* (2019), pp. 129–182.

[198] Christian Kuehn and Sebastian Throm. "Validity of amplitude equations for nonlocal nonlinearities". In: *Journal of Mathematical Physics* 59.7 (2018), p. 071510.

[199] David Morgan and Jonathan HP Dawes. "The Swift–Hohenberg equation with a nonlocal nonlinearity". In: *Physica D: Nonlinear Phenomena* 270 (2014), pp. 60–80.

[200] Cristóbal López and Emilio Hernández-García. "Fluctuations impact on a pattern-forming model of population dynamics with non-local interactions". In: *Physica D: Nonlinear Phenomena* 199.1-2 (2004), pp. 223–234.

[201] Grégory Faye and Matt Holzer. "Modulated traveling fronts for a nonlocal Fisher-KPP equation: a dynamical systems approach". In: *Journal of Differential Equations* 258.7 (2015), pp. 2257–2289.

[202] Simone Pigolotti, Cristóbal López, Emilio Hernández-García, et al. "How Gaussian competition leads to lumpy or uniform species distributions". In: *Theoretical Ecology* 3.2 (2010), pp. 89–96.

[203] Hugo Fort, Marten Scheffer, and Egbert H van Nes. "The paradox of the clumps mathematically explained". In: *Theoretical Ecology* 2.3 (2009), pp. 171–176.

[204] Ronald Aylmer Fisher. "The wave of advance of advantageous genes". In: *Annals of eugenics* 7.4 (1937), pp. 355–369.

[205] A Kolmogorov, I Petrovskii, and N Piskunov. "Study of a diffusion equation that is related to the growth of a quality of matter, and its application to a biological problem". In: *Byul. Mosk. Gos. Univ. Ser. A Mat. Mekh* 1.1 (1937), p. 26.

[206] Nicholas F Britton. "Spatial structures and periodic travelling waves in an integro-differential reaction-diffusion population model". In: *SIAM Journal on Applied Mathematics* 50.6 (1990), pp. 1663–1688.

[207] Stephen A Gourley. "Travelling front solutions of a nonlocal Fisher equation". In: *Journal of mathematical biology* 41.3 (2000), pp. 272–284.

[208] N Bessonov, Evgenia Babushkina, SF Golovashchenko, et al. "Numerical modelling of cell distribution in blood flow". In: *Mathematical Modelling of Natural Phenomena* 9.6 (2014), pp. 69–84.

[209] F Alvarez-Garrido, MG Clerc, and Gregorio Gonzalez-Cortes. "Transition to Spatiotemporal Intermittency and Defect Turbulence in Systems under Translational Coupling". In: *Physical review letters* 124.16 (2020), p. 164101.

[210] D Escaff. "Non-local defect interaction in one-dimension: weak versus strong non-locality". In: *The European Physical Journal D* 62.1 (2011), pp. 33–38.

[211] Cristian Fernandez-Oto, MG Clerc, Daniel Escaff, et al. "Strong nonlocal coupling stabilizes localized structures: an analysis based on front dynamics". In: *Physical review letters* 110.17 (2013), p. 174101.

[212] Jacopo Grilli, György Barabás, Matthew J Michalska-Smith, et al. "Higher-order interactions stabilize dynamics in competitive network models". In: *Nature* 548.7666 (2017), pp. 210–213.

[213] Tobias Galla. "Intrinsic fluctuations in stochastic delay systems: Theoretical description and application to a simple model of gene regulation". In: *Physical Review E* 80.2 (2009), p. 021909.

[214] Tobias Brett and Tobias Galla. "Stochastic processes with distributed delays: chemical Langevin equation and linear-noise approximation". In: *Physical Review Letters* 110.25 (2013), p. 250601.

[215] Manuel Barrio, Kevin Burrage, André Leier, et al. "Oscillatory regulation of Hes1: discrete stochastic delay modelling and simulation". In: *PLoS Comput Biol* 2.9 (2006), e117.

[216] Andre Leier and Tatiana T Marquez-Lago. "Delay chemical master equation: direct and closed-form solutions". In: *Proceedings of the Royal Society A: Mathematical, Physical and Engineering Sciences* 471.2179 (2015), p. 20150049.

[217] Uwe Küchler and Beatrice Mensch. "Langevins stochastic differential equation extended by a time-delayed term". In: *Stochastics: An International Journal of Probability and Stochastic Processes* 40.1-2 (1992), pp. 23–42.

[218] TD Frank and PJ Beek. "Stationary solutions of linear stochastic delay differential equations: Applications to biological systems". In: *Physical Review E* 64.2 (2001), p. 021917.

[219] TD Frank, PJ Beek, and R Friedrich. "Fokker-Planck perspective on stochastic delay systems: Exact solutions and data analysis of biological systems". In: *Physical Review E* 68.2 (2003), p. 021912.

[220] Robert M Corless, Gaston H Gonnet, David EG Hare, et al. "On the LambertW function". In: *Advances in Computational mathematics* 5.1 (1996), pp. 329–359.

[221] Michael Samoilov, Sergey Plyasunov, and Adam P Arkin. "Stochastic amplification and signaling in enzymatic futile cycles through noise-induced bistability with oscillations". In: *Proceedings of the National Academy of Sciences* 102.7 (2005), pp. 2310–2315.

[222] I Richard Lapidus and Ralph Schiller. "Model for the chemotactic response of a bacterial population". In: *Biophysical journal* 16.7 (1976), pp. 779–789.

[223] Marcus J Tindall, Philip K Maini, Steven L Porter, et al. "Overview of mathematical approaches used to model bacterial chemotaxis II: bacterial populations". In: *Bulletin of mathematical biology* 70.6 (2008), p. 1570.